frontiers | Research Topics

Integrated diagnostics and biomarker discovery in endocrinology and biomedical sciences, volume II

Edited by
Sijung Yun and Youngmi Ji

Published in
Frontiers in Endocrinology

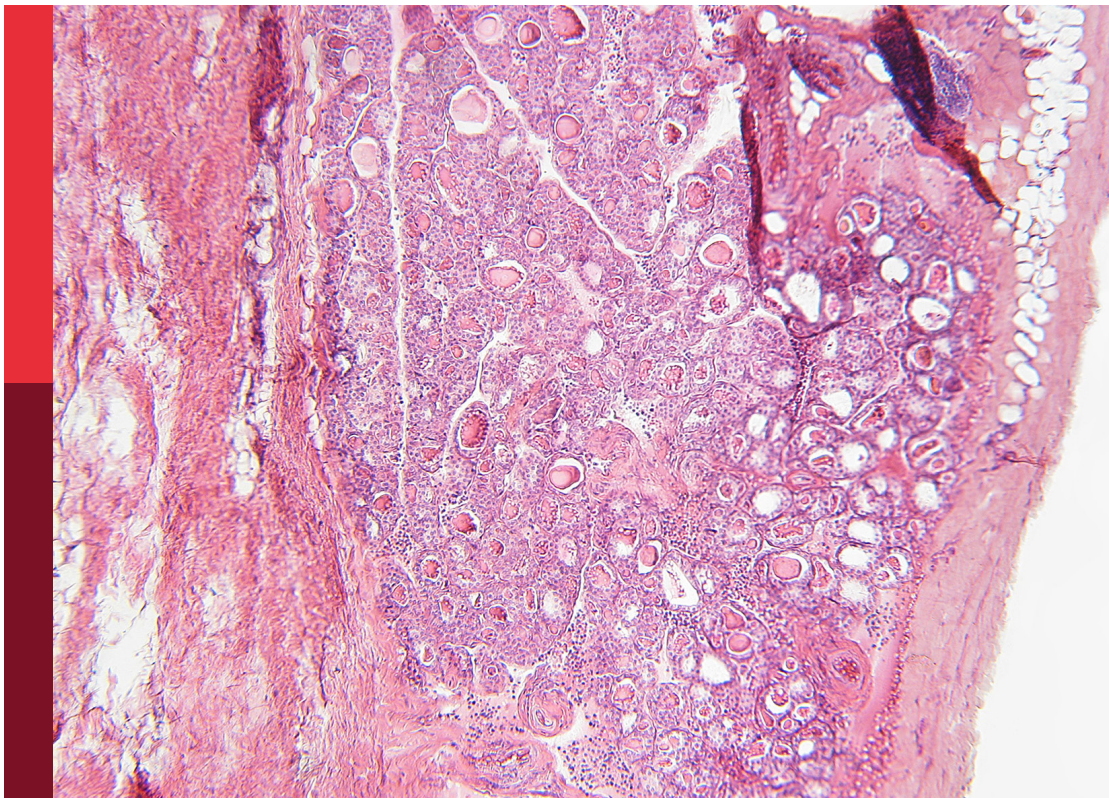

ISSN 1664-8714
ISBN 978-2-8325-7226-9
DOI 10.3389/978-2-8325-7226-9

Generative AI statement
Any alternative text (Alt text) provided alongside figures in the articles in this ebook has been generated by Frontiers with the support of artificial intelligence and reasonable efforts have been made to ensure accuracy, including review by the authors wherever possible. If you identify any issues, please contact us.

About Frontiers

Frontiers is more than just an open access publisher of scholarly articles: it is a pioneering approach to the world of academia, radically improving the way scholarly research is managed. The grand vision of Frontiers is a world where all people have an equal opportunity to seek, share and generate knowledge. Frontiers provides immediate and permanent online open access to all its publications, but this alone is not enough to realize our grand goals.

Frontiers journal series

The Frontiers journal series is a multi-tier and interdisciplinary set of open-access, online journals, promising a paradigm shift from the current review, selection and dissemination processes in academic publishing. All Frontiers journals are driven by researchers for researchers; therefore, they constitute a service to the scholarly community. At the same time, the *Frontiers journal series* operates on a revolutionary invention, the tiered publishing system, initially addressing specific communities of scholars, and gradually climbing up to broader public understanding, thus serving the interests of the lay society, too.

Dedication to quality

Each Frontiers article is a landmark of the highest quality, thanks to genuinely collaborative interactions between authors and review editors, who include some of the world's best academicians. Research must be certified by peers before entering a stream of knowledge that may eventually reach the public - and shape society; therefore, Frontiers only applies the most rigorous and unbiased reviews. Frontiers revolutionizes research publishing by freely delivering the most outstanding research, evaluated with no bias from both the academic and social point of view. By applying the most advanced information technologies, Frontiers is catapulting scholarly publishing into a new generation.

What are Frontiers Research Topics?

Frontiers Research Topics are very popular trademarks of the *Frontiers journals series*: they are collections of at least ten articles, all centered on a particular subject. With their unique mix of varied contributions from Original Research to Review Articles, Frontiers Research Topics unify the most influential researchers, the latest key findings and historical advances in a hot research area.

Find out more on how to host your own Frontiers Research Topic or contribute to one as an author by contacting the Frontiers editorial office: frontiersin.org/about/contact

Integrated diagnostics and biomarker discovery in endocrinology and biomedical sciences, volume II

Topic editors
Sijung Yun — Predictiv Care, Inc., United States
Youngmi Ji — National Institutes of Health (NIH), United States

Citation
Yun, S., Ji, Y., eds. (2025). *Integrated diagnostics and biomarker discovery in endocrinology and biomedical sciences, volume II*. Lausanne: Frontiers Media SA. doi: 10.3389/978-2-8325-7226-9

Dr. Yun is funded by Predictiv Care, Inc.

Table of contents

frontiers | Frontiers in Endocrinology

TYPE Editorial
PUBLISHED 21 November 2025
DOI 10.3389/fendo.2025.1739424

OPEN ACCESS

EDITED AND REVIEWED BY
Darko Stefanovski,
University of Pennsylvania, United States

*CORRESPONDENCE
Sijung Yun
syun16@jhu.edu
Youngmi Ji
charmgene@gmail.com

RECEIVED 04 November 2025
REVISED 07 November 2025
ACCEPTED 07 November 2025
PUBLISHED 21 November 2025

CITATION
Park K, Jin M, Kwon Y-M, Park Y, Kwon S-Y, Yun S, Ji Y and Yun S (2025) Editorial: Integrated diagnostics and biomarker discovery in endocrinology and biomedical sciences, volume II. *Front. Endocrinol.* 16:1739424. doi: 10.3389/fendo.2025.1739424

Editorial: Integrated diagnostics and biomarker discovery in endocrinology and biomedical sciences, volume II

Kinam Park[1], Mikyung Jin[1], Yong-Min Kwon[2], Yena Park[1], Soon-Yong Kwon[3], Sajung Yun[1,4,5], Youngmi Ji[6]* and Sijung Yun[4,7]*

[1]Predictive AI, Inc., Seongnam, Republic of Korea, [2]Department of Radiology, Youido St. Mary's Hospital, Catholic University of Korea, Seoul, Republic of Korea, [3]Seoul Bethesda Hospital, Seoul, Republic of Korea, [4]Johns Hopkins University, Baltimore, MD, United States, [5]US-Asia Technology Management Center, Stanford University, Stanford, CA, United States, [6]National Institute of Dental and Craniofacial Research, National Institutes of Health, Bethesda, MD, United States, [7]Predictiv Care, Inc., Mountain View, CA, United States

KEYWORDS

multi-omics, systems endocrinology, precision medicine, biomarker discovery, integrative analysis, endocrine disorders

Editorial on the Research Topic
Integrated diagnostics and biomarker discovery in endocrinology and biomedical sciences, volume II

The integration of multi-omics biological data, such as genomics, transcriptomics, proteomics, etc., is reshaping how we conceptualize and pursue biomarker discovery in endocrinology. Moving beyond reductionist paradigms, contemporary research now unites molecular, cellular, physiological, and population-level information to illuminate the complex regulatory architecture underlying endocrine health and disease. Integrated Diagnostics and Biomarker Discovery in Endocrinology and Biomedical Sciences: Volume II brings together nine original contributions that exemplify this transition toward a systems-oriented and data-driven discipline.

Spanning the spectrum from ionic ratios and proteomic signaling to transcriptomic networks, genomic variation, and ecological microbiome interactions, these studies demonstrate how diagnostic precision emerges through the convergence of molecular and systemic perspectives. Collectively, they trace a coherent trajectory - from basal biochemistry and molecular communication to clinical integration and population-scale modeling - illustrating how multi-scale data synthesis from ionic ratios to networks can refine both mechanistic understanding and translational application.

Taken together, this Research Topic reflects the growing maturity of integrative endocrinology, a field where multi-omics analytics, causal inference, and real-world data harmonization converge to enable predictive and personalized approaches to endocrine disorders. By highlighting these multi-scale insights, Volume II underscores the central message of modern biomarker science: meaningful diagnostic innovation arises not from any single data layer, but from their integration into a unified systems framework that connects molecules to medicine.

Lou et al. systematically validated the Glucose–Potassium Ratio (GPR) - a long-recognized broad clinical predictive marker (1) - as a prognostic biomarker for both short- and long-term all-cause mortality. They showed a strong association with mortality in both hospital and ICU settings. Mortality risk escalated sharply when GPR exceeded this threshold. Sensitivity analyses confirmed the robustness of these findings, positioning GPR as a valuable, non-invasive indicator for early identification and risk stratification of high-risk sepsis patients. This study opens the Research Topic by illustrating that integrated diagnostics can arise not only from macromolecular data but from fundamental ionic interactions reflecting systemic metabolic homeostasis.

Ji et al. utilized Tandem Mass Tag (TMT)-based quantitative proteomics on serum-derived exosomes to compare protein profiles among juvenile gout (J-Gout), juvenile hyperuricemia (J-HUA), and oligoarticular juvenile idiopathic arthritis (oJIA) patients. Subsequent ELISA validation confirmed that two proteins' concentrations were significantly high in J-Gout. Furthermore, their marker levels showed a positive correlation with clinical inflammatory indicators, C-reactive protein (CRP), and erythrocyte sedimentation rate (ESR). Bioinformatic analysis linked the differentially expressed proteins primarily to inflammatory mechanisms. These findings offer crucial molecular insight into J-Gout pathogenesis and serve as promising diagnostic or therapeutic biomarkers. Following the ionic analysis, this proteomic exploration demonstrates how molecular communication via exosomes encodes disease-specific inflammatory signatures.

Wang et al. analyzed the time-dependent biological variation (BV) of 16 biomarkers related to thyroid function, iron metabolism, and bone metabolism in 24 stable Type-2 Diabetes Mellitus (T2DM) patients. They also used variation values derived from healthy subjects, showing that some markers could be precisely monitored in T2DM patients by applying these reference change values. Conversely, for certain biomarkers, personalized monitoring was emphasized over using variation derived from healthy groups. This study illustrates the transition from individual molecular measures to dynamic systems of integrated biomarkers, reinforcing the need for personalized interpretation in metabolic diseases.

Wang and Zhu applied a two-sample Mendelian randomization (MR) analysis—an influential method for causal inference developed in the early 2000s (2)—using large-scale GWAS summary data comprising 1,195 rosacea cases and 211,139 controls to investigate the causal relationships between 179 plasma lipid species and rosacea. Two sterol esters (SE), two phosphatidylethanolamines (PE), and one sphingomyelin (SM) were identified as statistically significant protective factors against rosacea risk. This research enhances the understanding of rosacea pathogenesis by suggesting that these lipids are crucial for maintaining cell membrane function and regulating immune responses. It represents novel molecular targets for assessing and potentially treating this dermatological condition. Their work connects biochemical variability with genetic causality, demonstrating how lipid species can bridge metabolism, immunity, and dermatological pathology.

Ke et al. advanced the field of diagnostic marker discovery by applying bulk RNA analysis integrated with a comprehensive bioinformatics workflow - including differentially expressed gene (DEG) analysis, weighted gene co-expression network analysis (WGCNA), and machine learning - to identify potential diagnostic genes in patients with Diabetes Mellitus (DM). They further highlighted the biological significance by noting its strong correlation with variations in immune cell types, suggesting a pivotal role in DM's immunoregulatory mechanisms. This work leverages transcriptomic networks and machine learning to map the immune-metabolic landscape of endocrine disease.

Buzdin et al. introduced the EndoGene database, which is a repository documenting genetic variants identified via NGS and WES in 5,926 Russian patients with endocrine disorders. This work is valuable and meaningful from both an ethnic and population genetics perspective. This database is vital from a population-specific perspective due to the genetic heterogeneity of the Russian Federation. The study reported 2,073 unique genetic variants, with a striking 57% being previously undescribed at the time of genetic interpretation. EndoGene contributes essential population statistics and genetic background information, aiding clinicians in interpreting rare or population-specific mutations and ultimately enhancing the diagnostic accuracy and informative power of clinical NGS panels for endocrine pathologies. In the broader context, this database serves as an anchor point for genomic diversity, ensuring that future biomarker interpretation reflects population-specific genetic architecture.

Zhang et al. extended the concept of the Pan-Immune-Inflammation Value (PIV) - a composite biomarker integrating neutrophils, platelets, monocytes, and lymphocytes, originally proposed around 2020 as a prognostic indicator in cancer patients (3) - to broader applications encompassing general disease and mortality outcomes. They evaluated PIV as a predictor of mortality in the general population from a nationwide cohort study (NHANES, 48,662 samples). They found PIV levels were significantly and independently associated with an increased risk of all-cause mortality, as well as cause-specific deaths (cardiovascular, cancer, and diabetes-related). Moreover, a significant nonlinear dose-response relationship was observed between PIV and all-cause, cardiovascular disease, and cancer mortality. This research supports PIV's utility for public health risk stratification. Following the molecular and genomic studies, this large-scale investigation illustrates how integrated immune indices can extend biomarker discovery to population-level prediction.

Zhang et al. retrospectively analyzed 420 Chinese pregnant women with preeclampsia (PE) who had concomitant gestational hypothyroidism (GHT) to investigate the complex association between PE/GHT and neonatal birth weight (BW). Neonates born to mothers suffering from both PE and GHT exhibited significantly lower birth weight compared to those born to women with PE alone. Crucially, maternal Alanine Aminotransferase (ALT) levels, which were significantly elevated in the PE/GHT group, were identified as a potential partial mediator in this relationship. This highlights the necessity for clinicians to closely monitor maternal thyroid and liver function in PE patients to improve neonatal outcomes. Positioned toward the conclusion, their work exemplifies system-level biomarker integration, linking endocrine, hepatic, and obstetric parameters to clinical outcomes.

Cao et al. investigated the characteristics of the gut microbiome in 30 patients with Asymptomatic Hyperuricemia (AH) compared to 30 healthy controls using 16S rRNA sequencing. The AH group exhibited decreased overall gut microbial richness and ecological diversity. These microbial changes offer new insights and suggest that specific species may serve as potential biomarkers for early diagnosis and monitoring of AH. As the final piece, this study completes the integration spectrum by linking internal endocrine metabolism to external ecological networks, emphasizing that precision endocrinology now extends beyond the human genome into the microbiome.

Together, these nine contributions delineate a rapidly expanding frontier in integrated diagnostics, spanning the full continuum of biological organization—from ionic ratios and proteomic signatures to genomic databases and microbiome-derived ecological biomarkers. Collectively, they illustrate how endocrine science is evolving from isolated molecular characterization toward a fully systems-based discipline, in which the integration of multi-omics, clinical, and environmental data enhances both mechanistic insight and translational precision.

This convergence reflects the maturation of data-informed endocrinology, where diagnostic and prognostic innovation emerges from the synthesis of diverse data modalities rather than from any single layer of observation. By harmonizing biochemical, genetic, immunologic, and ecological perspectives, these studies redefine biomarker discovery as a process of multi-scale inference and integration - one that connects molecular precision with population-level relevance and real-world applicability. In this new framework, integration is not merely a methodological approach but a scientific imperative - transforming endocrinology into a discipline that systematically bridges molecules to medicine, and data to diagnosis.

Author contributions

KP: Writing – review & editing, Writing – original draft. MJ: Writing – review & editing, Writing – original draft. Y-MK: Writing – review & editing, Writing – original draft. YP: Writing – original draft, Writing – review & editing. S-YK: Writing – original draft, Writing – review & editing. YJ: Writing – review & editing, Writing – original draft. SaJY: Writing – review & editing, Writing – original draft. SiJY: Project administration, Supervision, Conceptualization, Writing – original draft, Writing – review & editing.

Conflict of interest

Authors KP, MJ, YP, SaJY were employed by Predictive AI, Inc. Author SijY was employed by Predictiv Care, Inc.

The remaining authors declare that the research was conducted in the absence of any commercial or financial relationships that could be construed as a potential conflict of interest.

Generative AI statement

The author(s) declare that no Generative AI was used in the creation of this manuscript.

Any alternative text (alt text) provided alongside figures in this article has been generated by Frontiers with the support of artificial intelligence and reasonable efforts have been made to ensure accuracy, including review by the authors wherever possible. If you identify any issues, please contact us.

Publisher's note

References

1. Lu Y, Ma X, Zhou X, Wang Y. The association between serum glucose to potassium ratio on admission and short-term mortality in ischemic stroke patients. *Sci Rep*. (2022) 12(1):8233. doi: 10.1038/s41598-022-12393-0

2. Smith GD, Ebrahim S. 'Mendelian randomization': can genetic epidemiology contribute to understanding environmental determinants of disease? *Int J Epidemiol*. (2003) 32(1):1–22. doi: 10.1093/ije/dyg070

3. Fucà G, Guarini V, Antoniotti C, Morano F, Moretto R, Corallo S, et al. The Pan-Immune-Inflammation Value is a new prognostic biomarker in metastatic colorectal cancer: results from a pooled analysis of the Valentino and TRIBE first-line trials. *Br J Cancer*. (2020) 123(3):403–9. doi: 10.1038/s41416-020-0894-7

frontiers | Frontiers in Endocrinology

TYPE Original Research
PUBLISHED 18 February 2025
DOI 10.3389/fendo.2025.1472754

OPEN ACCESS

EDITED BY
Sijung Yun,
Predictiv Care, Inc., United States

REVIEWED BY
Marcellus Andre Walker,
Johns Hopkins University, United States
Ching Chih Huang,
Johns Hopkins University, United States

*CORRESPONDENCE
Marianna A. Zolotovskaia
zolotovskaya.marianna@endocrincentr.ru

†These authors have contributed equally to this work

RECEIVED 30 July 2024
ACCEPTED 23 January 2025
PUBLISHED 18 February 2025

CITATION
Buzdin AA, Zolotovskaia MA, Roumiantsev SA, Emelyanova AG, Golounina OO, Pugacheva PA, Luppov DV, Kuzminyh AV, Alexeeva AO, Emelianova AA, Novoselov AL, Matrosova A, Slepukhina AA, Popov SV, Plaksina EV, Petrov VM, Guselnikova AR, Shagina AD, Suntsova MV, Zakharova VV, Belaya ZE, Vorontsova MV, Melnichenko GA, Mokrysheva NG, Chekhonin VP and Dedov II (2025) EndoGene database: reported genetic variants for 5,926 Russian patients diagnosed with endocrine disorders. *Front. Endocrinol.* 16:1472754. doi: 10.3389/fendo.2025.1472754

EndoGene database: reported genetic variants for 5,926 Russian patients diagnosed with endocrine disorders

Anton A. Buzdin[1,2,3,4†], Marianna A. Zolotovskaia[1,3*†], Sergey A. Roumiantsev[1], Aleksandra G. Emelyanova[1,3], Olga O. Golounina[1], Polina A. Pugacheva[1,3], Daniil V. Luppov[1,3], Anastasia V. Kuzminyh[3], Arseniya O. Alexeeva[1,3], Anna A. Emelianova[1,2], Alexey L. Novoselov[1], Alina Matrosova[1], Anastasia A. Slepukhina[5], Sergey V. Popov[1], Evgeniya V. Plaksina[1], Vasiliy M. Petrov[1], Anastasia R. Guselnikova[1], Anastasia D. Shagina[1], Maria V. Suntsova[1], Victoriya V. Zakharova[1], Zhanna E. Belaya[1], Maria V. Vorontsova[1,6], Galina A. Melnichenko[1], Natalia G. Mokrysheva[1], Vladimir P. Chekhonin[1] and Ivan I. Dedov[1]

[1]Laboratory of Bioinformatics, Endocrinology Research Center, Moscow, Russia, [2]Laboratory of Clinical and Genomic Bioinformatics, I.M. Sechenov First Moscow State Medical University, Moscow, Russia, [3]Moscow Center for Advanced Studies, Moscow, Russia, [4]Laboratory of Systems Biology, Shemyakin-Ovchinnikov Institute of Bioorganic Chemistry, Moscow, Russia, [5]Laboratory for Personalized Medicine, Institute of Chemical Biology and Fundamental Medicine, Novosibirsk, Russia, [6]Department of Internal Medicine, Lomonosov Moscow State University, Moscow, Russia

Introduction: Endocrine system disorders are a serious public health burden and can be caused by deleterious genetic variants in single genes or by the combined effects of multiple variants along with environmental and lifestyle factors.

Methods: The EndoGene database presents the results of next-generation sequencing assays used to genetically profile 5,926 patients who were diagnosed with 450 endocrine and concomitant diseases and were examined and treated at the National Medical Research Center for Endocrinology between November 2017 and January 2024. Among them, 494, 1,785, 692, and 1,941 patients were profiled using four internally developed genetic panels including 220, 250, 376, and 382 genes, respectively, selected based on a literature analysis and clinical recommendations, and 1,245 patients were profiled by whole exome sequencing covering 31,969 genes.

Results: 2,711 genetic variants were reported as clinically relevant by medical geneticists and are presented here along with genomic, technical, and clinical annotations.

Discussion: This publicly accessible database will be useful to those interested in genetics, epidemiology, population statistics, and a better understanding of the molecular basis of endocrine disorders.

KEYWORDS

genetic database, endocrine pathology, mutations, diabetes mellitus, Mendelian diseases, human genetic variants

1 Introduction

Endocrine diseases, including diabetes, thyroid dysfunction, and other hormonal imbalances, contribute significantly to the global burden of disease (1). These diseases not only affect public health but also lead to long-term disability and reduced quality of life for the affected individuals (1). The prevalence of these disorders is increasing, especially in the context of an aging population and the increasing incidence of metabolic disorders (2, 3).

These disorders can be caused by rare variants in a single gene (Mendelian or monogenic diseases), by the combined effects of multiple genetic variants, or by environmental and lifestyle factors (polygenic diseases such as type 2 diabetes mellitus or obesity). New techniques such as gene therapy offer hope when diseases cannot be effectively treated with traditional drugs. This is possible when the etiology of the inherited disease is known. Thus, a functional copy of a gene is introduced into the human body with the help of a gene therapy drug, slowing down the progression of the disease and, in some cases, even achieving significant improvement (4). In recent years, advancements in technology have facilitated the characterization of genomic diversity across a wide range of populations (5). Next-generation sequencing (NGS) and genome-wide association studies (GWASs) have been intensely used to study the genetic basis of endocrine diseases (6–9). However, the interpretation of identified variants using criteria widely recommended by the American College of Medical Genetics and the Association for Molecular Pathology (ACMG/AMP) (10) is challenging because detailed phenotypic information associated with specific variants is limited in most databases (11). To improve the accuracy of diagnosis, prognosis, and genetic counseling, the importance of variant databases in patients with specific diagnoses (12) is increasingly recognized. Such databases constitute systematically organized repositories of genetic variants, supplemented with clinical data (13). They facilitate communication between researchers, clinicians, and patients by allowing the sharing of information about genes, variants, and pathologic phenotypes (11).

Previous studies have created databases that include genetic variants associated with specific endocrinopathies. For example, the MEN2 RET database developed by Margraf et al. is a publicly accessible database that contains all *RET* sequence variants related to MEN2 syndromes as well as relevant clinical data (14). The "NGS and PPGL Study Group" also collected and classified variants in the *SDHB* gene, which is one of the major genes responsible for paraganglioma/pheochromocytoma predisposition (PPGL), leading to the creation of the *SDHB* variant database (15). In Argentina, a study of 170 patients with congenital hypopituitarism identified causative variants in both known and recently proposed candidate genes (9). In addition, a recent report presented a database containing comprehensive experimentally validated associations between endocrine diseases and long non-coding RNAs (16).

However, it is important to consider the potential role of population-specific variants in disease pathogenesis. Uncommon variants tend to be specific to certain populations (17). It has been observed that disease-causing variants often exhibit population specificity not only for rare but also for common diseases, which emphasizes the importance of considering pedigree in genetic studies and clinical diagnosis (18). The multinational population of the Russian Federation, comprising more than one hundred different ethnic groups, demonstrates genetic heterogeneity (19–21) and provides a unique but challenging opportunity to study the genetic basis of inherited pathogenic mutations and their contribution to disease etiology in different populations. A recent study presented a database on the frequency of genetic variants in Russia (22). In addition, several databases have been created for Russian patients with hereditary cancer syndromes (23, 24).

The aim of our study was to create the first representative database of genetic variants specifically targeting endocrine diseases in the Russian population. We collected information on pathogenic, likely pathogenic, and other genetic variants identified by panel NGS and/or whole exome sequencing (WES) in 5,926 patients with various endocrine pathologies. The database includes information on zygosity and pathogenicity classification according to ACMG/AMP recommendations and the presence of reported variants in previous scientific publications and in population frequency databases at the time of genetic interpretation. We also calculated gene mutation frequencies associated with each type of diagnosis.

In addition, we calculated the proportion of WES and smaller genetic panel analyses that resulted in the identification of variants for each type of endocrine diagnosis, allowing us to compare the performance of WES and panel target sequencing tests.

We believe that our database and the analysis of the statistics of reported genetic variants will contribute to a better understanding of the genetic basis of endocrine diseases, aid in the interpretation of mutations found in different populations, and suggest changes in the composition of diagnostic NGS panels to increase their informative power.

The ability to predict clinical outcomes based on genetic data may be improved by identifying pathogenic variants specific to certain populations (25). This study is the first to establish the frequency of pathogenic variants in Russian patients with endocrine diseases. To our knowledge, the presented database is also one of the world's largest genetic experimental knowledge bases on endocrine pathology. It contributes to the growing body of knowledge on the genetic basis of these diseases and opens the way for more accurate and personalized diagnosis and treatment.

2 Methods

2.1 Participant characteristics

The sample includes 5,926 patients who were subjected to NGS DNA sequencing tests performed in the National Medical Research Center for Endocrinology (Moscow) from November 2017 to January 2024. The patients either suffered from endocrine pathology or had unfavorable hereditary history. In all cases, written informed consent to participate in this study was acquired from the patients or from their legal representatives. The consent procedure and the design of the study were approved by the ethics committee of the National Medical Research Center for Endocrinology, Moscow, Russia.

Inclusion criteria were the availability of diagnosis and record with sequencing results interpreted by clinical geneticists according to the ACMG/AMP guidelines (10). Patients were not specifically selected based on their clinical diagnoses. However, given the specialization of the Endocrinology Research Center, the testing cohort predominantly included individuals with endocrine or endocrine-related pathology, and their relatives were considered potential carriers of pathogenic genetic variants. A complete set of ICD10 diagnoses associated with individual patients and specific genetic variants is available in the database file (https://doi.org/10.5281/zenodo.10894526) and the patients can be filtered by ICD10 code for specific disease types.

Exclusion criteria were records with genetic variants that were not confirmed by two or more identifiers or were not classified according to ACMG guidelines (e.g., due to the need for additional examination of the patient).

2.2 Library preparation and sequencing

Genomic DNA was extracted using a NucleoMag Blood Kit (Macherey–Nagel), MagPure Blood Dna, Kit (Magen), MagPure Universal Dna Kit (Magen), or HiPure Universal Dna Kit (Magen). DNA concentrations were measured on Qubit 4 fluorimeter. Library preparation was performed using a KAPA HyperPlus Kit (Roche), VAHTS Universal Plus DNA Library Prep Kit for Illumina V2 (Vazyme), or Illumina DNA Prep with Enrichment reagents (Illumina). To allow sample multiplexing, indexed primers or adapters were used as follows: KAPA UDI Primer Mixes (Roche), VAHTS DNA Adapters for Illumina (Vazyme), and IDT for Illumina UD Indexes (IDT). For target enrichment, DNA libraries were hybridized with biotinylated DNA probes for 16 to 18 h and then captured by streptavidin beads. Hybridization and capture procedures were performed according to the KAPA HyperCap Workflow, VAHTS Target Capture Hybridization and Wash protocol, or Illumina DNA Prep with Enrichment protocol with respective reagent kits. For whole exome enrichment, KAPA HyperExome Probes (Roche), a VAHTS Target Capture Core Exome Panel (Vazyme), or an IDT xGen Exome Hyb Panel (IDT) were used. Additionally, four custom probe panels were used for the enrichment of genes involved in endocrine disorders: Endo1, Endo2, Endome1, and Endome2 (Roche, designed in the National Medical Research Center for Endocrinology). Library quality was assessed using a 5200 Fragment Analyzer system (Agilent) with NGS Fragment Kits (1 to 6000bp). PE100 sequencing was performed on an Illumina NovaSeq 6000, NextSeq550, or MiSeq depending on the required number of reads per sample. The average mean exon coverage of x100 was obtained for both whole exome and target panel sequencing. Demultiplexing was performed using the Illumina Bcl2fastq2 program.

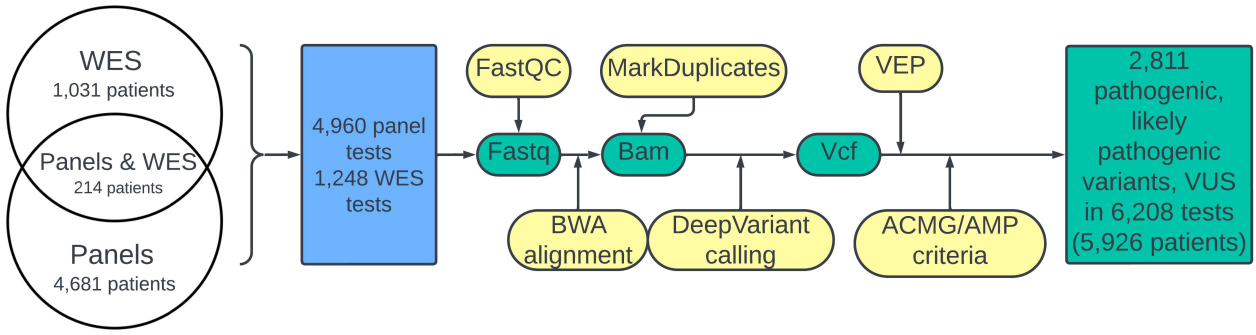

FIGURE 1
Flowchart of the study. The green color denotes molecular data; bioinformatic pipeline steps are shown in yellow. The blue block corresponds to performed NGS tests.

2.3 Data processing

The design of the study is schematized in Figure 1. A quality check of the fastq files was done using FastP (26). The reads were aligned to the human genome assembly GRCh38 using BWA-mem (27). Coordinates of target regions correspond to the enrichment used. BAM coverage was calculated against the BED file using mosdepth. Samtools software was used for BAM file indexing. Duplicate marking was performed using MarkDuplicates software. We used DeepVariant for variant calling (28). All variants with an allele frequency in the experimental read for a particular biosample of less 0.01 were removed from further analysis. VCF annotation was performed using the VEP (29) tool. Variant interpretation was performed in accordance with the ACMG/AMP guidelines considering information about clinical features including phenotype and family segregation, VEP annotation, which characterized its potential impact on protein function (variant type, scores from *in silico* predictors CADD, PolyPhen, BayesDel, MutPred, MetaRNN, SpliceAI, and LoF), and data from population and clinical databases (gnomAD, ClinVar, and HGMD public). A complete list of VEP annotation fields is available in Supplementary File 1. In addition, information from variant-related scientific articles found in the PubMed database was used to annotate the fields.

2.4 Designs of target panels for NGS

The targeted NGS panels were developed at the National Medical Research Center for Endocrinology to cover genes known to be associated with endocrine pathologies. Initially, at the beginning of the project, two separate NGS panels, called Endo1 and Endo2, were developed. Later, they were combined with some modifications into one comprehensive Endome1 panel, which was further expanded to the Endome2 panel (Figure 2). The composition of the genes in the used NGS panels is given in Supplementary File 2.

2.5 Text analysis

Interpreted genetic variants were available as text records in electronic medical cards. Genetic coordinates, type of mutation, gene name, zygosity, and novelty of variant at the moment of interpretation were parsed with R v4.3.1 (30) and checked manually. Diagnoses of patients were automatically downloaded from the "ICD10 code" fields in the electronic medical cards. If the "ICD10 code" field was empty, the diagnoses were extracted manually from another field in the electronic medical cards or available hard medical documents.

2.6 Patient diagnoses

Every patient case was assigned an ICD10 code of diagnosis according to the 10th revision of the International Statistical Classification of Diseases and Related Health Problems, a medical classification list created by the World Health Organization. The code of the last available clinical diagnosis before the sequencing was used. If information about concomitant diagnoses was available, we also included the ICD10 codes for them. If the patient had no documented evidence about their pathology or any medical consultation at the moment on sequencing, ICD10 code Z01.8 was assigned.

2.7 Database format

We created a single comma-separated file with the following columns: "Patient ID", "Age", "Gender", "ICD-10 code of the disease",

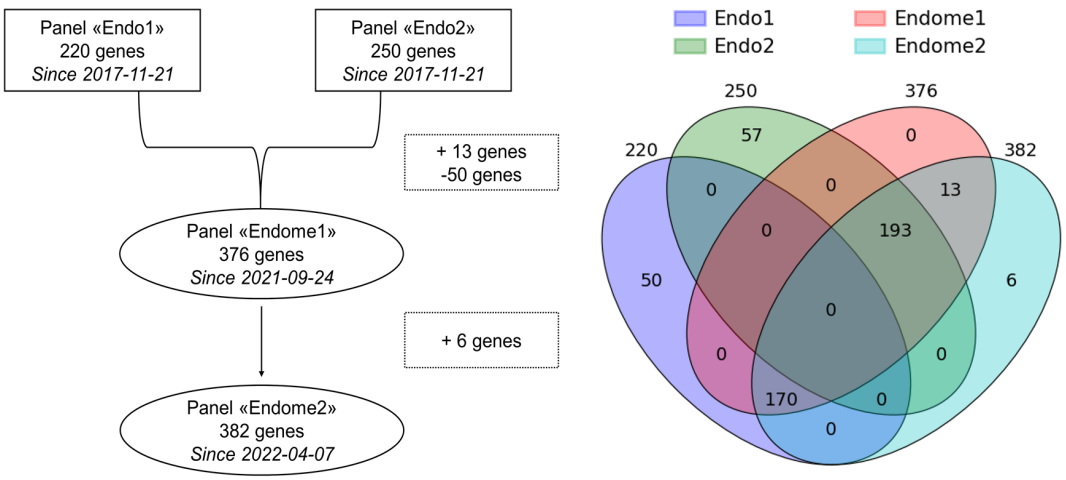

FIGURE 2
Relationship between the NGS panels used in this study. Intersections reflect the gene composition of panels under comparison.

"Sequencing type", "Panel design (if available)", "Variant reported", "Gene", "Zygosity", and "Described in the literature". If at least one variant was reported for a patient, each row corresponded to one variant. If the patient had no reported variants, one row corresponded to one patient and the fields for the reported variant were empty. All the ICD-10 codes for the patients are listed in each row with a semicolon as a separator.

2.8 Technical validation

2.8.1 Quality control of sequencing data

A data quality check was conducted on an Illumina SAV. A quality check of fastq files was conducted using FastP. All Illumina DNA short reads had a Phred score greater than 35 corresponding to a base accuracy greater than 99.9%.

2.8.2 Quality control of archive data

Metadata from the laboratory information system, such as WES or NGS panel version, were manually compared with the information from the text descriptions of the sequencing results. All the information obtained through text parsing was manually verified.

To prevent any operator mistakes, we validated the parsed variant description. We considered the variant valid if one of the following conditions was met:

1. The variant was written in both genomic and transcriptomic coordinates. We ensured that both types of coordinates described the same variant.
2. The variant had a dbSNP ID. We checked if the dbSNP variant indeed matched the variant parsed from the geneticist's report.
3. A *vcf* file was available and included the variant parsed from the geneticist's report.

To match genomic and cDNA coordinates, dbSNP ID, and vcf records, we used the Mutalyzer (31) and VariantValidator (32) tools.

Additionally, we used protein coordinates, HGMD ID, or PubMed ID (variant description from a scientific article) in manual mode to confirm the parsed variant.

In this study, we did not include any results obtained using a bioinformatic pipeline other than that outlined in Figure 1. Genetic variants with incomplete information (genome assembly, genomic coordinates, or ACMG/AMP classification) were filtered out and not included in the database. In this study, we did not consider genetic variants without final classification with only partially met ACMG/AMP criteria.

2.8.3 Control of clinical data

Interpretation of sequencing results for the individual patients was performed by clinical geneticists considering patient phenotype, medical documentation, and familial history when available. The correspondence of the patient diagnoses with the pathology group and with the results of NGS analysis was determined by the clinical endocrinologist.

3 Results and discussion

3.1 Overview of data records

We identified a total of 6,208 medical records with sequencing results for 5,926 patients. In total, 1,248 WES tests were performed for 1,245 patients, and 4,960 gene panel NGS tests were performed for 4895 patients. For 214 patients, both panel and WES tests were done. Some patients were tested several times due to technical or clinical reasons. Only genetic variants classified as "pathogenic," "likely pathogenic," or "of uncertain significance" were taken into consideration. Hereafter, they will be referred to as "reported variants". The complete database file is available at the following link: https://doi.org/10.5281/zenodo.10894526.

Relevant genetic variants were reported by clinical geneticists in 1,882 cases out of 4,960 NGS panel sequencing tests. Among them, 1,267 reports contained genetic variants classified as "pathogenic" and "likely pathogenic", and 700 were "variants of uncertain significance" (Figure 3). For WES tests, relevant genetic variants were reported for 448 out of 1,248 tests, including pathogenic and likely pathogenic variants in 203 cases and variants of uncertain significance in 284 cases (Figure 3). In some patient cases (267 for panel NGS and 129 for WES), more than one variant was annotated and reported. Interestingly, the percentage share of the cases with reported genetic variants was very similar for the results of WES and panel NGS (38% vs 36%, respectively).

For 43 genes, pathogenic and likely pathogenic variants were reported in both WES and panel NGS results. Pathogenic (*P*) and likely pathogenic (*LP*) variants were found in 108 and 186 genes in panel NGS or WES tests, respectively, with no intersections (Figure 3B). For variants of uncertain significance (*VUS*), 83 genes were common, and 161 and 251 were specific for the panel NGS and WES tests, respectively (Figure 3C). In total, 281 and 515 genes had at least one *P*, *LP*, or *VUS* reported variant for the panel NGS and WES tests, respectively, and 120 genes hosted reported genetic variants common in both tests (Supplementary Figure S1).

3.2 Analysis of groups of patients.

For statistical analyses, the patients were grouped according to their clinical diagnoses by ICD10 sections (240 groups, Supplementary File 3). The biggest groups, each containing more than 100 genetically profiled patients, are listed in Table 1.

In Table 1, some ICD10 diagnosis sections have broad definitions and include the following specific diagnoses for the clinical group under investigation:

a. for E03 *Other hypothyroidism*—E03.0 Congenital hypothyroidism with diffuse goitre, E03.1 Congenital hypothyroidism without goitre, E03.2 Hypothyroidism

10.3389/fendo.2025.1472754

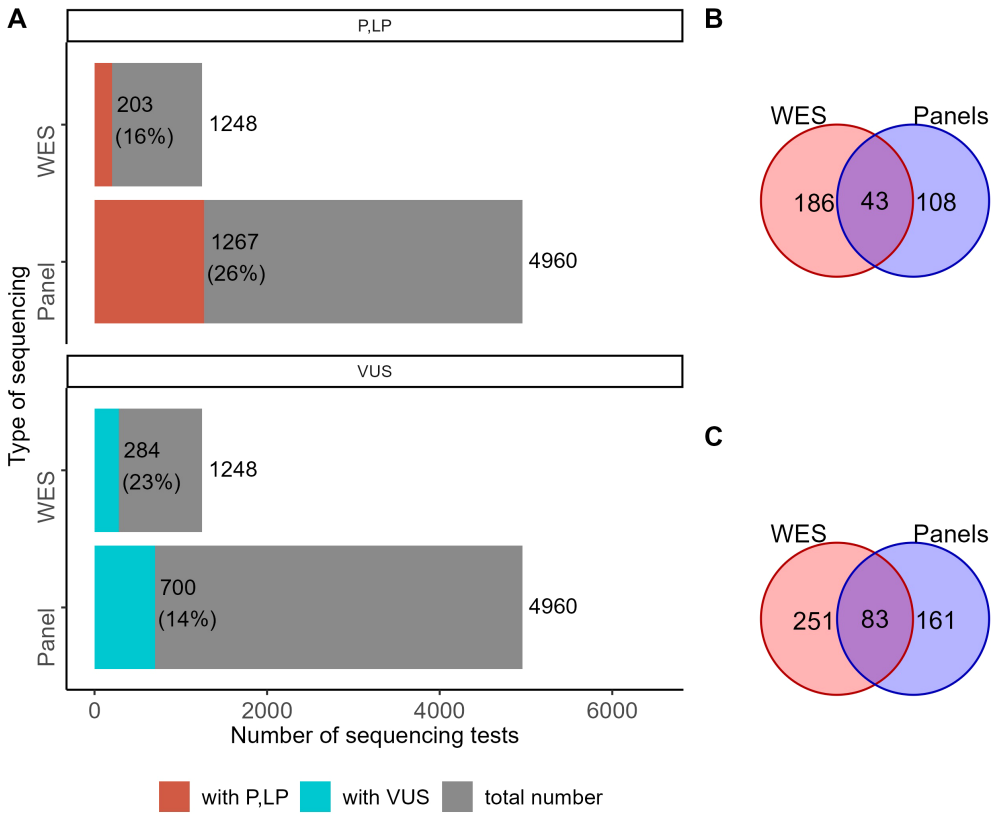

FIGURE 3
The proportion of NGS tests with reported genetic variants. **(A)** Number and percentage share of genetic tests with reported variants classified as "pathogenic" (P), "likely pathogenic" (LP), or "uncertain significance" (VUS) among the results of WES and panel NGS. **(B)** The number of genes hosting genetic variants classified as pathogenic or likely pathogenic in the results of WES and panel NGS. **(C)** The number of genes hosting genetic variants classified as VUS in the results of WES and panel NGS.

TABLE 1 ICD10 diagnostic sections containing more than 100 patients.

ICD10_section	WHO description	Diagnoses of the patients tested	Panel	WES	Total
E23	Hypofunction and other disorders of the pituitary gland	E23.0; E23.2; E23.3; E23.6; E23.7	574	112	686
E10	Type 1 diabetes mellitus	E10; E10.0; E10.1; E10.2; E10.3; E10.4; E10.6; E10.7; E10.8; E10.9	371	165	536
R73	Elevated blood glucose level	R73; R73.0; R73.9	408	2	410
E14	Unspecified diabetes mellitus	E14; E14.0; E14.7; E14.8; E14.9	392	7	399
E03	Other hypothyroidism	E03; E03.0; E03.1; E03.2; E03.8; E03.9	291	103	394
E34	Other endocrine disorders	E34; E34.3; E34.4; E34.5; E34.8; E34.9	230	128	358
E16	Other disorders of pancreatic internal secretion	E16.0; E16.1; E16.2; E16.4; E16.8; E16.9	248	97	345
E13	Other specified diabetes mellitus	E13; E13.2; E13.4; E13.7; E13.8; E13.9	297	10	307
E21	Hyperparathyroidism and other disorders of parathyroid gland	E21.0; E21.1; E21.2; E21.3; E21.4; E21.5	292	15	307
E66	Obesity	E66.0; E66.1; E66.8; E66.9	143	141	284
E25	Adrenogenital disorders	E25.0; E25.8; E25.9	261	21	282
E22	Hyperfunction of the pituitary gland	E22.0; E22.1; E22.8; E22.9	155	100	255
E27	Other disorders of the adrenal gland	E27; E27.0; E27.1; E27.3; E27.4; E27.5; E27.8; E27.9	207	32	239

(Continued)

TABLE 1 Continued

ICD10_section	WHO description	Diagnoses of the patients tested	Panel	WES	Total
E11	Type 2 diabetes mellitus	E11.2; E11.3; E11.4; E11.5; E11.6; E11.7; E11.8; E11.9	204	18	222
E83	Disorders of mineral metabolism	E83.3; E83.4; E83.5; E83.8; E83.9	194	11	205
E04	Other non-toxic goiter	E04.0; E04.1; E04.2	161	5	166
E31	Polyglandular dysfunction	E31; E31.0; E31.1; E31.8; E31.9	115	24	139
E30	Disorders of puberty, not elsewhere classified	E30; E30.0; E30.1; E30.8; E30.9	91	37	128

due to medicaments, E03.8 Other specified hypothyroidism, E03.9: Hypothyroidism, unspecified;

b. for E04 *Other nontoxic goiter*—E04.0 Non-toxic diffuse goiter, E04.1 Non-toxic single thyroid nodule, E04.2 Non-toxic multinodular goiter;
c. for E13 *Other specified diabetes mellitus*—E13.2 Other specified diabetes mellitus with renal complications, E13.4 Other specified diabetes mellitus with neurological complications, E13.7 Other specified diabetes mellitus with multiple complications, E13.8 Other specified diabetes mellitus with unspecified complications, E13.9 Other specified diabetes mellitus without complications;
d. for E16 *Other disorders of pancreatic internal secretion*—E16.0 Drug-induced hypoglycemia without coma, E16.1 Other hypoglycemia, E16.2 Hypoglycemia, unspecified, E16.4 Abnormal secretion of gastrin, E16.8 Other specified disorders of pancreatic internal secretion, E16.9 Disorder of pancreatic internal secretion, unspecified;
e. for E23 *Hypofunction and other disorders of pituitary gland* —E23.0 Hypopituitarism, E23.2: Diabetes insipidus,

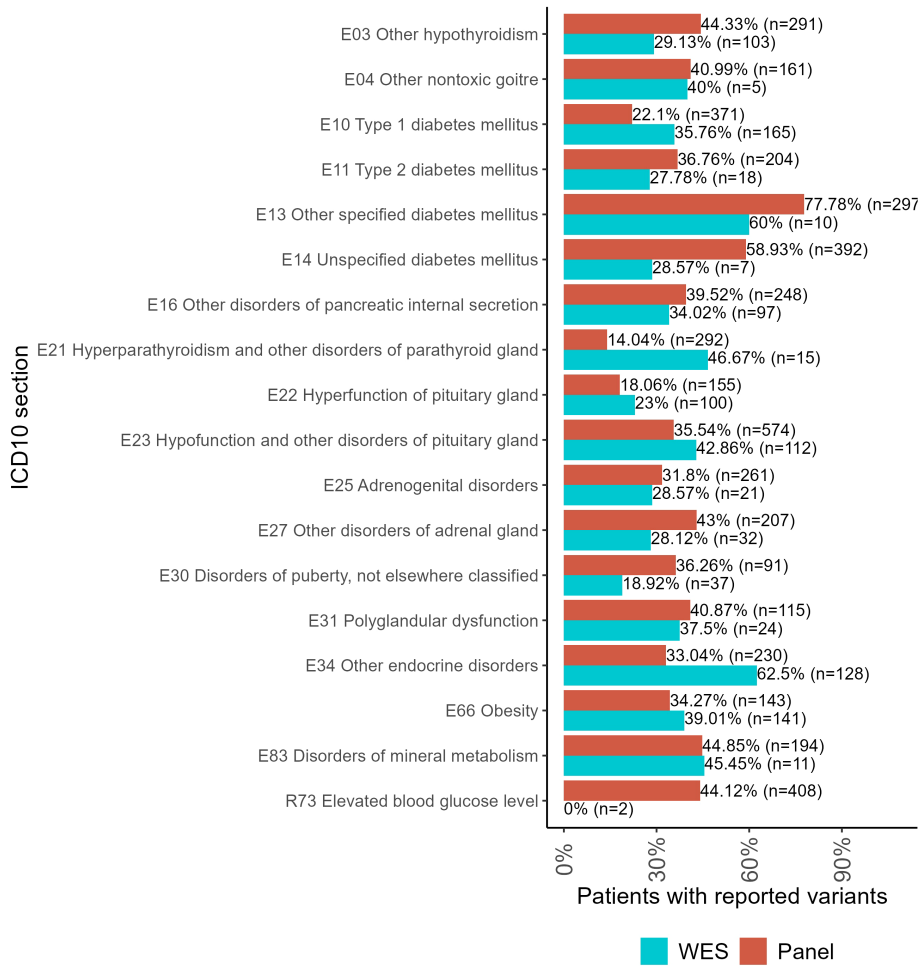

FIGURE 4
The proportion of patients with genetic variants classified as "pathogenic" (P), "likely pathogenic" (LP), or "uncertain significance" (VUS) in the results of panel NGS and WES tests for ICD10 diagnosis groups containing more than 100 genetically profiled patients with endocrine pathologies.

E23.3 Hypothalamic dysfunction, not elsewhere classified, E23.6 Other disorders of pituitary gland, E23.7 Disorder of pituitary gland, unspecified;

f. for E27 *Other disorders of adrenal gland*—E27.0 Other adrenocortical overactivity, E27.1 Primary adrenocortical insufficiency, E27.3 Drug-induced adrenocortical insufficiency, E27.4 Other and unspecified adrenocortical insufficiency, E27.5 Adrenomedullary hyperfunction, E27.8 Other specified disorders of adrenal gland, E27.9 Disorder of adrenal gland, unspecified;

g. for E30 *Disorders of puberty, not elsewhere classified*—E30.0 Delayed puberty, E30.1 Precocious puberty, E30.8 Other disorders of puberty, E30.9 Disorder of puberty, unspecified;

h. for E34 *Other endocrine disorders*—E34.3 Short stature, not elsewhere classified, E34.4 Constitutional tall stature, E34.5 Androgen resistance syndrome, E34.8 Other specified endocrine disorders, E34.9 Endocrine disorder, unspecified.

For the WES tests, the biggest proportion of reported variants was detected for the following patient groups (Figure 4): type 1 diabetes mellitus (E10), hyperparathyroidism and other disorders of parathyroid gland (E21), hyperfunction of pituitary gland (E22), hypofunction and other disorders of pituitary gland (E23), other endocrine disorders (E34), obesity (E66), and disorders of mineral metabolism (E83).

For panel NGS, the biggest proportion of reported variants was reported for the following groups: other hypothyroidism (E03); other non-toxic goiter (E04); type 2 diabetes mellitus (E11); other specified diabetes mellitus (E13); unspecified diabetes mellitus (E14); other disorders of pancreatic internal secretion (E16); adrenogenital disorders (E25); other disorders of the adrenal gland (E27); disorders of puberty, not elsewhere classified (E30); polyglandular dysfunction (E31); and elevated blood glucose level (R73).

For each individual patient, the *pathogenicity level* was assessed by the highest pathogenicity score of their reported variants (Figure 5). Thus, the highest level ("pathogenic") included patients with at least one pathogenic variant but who might have additional reported variants as well. Similarly, patients classified as having "likely pathogenic" variants could have other variants as well except for the "pathogenic" ones. The distribution of patients by pathogenicity level is shown in Figure 5.

Both panel NGS and WES profiles were available for 214 patients (Figure 6, Supplementary File 3). Thus, we compared the genetic variants reported in the same patients using alternative tests. In general, the WES results contained more reported variants than the panel NGS annotations. However, some variants were reported in the panel NGS results and then labeled as irrelevant to the patient's condition in the WES tests. Because the geneticists subjected the patients to WES after panel NGS in cases of doubt

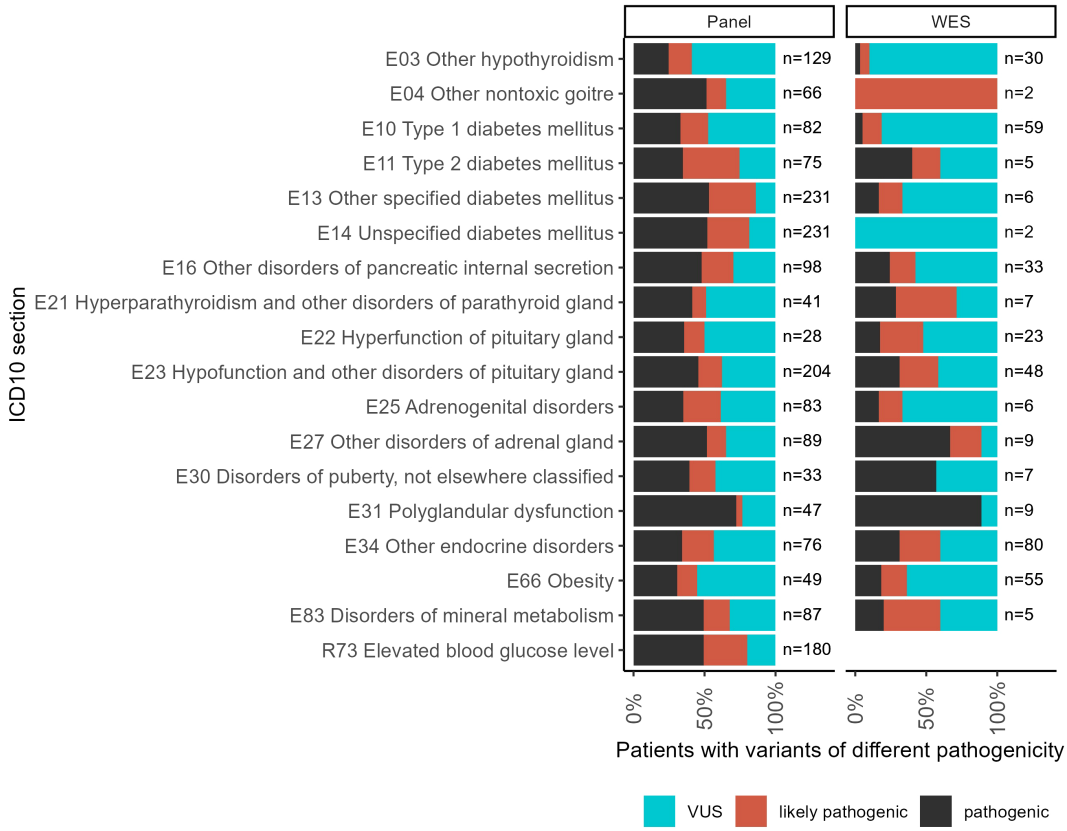

FIGURE 5
The proportion of patients with variants of different pathogenicity levels among all patients with reported variants for ICD10 diagnosis groups containing more than 100 genetically profiled patients with endocrine pathologies.

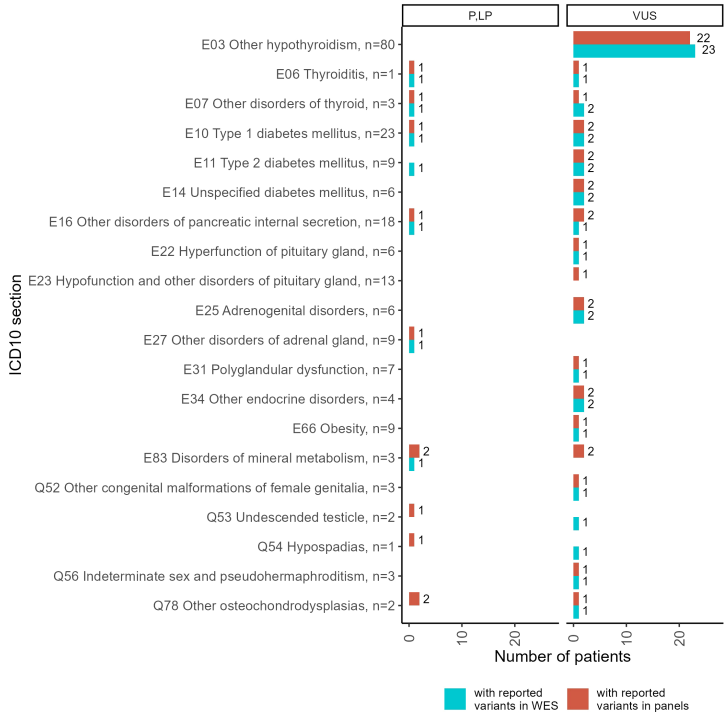

FIGURE 6
Statistics of patients with reported genetic variants classified as "pathogenic" (P), "likely pathogenic" (LP), or "uncertain significance" (VUS) in the results of double tests including panel NGS and WES, performed for 214 patients. Complete diagnoses of the patients tested are specified in Supplementary File 3.

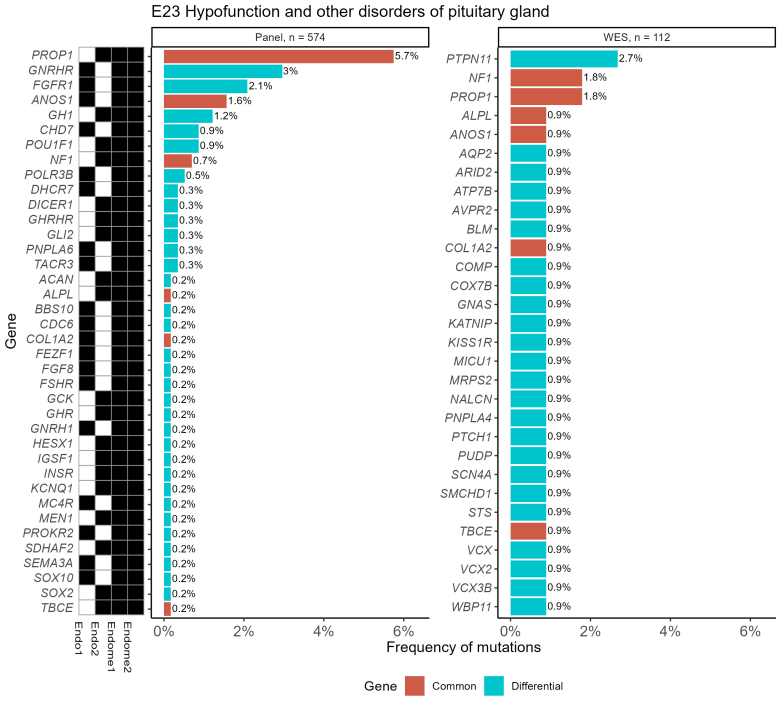

FIGURE 7
Frequencies of "pathogenic" (P) and "likely pathogenic" (LP) genetic variants for the ICD10 diagnosis group "E23 Hypofunction and other disorders of pituitary gland" identified using WES and panel NGS tests. Mutation frequency was calculated as the ratio of patients with gene mutations to the total number of patients in the group. Genes with pathogenic and likely pathogenic variants found in both panel NGS and WES tests are highlighted in orange (common items), otherwise shown in green (differential genes). The black marker shows whether the gene was included (black–yes, white–no) in the specific versions of the NGS panel used.

when the first test could not adequately explain the patient's phenotype, here we consider WES results as the gold standard for cases of such dual profiling.

A more detailed comparison of the molecular cases for the patients simultaneously profiled by panel NGS and WES including the distribution of gene mutation frequencies is given in Supplementary File 4.

We then compared the frequencies of *P* and *LP* variants in panel NGS and WES results. For this analysis, we excluded panel NGS results that were dismissed by WES tests for the same patients (eight patient cases).

In Figure 7, such an analysis is exemplified for the ICD10 diagnosis group "E23 *Hypofunction and other disorders of pituitary gland*". It can be seen that gene *PTPN11*, which was most frequently associated with the diagnosis "E34.3 *Short stature due to endocrine disorder*", was also useful for the analysis of the E23 group.

For other ICD10 diagnosis groups containing more than 100 genetically profiled patients with endocrine pathologies, complete

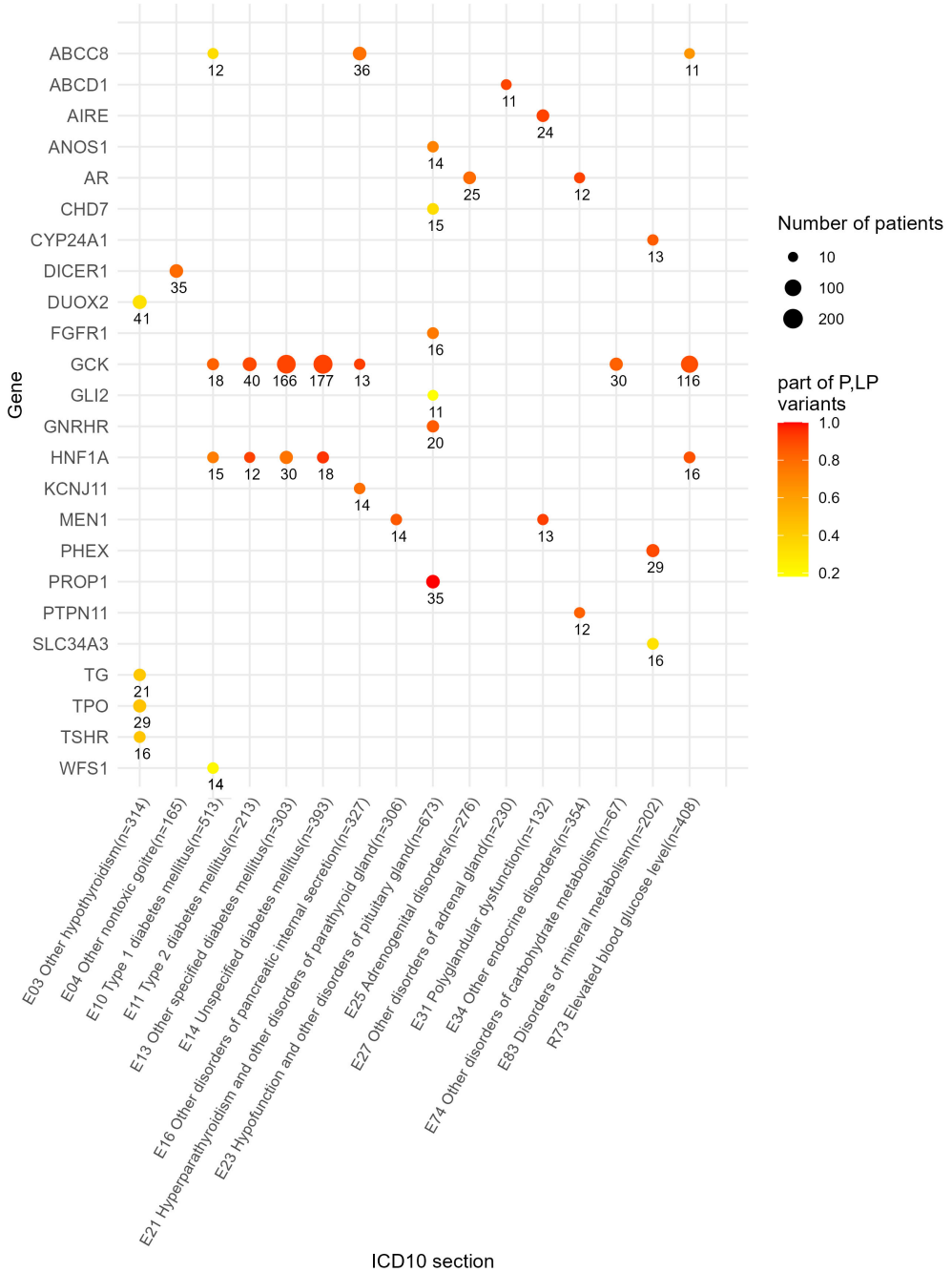

FIGURE 8
Genes with 10 times and greater occurrence in genetic reports in the whole patient cohort.

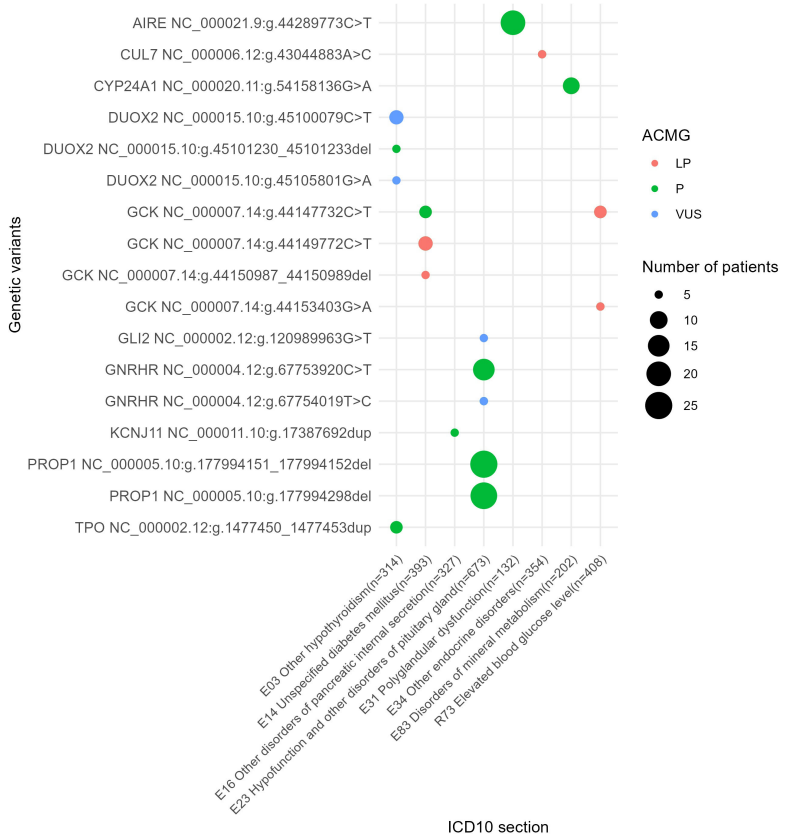

FIGURE 9
The most commonly reported genetic variants found in at least five patients under analysis.

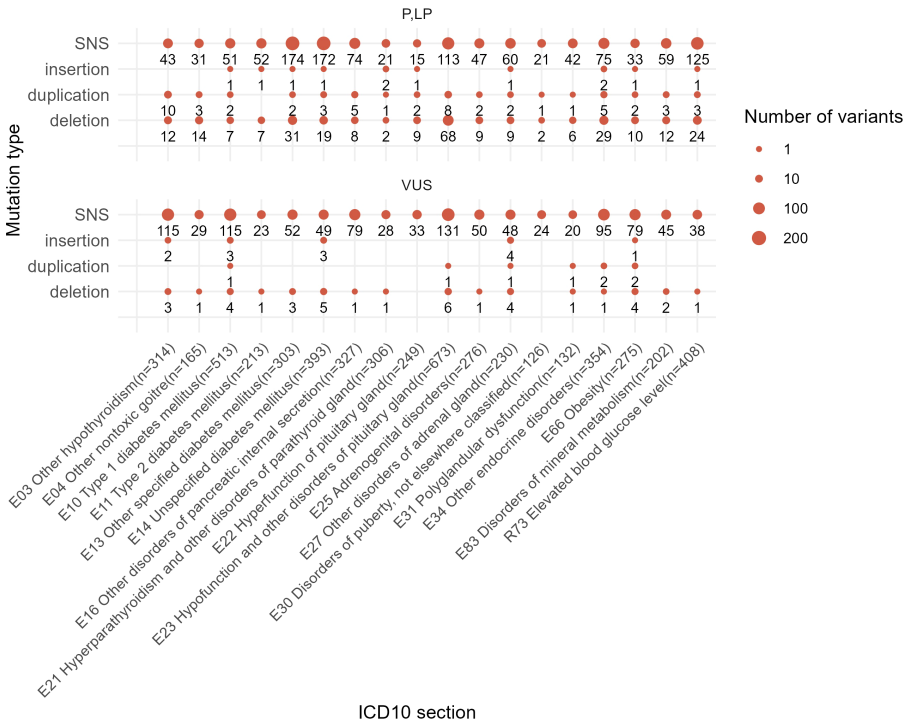

FIGURE 10
Statistics of different mutation types identified among the reported genetic variants in this study. One patient case may be included in several groups depending on the presence of mutations of a specific class.

lists of genes hosting reported variants and mutation frequency statistics are given in Supplementary File 5 for both WES and panel NGS tests.

We also identified a list of the most frequently mutated genes with a predominance of pathogenic and likely pathogenic reported variants that included genes *GCK* and *HNF1A* for diabetes mellitus phenotype or disorders of glucose metabolism (E10, E11, E13, E14, E74, an dR73); *KCNJ11*, *ABCC8* and *GCK* for other disorders of pancreatic internal secretion (E16); *AIRE* and *MEN1* for polyglandular dysfunction (E31); *AR* and *PTPN11* for the other endocrine disorders section including constitutional short stature; *GNRHR* and *PROP1* for hypofunction and other disorders of pituitary gland (E23); *DICER1* for other non-toxic goiter (E04); and *CYP24A1* and *PHEX* for disorders of mineral metabolism (Figure 8). In addition, 10 genes harbored relatively frequently reported variants that occurred in at least five patients under analysis (Figure 9).

In total, 1,184 out of 2,073 (57%) reported unique genetic variants were not described at the moment of NGS data interpretation by the geneticists. In the EndoGene database published here (https://doi.org/10.5281/zenodo.10894526), this is shown by the "*yes*" or "*no*" flags in the "Described in literature" column. The reported variants included 2,412 single nucleotide substitutions (SNS), 301 deletions, six insertions, 19 complex insertions and deletions, and 73 duplications. Out of them, four deletions and four duplications were long rearrangements involving at least several genes, as could be judged from the results of the WES analysis (Figure 10). In total, 2,811 variants (2,073 unique) were reported that could be classified as pathogenic, likely pathogenic, or VUS.

3.3 Next steps and limitations

Here, we present a database of genetic variants reported in patients with endocrine diseases and endocrine-related pathologies and in individuals at risk. We provided the ICD10 diagnosis codes for each patient and calculated the frequencies of genetic variants for the patients with diagnoses from the same ICD10 section. However, this article describes the raw data collection and does not intend to comprehensively interpret the data obtained. Thus, further statistical analysis will be needed to identify any associations of genetic variants with specific diagnoses.

Here, we report clinically relevant genetic variants in the standard HGVS format and classify associated diagnoses according to the ICD10 system, thus allowing this information to be converted and merged with other relevant knowledge bases.

Data availability statement

The datasets presented in this study can be found in online repositories. The names of the repository/repositories and accession number(s) can be found in the article/Supplementary Material.

Ethics statement

The studies involving humans were approved by the Ethical committee of The National Medical Research Center for Endocrinology, Moscow, Russia. The studies were conducted in accordance with the local legislation and institutional requirements. Written informed consent for participation in this study was provided by the participants' legal guardians/next of kin.

Author contributions

AB: Conceptualization, Data curation, Funding acquisition, Investigation, Methodology, Project administration, Resources, Supervision, Validation, Writing – review & editing. MZ: Conceptualization, Data curation, Formal Analysis, Investigation, Methodology, Project administration, Supervision, Validation, Visualization, Writing – original draft. SR: Conceptualization, Investigation, Writing – review & editing. AGE: Writing – original draft, Data curation, Formal Analysis, Validation, Visualization. OG: Writing – original draft, Data curation, Methodology, Validation. PP: Writing – original draft, Data curation. DL: Writing – original draft, Data curation. AK: Writing – original draft, Data curation. AA: Writing – original draft, Data curation. AAE: Writing – original draft, Data curation. AN: Writing – original draft, Formal Analysis, Software. AM: Writing – original draft, Data curation, Investigation, Methodology. AAS: Writing – review & editing, Conceptualization, Methodology, Supervision, Validation. SP: Writing – review & editing, Data curation, Investigation, Methodology. EP: Writing – original draft, Investigation. VP: Writing – original draft, Investigation. AG: Writing – original draft, Investigation. ADS: Writing – original draft, Data curation, Investigation. MS: Writing – original draft, Data curation. VZ: Writing – original draft, Data curation, Investigation, Methodology. ZB: Writing – original draft, Data curation. MV: Writing – review & editing, Methodology, Supervision. GM: Writing – review & editing, Conceptualization, Project administration, Supervision. NM: Writing – review & editing, Conceptualization, Funding acquisition, Project administration. VC: Writing – review & editing, Conceptualization, Funding acquisition, Methodology, Project administration, Supervision. ID: Writing – review & editing, Conceptualization, Funding acquisition, Methodology, Project administration, Supervision.

Funding

The author(s) declare financial support was received for the research, authorship, and/or publication of this article. This study was supported by the Ministry of Science and Higher Education of the Russian Federation (Agreement No. 075-15-2022-310 dated April 20, 2022). Validation of genomic variants from text records was supported by the Russian Science Foundation grant 22-74-10031.

Acknowledgments

We thank all the treating doctors of the Endocrinology Research Center who were guiding the patients included in this study. Genetic profiling was partly sponsored by the Alfa Endo charity foundation. We thank Dr. Dmitry Shtokalo (A.P. Ershov Institute of Informatics Systems, Novosibirsk) for the useful discussion.

Conflict of interest

The authors declare that the research was conducted in the absence of any commercial or financial relationships that could be construed as a potential conflict of interest.

The author(s) declared that they were an editorial board member of Frontiers, at the time of submission. This had no impact on the peer review process and the final decision.

Publisher's note

Supplementary material

The Supplementary Material for this article can be found online at: https://www.frontiersin.org/articles/10.3389/fendo.2025.1472754/full#supplementary-material

SUPPLEMENTARY FILE 1
List of VEP - annotation fields for vcf files.

SUPPLEMENTARY FILE 2
Gene compositions of the NGS panels: Endo1, Endo2, Endome1, Endome2.

SUPPLEMENTARY FILE 3
Groups of patients by ICD10 diagnosis sections.

SUPPLEMENTARY FILE 4
Gene mutation frequencies for the patients who were simultaneously profiled by panel NGS and WES.

SUPPLEMENTARY FILE 5
Genes with frequencies of pathogenic and likely pathogenic variants for all groups of patients.

SUPPLEMENTARY FIGURE 1
The number of genes hosting genetic variants classified as being of pathogenic, likely pathogenic, and uncertain significance in the results of WES and panel NGS.

References

1. Crafa A, Calogero AE, Cannarella R, Mongioi' LM, Condorelli RA, Greco EA, et al. The burden of hormonal disorders: A worldwide overview with a particular look in Italy. *Front Endocrinol (Lausanne)*. (2021) 12:694325. doi: 10.3389/fendo.2021.694325

2. Cao Q, Zheng R, He R, Wang T, Xu M, Lu J, et al. Age-specific prevalence, subtypes and risk factors of metabolic diseases in Chinese adults and the different patterns from other racial/ethnic populations. *BMC Public Health*. (2022) 22:2078. doi: 10.1186/s12889-022-14555-1

3. Palmer AK, Jensen MD. Metabolic changes in aging humans: current evidence and therapeutic strategies. *J Clin Invest*. (2022) 132:e158451. doi: 10.1172/JCI158451

4. Glazova O, Bastrich A, Deviatkin A, Onyanov N, Kaziakhmedova S, Shevkova L, et al. Models of congenital adrenal hyperplasia for gene therapies testing. *Int J Mol Sci*. (2023) 24:5365. doi: 10.3390/ijms24065365

5. Bick AG, Metcalf GA, Mayo KR, Lichtenstein L, Rura S, Carroll RJ, et al. Genomic data in the all of us research program. *Nature*. (2024) 627:340–6. doi: 10.1038/s41586-023-06957-x

6. Dapas M, Sisk R, Legro RS, Urbanek M, Dunaif A, Hayes MG. Family-based quantitative trait meta-analysis implicates rare noncoding variants in DENND1A in polycystic ovary syndrome. *J Clin Endocrinol Metab*. (2019) 104:3835–50. doi: 10.1210/jc.2018-02496

7. Kim JH, Choi J-H. Applications of genomic research in pediatric endocrine diseases. *Clin Exp Pediatr*. (2023) 66:520–30. doi: 10.3345/cep.2022.00948

8. Park SY, Seo MH, Lee S. Search for novel mutational targets in human endocrine diseases. *Endocrinol Metab (Seoul)*. (2019) 34:23–8. doi: 10.3803/EnM.2019.34.1.23

9. Vishnopolska SA, Mercogliano MF, Camilletti MA, Mortensen AH, Braslavsky D, Keselman A, et al. Comprehensive identification of pathogenic gene variants in patients with neuroendocrine disorders. *J Clin Endocrinol Metab*. (2021) 106:1956–76. doi: 10.1210/clinem/dgab177

10. Richards S, Aziz N, Bale S, Bick D, Das S, Gastier-Foster J, et al. Standards and guidelines for the interpretation of sequence variants: a joint consensus recommendation of the American College of Medical Genetics and Genomics and the Association for Molecular Pathology. *Genet Med*. (2015) 17:405–24. doi: 10.1038/gim.2015.30

11. Rodrigues E, Rodrigues E da S, Griffith S, Martin R, Antonescu C, Posey JE, Coban-Akdemir Z, et al. Variant-level matching for diagnosis and discovery: Challenges and opportunities. *Hum Mutat*. (2022) 43:782–90. doi: 10.1002/humu.24359

12. Wright CF, Ware JS, Lucassen AM, Hall A, Middleton A, Rahman N, et al. Genomic variant sharing: a position statement. *Wellcome Open Res*. (2019) 4:22. doi: 10.12688/wellcomeopenres

13. Gibbons SMC, Kaye J. Governing genetic databases: collection, storage and use. *Kings Law J*. (2007) 18:201–8. doi: 10.1080/09615768.2007.11427673

14. Margraf RL, Crockett DK, Krautscheid PMF, Seamons R, Calderon FRO, Wittwer CT, et al. Multiple endocrine neoplasia type 2 RET protooncogene database: repository of MEN2-associated RET sequence variation and reference for genotype/phenotype correlations. *Hum Mutat*. (2009) 30:548–56. doi: 10.1002/humu.20928

15. Aim LB, Maher ER, Cascon A, Barlier A, Giraud S, Ercolino T, et al. International initiative for a curated SDHB variant database improving the diagnosis of hereditary paraganglioma and pheochromocytoma. *J Med Genet*. (2022) 59:785–92. doi: 10.1136/jmedgenet-2020-107652

16. Hao M, Qi Y, Xu R, Zhao K, Li M, Shan Y, et al. ENCD: a manually curated database of experimentally supported endocrine system disease and lncRNA associations. *Database*. (2023) 2023:baac113. doi: 10.1093/database/baac113

17. Karczewski KJ, Francioli LC, Tiao G, Cummings BB, Alföldi J, et al. The mutational constraint spectrum quantified from variation in 141,456 humans. *Nature*. (2020) 581:434–43. doi: 10.1038/s41586-020-2308-7

18. Sirugo G, Williams SM, Tishkoff SA. The missing diversity in human genetic studies. *Cell*. (2019) 177:26–31. doi: 10.1016/j.cell.2019.02.048

19. Khrunin AV, Khokhrin DV, Filippova IN, Esko T, Nelis M, Bebyakova NA, et al. A genome-wide analysis of populations from European Russia reveals a new pole of genetic diversity in Northern Europe. *PloS One*. (2013) 8:e58552. doi: 10.1371/journal.pone.0058552

20. Oleksyk TK, Brukhin V, O'Brien SJ. The Genome Russia project: closing the largest remaining omission on the world Genome map. *Gigascience*. (2015) 4:53. doi: 10.1186/s13742-015-0095-0

21. Zhernakova DV, Brukhin V, Malov S, Oleksyk TK, Koepfli KP, Zhuk A, et al. Genome-wide sequence analyses of ethnic populations across Russia. *Genomics*. (2020) 112:442–58. doi: 10.1016/j.ygeno.2019.03.007

22. Barbitoff YA, Khmelkova DN, Pomerantseva EA, Slepchenkov AV, Zubashenko NA, Mironova IV, et al. Expanding the Russian allele frequency reference via cross-laboratory data integration: insights from 7,452 exome samples. *Natl Sci Rev*. (2022) 11:nwae326. doi: 10.1101/2021.11.02.21265801

23. Abramov IS, Lisitsa TS, Stroganova AM, Ryabaya OO, Danishevich AM, Khakhina AO, et al. Diagnostics of hereditary cancer syndromes by ngs. A database creation experience. *J Clin Pract*. (2021) 12:36–42. doi: 10.17816/clinpract76383

24. Nikitin AG, Герогиевича НА, Brovkina OI, Игоревна БО, Khodyrev DS, Сергеича ХД, et al. Creating a public mutation database oncoBRCA: bioinformatic problems and solutions. *J Clin Pract*. (2020) 11:21–9. doi: 10.17816/clinpract25860

25. Bean L, Hegde MR. Gene variant databases and sharing: creating a global genomic variant database for personalized medicine. *Hum Mutat*. (2016) 37:559–63. doi: 10.1002/humu.22982

26. Chen S, Zhou Y, Chen Y, Gu J. fastp: an ultra-fast all-in-one FASTQ preprocessor. *Bioinformatics*. (2018) 34:i884–90. doi: 10.1093/bioinformatics/bty560

27. Li H. Aligning sequence reads, clone sequences and assembly contigs with BWA-MEM. (2013). doi: 10.48550/arXiv.1303.3997. Preprint.

28. Poplin R, Chang P-C, Alexander D, Schwartz S, Colthurst T, Ku A, et al. A universal SNP and small-indel variant caller using deep neural networks. *Nat Biotechnol*. (2018) 36:983–7. doi: 10.1038/nbt.4235

29. McLaren W, Gil L, Hunt SE, Riat HS, Ritchie GRS, Thormann A, et al. The ensembl variant effect predictor. *Genome Biol*. (2016) 17:122. doi: 10.1186/s13059-016-0974-4

30. R Core Team. *R: A language and environment for statistical computing*. Vienna, Austria: R Foundation for Statistical Computing (2020).

31. Lefter M, Vis JK, Vermaat M, den Dunnen JT, Taschner PEM, Laros JFJ. Mutalyzer 2: next generation HGVS nomenclature checker. *Bioinformatics*. (2021) 37:2811–7. doi: 10.1093/bioinformatics/btab051

32. Freeman PJ, Hart RK, Gretton LJ, Brookes AJ, Dalgleish R. VariantValidator: Accurate validation, mapping, and formatting of sequence variation descriptions. *Hum Mutat*. (2018) 39:61–8. doi: 10.1002/humu.2018.39.issue-1

frontiers | Frontiers in Endocrinology

TYPE Original Research
PUBLISHED 28 April 2025
DOI 10.3389/fendo.2025.1427656

OPEN ACCESS

EDITED BY
Darko Stefanovski,
University of Pennsylvania, United States

REVIEWED BY
Terri Kang Johnson,
Edwards Lifesciences, United States
Mangala Hegde,
Indian Institute of Technology Guwahati, India

*CORRESPONDENCE
Zexin Zhu
zhuzexinmd@163.com

RECEIVED 04 May 2024
ACCEPTED 07 April 2025
PUBLISHED 28 April 2025

CITATION
Wang X and Zhu Z (2025) Causal relationship between plasma lipidome and rosacea: a Mendelian randomization analysis.
Front. Endocrinol. 16:1427656.
doi: 10.3389/fendo.2025.1427656

Causal relationship between plasma lipidome and rosacea: a Mendelian randomization analysis

Xiaoxue Wang[1] and Zexin Zhu[2*]

[1]Department of Dermatology, The Second Affiliated Hospital of Xi'an Jiaotong University, Xi'an, China, [2]Department of Surgical Oncology, The Comprehensive Breast Care Center, The Second Affiliated Hospital of Xi'an Jiaotong University, Xi'an, China

Background: Rosacea is a common chronic inflammatory skin disease. Limited studies reported the association between plasma lipidome and rosacea.

Methods: We employed a two-sample Mendelian randomization (MR) study to assess the causality between plasma lipidome and rosacea. Plasma lipidome association genome-wide association study (GWAS) data were collected. The inverse variance weighted (IVW) method was utilized as the principal method in our Mendelian randomization (MR) study; we also used the MR-Egger, weighted median, simple mode, and weighted mode methods. The MR-Egger intercept test, Cochran's Q test, MR-Pleiotropy RESidual Sum and Outlier (MR-PRESSO), and leave-one-out analysis were conducted to identify heterogeneity and pleiotropy.

Results: A total of 179 lipid species were analyzed; among them, five lipid species were closely related to rosacea. Two species of sterol ester [sterol ester (27:1/22:6) and sterol ester (27:1/15:0)], two species of phosphatidylethanolamine [phosphatidylethanolamine (O-18:2_20:4) and phosphatidylethanolamine (18:0_20:4)], and one species of sphingomyelin [sphingomyelin (d34:0)] were causally associated with rosacea ($P < 0.05$). All of them play protective roles in patients with rosacea. No heterogeneity or pleiotropy was observed.

Conclusion: This study provided new evidence of the relationship between plasma lipidome and rosacea. Our MR suggested that five lipid species play protective roles in rosacea progression. These could be novel and effective ways to treat rosacea.

KEYWORDS

plasma lipidome, rosacea, Mendelian randomization, causal inference, protective

1 Introduction

Rosacea is a prevalent chronic inflammatory dermatological condition that primarily impacts the cheeks, chin, nose, forehead, and ocular regions (1, 2). The reported prevalence of rosacea varies significantly, ranging from 1% to 22%, a variation attributed to geographical and demographic factors (3, 4). A recent systematic review estimated the global prevalence of rosacea to be approximately 5.5% among the adult population (5). Contrary to earlier studies that indicated a higher prevalence in females (1, 2), the findings of this systematic review suggest that both men and women are equally affected by the condition (5). The pathophysiology of rosacea remains inadequately understood. Mechanistically, the pathogenesis of rosacea is associated with various inflammatory pathways, which involve the dysregulation of both the innate and adaptive immune systems (2, 6). Investigations into single nucleotide polymorphisms (SNPs) in genes linked to rosacea indicate that genetic factors may also play a role (7). Factors such as stress, ultraviolet radiation, consumption of spicy foods, smoking, and alcohol intake have been identified as potential exacerbators of symptoms (1). The diagnosis of rosacea is primarily based on clinical manifestations and skin biopsy findings (1). Treatment options for rosacea include skin care regimens, topical medications such as brimonidine and ivermectin (8), oral antibiotics like doxycycline and minocycline (9), as well as biologic agents such as Secukinumab (10) and Erenumab (2). It is important to note that rosacea is a chronic condition; while patients may experience periods of remission due to various treatments, relapses are frequently observed (1).

Plasma lipids, including high-density lipoprotein cholesterol (HDL-C), low-density lipoprotein cholesterol (LDL-C), triglycerides (TG), and total cholesterol (TC), are routinely assessed and have been established as significant risk factors for various health conditions, particularly cardiovascular disease (CVD). Recent studies have expanded our comprehension of circulating lipid diversity by identifying additional lipid species, such as cholesterol esters (CE), lysophosphatidylcholines (LPC), phosphatidylcholines (PC), phosphatidylethanolamines (PE), and sphingomyelins (SM) (11).

Several studies reported the relationship between plasma lipids and skin disease. For instance, a significant reduction in serum high-density lipoprotein cholesterol (HDL-C) levels has been documented in patients with chronic spontaneous urticaria (12); on the other hand, patients suffering from atopic dermatitis exhibited a notable decrease in cholesteryl esters, free cholesterol, lysophosphatidylcholine (particularly the 16:0 species), and phosphatidylethanolamine (13). Additionally, adolescents diagnosed with atopic dermatitis (AD) within the Asian demographic demonstrated significantly elevated levels of total cholesterol (TC) and low-density lipoprotein cholesterol (LDL-C).

Mendelian randomization (MR) utilizes one or more genetic variants as instrumental variables (IVs) based on genome-wide association studies (GWAS). MR studies can infer the causal effects of exposure on an outcome. Recently, MR analysis also reported the causal relationship between lipids and skin diseases. For instance, MR analysis showed that HDL deficiency and high LDL-C and TG have a causal relationship with incident psoriasis genetically (14, 15). To our knowledge, no study has yet investigated the causal effect of plasma lipidome on the risk of rosacea using Mendelian randomization. Our investigation aimed to explore the plasma lipidome risk variants as instrumental variables for rosacea utilizing two-sample MR.

2 Materials and methods

2.1 Study design

According to the MR framework (Figure 1), three key assumptions are included (1): Relevance Assumption: Single nucleotide polymorphisms (SNPs) that are substantially linked to exposures are used as instrumental variables (IVs). (2) Independence Assumption: These SNPs (IVs) should not show any correlation with the relevant confounding factor. (3) Exclusivity Assumption: These SNPs (IVs) should affect outcomes only through its effect on exposure (16, 17).

2.2 Data sources

The plasma lipidome GWAS data were obtained from the prospective GeneRISK cohort including 7,174 individuals (18), summarized by Ottensmann L et al. (11). A total of 179 lipid species [GWAS Catalog (https://www.ebi.ac.uk/gwas/, GCST90277238–GCST90277416)] belonging to 13 lipid classes covering four major lipid categories (glycerolipids, glycerophospholipids, sphingolipids, and sterols) were detected. The GWAS data related to rosacea was obtained from the IEU OpenGWAS project, GWAS ID: finn-b-L12_ROSACEA, which included 1,195 cases and 211,139 controls, featuring 16,380,452 SNPs, with the study population being of European descent. All participants provided informed written consent, and all studies were reviewed and approved by institutional ethics review committees at the involved institutions.

2.3 Instrumental variables selection

Related IVs (plasma lipidome) for MR analysis followed particular principles: SNPs should be associated with exposures at the locus-wide significance level: $P < 5e{-}06$. In addition, linkage disequilibrium (LD) coefficient r^2 should be less than 0.001, not closely related (clumping window more than 10,000 kb) to ensure exposure instrument independence. The F statistic was employed to assess the strength of the IVs, with values exceeding 10, thereby suggesting the absence of weak instrumental variable bias. The F-value is calculated using the formula $F = R^2(N - 2)/(1 - R^2)$, where R^2 denotes the proportion of variance accounted for by SNPs in the exposure dataset, and N represents the sample size of the GWAS (16, 17).

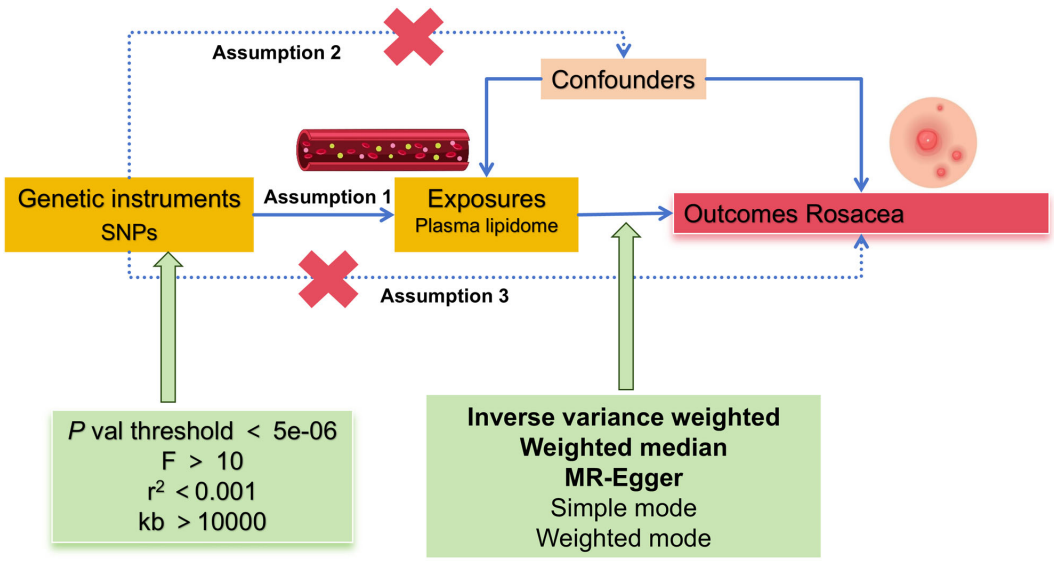

FIGURE 1
Flowchart schematic diagram followed by the MR analysis's principle of this study.

2.4 MR analysis

Causal associations between plasma lipidome and rosacea were determined using MR analysis. In the exposure–outcome analysis, we employed MR with more than two SNPs serving as IVs. Our MR analysis used each of the five methods: inverse variance weighted (IVW) was performed as the primary statistical analysis method in our MR analysis for evaluating causal effects, with additional methodologies, namely, simple mode, weighted median, weighted mode, and MR-Egger, being utilized to further corroborate the findings. The MR-Egger method is implemented through a straightforward modification of the weighted linear regression technique previously outlined. MR-Egger was specifically employed to evaluate the robustness of the MR results as a form of validation (16, 17, 19).

The heterogeneity of the chosen SNPs was evaluated using Cochrane's Q test, where a *P*-value of more than 0.05 suggested the lack of heterogeneity. The random effects model was used once significant heterogeneity has been identified. We evaluated the possible bias from horizontal pleiotropy using the weighted median and MR-Egger regression in order to gauge the robustness of the IVW method. The MR-PRESSO (MR-Pleiotropy RESidual Sum and Outlier) test was used to appraise outliers that might have been influenced by horizontal pleiotropy. The causal-effect estimates for individual variants were displayed using a scatter plot. Thereafter, we performed a leave-one-out analysis to examine the stability of the results in the context of a single SNP's influence and presented the findings in a forest plot (16, 17, 19).

2.5 Statistical analysis

All statistical analysis were conducted in R software (Version 4.3.2) using the TwoSampleMR package (Version 0.5.8). The statistical significance level is P <0.05. Pooled odds ratio (OR) with 95% confidence interval (CI) were calculated. The IVW method was primarily employed to evaluate the causal relationships between 179 lipid species and rosacea, with the findings illustrated through a volcano plot; significant results were subsequently represented using a forest plot. The false discovery rate (FDR) correction was applied to adjust all *P*-value thresholds, whereby *P*-values exceeding the FDR-corrected threshold but remaining below 0.05 were regarded as indicative of potential causal associations.

3 Results

3.1 MR analysis

Totally, we analyzed the plasma lipidome (1,893 SNPs, detailed in Supplementary Table S1) for their causal association with rosacea. As mentioned, the inverse variance weighted (IVW) method was chosen as the primary statistical analysis method. MR analysis revealed that among the 179 lipid species, according to the results of the IVW method ($P < 0.05$, Figure 2), five lipid species exhibited a significant association with the outcome variable of rosacea. Notably, all of these lipid species demonstrated an odds ratio (OR) of less than 1 (Figure 3, detailed in Table 1). Among them, two species of sterol ester [sterol ester (27:1/22:6) (OR = 0.757, 95% CI = 0.613–0.935, P = 0.01) and sterol ester (27:1/15:0) (OR = 0.691, 95% CI = 0.495–0.965, P = 0.03] resulted in a protective factor for rosacea; two species of phosphatidylethanolamine [phosphatidylethanolamine (O-18:2_20:4) (OR = 0.761, 95% CI = 0.589–0.984, P = 0.03) and phosphatidylethanolamine (18:0_20:4) (OR = 0.864, 95% CI = 0.753–0.992, P = 0.03)] showed a protective effect on rosacea; one species of sphingomyelin [sphingomyelin (d34:0) (OR = 0.835, 95% CI = 0.702–0.992, P = 0.04)] also resulted in a causal protective relationship with

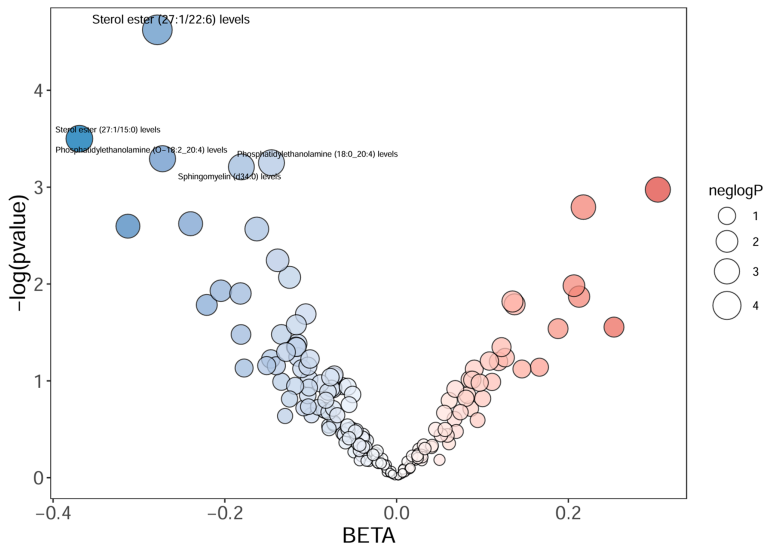

FIGURE 2
The volcano plot shows the association between 179 lipid species and rosacea risk. The X-axis represents the β value, and the Y-axis shows the logarithmic *p*-value in base 10. Sterol ester (27:1/22:6), sterol ester (27:1/15:0), phosphatidylethanolamine (O-18:2_20:4), phosphatidylethanolamine (18:0_20:4), and sphingomyelin (d34:0) indicate the *P*-value <0.05.

rosacea. The scatter plots for the causal relationship between plasma lipidome and rosacea are presented in Figure 4. It is noteworthy that all five lipid species exhibited a negative correlation with rosacea, indicating that these lipid types may have a causal protective effect against the condition. A detailed analysis of the components of each lipid species is provided in the Supplementary Materials.

3.2 Sensitivity analysis

According to the Cochran Q test, our IVW–MR analysis results demonstrated no evidence of heterogeneity among our reported results. The MR-Egger regression analysis results provided evidence that there was no other significant horizontal pleiotropy (Table 2). We also conducted the leave-one-out method to identify and delete abnormal instrumental variables. The results showed the robustness of our results (Supplementary Figure S1). These results suggest that the MR analysis results were relatively stable.

4 Discussion

We conducted an MR analysis to investigate the causal relationship between plasma lipidome and rosacea utilizing GWAS summary-level data. Our results showed that five lipid species have negative causal relationship on rosacea, specifically, two species of sterol ester, two species of phosphatidylethanolamine, and one species of sphingomyelin. To the best of our knowledge, the

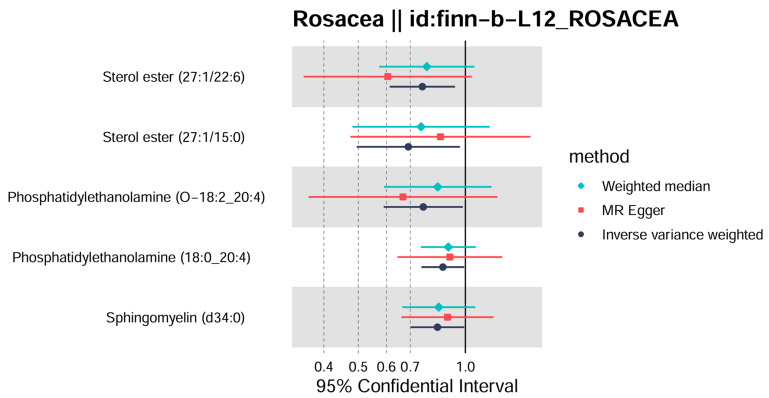

FIGURE 3
Forest plot of Mendelian randomization analysis for sterol ester (27:1/22:6), sterol ester (27:1/15:0), phosphatidylethanolamine (O-18:2_20:4), phosphatidylethanolamine (18:0_20:4), sphingomyelin (d34:0), and rosacea risk. The results of inverse variance weighted (IVW), weighted median, and MR-Egger are shown.

TABLE 1 Causal relationship between the plasma lipidome and rosacea.

Exposure	Methods	OR	Low 95% CI	Up 95% CI	*P*
	Inverse variance weighted	0.757	0.613	0.935	0.010
Sterol ester (27:1/22:6)	Weighted median	0.779	0.572	1.060	0.112
	MR-Egger	0.605	0.351	1.043	0.092
	Inverse variance weighted	0.691	0.495	0.965	0.030
Sterol ester (27:1/15:0)	Weighted median	0.751	0.481	1.171	0.206
	MR-Egger	0.851	0.475	1.524	0.607
	Inverse variance weighted	0.761	0.589	0.984	0.037
Phosphatidylethanolamine (O-18:2_20:4)	Weighted median	0.836	0.590	1.184	0.313
	MR-Egger	0.668	0.362	1.230	0.227
	Inverse variance weighted	0.864	0.753	0.992	0.039
Phosphatidylethanolamine (18:0_20:4)	Weighted median	0.896	0.750	1.070	0.224
	MR-Egger	0.904	0.644	1.269	0.570
	Inverse variance weighted	0.835	0.702	0.992	0.040
Sphingomyelin (d34:0)	Weighted median	0.842	0.665	1.066	0.152
	MR-Egger	0.891	0.661	1.199	0.457

current analysis of plasma lipidome on rosacea is limited, and the relationship between plasma lipidome and rosacea has not been reported.

Sterol ester, formed through the esterification of sterols and fatty acids, belongs to the sterols category, playing a crucial role in maintaining the structural and functional integrity of cellular membranes. They modulate membrane fluidity and stability, which in turn affect cellular responsiveness to external stimuli and signal transduction (20, 21). Generally, sterols are primarily taken up through dietary sources and synthesized in the liver. Additionally, cholesterol biosynthesis enzymes are expressed in primary and secondary lymphoid organs, which suggested that sterols play a role in immune regulation. Accordingly, systemic sterols modulate immune cell biology (22); furthermore, in inflammatory processes, sterol esters may act as signaling molecules or a regulatory agent (23). Meanwhile, our understanding of how sterols modulate specific immune cell biology is limited (20, 24).

Phosphatidylethanolamine (PE) is one of the most abundant phospholipids in plasma membranes (25). Besides being a passive membrane constituent, PE is also functionally associated with protein biogenesis and activity (26), oxidative phosphorylation (27), and autophagy (28) and is an important precursor of other lipids (29). The localization of PE changes during cell death. PE resides predominantly in the inner leaflet of the cell membrane in healthy cells; on the other hand, PE is externalized to the outer leaflet of the plasma membrane in dead or dying cells (25). It is demonstrated that PE is associated with Alzheimer's and Parkinson's disease and liver steatosis and steatohepatitis (29).

Sphingomyelin (SM) is one of the main phospholipids that make up the hydrophobic matrix of mammalian membranes, which are considered a "structural" lipid and contribute to the geometrical stability of the cell membranes (30). Recently, studies reported that the SM metabolic pathway contributes significantly to cell signaling, especially in regulating tumor cell growth, differentiation, senescence, and survival (31). Accordingly, SM acts as a critical molecule for brain physiopathology, playing a role in Parkinson's disease progression (32). In addition, SM regulates cell growth, differentiation, and apoptosis in colorectal cancer and decreases colonic inflammation and inflammation-driven colorectal cancer (33).

Although no MR analysis reported the causal relationship between plasma lipidome and rosacea, some MR analyses reported the causal relationship between plasma lipidome and other illness. MR analysis revealed that phosphatidylinositol and triglyceride levels decreased the risk of breast cancer (BC) (34); genetically increased triglycerides were closely related to an elevated risk of Barrett's esophagus (BE) (35).

Studies also reported the role of plasma lipidome in rosacea. Neutrophils and HDL, instead of LDL, have effects on the risk or severity of rosacea (36). Moreover, a meta-analysis performed on large groups of patients with rosacea and controls revealed that rosacea is significantly associated with dyslipidemia and higher total cholesterol, LDL, and triglyceride concentrations (37). The explanation for the association between rosacea and dyslipidemia is uncertain. Studies showed the activation of nucleotide binding oligomerization domain-like receptor 3, which can cause IL-1β release and induce structural changes of lipoproteins, decreasing their ability to break down and transport cholesterol (37, 38). An earlier study on the skin surface lipids in rosacea revealed that the lipid contents in the skin, particularly cholesterol, free fatty acids, triglycerides, esters, and squalene, were no different between patients and controls without rosacea (39). It should be noted

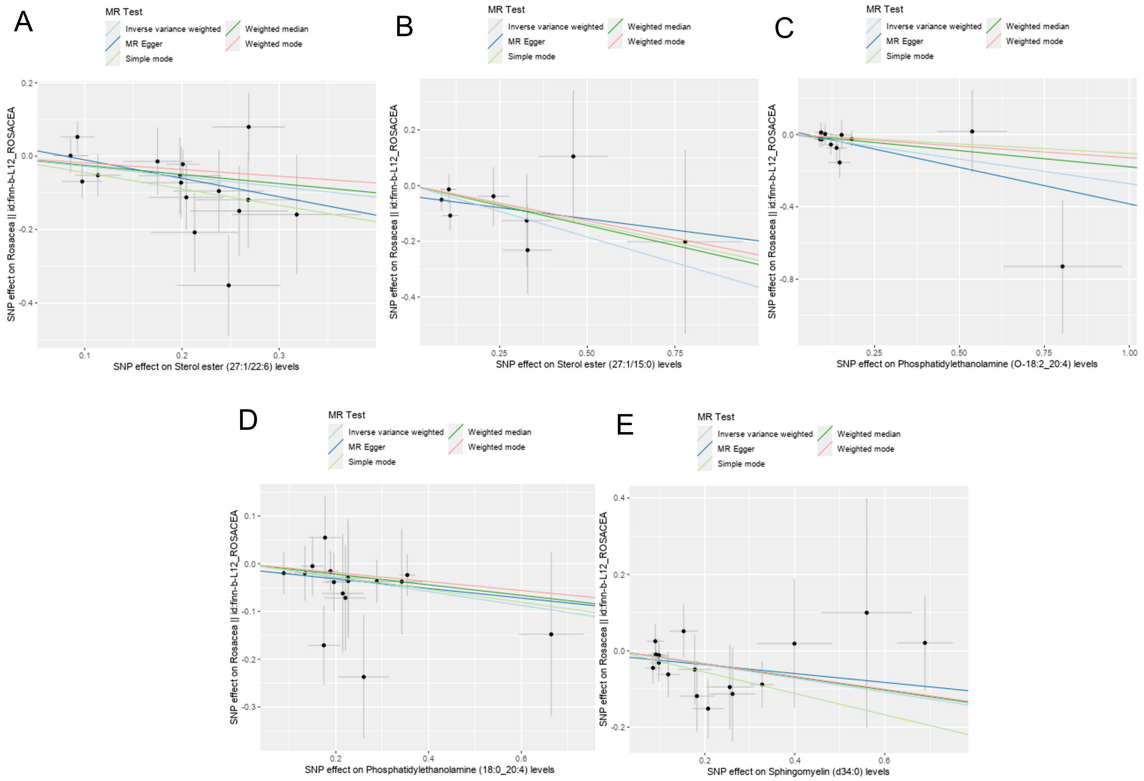

FIGURE 4
Scatter plots showing significant causal effects between plasma lipidome and rosacea. **(A)** Sterol ester (27:1/22:6). **(B)** Sterol ester (27:1/15:0). **(C)** Phosphatidylethanolamine (O-18:2_20:4). **(D)** Phosphatidylethanolamine (18:0_20:4). **(E)** Sphingomyelin (d34:0).

that this research was performed on a small group of patients (N=31) and focused on skin lipidomics, not plasma lipidome. In actuality, research examining the roles of sterol esters, PE, and SM in the context of rosacea is relatively scarce.

Our research employed MR analysis to investigate the causal relationship between various plasma components and rosacea. The results suggest that sterol esters, PE, and SM may serve as protective factors against rosacea. Identifying novel biomarkers could enhance our understanding of the pathogenesis of rosacea and facilitate improved assessment of patients suffering from this dermatological condition. The implications of our findings may extend to both experimental design and clinical practice. Future investigations will focus on the roles of sterol esters, PE, and SM in rosacea, utilizing cell culture and animal models for further exploration.

There are several limitations to our study. First, due to the original GWAS statistics, we were unable to divide the cohorts or perform subgroup analyses. Second, our analysis only included individuals of the European population. Although using a single European population to investigate causal relationships can minimize population stratification bias, it is important to interpret these findings with caution regarding their applicability to other populations; in addition, there was no validation performed using a different set of data.

Our findings reported that sterol ester, PE, and SM have nominal causal connections with rosacea, but these correlations vanished after applying the FDR correction. It is important to note that the FDR correction can result in false negatives (40).

TABLE 2 Sensitivity analysis of plasma lipidome on rosacea.

Exposure	Q	*P*-value for Cochran Q test	Egger-intercept	*P*-value for MR-Egger intercept
Sterol ester (27:1/22:6)	14.612	0.405	0.040	0.395
Sterol ester (27:1/15:0)	3.326	0.767	−0.039	0.426
Phosphatidylethanolamine(O-18:2_20:4)	5.899	0.750	0.020	0.653
Phosphatidylethanolamine (18:0_20:4)	7.134	0.929	−0.012	0.780
Sphingomyelin (d34:0)	8.819	0.887	−0.013	0.607

We have established a causal relationship between sterol ester, PE, and SM in relation to rosacea; however, the expression levels of specific liposomes in patients with rosacea remain uncertain. Furthermore, the underlying mechanisms by which these lipids exert their effects are not yet fully understood, necessitating further investigation. It is important to emphasize that while our study did not identify any associations between other subtypes of the plasma lipidome and the risk of rosacea, this absence of evidence does not imply that these other subtypes lack an influence on the condition. Our research serves as a hypothesis-generating endeavor for exploratory purposes.

5 Conclusion

In summary, our MR study presents evidence suggesting that sterol esters, phosphatidylethanolamine (PE), and sphingomyelin (SM) exert a negative causal influence on rosacea. This finding indicates that sterol esters, PE, and SM may play a protective role in the pathophysiology of rosacea. Future investigations into the plasma lipidome may yield innovative therapeutic targets and clinical strategies for the management of rosacea.

Data availability statement

The original contributions presented in the study are included in the article/Supplementary Material. Further inquiries can be directed to the corresponding author.

Ethics statement

Ethical approval was not required for the study involving humans in accordance with the local legislation and institutional requirements. Written informed consent to participate in this study was not required from the participants or the participants' legal guardians/next of kin in accordance with the national legislation and the institutional requirements.

Author contributions

XW: Conceptualization, Data curation, Formal analysis, Software, Writing – review & editing. ZZ: Validation, Visualization, Writing – original draft, Writing – review & editing.

Funding

The author(s) declare that financial support was received for the research and/or publication of this article. This work has been funded by the National Natural Science Foundation of China (82404921).

Acknowledgments

We acknowledge GWAS's database for providing their platforms and contributors for uploading their meaningful datasets.

Conflict of interest

The authors declare that the research was conducted in the absence of any commercial or financial relationships that could be construed as a potential conflict of interest.

Publisher's note

Supplementary material

The Supplementary Material for this article can be found online at: https://www.frontiersin.org/articles/10.3389/fendo.2025.1427656/full#supplementary-material

SUPPLEMENTARY FIGURE 1
Results of "leave-one-out" sensitivity analysis in the discovery and validation datasets. **(A)** Sterol ester (27:1/22:6). **(B)** Sterol ester (27:1/15:0). **(C)** Phosphatidylethanolamine (O-18:2_20:4). **(D)** Phosphatidylethanolamine (18:0_20:4). **(E)** Sphingomyelin (d34:0).

References

1. van Zuuren EJ. Rosacea. *New Engl J Med*. (2017) 377:1754–64. doi: 10.1056/nejmcp1506630

2. van Zuuren EJ, Arents BWM, van der Linden MMD, Vermeulen S, Fedorowicz Z, Tan J. Rosacea: new concepts in classification and treatment. *Am J Clin Dermatol*. (2021) 22:457–65. doi: 10.1007/s40257-021-00595-7

3. Tan J, Berg M. Rosacea: Current state of epidemiology. *J Am Acad Dermatol*. (2013) 69:S27–35. doi: 10.1016/j.jaad.2013.04.043

4. Tan J, Schöfer H, Araviiskaia E, Audibert F, Kerrouche N, Berg M. Prevalence of rosacea in the general population of Germany and Russia – The RISE study. *J Eur Acad Dermatol Venereology*. (2016) 30:428–34. doi: 10.1111/jdv.13556

5. Gether L, Overgaard LK, Egeberg A, Thyssen JP. Incidence and prevalence of rosacea: a systematic review and meta-analysis. *Br J Dermatol*. (2018) 179(2):282–9. doi: 10.1111/bjd.16481

6. Steinhoff M, Schauber J, Leyden JJ. New insights into rosacea pathophysiology: A review of recent findings. *J Am Acad Dermatol*. (2013) 69:S15–26. doi: 10.1016/j.jaad.2013.04.045

7. Chang ALS, Raber I, Xu J, Li R, Spitale R, Chen J, et al. Assessment of the genetic basis of rosacea by genome-wide association study. *J Invest Dermatol*. (2015) 135:1548–55. doi: 10.1038/jid.2015.53

8. Schaller M, Kemény L, Havlickova B, Jackson JM, Ambroziak M, Lynde C, et al. A randomized phase 3b/4 study to evaluate concomitant use of topical ivermectin 1% cream and doxycycline 40-mg modified-release capsules, versus topical ivermectin 1% cream and placebo in the treatment of severe rosacea. *J Am Acad Dermatol*. (2020) 82:336–43. doi: 10.1016/j.jaad.2019.05.063

9. van der Linden MMD, van Ratingen AR, van Rappard DC, Nieuwenburg SA, Spuls P. DOMINO, doxycycline 40 mg vs. minocycline 100 mg in the treatment of rosacea: a randomized, single-blinded, noninferiority trial, comparing efficacy and safety. *Br J Dermatol*. (2017) 176:1465–74. doi: 10.1111/bjd.15155

10. Kumar A, Chiou AS, Shih YH, Li S, Lynn A. An exploratory, open-label, investigator-initiated study of interleukin-17 blockade in patients with moderate-to-severe papulopustular rosacea. *Br J Dermatol*. (2020) 183:942–3. doi: 10.1111/bjd.19172

11. Ottensmann L, Tabassum R, Ruotsalainen SE, Gerl MJ, Klose C, Widén E, et al. Genome-wide association analysis of plasma lipidome identifies 495 genetic associations. *Nat Commun*. (2023) 14:6934. doi: 10.1038/s41467-023-42532-8

12. Maged Amin M, Rushdy M. Hyperlipidemia in association with pro-inflammatory cytokines among chronic spon-taneous urticaria: case-control study. *Eur Ann Allergy Clin Immunol*. (2018) 50:254. doi: 10.23822/eurannaci.1764-1489.68

13. Trieb M, Wolf P, Knuplez E, Weger W, Schuster C, Peinhaupt M, et al. Abnormal composition and function of high-density lipoproteins in atopic dermatitis patients. *Allergy*. (2018) 74:398–402. doi: 10.1111/all.13620

14. Xiao Y, Jing D, Tang Z, Peng C, Yin M, Liu H, et al. Serum lipids and risk of incident psoriasis: A prospective cohort study from the UK biobank study and Mendelian randomization analysis. *J Invest Dermatol*. (2022) 142:3192–99.e12. doi: 10.1016/j.jid.2022.06.015

15. Zhang Z-Y-O, Jian Z-Y, Tang Y, Li W. The relationship between blood lipid and risk of psoriasis: univariable and multivariable Mendelian randomization analysis. *Front Immunol*. (2023) 14:2023.1174998. doi: 10.3389/fimmu.2023.1174998

16. Bowden J, Del Greco MF, Minelli C, Davey Smith G, Sheehan N, Thompson J. A framework for the investigation of pleiotropy in two-sample summary data Mendelian randomization. *Stat Med*. (2017) 36:1783–802. doi: 10.1002/sim.7221

17. Boef AGC, Dekkers OM, le Cessie S. Mendelian randomization studies: a review of the approaches used and the quality of reporting. *Int J Epidemiol*. (2015) 44:496–511. doi: 10.1093/ije/dyv071

18. Widén E, Junna N, Ruotsalainen S, Surakka I, Mars N, Ripatti P, et al. How communicating polygenic and clinical risk for atherosclerotic cardiovascular disease impacts health behavior: an observational follow-up study. *Circulation: Genomic Precis Med*. (2022) 15(2):e003459. doi: 10.1161/circgen.121.003459

19. Bowden J, Davey Smith G, Burgess S. Mendelian randomization with invalid instruments: effect estimation and bias detection through Egger regression. *Int J Epidemiol*. (2015) 44:512–25. doi: 10.1093/ije/dyv080

20. Hegele RA. Plasma lipoproteins: genetic influences and clinical implications. *Nat Rev Genet*. (2009) 10:109–21. doi: 10.1038/nrg2481

21. Huang M, Liu Y, Cheng Y, Dai W. Role of inflammatory biomarkers in mediating the effect of lipids on spontaneous intracerebral hemorrhage: a two-step, two-sample Mendelian randomization study. *Front Neurol*. (2024) 15:2024.1411555. doi: 10.3389/fneur.2024.1411555

22. Fessler MB. Regulation of adaptive immunity in health and disease by cholesterol metabolism. *Curr Allergy Asthma Rep*. (2015) 15(8):48. doi: 10.1007/s11882-015-0548-7

23. Saher G, Quintes S, Nave K-A. Cholesterol: a novel regulatory role in myelin formation. *Neuroscientist: A Rev J Bringing Neurobiology Neurol Psychiatry*. (2011) 17:79–93. doi: 10.1177/1073858410373835

24. Britt RD, Porter N, Grayson MH, Gowdy KM, Ballinger M, Wada K, et al. Sterols and immune mechanisms in asthma. *J Allergy Clin Immunol*. (2023) 151:47–59. doi: 10.1016/j.jaci.2022.09.025

25. Elvas F, Stroobants S, Wyffels L. Phosphatidylethanolamine targeting for cell death imaging in early treatment response evaluation and disease diagnosis. *Apoptosis*. (2017) 22:971–87. doi: 10.1007/s10495-017-1384-0

26. Becker T, Horvath SE, Böttinger L, Gebert N, Daum G, Pfanner N. Role of phosphatidylethanolamine in the biogenesis of mitochondrial outer membrane proteins. *J Biol Chem*. (2013) 288:16451–9. doi: 10.1074/jbc.m112.442392

27. Böttinger L, Horvath SE, Kleinschroth T, Hunte C, Daum G, Pfanner N, et al. Phosphatidylethanolamine and cardiolipin differentially affect the stability of mitochondrial respiratory chain supercomplexes. *J Mol Biol*. (2012) 423-248:677–86. doi: 10.1016/j.jmb.2012.09.001

28. Ichimura Y, Kirisako T, Takao T, Satomi Y, Shimonishi Y, Ishihara N, et al. A ubiquitin-like system mediates protein lipidation. *Nature*. (2000) 408:488–92. doi: 10.1038/35044114

29. Calzada E, Onguka O, Claypool SM. Phosphatidylethanolamine metabolism in health and disease. *Int Rev Cell Mol Biol*. (2016) 321:29–88. doi: 10.1016/bs.ircmb.2015.10.001

30. Goñi FM. Sphingomyelin: What is it good for? *Biochem Biophys Res Commun*. (2022) 633:23–5. doi: 10.1016/j.bbrc.2022.08.074

31. Zhu H, Chen H-J, Wen H-Y, Wang Z-G, Liu S-L. Engineered lipidic nanomaterials inspired by sphingomyelin metabolism for cancer therapy. *Molecules/Molecules online/Molecules Annu*. (2023) 28:5366–6. doi: 10.3390/molecules28145366

32. Signorelli P, Conte C, Albi E. The multiple roles of sphingomyelin in Parkinson's disease. *Biomolecules*. (2021) 11:1311. doi: 10.3390/biom11091311

33. Jiang C, Cheong L-Z, Zhang X, Ali AH, Jin Q, Wei W, et al. Dietary sphingomyelin metabolism and roles in gut health and cognitive development. *Adv Nutr*. (2022) 13:474–91. doi: 10.1093/advances/nmab117

34. Cao Y, Ai M, Liu C. The impact of lipidome on breast cancer: a Mendelian randomization study. *Lipids Health Dis*. (2024) 23(1):109. doi: 10.1186/s12944-024-02103-2

35. Li B, Li M, Qi X, Tong T, Zhang G. The causal associations of circulating lipids with Barrett's Esophagus and Esophageal Cancer: a bi-directional, two sample mendelian randomization analysis. *Hum Genomics*. (2024) 18(1):37. doi: 10.1186/s40246-024-00608-6

36. Xiao W, Li J, Huang X, Zhu Q, Liu T, Xie H, et al. Mediation roles of neutrophils and high-density lipoprotein (HDL) on the relationship between HLA-DQB1 and rosacea. *Ann Med (Helsinki)/Annals Med*. (2022) 54:1530–7. doi: 10.1080/07853890.2022.2077427

37. Chen Q, Shi X, Tang Y, Wang B, Xie HF, Shi W, et al. Association between rosacea and cardiometabolic disease: A systematic review and meta-analysis. *J Am Acad Dermatol*. (2020) 83:1331–40. doi: 10.1016/j.jaad.2020.04.113

38. Nowowiejska J, Baran A, Flisiak I. Lipid alterations and metabolism disturbances in selected inflammatory skin diseases. *Int J Mol Sci*. (2023) 24:7053. doi: 10.3390/ijms24087053

39. Pye RJ, Meyrick G, Burton JL. Skin surface lipid composition in rosacea. *Br J dermatology/British J dermatology Supplement*. (1976) 94:161–4. doi: 10.1111/j.1365-2133.1976.tb04365.x

40. Larsson SC, Traylor M, Malik R, Dichgans M, Burgess S, Markus HS. Modifiable pathways in Alzheimer's disease: Mendelian randomisation analysis. *BMJ*. (2017) 6:359:j5375. doi: 10.1136/bmj.j5375

frontiers | Frontiers in Endocrinology

TYPE Original Research
PUBLISHED 30 April 2025
DOI 10.3389/fendo.2025.1534018

OPEN ACCESS

EDITED BY
Sijung Yun,
Predictiv Care, Inc., United States

REVIEWED BY
Mariana Lorena Tellechea,
National Scientific and Technical Research Council (CONICET), Argentina
Alfredo Caturano,
Università Telematica San Raffaele, Italy

*CORRESPONDENCE
Ye Zhang
493305441@qq.com

†These authors have contributed equally to this work and share first authorship

RECEIVED 25 November 2024
ACCEPTED 10 April 2025
PUBLISHED 30 April 2025

CITATION
Zhang Y, Yue Y, Sun Z, Li P, Wang X, Cheng G, Huang H and Li Z (2025) Pan-immune-inflammation value and its association with all-cause and cause-specific mortality in the general population: a nationwide cohort study. *Front. Endocrinol.* 16:1534018. doi: 10.3389/fendo.2025.1534018

Pan-immune-inflammation value and its association with all-cause and cause-specific mortality in the general population: a nationwide cohort study

Ye Zhang[1*†], Yong Yue[2,3†], Zhengyu Sun[4], Pengcheng Li[5], Xiaoyi Wang[1], Gang Cheng[1], Hailin Huang[1] and Zongping Li[1]

[1]Department of Neurosurgery, Mianyang Central Hospital, School of Medicine, University of Electronic Science and Technology of China, Mianyang, Sichuan, China, [2]Division of Clinical Neuroscience, Chiba University Center for Forensic Mental Health, Chiba, Japan, [3]Department of Pharmacology, Chiba University Graduate School of Medicine, Chiba, Japan, [4]Department of Plastic and Aesthetic, Jintang First People's Hospital, Chengdu, Sichuan, China, [5]The Department of Oncology, The First Affiliated Hospital of the Chengdu Medical College, Chengdu, Sichuan, China

Introduction: The Pan-Immune-Inflammation Value (PIV) is a novel biomarker derived from counts of neutrophils, platelets, monocytes, and lymphocytes, providing a comprehensive measure of systemic immune and inflammatory status. While it has shown prognostic value in specific disease settings, its association with mortality in the general population remains unclear. This study aims to evaluate the predictive value of PIV for all-cause and cause-specific mortality, including cardiovascular, cancer, and diabetes-related deaths, within a general adult population.

Methods: Data were obtained from the NHANES cohort, with 48,662 participants aged 20 and older. Participants were followed for an average of 117.44 months, with PIV quartiles calculated at baseline. Cox proportional hazard models were used to assess mortality risk across PIV quartiles, while restricted cubic spline models examined nonlinear dose-response relationships. Subgroup and sensitivity analyses further explored the robustness of PIV's associations.

Results: Higher PIV levels were significantly associated with increased risks of all-cause, cardiovascular, cancer, and diabetes mortality. Nonlinear relationships were observed between PIV and all-cause, cardiovascular, and cancer mortality, with a risk threshold at PIV values above 254.07. Subgroup analyses supported these findings, and sensitivity analyses confirmed the consistency of PIV's prognostic value.

Conclusion: Elevated PIV serves as an independent risk factor for multiple mortality outcomes in the general population. This study underscores the potential of PIV as a predictive biomarker for mortality risk, with implications for its use in clinical and epidemiological settings. Further studies are needed to confirm PIV's clinical utility across diverse populations and conditions.

KEYWORDS

pan-immune-inflammation value, mortality, inflammation, biomarker, NHANES

Introduction

Inflammatory responses are fundamental to maintaining health and protecting the body from external threats. Acute inflammation is a normal physiological reaction to infections, injuries, and other external stimuli, where the immune system is activated to eliminate pathogens and promote tissue repair (1). However, chronic inflammation has been strongly linked to the development of various diseases, including cardiovascular diseases, cancer, diabetes, and metabolic disorders (2–7). Persistent inflammatory responses can result in tissue damage, disrupt homeostasis, and accelerate disease onset and progression (6).

Immune-inflammatory biomarkers (IIBs), such as neutrophils (NEUs), lymphocytes (LYMs), monocytes (MONs), and platelets (PLTs), reflect the balance between the host's immune and inflammatory states and are critical for assessing disease conditions. Several inflammatory indices derived from CBC parameters, such as the monocyte-to-lymphocyte ratio (MLR), neutrophil-to-lymphocyte ratio (NLR), platelet-to-lymphocyte ratio (PLR), systemic inflammation response index (SIRI), lymphocyte-to-monocyte ratio (LMR), and systemic immune-inflammation index (SII), are widely used for disease risk assessment and prognosis. Multiple studies have demonstrated that NLR, PLR, and LMR are effective predictors of disease progression and prognosis across diverse conditions, including cancer, cardiovascular diseases, and inflammatory disorders (8–13). Additionally, these indices have been employed to distinguish between different types of chronic inflammatory diseases, such as Crohn's disease, further underscoring their broad clinical utility (14). Among these, SII has emerged as a valuable marker of inflammation, showing significant prognostic value in chronic conditions such as cancer and inflammatory diseases (8, 15, 16). Research conducted on general populations has also highlighted the potential of SII in assessing systemic inflammation (17, 18).

More recently, a novel and more comprehensive immune-inflammatory index, the Pan-Immune-Inflammation Value (PIV), has been developed. PIV integrates the counts of NEUs, PLTs, MONs, and LYMs, offering a more holistic assessment of the systemic immune and inflammatory status (19). Preliminary studies suggest that PIV has greater prognostic accuracy compared to traditional IIBs such as NLR and PLR, particularly in predicting outcomes for patients with cancers such as advanced colorectal cancer, hepatocellular carcinoma, and breast cancer (19–21). Although PIV has shown promise in predicting outcomes for cancer patients, its association with overall and cause-specific mortality in the general population remains understudied. Therefore, this study aims to evaluate the relationship between PIV and mortality rates in the U.S. population, with the goal of determining its potential as a prognostic marker and providing valuable insights to inform public health strategies.

Methods

Data source and study population

This study employed a prospective cohort design, with all data drawn from the NHANES database. NHANES, administered by the National Center for Health Statistics (NCHS), uses a multistage, stratified, and subgroup probability sampling method to select a representative sample of the American population. Its objective is to evaluate the health and nutritional status of adults and children in the United States (22). The survey's original protocol underwent a comprehensive ethical review and was approved by the CDC's Institutional Review Board. Informed consent was obtained from all participants, who signed consent forms prior to their participation (23) Additional details regarding the study are accessible online: www.cdc.gov/nchs/nhanes/irba98.htm.

We enrolled a total of 101,326 participants from NHANES, covering data of ten circles from 1999 to 2018 in this research. Participants younger than 20 years old and those missing data on neutrophil counts, monocyte counts, or mortality information were excluded. The process of participant selection is depicted in Figure 1.

Definition of CBC-derived inflammatory indices

The complete blood count (CBC) parameters were derived using the Beckman Coulter method for cell counting and sizing, with an automated diluting and mixing device for sample

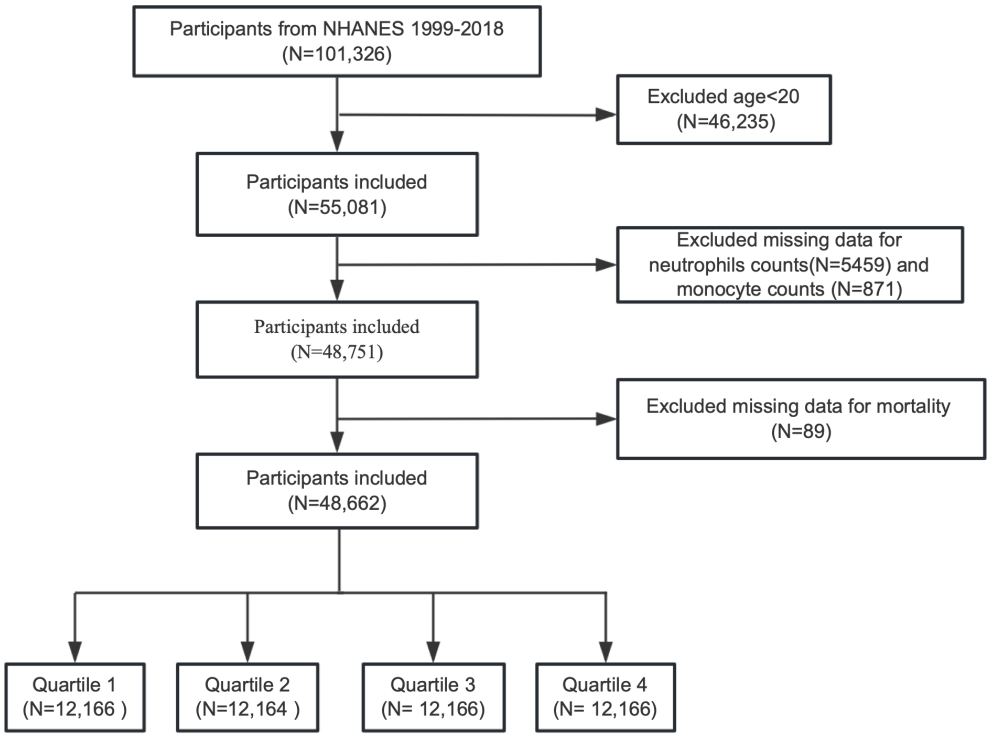

FIGURE 1
Flow chart depicting the incision and exclusion of participants from NHANES 1999-2018.

processing. All cell counts were measured in $\times 10^9$/L. The inflammatory indicators were calculated using the following formulas (19, 24):

$$MLR = monocytes/lymphocytes;$$

$$NLR = neutrophils/lymphocytes;$$

$$PLR = platelets/lymphocytes;$$

$$SII = platelets \times neutrophils/lymphocytes;$$

$$SIRI = neutrophils \times monocytes/lympocytes;$$

$$PIV = neutrophils \times monocytes \times platelets/lymphocytes;$$

As all components are expressed as counts per $\times 10^9$/L, the units cancel out during calculation, and all indices, including PIV, are dimensionless values. Among these indices, PIV uniquely integrates four key circulating immune cells — neutrophils, monocytes, platelets, and lymphocytes — representing both innate and adaptive immunity. Compared with simpler indices such as NLR and PLR, PIV provides a more comprehensive assessment of systemic immune-inflammatory status and has been identified as a promising prognostic marker in recent studies. In this study, PIV was analyzed both as a continuous variable and as a categorical variable by dividing participants into quartiles according to their PIV levels for subsequent analyses.

Assessment of all-cause and cause-specific mortality

The primary outcomes of interest were all-cause mortality, along with mortality due to cardiovascular disease (CVD), diabetes and cancer. Mortality information in NHANES is available via the National Death Index (NDI) death certificate records (www.cdc.gov/nchs/data-linkage/mortality_public.htm). Participant mortality status was determined by linking their data with the National Mortality Index through December 31, 2019. Disease-specific deaths were classified according to the International Classification of Diseases (ICD)-10. Cardiovascular mortality included deaths related to heart disease, cerebrovascular conditions, and/or hypertension. Specifically, heart disease mortality corresponded to codes I00-09, I11, I13, and I20-51, while cerebrovascular mortality was defined by codes I60-I69. Diabetes-related deaths were classified under codes E10-E14, and cancer-related deaths under codes C00-C97.

Potential covariates

Sociodemographic information assessed included age, gender, race, education level, and family income-to-poverty ratio, as well as marital status. Lifestyle and health-related factors comprised body mass index (BMI), smoking, and drinking. Laboratory parameters included red blood cell (RBC) count, white blood cell (WBC) count,

lymphocyte count, neutrophil count, monocyte count, platelet count, hemoglobin, aspartate transaminase (AST), alanine transaminase (ALT), total cholesterol (TC), blood urea nitrogen (BUN), uric acid, creatinine, albumin, and glycosylated hemoglobin A1c (HbA1c). Medical conditions considered were hypertension, diabetes, kidney disease, congestive heart failure(CHF), coronary heart disease(CHD),heart attack, angina pectoris, stroke, liver disease, and cancer.

Statistical analysis

In this study, statistical analyses accounted for the sample weights, clustering, and stratification resulting from the complex multistage stratified probability design used in NHANES. All analyses adhered to CDC guidelines (http://www.cdc.gov/nchs/tutorials/default.aspx). For two circles in NHANES 1999-2002, we applied the WTMEC4YR weights, while for the remaining 8 circles in NHANES 2003-2018, the WTMEC2YR weights were used. In accordance with the analytical recommendations, we calculated sampling weights for the 1999–2018 period as 1/5 of the 1999–2002 weight or 1/10 of the 2003–2018 weight.

Baseline characteristics of all participants were presented depending on PIV quartiles. Continuous variables were expressed as weighted means (95% confidence interval, 95%CI), while categorical variables were described in terms of weighted percentages. Differences in continuous and categorical variables were analyzed using linear regression models and chi-square tests, respectively. Multivariable Cox proportional hazards model was utilized to estimate the association between PIV and both all-cause and cause-specific mortality, reported through hazard ratios (HRs) and 95%CI. Model 1 represented the non-adjusted analysis. Model 2 adjusted for age, gender, race, family income to poverty ratio, education level, and marital status. Model 3 further adjusted for BMI, albumin, ALT, AST, BUN, creatinine, HbA1c, hemoglobin, RBC, TC, and uric acid. Finally, Model 4 included all variables from Model 3, along with adjustments for drinking, smoking, hypertension, diabetes, kidney disease, CHF, CHD, angina pectoris, heart attack, stroke, liver disease, and cancer. Survival was evaluated using the Kaplan-Meier method, and HRs for all-cause and specific mortality were derived using the log-rank test. To investigate potential non-linear associations between PIV and mortality outcomes, restricted cubic spline (RCS) analyses with four knots were performed, adjusting for the same variables as in Model 4. The knots were positioned at the 5th, 35th, 65th, and 95th percentiles of PIV distribution. Four knots were placed to exclude the most extreme 5% of values, minimizing the potential influence of outliers. Non-linearity relationship was assessed via the likelihood ratio test. In cases where a nonlinear relationship was identified, a threshold effect analysis was conducted. This involved applying a two-piece Cox proportional hazards model on either side of the inflection point to assess the association between PIV and the risk of all-cause and cause-specific mortality. Subgroup analyses were carried out to identify potential effect modifications by crucial factors, including age, gender, race, education level, family income-to-poverty ratio, marital status, smoking, drinking, BMI. The diagnostic efficacy of PIV and other inflammatory indices was evaluated using receiver operating characteristic (ROC) curve analysis. To quantify their predictive accuracy, the area under the curve (AUC) was calculated, providing a comprehensive measure of their performance in distinguishing outcomes. Finally, sensitivity analyses were performed as follows: (1) repeating the Multivariable Cox proportional hazards regression on the complete dataset (33,710 participants) without multiple imputation; (2) repeating the analyses after excluding participants with cancer, cardiovascular disease, or diabetes; and (3) calculating the E-value to determine the influence of unmeasured confounders on the study's findings (25).

The proportion of missing data for all variables was less than 10% in our study. To address potential bias from missing data, multiple imputation was performed (26, 27). A two-sided P-value of less than 0.05 was considered statistically significant. All statistical analyses were executed using R software version 4.3.2 (R Foundation for Statistical Computing) and Empower (R) version 4.2.

Results

Baseline population characteristics by PIV quartiles

After excluding 46,235 participants under 20 years of age, 5,459 participants with missing neutrophil counts, 871 participants with missing monocyte counts, and 89 participants with incomplete mortality information, a total of 48,662 participants were included in the final analysis. The demographic and clinical characteristics of the participants, stratified by PIV quartiles, are detailed in Table 1.

Participants were categorized into four quartiles based on their PIV levels at enrollment: Q1 (<164.18), Q2 (164.19–254.05), Q3 (254.06–393.66), and Q4 (>393.67). The overall mean PIV value for all participants was 327.0 (95% CI: 322.8–331.2). Median PIV values for each quartile were as follows: 116.9 (95% CI: 116.1–117.7) in Q1, 208.4 (95% CI: 207.8–209.0) in Q2, 316.4 (95% CI: 315.4–317.4) in Q3, and 640.1 (95% CI: 633.2–647.1) in Q4. Additional inflammatory markers, including MLR, NLR, PLR, SII, and SIRI, demonstrated a significant upward trend across the PIV quartiles. The mean MLR values increased from 0.21 (95% CI: 0.20–0.21) in Q1 to 0.38 (95% CI: 0.38–0.39) in Q4. Similarly, NLR rose from 1.40 (95% CI: 1.39–1.41) in Q1 to 3.25 (95% CI: 3.21–3.28) in Q4. PLR increased from 105.75 (95% CI: 104.68–106.83) in Q1 to 158.40 (95% CI: 156.77–160.03) in Q4, and SII climbed from 291.18 (95% CI: 288.34–294.01) in Q1 to 923.36 (95% CI: 912.94–933.78) in Q4. SIRI followed a similar pattern, rising from 0.57 (95% CI: 0.56–0.57) in Q1 to 2.26 (95% CI: 2.23–2.28) in Q4.

Participants in the highest PIV quartile (Q4) were characterized by older age (mean: 48.38 years), higher BMI, and a greater prevalence of females, Non-Hispanic Whites, and individuals with lower educational attainment (below high school and high school levels). They were more likely to have lower family income-to-

TABLE 1 The demographic characteristics of the study population with various PIV quartiles.

Variable	Total (N=48,662)	Q1 <164.18(N=12,166)	Q2 164.19-254.05 (N=12,164)	Q3 254.06-393.66 (N=12,166)	Q4 >393.67(N=12,166)	P-value
Age, years	47.19 (46.83 ,47.54)	46.15 (45.66 ,46.63)	46.80 (46.38 ,47.23)	47.29 (46.78 ,47.80)	48.38 (47.88 ,48.88)	<0.001
Gender (%)						0.727
Male	48.01 (47.58 ,48.45)	48.04 (46.91 ,49.18)	48.52 (47.43 ,49.61)	47.82 (46.86 ,48.78)	47.68 (46.63 ,48.72)	
Female	51.99 (51.55 ,52.42)	51.96 (50.82 ,53.09)	51.48 (50.39 ,52.57)	52.18 (51.22 ,53.14)	52.32 (51.28 ,53.37)	
Race (%)						<0.001
Mexican American	8.20 (7.19 ,9.35)	8.35 (7.29 ,9.56)	8.34 (7.25 ,9.58)	8.47 (7.40 ,9.67)	7.67 (6.59 ,8.90)	
Hispanics	5.60 (4.80 ,6.51)	5.63 (4.85 ,6.51)	5.81 (4.89 ,6.89)	5.71 (4.84 ,6.73)	5.25 (4.34 ,6.33)	
Non-Hispanic White	68.52 (66.43 ,70.55)	57.44 (54.85 ,59.99)	68.82 (66.58 ,70.98)	71.41 (69.30 ,73.44)	75.04 (72.95 ,77.01)	
Non-Hispanic Black	10.77 (9.71 ,11.93)	19.35 (17.52 ,21.31)	10.16 (9.12 ,11.30)	8.11 (7.23 ,9.09)	6.54 (5.78 ,7.38)	
Others	6.91 (6.32 ,7.54)	9.23 (8.28 ,10.28)	6.87 (6.08 ,7.75)	6.30 (5.64 ,7.04)	5.51 (4.91 ,6.18)	
Education level (%)						<0.001
Below high school	17.23 (16.36 ,18.13)	17.38 (16.30 ,18.51)	16.86 (15.77 ,18.02)	16.60 (15.48 ,17.80)	18.09 (17.03 ,19.19)	
High school	23.99 (23.22 ,24.78)	21.65 (20.50 ,22.84)	22.85 (21.67 ,24.07)	24.43 (23.44 ,25.45)	26.73 (25.51 ,27.99)	
Above high school	58.78 (57.46 ,60.09)	60.97 (59.22 ,62.70)	60.29 (58.63 ,61.92)	58.96 (57.41 ,60.50)	55.18 (53.51 ,56.84)	
Family income of poverty ratio(%)						<0.001
<1.3	21.26 (20.23 ,22.32)	21.25 (20.09 ,22.47)	19.97 (18.65 ,21.35)	21.61 (20.26 ,23.01)	22.21 (21.01 ,23.45)	
1.30-3.5	35.92 (34.94 ,36.91)	35.07 (33.52 ,36.65)	35.26 (33.86 ,36.67)	35.40 (33.95 ,36.87)	37.85 (36.57 ,39.14)	
≥3.50	42.82 (41.29 ,44.37)	43.68 (41.64 ,45.74)	44.78 (42.90 ,46.68)	43.00 (41.03 ,44.98)	39.94 (38.18 ,41.73)	
Smoking (%)						<0.001
No	54.07 (53.14 ,55.00)	60.10 (58.62 ,61.56)	56.34 (54.91 ,57.76)	52.90 (51.54 ,54.25)	47.69 (46.22 ,49.16)	
Yes	45.93 (45.00 ,46.86)	39.90 (38.44 ,41.38)	43.66 (42.24 ,45.09)	47.10 (45.75 ,48.46)	52.31 (50.84 ,53.78)	
Drinking (%)						0.004
No	22.73 (21.61 ,23.90)	24.25 (22.76 ,25.81)	22.09 (20.77 ,23.47)	22.84 (21.38 ,24.37)	21.95 (20.69 ,23.27)	
Yes	77.27 (76.10 ,78.39)	75.75 (74.19 ,77.24)	77.91 (76.53 ,79.23)	77.16 (75.63 ,78.62)	78.05 (76.73 ,79.31)	

(Continued)

10.3389/fendo.2025.1534018

TABLE 1 Continued

Variable	Total (N=48,662)	Q1 <164.18(N=12,166)	Q2 164.19-254.05 (N=12,164)	Q3 254.06-393.66 (N=12,166)	Q4 >393.67(N=12,166)	P-value
Marital status (%)						<0.001
Single	36.07 (35.14 ,37.01)	34.86 (33.48 ,36.27)	34.37 (33.10 ,35.65)	35.72 (34.38 ,37.08)	39.17 (37.90 ,40.46)	
Married or living with a partner	63.93 (62.99 ,64.86)	65.14 (63.73 ,66.52)	65.63 (64.35 ,66.90)	64.28 (62.92 ,65.62)	60.83 (59.54 ,62.10)	
BMI, kg/m2	28.79 (28.67 ,28.92)	27.67 (27.49 ,27.84)	28.34 (28.16 ,28.52)	29.20 (29.03 ,29.38)	29.83 (29.63 ,30.02)	<0.001
RBC, 10^{12}/L	4.70 (4.69 ,4.71)	4.65 (4.63 ,4.66)	4.71 (4.69 ,4.72)	4.73 (4.71 ,4.74)	4.71 (4.69 ,4.73)	<0.001
WBC,10^9/L	7.30 (7.26 ,7.34)	5.83 (5.77 ,5.89)	6.67 (6.62 ,6.71)	7.52 (7.47 ,7.57)	9.00 (8.94 ,9.05)	<0.001
Lymphocyte,10^9/L	2.16 (2.14 ,2.17)	2.28 (2.23 ,2.33)	2.16 (2.14 ,2.18)	2.15 (2.13 ,2.18)	2.05 (2.03 ,2.07)	<0.001
Neutrophils,10^9/L	4.34 (4.31 ,4.38)	2.88 (2.85 ,2.90)	3.75 (3.73 ,3.78)	4.55 (4.52 ,4.58)	6.01 (5.97 ,6.06)	<0.001
Monocyte,10^9/L	0.56 (0.56 ,0.57)	0.43 (0.42 ,0.43)	0.51 (0.51 ,0.52)	0.58 (0.58 ,0.59)	0.72 (0.71 ,0.72)	<0.001
Platelets,10^9/L	254.70 (253.38 ,256.02)	214.94 (213.46 ,216.42)	242.07 (240.57 ,243.58)	262.86 (261.35 ,264.38)	293.96 (291.73 ,296.20)	<0.001
Hemoglobin, g/dL	14.26 (14.22 ,14.30)	14.13 (14.08 ,14.18)	14.32 (14.28 ,14.37)	14.34 (14.30 ,14.39)	14.23 (14.17 ,14.28)	<0.001
AST, mmol/L	25.12 (24.94 ,25.30)	25.87 (25.50 ,26.24)	25.03 (24.70 ,25.35)	24.75 (24.48 ,25.02)	24.92 (24.57 ,25.27)	<0.001
ALT, mmol/L	25.29 (25.03 ,25.54)	24.92 (24.50 ,25.34)	25.53 (25.07 ,25.98)	25.23 (24.85 ,25.62)	25.43 (24.78 ,26.09)	0.191
TC, mmol/L	5.07 (5.05 ,5.09)	5.02 (4.99 ,5.05)	5.09 (5.06 ,5.11)	5.09 (5.06 ,5.12)	5.08 (5.05 ,5.10)	0.001
BUN, mmol/L	4.82 (4.78 ,4.86)	4.71 (4.65 ,4.76)	4.81 (4.77 ,4.86)	4.83 (4.78 ,4.89)	4.92 (4.86 ,4.97)	<0.001
Uric acid, umol/L	320.80 (319.63 ,321.97)	312.33 (310.20 ,314.47)	319.90 (317.77 ,322.02)	322.35 (320.48 ,324.21)	327.53 (325.20 ,329.86)	<0.001
Creatinine, umol/L	77.94 (77.50 ,78.37)	77.23 (76.60 ,77.86)	77.49 (76.84 ,78.13)	77.32 (76.63 ,78.00)	79.61 (78.81 ,80.42)	<0.001
Albumin, g/L	42.68 (42.60 ,42.76)	42.92 (42.82 ,43.03)	43.01 (42.90 ,43.11)	42.74 (42.63 ,42.85)	42.10 (42.00 ,42.20)	<0.001
HbA1c (%)	5.58 (5.56 ,5.59)	5.54 (5.52 ,5.56)	5.54 (5.52 ,5.56)	5.59 (5.56 ,5.61)	5.64 (5.62 ,5.66)	<0.001
Kidney disease (%)						<0.001
No	97.59 (97.40 ,97.76)	98.02 (97.69 ,98.31)	97.97 (97.62 ,98.27)	97.56 (97.22 ,97.86)	96.85 (96.50 ,97.16)	
Yes	2.41 (2.24 ,2.60)	1.98 (1.69 ,2.31)	2.03 (1.73 ,2.38)	2.44 (2.14 ,2.78)	3.15 (2.84 ,3.50)	
CHF (%)						<0.001
No	97.55 (97.36 ,97.74)	98.20 (97.95 ,98.42)	98.25 (97.96 ,98.49)	97.53 (97.12 ,97.87)	96.32 (95.93 ,96.68)	
Yes	2.45 (2.26 ,2.64)	1.80 (1.58 ,2.05)	1.75 (1.51 ,2.04)	2.47 (2.13 ,2.88)	3.68 (3.32 ,4.07)	

(Continued)

10.3389/fendo.2025.1534018

TABLE 1 Continued

Variable	Total (N=48,662)	Q1 <164.18(N=12,166)	Q2 164.19-254.05 (N=12,164)	Q3 254.06-393.66 (N=12,166)	Q4 >393.67(N=12,166)	P-value
CHD (%)						<0.001
No	96.44 (96.14 ,96.70)	97.37 (96.98 ,97.71)	96.71 (96.24 ,97.12)	96.40 (95.87 ,96.87)	95.37 (94.85 ,95.84)	
Yes	3.56 (3.30 ,3.86)	2.63 (2.29 ,3.02)	3.29 (2.88 ,3.76)	3.60 (3.13 ,4.13)	4.63 (4.16 ,5.15)	
Angina pectoris (%)						<0.001
No	97.51 (97.29 ,97.71)	98.11 (97.75 ,98.41)	97.61 (97.20 ,97.96)	97.45 (97.02 ,97.82)	96.94 (96.48 ,97.34)	
Yes	2.49 (2.29 ,2.71)	1.89 (1.59 ,2.25)	2.39 (2.04 ,2.80)	2.55 (2.18 ,2.98)	3.06 (2.66 ,3.52)	
Heart attack (%)						<0.001
No	96.56 (96.30 ,96.79)	97.19 (96.77 ,97.55)	97.11 (96.67 ,97.49)	96.57 (96.11 ,96.97)	95.44 (94.96 ,95.87)	
Yes	3.44 (3.21 ,3.70)	2.81 (2.45 ,3.23)	2.89 (2.51 ,3.33)	3.43 (3.03 ,3.89)	4.56 (4.13 ,5.04)	
Stroke (%)						<0.001
No	97.15 (96.94 ,97.34)	97.66 (97.26 ,98.00)	97.72 (97.35 ,98.03)	97.15 (96.72 ,97.53)	96.12 (95.68 ,96.52)	
Yes	2.85 (2.66 ,3.06)	2.34 (2.00 ,2.74)	2.28 (1.97 ,2.65)	2.85 (2.47 ,3.28)	3.88 (3.48 ,4.32)	
Liver disease (%)						0.128
No	96.45 (96.20 ,96.68)	96.04 (95.49 ,96.53)	96.47 (95.98 ,96.90)	96.81 (96.36 ,97.21)	96.42 (95.98 ,96.82)	
Yes	3.55 (3.32 ,3.80)	3.96 (3.47 ,4.51)	3.53 (3.10 ,4.02)	3.19 (2.79 ,3.64)	3.58 (3.18 ,4.02)	
Cancer (%)						<0.001
No	90.45 (90.06 ,90.82)	91.73 (91.01 ,92.39)	90.93 (90.21 ,91.61)	90.55 (89.80 ,91.24)	88.74 (87.88 ,89.55)	
Yes	9.55 (9.18 ,9.94)	8.27 (7.61 ,8.99)	9.07 (8.39 ,9.79)	9.45 (8.76 ,10.20)	11.26 (10.45 ,12.12)	
Hypertension(%)						<0.001
No	69.26 (68.46 ,70.05)	73.04 (71.85 ,74.20)	71.63 (70.40 ,72.83)	68.80 (67.56 ,70.01)	64.04 (62.85 ,65.21)	
Yes	30.74 (29.95 ,31.54)	26.96 (25.80 ,28.15)	28.37 (27.17 ,29.60)	31.20 (29.99 ,32.44)	35.96 (34.79 ,37.15)	
Diabetes (%)						<0.001
No	91.03 (90.66 ,91.39)	92.44 (91.77 ,93.06)	92.15 (91.54 ,92.72)	90.51 (89.75 ,91.23)	89.20 (88.47 ,89.89)	
Yes	8.97 (8.61 ,9.34)	7.56 (6.94 ,8.23)	7.85 (7.28 ,8.46)	9.49 (8.77 ,10.25)	10.80 (10.11 ,11.53)	

(Continued)

10.3389/fendo.2025.1534018

TABLE 1 Continued

Variable	Total (N=48,662)	Q1 <164.18(N=12,166)	Q2 164.19-254.05 (N=12,164)	Q3 254.06-393.66 (N=12,166)	Q4 >393.67(N=12,166)	P-value
All-cause mortality (%)						<0.001
No	88.83 (88.31 ,89.34)	91.49 (90.80 ,92.14)	90.63 (89.93 ,91.29)	89.28 (88.60 ,89.92)	84.27 (83.27 ,85.22)	
Yes	11.17 (10.66 ,11.69)	8.51 (7.86 ,9.20)	9.37 (8.71 ,10.07)	10.72 (10.08 ,11.40)	15.73 (14.78 ,16.73)	
Diabetes mortality (%)						0.001
No	99.61 (99.54 ,99.67)	99.75 (99.63 ,99.83)	99.66 (99.52 ,99.77)	99.64 (99.51 ,99.73)	99.41 (99.22 ,99.55)	
Yes	0.39 (0.33 ,0.46)	0.25 (0.17 ,0.37)	0.34 (0.23 ,0.48)	0.36 (0.27 ,0.49)	0.59 (0.45 ,0.78)	
Cancer mortality (%)						<0.001
No	97.43 (97.24 ,97.60)	97.83 (97.48 ,98.13)	97.66 (97.34 ,97.95)	97.78 (97.47 ,98.05)	96.49 (96.09 ,96.86)	
Yes	2.57 (2.40 ,2.76)	2.17 (1.87 ,2.52)	2.34 (2.05 ,2.66)	2.22 (1.95 ,2.53)	3.51 (3.14 ,3.91)	
Cardiovascular mortality (%)						<0.001
No	96.67 (96.41 ,96.91)	97.56 (97.15 ,97.91)	97.34 (96.99 ,97.65)	96.68 (96.29 ,97.03)	95.21 (94.77 ,95.62)	
Yes	3.33 (3.09 ,3.59)	2.44 (2.09 ,2.85)	2.66 (2.35 ,3.01)	3.32 (2.97 ,3.71)	4.79 (4.38 ,5.23)	
Follow-up time (months)	117.44 (115.55 ,119.34)	110.65 (108.28 ,113.03)	118.66 (116.39 ,120.94)	122.41 (119.92 ,124.90)	117.20 (114.59 ,119.81)	<0.001
MLR	0.28 (0.28 ,0.29)	0.21 (0.20 ,0.21)	0.25 (0.25 ,0.25)	0.29 (0.29 ,0.29)	0.38 (0.38 ,0.39)	<0.001
NLR	2.22 (2.20 ,2.23)	1.40 (1.39 ,1.41)	1.85 (1.83 ,1.87)	2.26 (2.24 ,2.28)	3.25 (3.21 ,3.28)	<0.001
PLR	129.99 (129.08 ,130.90)	105.75 (104.68 ,106.83)	120.86 (119.65 ,122.07)	131.93 (130.60 ,133.26)	158.40 (156.77 ,160.03)	<0.001
SII	563.98 (558.31 ,569.65)	291.18 (288.34 ,294.01)	433.75 (430.09 ,437.40)	573.61 (569.11 ,578.12)	923.36 (912.94 ,933.78)	<0.001
SIRI	1.27 (1.25 ,1.28)	0.57 (0.56 ,0.57)	0.90 (0.89 ,0.91)	1.26 (1.25 ,1.27)	2.26 (2.23 ,2.28)	<0.001
PIV	327.00 (322.80 ,331.20)	116.90 (116.10 ,117.70)	208.41 (207.82 ,209.00)	316.36 (315.37 ,317.36)	640.13 (633.21 ,647.06)	<0.001

For continuous variables: survey-weighted mean (95% CI), P-value was by survey-weighted linear regression. For categorical variables: survey-weighted percentage (95% CI), P-value was by survey-weighted Chi-square test.
BMI, body mass index; RBC, red blood cell; WBC, white blood cell; AST, aspartate transaminase; ALT, glutamic-pyruvic transaminase; TC, total cholesterol; BUN, blood urea nitrogen; HBA1c, glycosylated hemoglobin A1c; CHF, congestive heart failure; CHD, coronary heart disease; MLR, monocyte-to-lymphocyte ratio; PLR, platelet-to-lymphocyte ratio; NLR, neutrophil-to-lymphocyte ratio; SII, systemic immune-inflammation index; SIRI, systemic inflammation response index; PIV, pan-immune- inflammation value.

10.3389/fendo.2025.1534018

poverty ratios (<3.5), higher rates of smoking and drinking, and a single marital status. Moreover, these participants exhibited elevated levels of inflammatory markers (MLR, NLR, PLR, SII, and SIRI) and adverse metabolic indicators, including elevated BUN, creatinine, uric acid, and HbA1c. Comorbidities such as kidney disease, cancer, hypertension, diabetes, and cardiovascular conditions (e.g., CHF, CHD, angina pectoris, heart attack, and stroke) were more prevalent in participants in Q4 compared to those in Q1. Additionally, participants in Q4 exhibited significantly higher mortality rates, including all-cause mortality (15.73% vs. 8.51%), diabetes-related mortality (0.59% vs. 0.25%), cancer-related mortality (3.51% vs. 2.17%), and cardiovascular mortality (4.79% vs. 2.44%). The median follow-up duration was shorter in Q4 participants (117.20 months) compared to Q1 (110.65 months), likely reflecting the elevated mortality risks associated with this group.

Relationship between PIV and all-cause and cause-specific mortality

To explore the relationship between PIV and various mortality outcomes, including all-cause, cardiovascular, cancer, and diabetes-related mortality, we developed four weighted Cox proportional hazard models, as presented in Table 2. For every 100-unit increase in PIV, the unadjusted hazard ratios were 1.038 (95% CI: 1.030–1.047) for all-cause mortality, 1.039 (95% CI: 1.031–1.048) for cardiovascular mortality, 1.035 (95% CI: 1.028–1.042) for cancer mortality, and 1.035 (95% CI: 1.028–1.042) for diabetes mortality. The fully adjusted hazard ratios were 1.031 (95% CI: 1.024–1.038), 1.032 (95% CI: 1.024–1.040), 1.028 (95% CI: 1.020–1.035), and 1.040 (95% CI: 1.030–1.051), respectively. Furthermore, when PIV was divided into quartiles, a clear, stepwise increase in mortality risk was observed across the quartiles, even after adjusting for confounders (p for trend < 0.05).

Kaplan-Meier survival curves, shown in Figure 2, confirmed the differences in mortality rates across PIV quartiles. Significant disparities were observed in all-cause, cardiovascular, cancer, and diabetes-related mortality among the groups (log-rank test p-values < 0.001 for all).

Nonlinear association between PIV and mortality outcomes

To model the relationship between PIV and mortality outcomes flexibly, we used restricted cubic spline analyses. Figure 3 illustrates significant nonlinear dose-response relationships between PIV and all-cause, cardiovascular, and cancer mortality after adjusting for covariates in Model 4 (p for nonlinearity < 0.001, 0.001, and 0.019, respectively). No significant nonlinear relationship was found between PIV and diabetes-related mortality (p for nonlinearity = 0.101).

When nonlinear relationships were identified, a threshold effect analysis was performed using a two-piece Cox proportional hazards model. For PIV values below 254.07, no significant association with all-cause, cardiovascular, or cancer mortality was observed (log-likelihood ratio test p-values = 0.995, 0.838, and 0.776, respectively). However, for PIV values of 254.07 or higher, a positive association with increased risk of all-cause, cardiovascular, and cancer mortality was evident (log-likelihood ratio test p-values < 0.001 for all), as detailed in Supplementary Table S1.

Subgroup analysis

Subgroup analyses were performed to determine the association between PIV and both all-cause and cause-specific mortality, stratifying by variables including age, gender, race, family income-to-poverty ratio, marital status, education level, smoking, drinking, and BMI. Across most subgroups, PIV was consistently linked with a significantly higher risk of both all-cause and cause-specific mortality, as shown in Table 3. However, the interaction analysis produced nuanced results. While a significant association with all-cause and cardiovascular mortality was observed across all subgroups, except for the gender subgroup, the association for cancer mortality was significant only in the subgroups defined by race, family income-to-poverty ratio, drinking, and BMI. For diabetes mortality, significant associations were found in subgroups based on race, family income-to-poverty ratio, and drinking.

ROC analysis

ROC curve analyses (Figure 4) evaluated the predictive efficiency of PIV and other inflammatory markers. For all-cause mortality, PIV had an AUC of 0.581 (95% CI: 0.574–0.588), which was superior to PLR (AUC = 0.557) and SII (AUC = 0.567) (both p<0.001), but inferior to MLR (AUC = 0.627), NLR (AUC = 0.600), and SIRI (AUC = 0.609) (all p<0.001). Similar trends were observed for cardiovascular mortality, with PIV demonstrating better performance than PLR and SII (both p<0.001), but inferior to MLR, NLR, and SIRI (all p<0.001). For cancer mortality, PIV showed comparable performance to NLR and PLR, while outperforming SII (p<0.001) but being surpassed by MLR and SIRI. For diabetes-related mortality, PIV outperformed PLR (p<0.001) and was comparable to other markers (p>0.05).

Sensitivity analysis

To further assess the stability of the PIV-mortality relationships, we performed a sensitivity analysis by excluding participants with incomplete data, as well as those with pre-existing cardiovascular disease or cancer (Supplementary Table S2, Supplementary Table S3 and Supplementary Table S4). The results aligned with those of the primary analysis. Furthermore, based on Model 4, we calculated the E-value to determine the minimum strength of association that

10.3389/fendo.2025.1534018

TABLE 2 Association between PIV and all-cause mortality and cause-specific mortality.

	Model 1		Model 2		Model 3		Model 4	P-value
	HR (95% CI)	P-value	HR (95% CI)	P-value	HR (95% CI)	P-value	HR (95% CI)	
All-cause mortality								
PIV (per 100units)	1.038 (1.030,1.047)	<0.001	1.036 (1.028,1.043)	<0.001	1.030 (1.022,1.037)	<0.001	1.031 (1.024,1.038)	<0.001
Q1	Ref	Ref	Ref	Ref	Ref	Ref	Ref	Ref
Q2	1.013 (0.920, 1.116)	0.787	0.956 (0.871,1.048)	0.336	0.961 (0.874,1.057)	0.411	0.977 (0.891,1.071)	0.614
Q3	1.116 (1.021, 1.220)	0.016	1.012 (0.932,1.099)	0.771	1.003 (0.920,1.094)	0.945	0.993 (0.910,1.083)	0.869
Q4	1.718 (1.570,1.880)	<0.001	1.423 (1.312,1.544)	<0.001	1.365 (1.253,1.486)	<0.001	1.334 (1.225,1.452)	<0.001
P for trend	<0.001		<0.001		<0.001		<0.001	
Cardiovascular mortality								
PIV (per 100units)	1.039 (1.031,1.048)	<0.001	1.037 (1.029,1.045)	<0.001	1.031 (1.022,1.039)	<0.001	1.032 (1.024,1.040)	<0.001
Q1	Ref	Ref	Ref	Ref	Ref	Ref	Ref	Ref
Q2	1.004 (0.843,1.195)	0.964	0.948 (0.804, 1.118)	0.527	0.925 (0.779,1.097)	0.370	0.934 (0.788,1.109)	0.436
Q3	1.208 (1.004, 1.452)	0.045	1.098 (0.923, 1.307)	0.291	1.038 (0.869,1.240)	0.682	1.029 (0.864,1.226)	0.746
Q4	1.827 (1.562,2.136)	<0.001	1.481 (1.273, 1.724)	<0.001	1.337 (1.145,1.562)	<0.001	1.313 (1.126,1.532)	<0.001
P for trend	<0.001		<0.001		<0.001		<0.001	
Cancer mortality								
PIV (per 100units)	1.035 (1.028,1.042)	<0.001	1.030 (1.024,1.037)	<0.001	1.028 (1.021,1.035)	<0.001	1.028 (1.020,1.035)	<0.001
Q1	Ref	Ref	Ref	Ref	Ref	Ref	Ref	Ref
Q2	0.992 (0.813,1.209)	0.933	0.939 (0.772,1.141)	0.526	0.978 (0.801,1.194)	0.826	0.985 (0.806,1.204)	0.883
Q3	0.907 (0.764, 1.076)	0.263	0.830 (0.695,0.990)	0.039	0.864 (0.719,1.039)	0.120	0.855 (0.709,1.030)	0.100
Q4	1.505 (1.257, 1.802)	<0.001	1.275 (1.072,1.517)	0.006	1.317 (1.100,1.575)	0.003	1.272 (1.066,1.519)	0.008
P for trend	<0.001		<0.001		<0.001		<0.001	
Diabetes mortality								
PIV (per 100units)	1.035 (1.028,1.042)	<0.001	1.041 (1.031,1.051)	<0.001	1.028 (1.015,1.042)	<0.001	1.040 (1.030,1.051)	<0.001
Q1	Ref	Ref	Ref	Ref	Ref	Ref	Ref	Ref
Q2	1.230 (0.705,2.146)	0.467	1.214 (0.690,2.138)	0.501	1.041 (0.581,1.862)	0.894	0.981 (0.534,1.80)	0.949
Q3	1.267 (0.801, 2.002)	0.312	1.245 (0.769,2.014)	0.372	0.983 (0.583,1.657)	0.949	0.989 (0.598,1.635)	0.965
Q4	2.181 (1.368,3.477)	0.001	2.033 (1.219, 3.391)	0.007	1.580 (0.939,2.658)	0.085	1.523 (0.900, 2.577)	0.117
P for trend	<0.001		<0.001		0.004		0.011	

Model 1: Non-adjusted.
Model 2: Adjusted for age, gender, race, family income of poverty ratio, education level, marital status.
Model 3: Adjusted for age, gender, race, family income of poverty ratio, education level, marital status, BMI, albumin, ALT, AST, BUN, creatinine, HbA1c, Hemoglobin, RBC, TC, uric acid.
Model 4: Adjusted for age, gender, race, family income of poverty ratio, education level, marital status, BMI, albumin, ALT, AST, BUN, creatinine, HbA1c, Hemoglobin, RBC, TC, uric acid, drinking, smoking, hypertension, diabetes, kidney disease, CHF, CHD, angina pectoris, heart attack, stroke, liver disease, cancer.
BMI, body mass index; RBC, red blood cell; AST, aspartate transaminase; ALT, glutamic-pyruvic transaminase; TC, total cholesterol; BUN, blood urea nitrogen; HbA1c, glycosylated hemoglobin A1c; CHF, congestive heart failure; CHD, coronary heart disease; PIV, pan-immune- inflammation value; CI, confidence interval; HR, hazard ratios.

an unmeasured confounder would need to negate the observed PIV-mortality relationships. The E-values for PIV and all-cause mortality, cardiovascular mortality, cancer mortality, and diabetes mortality were 1.21, 1.21, 1.20, and 1.24, respectively. These E-values indicate that relatively small unmeasured confounding would be sufficient to explain the observed hazard ratios.

Discussion

This study investigated whether the PIV could predict long-term outcomes in a general population. Our results demonstrated that PIV is significantly associated with mortality across multiple causes in this population. A high PIV level was shown to be an

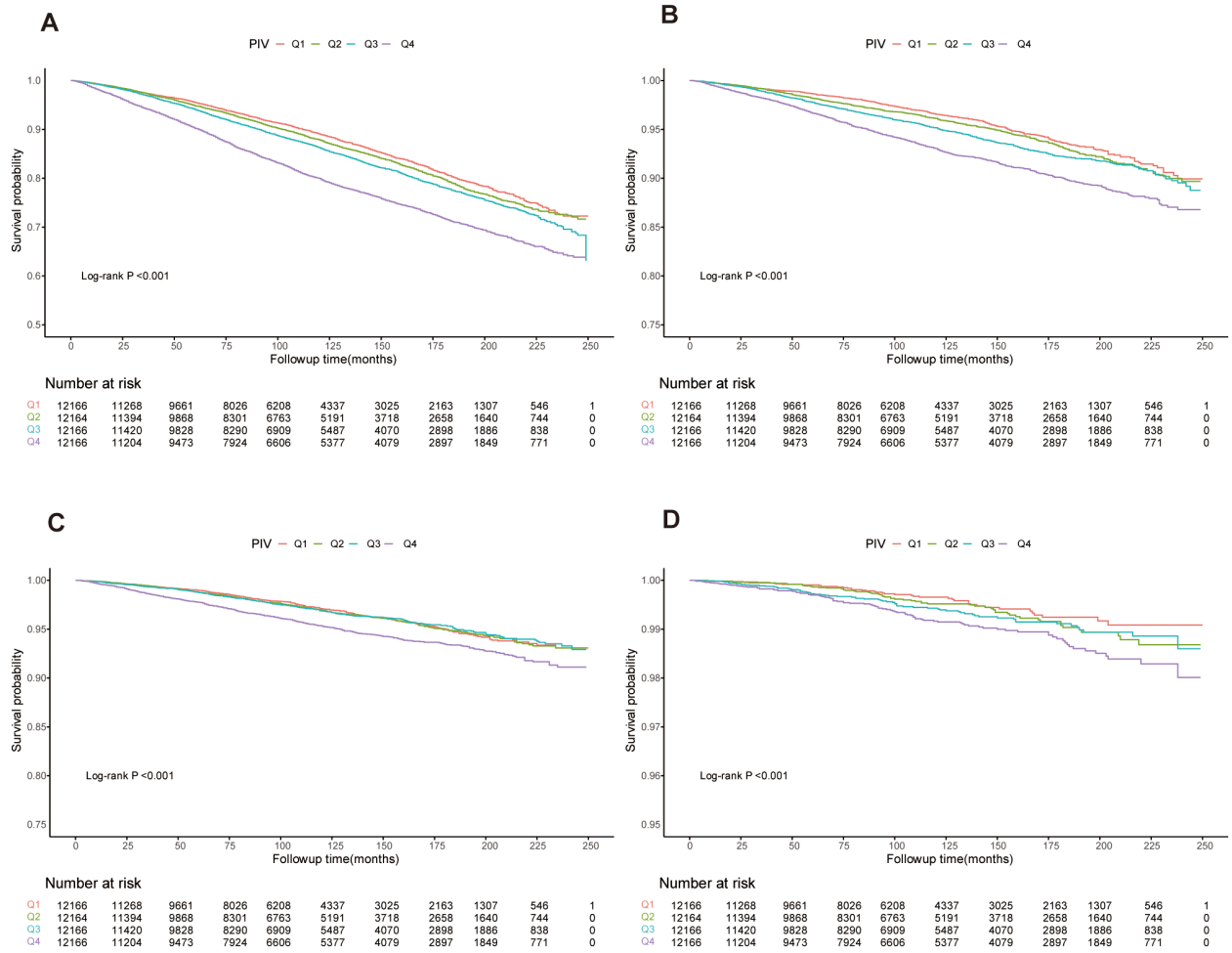

FIGURE 2
Kaplan-Meier curves showing survival rates and population numbers for us adults stratified by PIV quartiles. **(A)** All-cause mortality. **(B)** Cardiovascular mortality. **(C)** Cancer mortality. **(D)** Diabetes mortality.

independent risk factor for all-cause mortality and cause-specific mortality. Additionally, PIV exhibited a nonlinear relationship with all-cause, cardiovascular, and cancer mortality, while displaying a linear association with diabetes mortality.

The PIV is a novel biomarker derived from neutrophils, platelets, monocytes, and lymphocytes, providing an integrative view of a patient's immune and inflammatory status. Originally studied in the context of metastatic colorectal cancer, PIV has shown superior prognostic power over traditional inflammatory markers, such as NLR and PLR (19). Its simplicity, along with its ability to combine multiple immune components into a single measure, makes PIV a valuable and non-invasive tool for assessing systemic inflammation across a variety of clinical settings.

PIV has been well-established as a prognostic marker in oncology, where elevated levels are associated with worse prognosis, rapid disease progression, and therapy resistance. Researches have shown that high PIV correlates with poor survival outcomes in multiple cancers, including pancreatic (28), colorectal (29, 30), lung (31, 32), ovarian (33) esophageal (34), and breast cancers (35, 36). In newly diagnosed glioblastoma multiforme (GBM), E. Topkan et al. reported a significant association between elevated PIV levels and shorter progression-free survival (PFS) and overall survival (OS) outcomes (37). Furthermore, dynamic changes in PIV during immune checkpoint inhibitor (ICI) treatment have been linked to patient outcomes in colorectal cancer, with higher PIV levels indicating poor response and survival (38) Additionally, PIV serves as an indicator of chemotherapy resistance; for instance, in breast cancer patients undergoing neoadjuvant chemotherapy, lower PIV levels have been associated with better responses and improved survival (35). Elevated PIV levels also predict enhanced tumor progression, aiding clinicians in tailoring treatment plans and identifying patients at higher risk of recurrence. PIV not only plays a critical role in prognostic assessment but also shows potential in tumor diagnosis and recurrence monitoring. Y.T. Yang et al. highlighted that PIV has high sensitivity and specificity for diagnosing brain tumors, particularly gliomas (39). In Merkel cell carcinoma (MCC), T. Gambichler's study confirmed that PIV levels correlate with disease stage and are independent predictors of MCC recurrence (40).

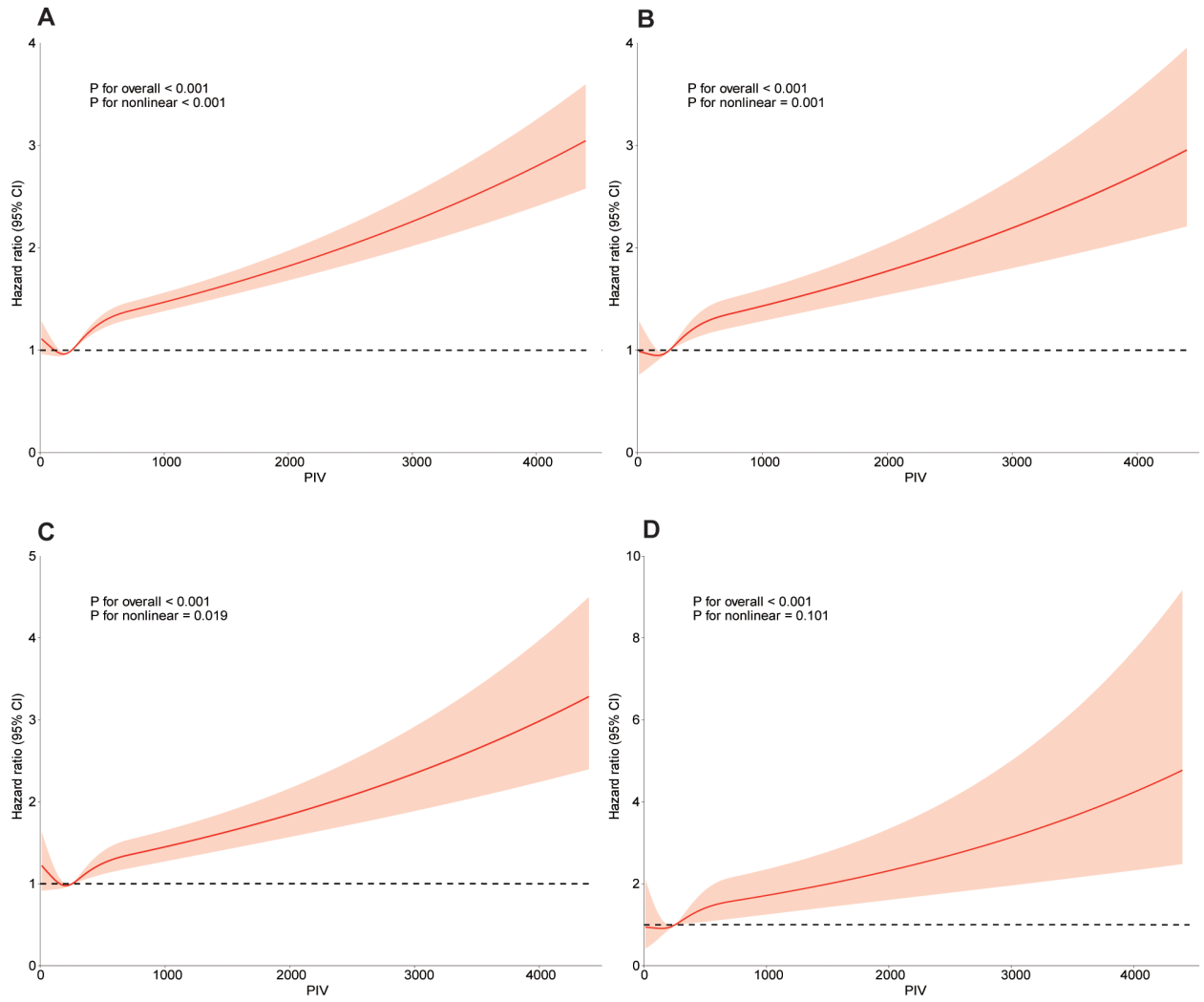

FIGURE 3
Dose-response curve of PIV and all-cause mortality and specific-mortality. A restricted cubic spline was fitted to model each curve, with 4 knots fixed at the 5th, 35th, 65th and 95th percentiles for all smooth curves. Solid lines represent the point estimates of HRs for incident all-cause mortality **(A)**, CVD mortality **(B)**, cancer mortality **(C)**, diabetes mortality **(D)**. Orange area represents their corresponding 95% CIs. Adjusted for age, gender, race, family income of poverty ratio, education level, marital status, BMI, albumin, ALT, AST, BUN, creatine, HbA1c, Hemoglobin, RBC, TC, uric acid, drinking, smoking, hypertension, diabetes, kidney disease, CHF, CHD, angina pectoris, heart attack, stroke, liver disease, cancer. PIV, pan-immune-inflammation value; BMI, body mass index; RBC, red blood cell; AST, aspartate transaminase; ALT, glutamic-pyruvic transaminase; TC, total cholesterol; BUN, blood urea nitrogen; HBA1c, glycosylated hemoglobin A1c; CHF, congestive heart failure; CHD, coronary heart disease; CI, confidence interval; HR, hazard ratios.

Chronic inflammation is a central factor in cardiovascular diseases, and PIV provides a comprehensive measure of inflammatory burden in conditions such as ST-segment elevation myocardial infarction (STEMI) and hypertension. Elevated PIV levels are predictive of both short-term and long-term mortality following STEMI, underscoring its value in risk stratification (9). Among hypertensive patients, high PIV levels have been linked to increased cardiovascular mortality due to their role in promoting thrombosis and exacerbating atherosclerosis (41). PIV's capacity to integrate immune and inflammatory markers makes it a valuable tool for tracking disease progression and tailoring interventions in cardiovascular care.

Beyond oncology and cardiovascular disease, PIV has shown promise across a broad spectrum of conditions. In autoimmune diseases like systemic lupus erythematosus (SLE), PIV levels are significantly elevated compared to healthy controls (42). This elevation captures both inflammatory activity and immune dysregulation, which are critical in autoimmune disease pathogenesis. In rheumatoid arthritis, where chronic inflammation drives joint damage and cardiovascular complications, PIV serves as a useful index of inflammatory burden (43) Additionally, PIV is a significant nonlinear predictor of 28-day and 90-day mortality in septic patients, with higher levels correlating with increased mortality risk beyond a specific threshold

TABLE 3 Subgroup analysis of the associations between PIV (per 100units) and all-cause and cause-specific mortality.

Variables	All-cause mortality			Cardiovascular mortality			Cancer mortality			Diabetes mortality		
	HR (95%CI)	P for value	P for interaction	HR (95%CI)	P for value	P for interaction	HR (95%CI)	P for value	P for interaction	HR (95%CI)	P for value	P for interaction
Age			0.008			0.007			0.805			0.101
<60	1.05 (1.03,1.06)	<0.001		1.07 (1.04,1.09)	<0.001		1.02(0.98,1.06)	0.279		1.08 (1.03,1.13)	0.002	
≥60	1.03 (1.02,1.03)	<0.001		1.03 (1.02,1.03)	<0.001		1.03(1.02,1.03)	<0.001		1.03 (1.02,1.04)	<0.001	
Gender			0.032			0.137			0.143			0.615
Male	1.03 (1.03,1.03)	<0.001		1.03 (1.02,1.03)	<0.001		1.03(1.02,1.03)	<0.001		1.03 (1.02,1.04)	<0.001	
Female	1.04 (1.03,1.04)	<0.001		1.04 (1.03,1.05)	<0.001		1.01(0.99,1.04)	0.351		1.04 (1.01,1.07)	0.002	
Race			<0.001			<0.001			0.008			0.006
Mexican American	1.02 (1.02,1.03)	<0.001		1.02 (1.01,1.04)			1.03(1.02,1.04)	<0.001		1.02 (0.99,1.05)	0.152	
Hispanics	1.05 (1.01,1.09)	0.019		1.06 (0.99,1.13)			1.06(0.99,1.14)	0.099		1.10 (0.96,1.25)	0.162	
Non-Hispanic White	1.07 (1.06,1.07)	<0.001		1.07 (1.06,1.08)			1.05(1.03,1.07)	<0.001		1.09 (1.07,1.12)	<0.001	
Non-Hispanic Black	1.04 (1.02,1.06)	<0.001		1.04 (1.01,1.07)			1.04(1.01,1.08)	0.21		1.02 (0.92,1.13)	0.728	
Others	1.09 (1.06,1.12)	<0.001		1.09 (1.04,1.15)			1.11(1.06,1.17)	<0.001		1.04 (0.82,1.33)	0.742	
Family income of poverty ratio			<0.001			<0.001			0.047			0.004
<1.3	1.03 (1.03,1.04)	<0.001		1.04 (1.03,1.04)	<0.001		1.03(1.01,1.04)	<0.001		1.04 (1.02,1.06)	<0.001	
1.3-3.5	1.03 (1.02,1.03)	<0.001		1.03 (1.02,1.03)	<0.001		1.03(1.02,1.03)	<0.001		1.03 (1.00,1.05)	0.026	
≥3.5	1.08 (1.07,1.10)	<0.001		1.08 (1.06,1.11)	<0.001		1.07(1.04,1.09)	<0.001		1.13 (1.08,1.17)	<0.001	
Marital status			<0.001			<0.001			0.509			0.113
Single	1.03 (1.02,1.03)	<0.001		1.03 (1.02,1.03)	<0.001		1.03(1.02,1.03)	<0.001		1.03 (1.01,1.04)	<0.001	
Married or living with partner	1.04 (1.04,1.05)	<0.001		1.04 (1.04,1.05)	<0.001		1.03(1.02,1.05)	<0.001		1.05 (1.03,01.07)	<0.001	
Education level			<0.001			<0.001			0.321			0.481
Under high school	1.03 (1.03,1.04)	<0.001		1.03 (1.02,1.04)	<0.001		1.03(1.01,1.04)	<0.001		1.04 (1.01,1.06)	0.006	
High school	1.06 (1.05,1.07)	<0.001		1.07 (1.05,1.09)	<0.001		1.05(1.03,1.08)	<0.001		1.07 (1.02,1.13)	0.008	
Above high school	1.06 (1.05,1.07)	<0.001		1.03 (1.03,1.04)	<0.001		1.03(1.02,1.04)	<0.001		1.03 (1.02,1.05)	<0.001	

(Continued)

10.3389/fendo.2025.1534018

TABLE 3 Continued

Variables	All-cause mortality			Cardiovascular mortality			Cancer mortality			Diabetes mortality		
	HR (95%CI)	P for value	P for interaction	HR (95%CI)	P for value	P for interaction	HR (95%CI)	P for value	P for interaction	HR (95%CI)	P for value	P for interaction
Smoking			<0.001			<0.001			0.203			0.148
No	1.03 (1.02,1.03)	<0.001		1.03 (1.02,1.03)	<0.001		1.03(1.02,1.04)	<0.001		1.03 (1.01,1.05)	0.001	
Yes	1.04 (1.04,1.04)	<0.001		1.04 (1.03,1.05)	<0.001		1.03(1.02,1.04)	<0.001		1.05 (1.03,1.06)	<0.001	
Drinking			<0.001			<0.001			0.003			0.004
No	1.03 (1.02,1.03)	<0.001		1.02 (1.02,1.03)	<0.001		1.03(1.02,1.03)	<0.001		1.02 (1.01,1.04)	0.002	
Yes	1.07 (1.06,1.07)	<0.001		1.07 (1.06,1.08)	<0.001		1.05(1.04,1.07)	<0.001		1.08 (1.05,1.11)	<0.001	
BMI			<0.001			<0.001			<0.001			0.057
<25	1.08 (1.07,1.09)	<0.001		1.08 (1.06,1.09)	<0.001		1.07(1.05,1.09)	<0.001		1.09 (1.04,1.14)	<0.001	
25-30	1.03 (1.02,1.03)	<0.001		1.03 (1.02,1.03)	<0.001		1.03(1.02,1.03)	<0.001		1.03 (1.01,1.05)	<0.001	
≥ 30	1.06 (1.05,1.07)	<0.001		1.07 (1.05,1.08)	<0.001		1.03(1.00,1.06)	0.021		1.06 (1.02,1.11)	0.002	

BMI, body mass index; RBC, red blood cell; AST, aspartate transaminase; ALT, glutamic-pyruvic transaminase; TC, total cholesterol; BUN, blood urea nitrogen; HbA1c, glycosylated hemoglobin A1c; CHF, congestive heart failure; CHD, coronary heart disease; PIV, pan-immune- inflammation value; CI, confidence interval; HR, hazard ratios.

10.3389/fendo.2025.1534018

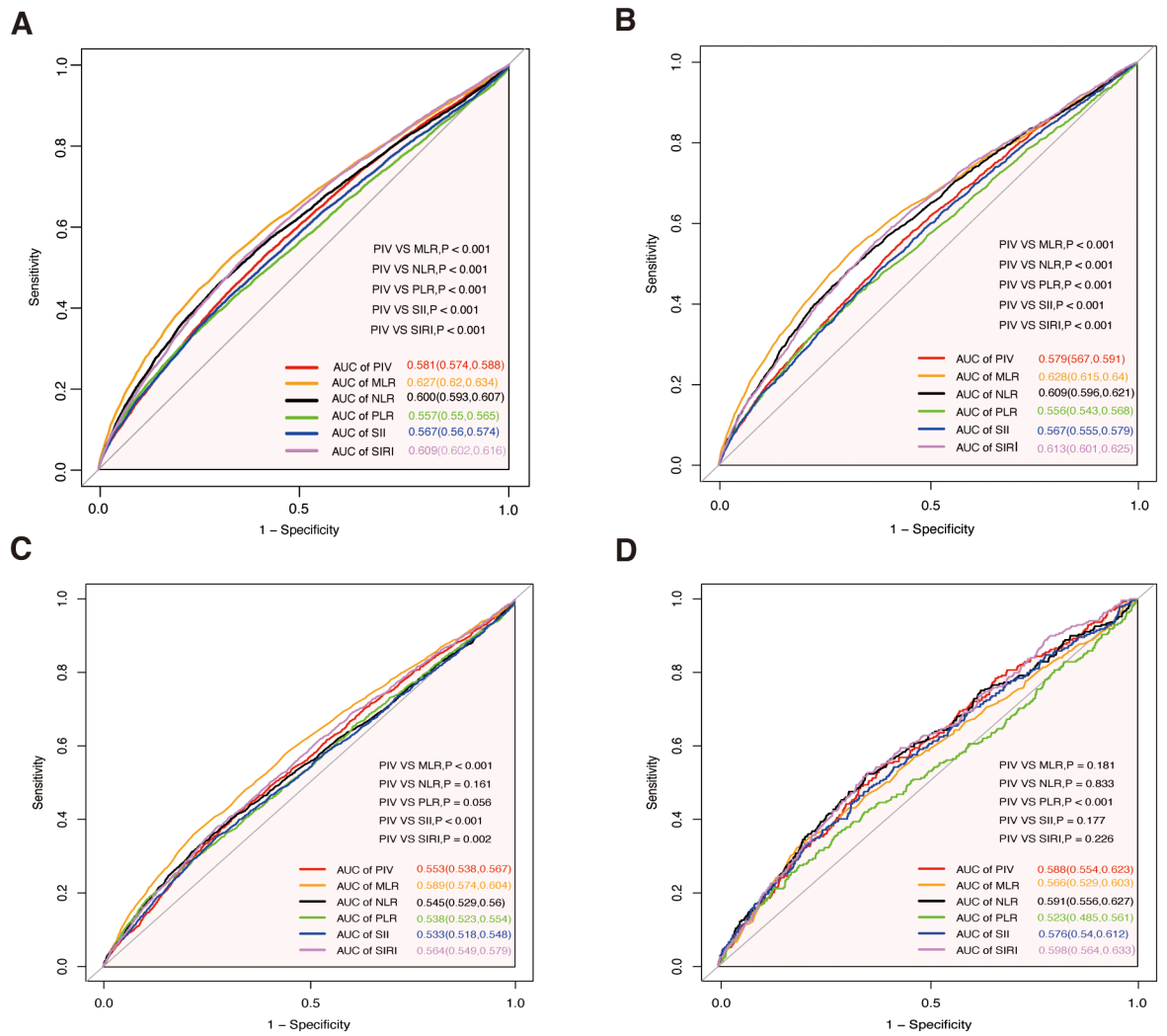

FIGURE 4
Receiver operating characteristic curves for PIV, MLR, NLR, PLR, SII, and SIRI in predicting all-cause and cause-specific mortality. **(A)** All-cause mortality. **(B)** Cardiovascular mortality. **(C)** Cancer mortality. **(D)** Diabetes mortality. MLR, monocyte-to-lymphocyte ratio; PLR, platelet-to-lymphocyte ratio; NLR, neutrophil-to-lymphocyte ratio; SII, systemic immune-inflammation index; SIRI, systemic inflammation response index; PIV, pan-immune- inflammation value; AUC, area under the curve.

(44). In critically ill patients with non-traumatic subarachnoid hemorrhage (SAH), elevated admission PIV is independently associated with increased mortality across ICU, in-hospital, 30-day, 90-day, and 1-year outcomes (45). For patients with fatty liver disease (FLD), Pan and colleagues demonstrated that PIV, alongside the SII, is closely associated with all-cause mortality, particularly highlighting its link to cardiovascular mortality (46). Jiang and colleagues further showed that PIV, rather than SII, is associated with the prevalence of NAFLD and hepatic fibrosis, particularly in individuals under 60, positioning it as a valuable marker for liver health (47). In hypertensive patients, Long and colleagues identified elevated PIV as a significant predictor of sarcopenia, especially in those with coexisting diabetes (48). Guo and colleagues reported that PIV, along with SII and SIRI, is inversely associated with cognitive performance in older adults, suggesting its potential as a biomarker for cognitive decline (49). Qiu and colleagues found that higher PIV levels are associated with increased COPD prevalence and all-cause mortality, with nonlinear relationships displaying a J-shaped association for prevalence and a U-shaped association for mortality risk (50). In the study by Tang et al (24), elevated levels of NLR, MLR, PLR, SII, SIRI, and PIV were positively associated with frailty risk in middle-aged and older adults, while lower PLR levels were inversely related. In frail individuals, all six inflammatory markers were linked to increased all-cause mortality, with MLR exhibiting the strongest predictive value. Among pre-frail individuals, elevated NLR, MLR, SII, SIRI, and PIV, alongside increased neutrophil counts, were associated with higher mortality risk, whereas higher lymphocyte counts were protective. Notably, a U-shaped relationship between NLR, MLR, SIRI, and PIV with mortality was observed in pre-frail individuals, where

excessively low or high levels increased mortality risk. The predictive superiority of MLR likely arises from its ability to reflect immune senescence, as elevated monocytes indicate systemic inflammation, and reduced lymphocytes represent immune dysfunction—both critical drivers of frailty progression and mortality. Our study aligns with the findings of Tang et al., demonstrating that MLR exhibits the highest predictive value for all-cause mortality risk. However, their research didn't extend to the investigation of other cause-specific mortality risks.

Taken together, these findings underscore the versatility and clinical relevance of PIV across diverse medical conditions, including liver disease, sarcopenia, cognitive decline, respiratory diseases, autoimmune disorders, sepsis, and others. PIV's ability to integrate systemic inflammation and immune dysregulation highlights its value as a robust biomarker for risk assessment and disease prognosis across various populations.

These findings underscore the versatility and clinical relevance of PIV across diverse medical conditions, including liver disease, sarcopenia, cognitive decline, respiratory diseases, autoimmune disorders, sepsis, and others. PIV's ability to integrate systemic inflammation and immune dysregulation highlights its value as a robust biomarker for risk assessment and disease prognosis across various populations.

While the precise mechanisms underlying PIV's prognostic value in various diseases remain uncertain, several explanations are emerging. Firstly, neutrophils, once considered straightforward immune defenders, are now understood to regulate diverse processes, including tissue repair, cancer progression, autoimmunity, and chronic inflammation. Low neutrophil levels can lead to severe immunodeficiency, while their excessive activation can damage host tissues (51). In cancer, neutrophils release VEGF, IL-6, and MMPs, which promote angiogenesis, tumor growth, and metastasis (52). However, they also suppress adaptive immunity by inhibiting T-cell activity through nitric oxide and reactive oxygen species (ROS), enabling tumor immune evasion (53). In ischemic heart failure, neutrophils initially assist in cardiac repair by initiating inflammation and clearing necrotic myocardial debris, but prolonged activation may lead to chronic inflammation, impairing cardiac function (54). Secondly, platelets are known for their complex roles in both physiological and pathological conditions. Beyond hemostasis and thrombosis, platelets regulate immune responses, chronic inflammation, and disease progression. In sterile inflammation (e.g., atherosclerosis), platelets bind damage-associated molecular patterns (DAMPs), activate signaling pathways such as MAPK and NF-κB, and release potent inflammatory mediators like HMGB1 (55, 56) Additionally, they interact with bacteria, initiate immune responses, and release inflammatory mediators through Toll-like receptors (TLRs), aiding in pathogen defense (55) Platelets also play a crucial role in cancer metastasis by cloaking circulating tumor cells, promoting endothelial adhesion, and facilitating tumor invasion and metastasis (57, 58). Thirdly, monocytes play central roles in immune defense and inflammation. Classical monocytes are recruited to infection and inflammation sites via the CCL2/CCR2 pathway, releasing cytokines like TNF-α and iNOS to kill pathogens and enhance adaptive immunity. while non-classical monocytes patrol the vascular endothelium to monitor for tissue injury via the CX3CL1/CX3CR1 axis. In conditions like atherosclerosis, monocytes differentiate into foam cells, sustaining chronic inflammation and plaque formation (59). In tumors, monocytes differentiate into tumor-associated macrophages (TAMs), which promote immunosuppression and angiogenesis, allowing tumor cells to evade immune surveillance (60). Lastly, lymphocytes are pivotal in immune surveillance and inflammation. In chronic inflammation, such as atherosclerosis, lymphocytes mediate immune responses against pathogens and contribute to tissue repair, though excessive activity can exacerbate inflammation and tissue damage (61–63). Within tumors, tumor-infiltrating lymphocytes (TILs) recognize and kill cancer cells, particularly in high mutation-load cancers (64, 65). Conversely, lymphopenia—a low lymphocyte count—is linked with poor outcomes, reflecting impaired immune competence and heightened disease susceptibility (66). Overall, these mechanisms highlight PIV's potential to capture the complex interplay between immunity and inflammation across diverse diseases.

Our findings underscore a significant association between PIV and various mortality outcomes. We observed a dose-dependent increase in the risk of all-cause, cardiovascular, cancer, and diabetes-related mortality with elevated PIV levels. Even after adjusting for potential confounders, high PIV levels remained consistently associated with increased mortality risks. Kaplan-Meier survival curves further validated these disparities across PIV quartiles, demonstrating that individuals with higher PIV indices had markedly elevated long-term mortality risks. Notably, restricted cubic spline analysis revealed nonlinear dose-response relationships between PIV and all-cause, cardiovascular, and cancer mortality. Specifically, when PIV levels were below 254.07, no significant association with mortality risk was observed, but once this threshold was exceeded, the risks rose sharply. This threshold effect suggests that while low PIV levels may have minimal impact, elevated PIV could play a critical role in disease progression. Sensitivity and subgroup analyses reinforced the robustness of these associations, underscoring PIV's potential as a reliable prognostic marker across diverse populations.

Additionally, our findings highlight the comparative predictive efficiency of PIV against other inflammatory markers in mortality risk assessment. ROC curve analyses demonstrated that PIV provides reasonable predictive performance for all-cause, cardiovascular, cancer, and diabetes-related mortality. Notably, PIV outperformed simpler markers such as PLR and SII, emphasizing its greater utility in reflecting systemic inflammatory responses. However, its predictive capability was surpassed by more comprehensive indices, including MLR, NLR, and SIRI, which likely integrate broader aspects of inflammatory and immune dynamics. For cancer mortality, PIV exhibited comparable performance to NLR and PLR but was inferior to MLR and SIRI, suggesting that

composite indices may better capture the complexity of inflammation-driven processes in cancer progression. Similarly, for diabetes-related mortality, PIV demonstrated consistent and comparable predictive performance relative to other markers, further supporting its reliability in specific contexts. Taken together, these findings highlight PIV as a practical and accessible prognostic marker with considerable potential for mortality risk stratification. However, the superior performance of MLR, NLR, and SIRI indicates that combining PIV with complementary markers could enhance predictive accuracy. Future studies should prioritize investigating the synergistic use of PIV alongside other inflammatory indices to improve risk stratification and inform clinical decision-making across diverse populations and mortality outcomes.

In this study, we conducted a comprehensive comparison of baseline characteristics between participants who were excluded and those included in the final analysis (Supplementary Table S5). Significant differences were observed in various demographic, clinical, and laboratory parameters, including age, race, educational attainment, family income-to-poverty ratio, smoking behavior, marital status, BMI, and laboratory measurements such as RBC count, lymphocyte count, platelet count, hemoglobin, ALT, TC, BUN, uric acid, creatinine, albumin, and HbA1c. Additionally, differences were notable in the prevalence of comorbidities, such as kidney disease, CHF, CHD, heart attack, stroke, and cancer, as well as in causes of mortality. Conversely, no significant differences were identified in gender, WBC count, neutrophil count, monocyte count, AST levels, or in the prevalence of angina pectoris, liver disease, hypertension, diabetes, and follow-up duration. Furthermore, inflammatory markers, including NLR, PLR, SII, and PIV, also showed no significant differences between the two groups. We recognize the potential for selection bias arising from these differences. To address this, we employed rigorous statistical adjustments, incorporating a variety of confounding variables into our analysis. Multiple models were constructed to validate the consistency and reliability of our findings, all of which demonstrated concordant trends. Despite the inherent limitations in sample selection, the robustness of our results underscores the credibility of our conclusions. This study provides a strong foundation for future research exploring the clinical relevance of PIV and related outcomes in diverse populations.

Our findings also have important clinical implications. First, as a composite biomarker derived from routine complete blood count (CBC) parameters, PIV is a cost-effective, readily available, and non-invasive marker that can be easily applied in daily clinical practice, including in primary care and resource-limited settings. Second, given its strong association with all-cause and cause-specific mortality, PIV may serve as an effective tool for early identification of individuals at high risk of adverse outcomes, who may benefit from targeted preventive interventions and more intensive clinical monitoring. For instance, individuals with elevated PIV levels could be prioritized for cardiovascular risk management, cancer screening, or metabolic evaluations. Third, since PIV reflects both innate and adaptive immune responses, as well as systemic inflammation, it offers a broader perspective on the overall immune-inflammatory status than traditional indices such as NLR or PLR, supporting its potential role in comprehensive risk stratification models. Furthermore, considering the dynamic nature of inflammation, repeated assessments of PIV over time may help monitor disease progression and evaluate treatment responses. Lastly, integrating PIV with other clinical information, including comorbidities, lifestyle factors, and biochemical markers, could improve personalized risk prediction and support clinical decision-making in preventive and therapeutic strategies. Further prospective and interventional studies are warranted to validate these clinical applications and to establish optimal PIV thresholds for risk stratification and clinical management.

Strengths, limitations, and future directions

Our study, leveraging a large cohort and extensive follow-up, provided valuable insights into the association between PIV and mortality outcomes, including all-cause, cardiovascular, cancer, and diabetes-related mortality in the general population. The use of restricted cubic spline models enabled us to explore nonlinear relationships between PIV and mortality, revealing nuanced dose-response patterns and potential threshold effects.

However, several limitations warrant discussion. This study is cross-sectional in design, which inherently limits its ability to establish causal relationships between PIV and mortality outcomes. While the observed associations provide valuable insights, the lack of longitudinal data prevents us from fully elucidating the temporal dynamics and causal pathways underlying these relationships. This limitation is particularly relevant given the multifactorial nature of inflammation and its interactions with mortality risks over time. First and foremost, PIV was measured only at baseline, which restricts our ability to capture dynamic changes in inflammatory status during follow-up. Inflammation is a highly variable and dynamic process, and the absence of longitudinal PIV measurements may obscure important temporal trends or fluctuations that could further clarify its association with mortality. For instance, repeated measures of PIV could reveal patterns of sustained inflammation or fluctuations that are more predictive of adverse outcomes. Future studies should consider incorporating multiple PIV assessments at different time points to better evaluate its trajectory and time-dependent predictive value. Second, baseline data on complications and lifestyle factors were self-reported, which introduces the potential for recall bias and inaccuracies in the data. This limitation may have impacted the reliability of certain variables, particularly those related to behavioral factors or self-perceived health conditions. Future research should prioritize the use of objective, validated measures and standardized data collection protocols to minimize these biases and enhance the reliability of

findings. Third, while we adjusted for a wide range of potential confounders, there is always the possibility of residual confounding from unmeasured variables. Factors such as genetic predisposition, environmental exposures, access to healthcare, and specific treatments during follow-up may have influenced our results. Addressing these unmeasured variables in future research through more comprehensive data collection and advanced statistical techniques, such as causal inference models, will be critical. Finally, the generalizability of our findings is limited by the single-cohort design and population characteristics. The results may not fully reflect the diverse inflammatory and mortality profiles present across different regions or healthcare systems.

To address these limitations, future research should focus on several key areas. First, well-designed longitudinal cohort studies with repeated PIV measurements are warranted to capture the dynamic changes in inflammatory status over time and to better elucidate the temporal relationship between PIV fluctuations and mortality outcomes. These studies should explore whether persistent elevation or changes in PIV trajectories are more predictive of adverse outcomes compared to single baseline measurements. Second, further investigation is needed to determine optimal PIV cut-off values for risk stratification in diverse populations, considering differences in age, sex, ethnicity, and comorbid conditions, to enhance its clinical applicability. Third, mechanistic studies incorporating multi-omics approaches, including transcriptomics, proteomics, and metabolomics, could provide deeper insights into the biological pathways linking PIV with systemic inflammation and disease progression. Fourth, intervention-based studies, such as randomized controlled trials, should assess whether modulating systemic inflammation to reduce PIV levels can translate into improved clinical outcomes, thereby establishing PIV not only as a prognostic biomarker but also as a potential target for therapeutic interventions. Additionally, future studies should integrate PIV with advanced analytical techniques, including artificial intelligence and machine learning models, to develop robust, individualized prediction tools that can dynamically assess risk based on PIV trajectories and other clinical parameters. Finally, large multi-center and international studies are essential to validate the generalizability of PIV and to facilitate its integration into global clinical practice guidelines.

Despite these limitations, our study highlights the significant prognostic value of PIV as a biomarker for mortality risks. It provides a robust foundation for future investigations into inflammation-based risk stratification, paving the way for large-scale, longitudinal, and multi-center studies to further elucidate the clinical utility of PIV in predicting diverse mortality outcomes.

Conclusion

The PIV is a robust and versatile biomarker that integrates inflammation and immune status, providing valuable insights into disease progression, treatment response, and patient outcomes. Its prognostic utility has been demonstrated across various diseases, including cancer, cardiovascular conditions, autoimmune disorders, and infectious diseases. The individual contributions of neutrophils, platelets, monocytes, and lymphocytes reflect the intricate dynamics driving disease progression, underscoring the clinical relevance of PIV. As research advances, PIV holds substantial promise for personalized medicine, enabling clinicians to optimize treatment strategies, improve patient outcomes, and enhance healthcare delivery.

Data availability statement

The raw data supporting the conclusions of this article will be made available by the authors, without undue reservation.

Ethics statement

The studies involving human participants were approved by the Institutional Review Boards of the Massachusetts Institute of Technology (Cambridge, MA, USA) and Beth Israel Deaconess Medical Center (Boston, MA, USA). All procedures were conducted in compliance with local legislation and institutional requirements. Written informed consent for participation was not obtained from participants or their legal guardians/next of kin because, under national legislation and institutional guidelines, written informed consent was not required for this study. The studies were conducted in accordance with the local legislation and institutional requirements. The participants provided their written informed consent to participate in this study. Written informed consent was obtained from the individual(s) for the publication of any potentially identifiable images or data included in this article.

Author contributions

YZ: Conceptualization, Data curation, Formal Analysis, Funding acquisition, Investigation, Methodology, Project administration, Resources, Software, Supervision, Validation, Visualization, Writing – original draft, Writing – review & editing. YY: Conceptualization, Data curation, Formal Analysis, Funding acquisition, Investigation, Methodology, Project administration, Resources, Software, Supervision, Validation, Visualization, Writing – original draft, Writing – review & editing. ZS: Formal Analysis, Methodology, Software, Writing – original draft, Writing – review & editing. PL: Formal Analysis, Methodology, Software, Writing – original draft, Writing – review & editing. XW: Data curation, Software, Writing – original draft, Writing – review & editing. GC: Data curation, Software, Writing – original draft, Writing – review & editing. HH: Data curation, Software, Writing – original draft, Writing – review & editing. ZL: Data curation, Software, Writing – original draft, Writing – review & editing.

Funding

The author(s) declare that no financial support was received for the research and/or publication of this article.

Conflict of interest

The authors declare that this research was conducted without any commercial or financial relationships that could be interpreted as a potential conflict of interest.

Generative AI statement

The author(s) declare that no Generative AI was used in the creation of this manuscript.

Publisher's note

Supplementary material

The Supplementary Material for this article can be found online at: https://www.frontiersin.org/articles/10.3389/fendo.2025.1534018/full#supplementary-material

References

1. Medzhitov R. Origin and physiological roles of inflammation. *Nature*. (2008) 454:428–35. doi: 10.1038/nature07201

2. Diakos CI, Charles KA, McMillan DC, Clarke SJ. Cancer-related inflammation and treatment effectiveness. *Lancet Oncol*. (2014) 15:e493–503. doi: 10.1016/S1470-2045(14)70263-3

3. Frostegard J. Immunity, atherosclerosis and cardiovascular disease. *BMC Med*. (2013) 11:117. doi: 10.1186/1741-7015-11-117

4. Hotamisligil GS. Inflammation, metaflammation and immunometabolic disorders. *Nature*. (2017) 542:177–85. doi: 10.1038/nature21363

5. Karam BS, Chavez-Moreno A, Koh W, Akar JG, Akar FG. Oxidative stress and inflammation as central mediators of atrial fibrillation in obesity and diabetes. *Cardiovasc Diabetol*. (2017) 16(1):120. doi: 10.1186/s12933-017-0604-9

6. Kotas ME, Medzhitov R. Homeostasis, inflammation, and disease susceptibility. *Cell*. (2015) 160:816–27. doi: 10.1016/j.cell.2015.02.010

7. Lee YS, Olefsky J. Chronic tissue inflammation and metabolic disease. *Genes Dev*. (2021) 35:307–28. doi: 10.1101/gad.346312.120

8. Gavriilidis P, Pawlik TM. Inflammatory indicators such as systemic immune inflammation index (SIII), systemic inflammatory response index (SIRI), neutrophil-to-lymphocyte ratio (NLR) and platelet-to-lymphocyte ratio (PLR) as prognostic factors of curative hepatic resections for hepatocellular carcinoma. *Hepatobil Surg Nutr*. (2024) 13:509–11. doi: 10.21037/hbsn-23-631

9. Murat B, Murat S, Ozgeyik M, Bilgin M. Comparison of pan-immune-inflammation value with other inflammation markers of long-term survival after ST-segment elevation myocardial infarction. *Eur J Clin Invest*. (2023) 53(1):e13872. doi: 10.1111/eci.13872

10. Wang RH, Wen WX, Jiang ZP, Du ZP, Ma ZH, Lu AL, et al. The clinical value of neutrophil-to-lymphocyte ratio (NLR), systemic immune-inflammation index (SII), platelet-to-lymphocyte ratio (PLR) and systemic inflammation response index (SIRI) for predicting the occurrence and severity of pneumonia in patients with intracerebral hemorrhage. *Front Immunol*. (2023) 14:1115031. doi: 10.3389/fimmu.2023.1115031

11. Yi C, Zhou YN, Guo J, Chen J, She X. Novel predictors of intravenous immunoglobulin resistance in patients with Kawasaki disease: a retrospective study. *Front Immunol*. (2024) 15. doi: 10.3389/fimmu.2024.1399150

12. Yu HJ, Ren Y, Xia JQ. Prognostic significance of the pretreatment pan-immune-inflammation value in cancer patients: an updated meta-analysis of 30 studies. *Front Nutr*. (2023) 10:1259929. doi: 10.3389/fnut.2023.1259929

13. Zinellu A, Zinellu E, Mangoni AA, Pau MC, Carru C, Pirina P, et al. Clinical significance of the neutrophil-to-lymphocyte ratio and platelet-to-lymphocyte ratio in acute exacerbations of COPD: present and future. *Eur Respir Rev*. (2022) 31 (166):220095. doi: 10.1183/16000617.0095-2022

14. Nassri A, Muftah M, Nassri R, Fialho A, Fialho A, Ribeiro B, et al. Novel inflammatory-nutritional biomarkers as predictors of histological activity in crohn's disease. *Clin Lab*. (2020) 66:1173–81. doi: 10.7754/Clin.Lab.2019.190816

15. Xia YY, Xia CL, Wu LD, Li Z, Li H, Zhang JX. Systemic immune inflammation index (SII), system inflammation response index (SIRI) and risk of all-cause mortality and cardiovascular mortality: A 20-year follow-up cohort study of 42,875 US adults. *J Clin Med*. (2023) 12(3):1128. doi: 10.3390/jcm12031128

16. Cao Y, Li PX, Zhang Y, Qiu MH, Li J, Ma SC, et al. Association of systemic immune inflammatory index with all-cause and cause-specific mortality in hypertensive individuals: Results from NHANES. *Front Immunol*. (2023) 14. doi: 10.3389/fimmu.2023.1087345

17. Wang H, Nie HY, Bu G, Tong XN, Bai XF. Systemic immune-inflammation index (SII) and the risk of all-cause, cardiovascular, and cardio-cerebrovascular mortality in the general population. *Eur J Med Res*. (2023) 28(1):575. doi: 10.1186/s40001-023-01529-1

18. Wang PB, Guo XF, Zhou Y, Li Z, Yu SS, Sun YX, et al. Monocyte-to-high-density lipoprotein ratio and systemic inflammation response index are associated with the risk of metabolic disorders and cardiovascular diseases in general rural population. *Front Endocrinol*. (2022) 13. doi: 10.3389/fendo.2022.944991

19. Fucà G, Guarini V, Antoniotti C, Morano F, Moretto R, Corallo S, et al. The Pan-Immune-Inflammation Value is a new prognostic biomarker in metastatic colorectal cancer: results from a pooled-analysis of the and TRIBE first-line trials. *Brit J Cancer*. (2020) 123:403–9. doi: 10.1038/s41416-020-0894-7

20. Karadag I, Karakaya S, Yilmaz ME, Öksüzoglu OBC. The potential prognostic novel markers PIV and PILE score to predict survival outcomes at hepatocellular cancer. *Eur Rev Med Pharmacol Sci*. (2022) 26:7679–86. doi: 10.26355/eurrev_202210_30044

21. Lin F, Zhang LP, Xie SY, Huang HY, Chen XY, Jiang TC, et al. Pan-immune-inflammation value: A new prognostic index in operative breast cancer. *Front Oncol*. (2022) 12. doi: 10.3389/fonc.2022.830138

22. Johnson CL, Dohrmann SM, Burt VL, Mohadjer LK. National health and nutrition examination survey: sample design, 2011-2014. *Vital Health Stat*. (2014) 2:1–33.

23. Zipf G, Chiappa M, Porter KS, Ostchega Y, Lewis BG, Dostal J. National health and nutrition examination survey: plan and operations, 1999-2010. *Vital Health Stat*. (2013) 1:1–37.

24. Tang Y, Zhai Y, Song W, Zhu T, Xu Z, Jiang L, et al. Association between complete blood count-derived inflammatory markers and the risk of frailty and mortality in middle-aged and older adults. *Front Public Health*. (2024) 12:1427546. doi: 10.3389/fpubh.2024.1427546

25. VanderWeele TJ, Ding P. Sensitivity analysis in observational research: introducing the E-value. *Ann Intern Med*. (2017) 167:268–+. doi: 10.7326/M16-2607

26. Austin PC, White IR, Lee DS, van Buuren S. Missing data in clinical research: A tutorial on multiple imputation. *Can J Cardiol*. (2021) 37:1322–31. doi: 10.1016/j.cjca.2020.11.010

27. White IR, Royston P, Wood AM. Multiple imputation using chained equations: Issues and guidance for practice. *Stat Med*. (2011) 30:377–99. doi: 10.1002/sim.v30.4

28. Topkan E, Selek U, Kucuk A, Pehlivan B. Low pre-chemoradiotherapy pan-immune-inflammation value (PIV) measures predict better survival outcomes in locally advanced pancreatic adenocarcinomas. *J Inflammation Res*. (2022) 15:5413–23. doi: 10.2147/JIR.S385328

29. Liu QH, Wang HH, Chen QJ, Luo RY, Luo CJ. Nomogram incorporating preoperative pan-immune-inflammation value and monocyte to high-density lipoprotein ratio for survival prediction in patients with colorectal cancer: a retrospective study. *BMC Cancer*. (2024) 24(1):74. doi: 10.1186/s12885-024-12509-x

30. Zhao HZ, Chen XY, Zhang WH, Cheng D, Lu YJ, Wang C, et al. Pan-immune-inflammation value is associated with the clinical stage of colorectal cancer. *Front Surg.* (2022) 9. doi: 10.3389/fsurg.2022.996844

31. Lei WQ, Wang W, Qin SX, Yao WR. Predictive value of inflammation and nutritional index in immunotherapy for stage IV non-small cell lung cancer and model construction. *Sci Rep-Uk.* (2024) 14(1):11751. doi: 10.1038/s41598-024-66813-4

32. Zeng R, Liu F, Fang C, Yang J, Luo LF, Yue P, et al. PIV and PILE score at baseline predict clinical outcome of anti-PD-1/PD-L1 inhibitor combined with chemotherapy in extensive-stage small cell lung cancer patients. *Front Immunol.* (2021) 12. doi: 10.3389/fimmu.2021.724443

33. Liao WJ, Li J, Feng WY, Kong WA, Shen YJ, Chen ZJ, et al. Pan-immune-inflammation value: a new prognostic index in epithelial ovarian cancer. *BMC Cancer.* (2024) 24(1):1052. doi: 10.1186/s12885-024-12809-2

34. Feng JF, Wang L, Yang X, Chen QX, Cheng XD. Pretreatment pan-immune-inflammation value (PIV) in predicting therapeutic response and clinical outcomes of neoadjuvant immunochemotherapy for esophageal squamous cell carcinoma. *Ann Surg Oncol.* (2024) 31:272–83. doi: 10.1245/s10434-023-14430-2

35. Gasparri ML, Albasini S, Truffi M, Favilla K, Tagliaferri B, Piccotti F, et al. Low neutrophil-to-lymphocyte ratio and pan-immune-inflammation-value predict nodal pathologic complete response in 1274 breast cancer patients treated with neoadjuvant chemotherapy: a multicenter analysis. *Ther Adv Med Oncol.* (2023) 15:17588359231193732. doi: 10.1177/17588359231193732

36. Cheng HW, Wang T, Yu GC, Xie LY, Shi B. Prognostic role of the systemic immune-inflammation index and pan-immune inflammation value for outcomes of breast cancer: a systematic review and meta-analysis. *Eur Rev Med Pharmacol Sci.* (2024) 28:180–90. doi: 10.26355/eurrev_202401_34903

37. Topkan E, Kucuk A, Selek U. Pretreatment pan-immune-inflammation value efficiently predicts survival outcomes in glioblastoma multiforme patients receiving radiotherapy and temozolomide. *J Immunol Res.* (2022) 2022:1346094. doi: 10.1155/2022/1346094

38. Corti F, Lonardi S, Intini R, Salati M, Fenocchio E, Belli C, et al. The Pan-Immune-Inflammation Value in microsatellite instability-high metastatic colorectal cancer patients treated with immune checkpoint inhibitors. *Eur J Cancer.* (2021) 150:155–67. doi: 10.1016/j.ejca.2021.03.043

39. Yang YT, Hu F, Wu S, Huang ZL, Wei K, Ma Y, et al. Blood-based biomarkers: diagnostic value in brain tumors (focus on gliomas). *Front Neurol.* (2023) 14. doi: 10.3389/fneur.2023.1297835

40. Gambichler T, Said S, Abu Rached N, Scheel CH, Susok L, Stranzenbach R, et al. Pan-immune-inflammation value independently predicts disease recurrence in patients with Merkel cell carcinoma. *J Cancer Res Clin.* (2022) 148:3183–9. doi: 10.1007/s00432-022-03929-y

41. Wu B, Zhang CL, Lin SQ, Zhang YB, Ding S, Song W. The relationship between the pan-immune-inflammation value and long-term prognoses in patients with hypertension: National Health and Nutrition Examination Study, 1999-2018. *Front Cardiovasc Med.* (2023) 10. doi: 10.3389/fcvm.2023.1099427

42. Gambichler T, Numanovic Z, Apel I, Hessam S, Susok L, Xenofon B, et al. Do novel inflammation biomarkers arising from routine complete blood count play a role in patients with systemic lupus erythematosus? *Lupus.* (2024) 33(14):1556–61. doi: 10.1177/09612033241295865

43. Tutan D, Dogan AG. Pan-immune-inflammation index as a biomarker for rheumatoid arthritis progression and diagnosis. *Cureus J Med Sci.* (2023) 15(10): e46609. doi: 10.7759/cureus.46609

44. Xu HB, Xu YH, He Y, Lin XH, Suo ZJ, Shu HQ, et al. Association between admission pan-immune-inflammation value and short-term mortality in septic patients: a retrospective cohort study. *Sci Rep-Uk.* (2024) 14(1):15205. doi: 10.1038/s41598-024-66142-6

45. Huang YW, Zhang Y, Li ZP, Yin XS. Association between a four-parameter inflammatory index and all-cause mortality in critical ill patients with non-traumatic subarachnoid hemorrhage: a retrospective analysis of the MIMIC-IV database (2012-2019). *Front Immunol.* (2023) 14. doi: 10.3389/fimmu.2023.1235266

46. Pan X, Lv J, Liu M, Li Y, Zhang Y, Zhang R, et al. Chronic systemic inflammation predicts long-term mortality among patients with fatty liver disease: Data from the National Health and Nutrition Examination Survey 2007-2018. *PloS One.* (2024) 19: e0312877. doi: 10.1371/journal.pone.0312877

47. Jiang R, Hua Y, Hu X, Hong Z. The pan immune inflammatory value in relation to non-alcoholic fatty liver disease and hepatic fibrosis. *Clin Res Hepatol Gastroenterol.* (2024) 48:102393. doi: 10.1016/j.clinre.2024.102393

48. Long L, Xiong B, Luo Z, Yang H, She Q. Association between pan-immune inflammation value and sarcopenia in hypertensive patients, NHANES 1999-2018. *J Clin Hypertens (Greenwich).* (2025) 27(1):e14944. doi: 10.1111/jch.14944

49. Guo Z, Zheng Y, Geng J, Wu Z, Wei T, Shan G, et al. Unveiling the link between systemic inflammation markers and cognitive performance among older adults in the US: A population-based study using NHANES 2011–2014 data. *J Clin Neurosci.* (2024) 119:45–51. doi: 10.1016/j.jocn.2023.11.004

50. Qiu S, Jiang Q, Li Y. The association between pan-immune-inflammation value and chronic obstructive pulmonary disease: data from NHANES 1999-2018. *Front Physiol.* (2024) 15:1440264. doi: 10.3389/fphys.2024.1440264

51. Liew PX, Kubes P. The neutrophil's role during health and disease. *Physiol Rev.* (2019) 99:1223–48. doi: 10.1152/physrev.00012.2018

52. Ocana A, Nieto-Jimenez C, Pandiella A, Templeton AJ. Neutrophils in cancer: prognostic role and therapeutic strategies. *Mol Cancer.* (2017) 16:137. doi: 10.1186/s12943-017-0707-7

53. Jaillon S, Ponzetta A, Di Mitri D, Santoni A, Bonecchi R, Mantovani A. Neutrophil diversity and plasticity in tumour progression and therapy. *Nat Rev Cancer.* (2020) 20:485–503. doi: 10.1038/s41568-020-0281-y

54. Kain V, Halade GV. Role of neutrophils in ischemic heart failure. *Pharmacol Therapeut.* (2020) 205:107424. doi: 10.1016/j.pharmthera.2019.107424

55. Thomas MR, Storey RF. The role of platelets in inflammation. *Thromb Haemost.* (2015) 114:449–58. doi: 10.1160/TH14-12-1067

56. Khodadi E. Platelet function in cardiovascular disease: activation of molecules and activation by molecules. *Cardiovasc Toxicol.* (2020) 20:1–10. doi: 10.1007/s12012-019-09555-4

57. Schlesinger M. Role of platelets and platelet receptors in cancer metastasis. *J Hematol Oncol.* (2018) 11:125. doi: 10.1186/s13045-018-0669-2

58. Franco AT, Corken A, Ware J. Platelets at the interface of thrombosis, inflammation, and cancer. *Blood.* (2015) 126:582–8. doi: 10.1182/blood-2014-08-531582

59. Shi C, Pamer EG. Monocyte recruitment during infection and inflammation. *Nat Rev Immunol.* (2011) 11:762–74. doi: 10.1038/nri3070

60. Huang CB, Li ZX, Li N, Li Y, Chang AT, Zhao TS, et al. Interleukin 35 expression correlates with microvessel density in pancreatic ductal adenocarcinoma, recruits monocytes, and promotes growth and angiogenesis of xenograft tumors in mice. *Gastroenterology.* (2018) 154:675–88. doi: 10.1053/j.gastro.2017.09.039

61. Wang J, Duan Y, Sluijter JP, Xiao J. Lymphocytic subsets play distinct roles in heart diseases. *Theranostics.* (2019) 9:4030–46. doi: 10.7150/thno.33112

62. Sakai Y, Kobayashi M. Lymphocyte "homing' and chronic inflammation. *Pathol Int.* (2015) 65:344–54. doi: 10.1111/pin.2015.65.issue-7

63. Epelman S, Liu PP, Mann DL. Role of innate and adaptive immune mechanisms in cardiac injury and repair. *Nat Rev Immunol.* (2015) 15:117–29. doi: 10.1038/nri3800

64. Lin B, Du L, Li H, Zhu X, Cui L, Li X. Tumor-infiltrating lymphocytes: Warriors fight against tumors powerfully. *BioMed Pharmacother.* (2020) 132:110873. doi: 10.1016/j.biopha.2020.110873

65. Monberg TJ, Borch TH, Svane IM, Donia M. TIL therapy: facts and hopes. *Clin Cancer Res.* (2023) 29:3275–83. doi: 10.1158/1078-0432.CCR-22-2428

66. Wu ES, Oduyebo T, Cobb LP, Cholakian D, Kong XR, Fader AN, et al. Lymphopenia and its association with survival in patients with locally advanced cervical cancer. *Gynecol Oncol.* (2016) 140:76–82. doi: 10.1016/j.ygyno.2015.11.013

frontiers | Frontiers in Endocrinology

TYPE Original Research
PUBLISHED 15 May 2025
DOI 10.3389/fendo.2025.1460218

OPEN ACCESS

EDITED BY
Sijung Yun,
Predictiv Care, Inc., United States

REVIEWED BY
Hong Zan,
Prellis Biologics, United States
Eloi Franco-Trepat,
IrsiCaixa, Spain

*CORRESPONDENCE
Xia Pan
762757384@qq.com
Tianwang Li
litian-wang@163.com
Yukai Huang
348855048@qq.com

†These authors have contributed equally to this work

RECEIVED 05 July 2024
ACCEPTED 10 April 2025
PUBLISHED 15 May 2025

CITATION
Ji Z, Zheng S, Liang L, Huang L, Sun S, Huang Z, He Y, Pan X, Li T and Huang Y (2025) TMT-based quantitative proteomics analysis of serum-derived exosomes in patients with juvenile gout. *Front. Endocrinol.* 16:1460218. doi: 10.3389/fendo.2025.1460218

TMT-based quantitative proteomics analysis of serum-derived exosomes in patients with juvenile gout

Zhuyi Ji[3,1†], Shaoling Zheng[1†], Ling Liang[4†], Lixin Huang[1†], Shanmiao Sun[1], Zhixiang Huang[1], Yuebing He[1], Xia Pan[1*], Tianwang Li[1,2*] and Yukai Huang[1*]

[1]The Affiliated Guangdong Second Provincial General Hospital of Jinan University, Guangzhou, China, [2]Department of Rheumatology and Immunology, Zhaoqing Central People's Hospital, Zhaoqing, China, [3]Department of Rheumatology and Immunology, The Third People's Hospital of Chengdu, Chengdu, China, [4]The Second Affiliated Hospital, Guangzhou Medical University, Guangzhou, China

Objectives: The purpose of this study was to compare the proteomics of serum-derived exosomes in juvenile gout (J-Gout), juvenile hyperuricemia (J-HUA) and oligoarticular juvenile idiopathic arthritis (oJIA).

Methods: Serum-derived exosomes were isolated from patients using a qEV column combined with the ExoQuick-TC kit. The proteomics of serum-derived exosomes was analyzed by tandem mass tag (TMT)-labeled liquid chromatography-mass spectrometry (LC-MS/MS) technology. Proteins differentially expressed in J-Gout and the other two groups were identified. This was followed by volcano plot, hierarchical cluster, Venn diagram, gene ontology (GO), and Kyoto Encyclopedia of Genes and Genome (KEGG) pathway analyses.

Results: A total of 838 credible proteins were identified in serum-derived exosomes from the three groups. Eighty-eight differentially expressed proteins (13 upregulated and 75 downregulated) were identified in J-Gout when compared with J-HUA. One hundred twenty-one differentially expressed proteins (20 upregulated and 101 downregulated) were identified in J-Gout when compared with oJIA. A total of 166 differentially expressed proteins were identified in J-Gout, compared with J-HUA and oJIA respectively. Bioinformatic analysis indicated that the 166 differentially expressed proteins were significantly involved in "immune response", "Fc epsilon RI signaling pathway" and "B cell receptor signaling pathway". A total of 43 differentially expressed proteins were identified in J-Gout, compared with J-HUA and oJIA simultaneously. Six proteins were found highly expressed in J-Gout uniquely. ELISA results showed that dipeptidyl peptidase 4 (DPP4) and heparin cofactor 2 (SERPIND1) were the highest in J-Gout, which was consistent with the proteomic results. Correlation analysis revealed that exosome-derived DPP4 and SERPIND1 were positively correlated with C-reactive protein (CRP) and erythrocyte sedimentation rate (ESR).

Conclusion: The protein composition of serum-derived exosomes in J-Gout was significantly differed from that in J-HUA and oJIA. DPP4 and SERPIND1 were uniquely highly expressed in J-Gout. Some possible mechanisms regarding the inflammatory response and coagulation complement system were proposed, which may provide helpful diagnostic and therapeutic insights for J-Gout.

KEYWORDS

juvenile gout, exosomes, TMT, proteomics, biomarker

1 Introduction

Gout is an inflammatory form of arthritis that can be attributed to monosodium urate (MSU) deposition resulting from hyperuricemia (1). Recent data suggest that the incidence and prevalence of juvenile gout (J-Gout) are increasing, and childhood obesity parallels the increased incidence of gout at younger ages (2, 3). A survey based on Chinese children and adolescents showed an overall prevalence of hyperuricemia of 23.3% (4). At present, few studies exploring J-Gout have been conducted, and many challenges still exist in J-Gout diagnosis and treatment. A previous study showed that compared with adult gout, J-Gout has a higher average level of serum uric acid and faster progression of joint destruction (5). In addition, most J-Gout patients meet the diagnostic criteria for juvenile idiopathic arthritis (JIA), especially oligoarticular juvenile idiopathic arthritis (oJIA) (6). Therefore, it is of vital significance to find biomarkers for J-Gout and further explore its pathogenesis.

Exosomes are nanoscale membrane vesicles with a diameter of 30–150 nm that contain proteins and RNAs and are present in serum, synovial fluid, urine, and milk. Exosomes are thought to be an essential mediators of intercellular communication and carriers of cargoes involved in cellular processes, including extracellular matrix degradation, inflammation regulation, and antigen presentation (7–9). Yoo identified that exosomal serum amyloid A (SAA) and lymphatic endothelial hyaluronic acid receptor-1 (LYVE-1) were important in the rheumatoid arthritis (RA) pathogenic process and could serve as novel biomarkers of activity and remission (10). Ying screened and identified differentially expressed proteins using proteomics and found that the TBB4A protein may be involved in the pathogenesis of gout (11). Li analyzed the protein profiles of synovial fluid-derived exosomes from adult gout patients and proposed some potential biomarkers (12). However, no study has been conducted examining the proteomics of serum-derived exosomes in J-Gout.

In our study, serum-derived exosomes were isolated from J-Gout, juvenile hyperuricemia (J-HUA) and oJIA patients. Quantitative proteomics with tandem mass tag (TMT) labeling combined with LC-MS/MS was used to explore differentially expressed proteins. This study may provide clues for identifying potential biomarkers and further exploring the molecular mechanism of J-Gout.

2 Materials and methods

2.1 Participants

Because J-Gout and J-HUA do not have official acronyms, we customized the study subjects for the experiment. Gout and hyperuricemia were diagnosed according to adult criteria, but all subjects were aged <18 years.

In this study, a total of 6 J-Gout patients with acute attacks, 6 J-HUA patients and 6 oJIA patients from October 2018 to August 2022 in our hospital were enrolled. The inclusion criteria were as follows: all cases were aged <18 years. Gout was diagnosed in accordance with the 2015 American College of Rheumatology/European League Against Rheumatism classification criteria for primary gout (13). The diagnosis of HUA was consistent with serum uric acid (sUA) levels greater than 420 μmol/L for boys and 360 μmol/L for girls, no history of acute attack gout and no medical treatment (14). OJIA was diagnosed according to the International League of Associations for Rheumatology (ILAR) criteria (15). The serum was centrifuged, and the supernatant was stored at −80°C. Samples were collected after obtaining informed consent from all participants. This study was approved by the Ethics Committee of the Guangdong Second Provincial General Hospital (2019-QNJJ-17-02).

2.2 Isolation and identification of exosomes

Serum-derived exosomes were isolated from patients using a qEV column combined with the ExoQuick-TC kit. The morphology of exosomes was observed by transmission electron microscopy (TEM). The size and concentration of exosomes were measured by high-sensitivity flow cytometry (HSFC) for nanoparticle analysis. Western blotting was used to examine the levels of exosome protein markers (TSG101 and CD81).

2.3 Tryptic digestion

Six samples in the same group were mixed pairwise into three samples to be tested per group. Corresponding volumes of 25 mM

dithiothreitol and 100 mM iodoacetamide were added. After incubating away from light, acetone was added (6 times volume) to precipitate the protein. After being left overnight, the precipitate was collected by centrifugation at 8000 g for 10 min, and 200 mM tetraethylammonium bromide was added to bring the volume to 100 µl. The samples were digested with trypsin overnight at 37°C in a 50:1 ratio (protein: enzyme), followed by lyophilization.

2.4 TMT labeling

The lyophilized samples were added to 100 mM tetraethylammonium bromide, followed by the addition of TMT pro reagent mixed with anhydrous acetonitrile. After leaving for 1 h, 5% hydroxylamine was added to react for 15 min. The labeled peptide solutions were lyophilized.

2.5 Reversed-phase chromatography separation

The samples were fractionated by reversed-phase 1100 HPLC using an Agilent Zorbax Extend-C18 narrow diameter column (2.1×150 mm, 5µm, Agilent, USA). The detection wavelengths were set to 210 nm and 280 nm. The flow rate was set to 300 µL/min, mobile phase A (2% acetonitrile in HPLC water) and mobile phase B (90% acetonitrile in HPLC water). Samples were collected by gradient elution for 8–60 min, and the eluate was collected in centrifuge tubes every minute. The centrifuge tubes were marked 1-15, and samples were repeatedly collected in these tubes. The separated samples were lyophilized for mass spectrometry analysis.

2.6 Chromatography and mass spectrometry conditions

The samples were loaded onto the precolumn Acclaim PepMap100 (Thermo, USA), setting at a flow rate of 350 nL/min and separated using an Acclaim PepMap RSLC (RP-C18, Thermo Fisher, USA) separation column. Full MS scans were acquired in the mass range of 350–1500 m/z with a mass resolution of 60,000, an AGC target of 3e6 and a maximum injection time of 50 ms. MS/MS spectra were obtained with a resolution of 45,000, an AGC target of 2e5 and a maximum injection time of 80 ms. All MS/MS spectra were obtained in positive ion mode, and the dynamic exclusion time was set to 30 s.

2.7 Database search

The resulting MS/MS data were processed using Proteome Discoverer 2.4.1.15 (Thermo Fisher Scientific, USA). Trypsin was specified as a cleavage enzyme allowing up to 2 missing cleavages. The primary MS error range was 10 ppm, and the fragment ion mass tolerance was 0.02 Da.

2.8 Bioinformatics analysis

Differential proteins were screened according to the criteria of fold change ≥ 1.2 and p value < 0.05 and analyzed by volcano plot, hierarchical clustering heatmap and Venn diagram. The functions of the differentially expressed proteins were assessed by GO enrichment analysis, which comprehensively describes the functions of genes and products in organisms in terms of biological processes, cellular components, and molecular functions. The Kyoto Encyclopedia of Genes and Genomes (KEGG) (http://www.genome.jp/kegg/ and https://david.ncifcrf.gov/) was used to analyze the biological regulatory pathways and functional roles of proteins with significantly differential expression.

2.9 ELISA

Protein samples of serum-derived exosomes from 6 J-Gout, 6 J-HUA and 6 oJIA patients were measured for the expression levels of DPP4 and SERPIND1 using ELISA kits (ZCIBIO-32912, ZCIBIO-56060) according to the manufacturer's instructions.

2.10 Statistical analysis

All statistical analyses were conducted using SPSS 23.0 or GraphPad Prism 8 software. Continuous variables are described as the mean ± standard deviation (mean ± SD) in the patient's basic information, and categorical variables are described as frequencies. One-way ANOVA or nonparametric tests were used for continuous variables, and differences between groups were assessed using categorical variables and chi-square tests or Fisher's exact probability method. Bivariate correlation analysis was performed using Pearson correlation analysis. A p value < 0.05 was accepted as statistically significant.

3 Results

3.1 Clinical characteristics of the participants

J-Gout patients were older than oJIA patients. J-Gout patients had higher levels of white blood cell counts than J-HUA patients. Hemoglobin levels were higher in J-Gout patients than in oJIA patients. J-Gout patients had the highest sUA levels compared to oJIA and J-HUA patients. All differences were statistically significant (p < 0.05) (Table 1).

3.2 Isolation and identification of serum-derived exosomes

Morphological analysis using TEM showed that exosomes were round to oval vesicular structures with darker stained lipid bilayers and

10.3389/fendo.2025.1460218

TABLE 1 Basic characteristics of the participants.

	J-Gout (n=6)	J-HUA (n=6)	oJIA (n=6)	*p* value
Age (years)	14.33 ± 1.63	12.17 ± 3.97	6.00 ± 3.95*	0.002
Sex (male/female)	6/0	5/1	2/4	0.027
WBC (10^9/mL)	8.36 ± 1.12	5.42 ± 1.81*	10.30 ± 2.60	0.004
NE# (10^9/mL)	4.84 ± 0.97	3.16 ± 1.32	5.83 ± 1.80	0.024
PLT (10^9/mL)	307.67 ± 59.95	232.00 ± 69.15	386.83 ± 68.68	0.006
HGB (g/L)	152.33 ± 6.15	140.00 ± 14.54	124.67 ± 8.57*	0.001
CRP (mg/L)	14.02 ± 27.60	0.78 ± 1.56	20.58 ± 21.65	0.394
ESR (mm/h)	24.52 ± 25.03	5.28 ± 4.29	47.20 ± 26.75	0.029
sUA (umol/L)	606.17 ± 132.52	443 ± 92.46*	273.50 ± 36.23*	<0.001
RF (IU/mL)	2.04 ± 2.81	4.2 ± 3.54	3.95 ± 1.55	0.388
CCP (U/mL)	10.72 ± 3.03	18.27 ± 2.73	15.47 ± 12.76	0.492

*$p < 0.05$ vs. J-Gout group.

lighter stained low electron density material (Figure 1A). The HSFC nanoparticle analysis indicated that the exosome diameters were 78.69 ± 21.41 nm, and their concentration was 256 x 10^{10} particles/ml (Figure 1B). Western blot results showed that CD81 and TSG101 were significantly expressed (Figure 1C). The results indicated that the isolated exosomes had further experimental feasibility.

3.3 Quality control of proteomics data

Principal component analysis (PCA) revealed differences between samples from different dimensions, and the results showed that the protein expression profiles of samples in the same group were basically stable (Figure 2A). Corrplot analysis showed that samples from the same group were strongly correlated (Figure 2B). Box and density plot analyses of credible protein expression revealed small fluctuations across samples and concentrations (Figures 2C, D). These results indicated sample stability and reproducibility.

3.4 Screening and functional analysis of differentially expressed proteins

A total of 838 credible proteins were identified in serum-derived exosomes from the three groups. Eighty-eight differentially expressed proteins were identified in J-Gout when compared with J-HUA. One hundred twenty-one differentially expressed proteins were identified in J-Gout when compared with oJIA. A total of 166 differentially expressed proteins were identified in J-Gout, compared with J-HUA and oJIA respectively. A total of 43 differentially expressed proteins were identified in J-Gout, compared with J-HUA and oJIA simultaneously. Six proteins were found highly expressed in J-Gout uniquely. All screens were based on criteria of log2 | fold change | ≥ 1.2 and $p < 0.05$. The Kyoto Encyclopedia of Genes and Genomes (KEGG) (http://www.genome.jp/kegg/ and https://david.ncifcrf.gov/) was used to analyze the biological regulatory pathways and functional roles of proteins with significantly differential expression.

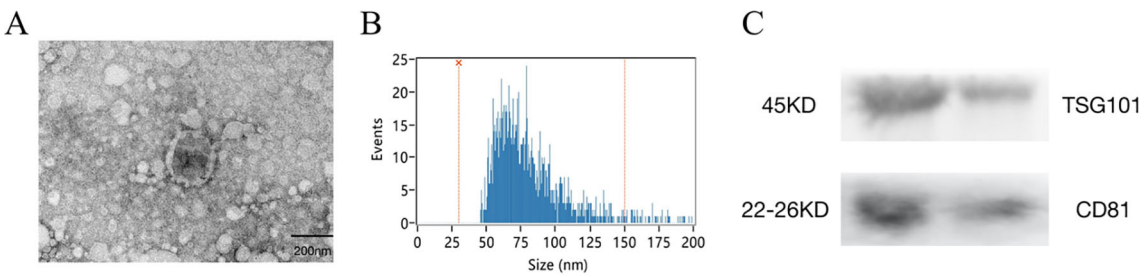

FIGURE 1
Isolation and identification of serum-derived exosomes. **(A)** The morphology of exosomes was shown by transmission electron microscopy (TEM), Scale bar=200 nm. **(B)** The size of exosomes was detected by high -sensitivity flow cytometry (HSFC) nanoparticle analysis. **(C)** The expression of CD81 and TSG101 was detected by western blotting.

10.3389/fendo.2025.1460218

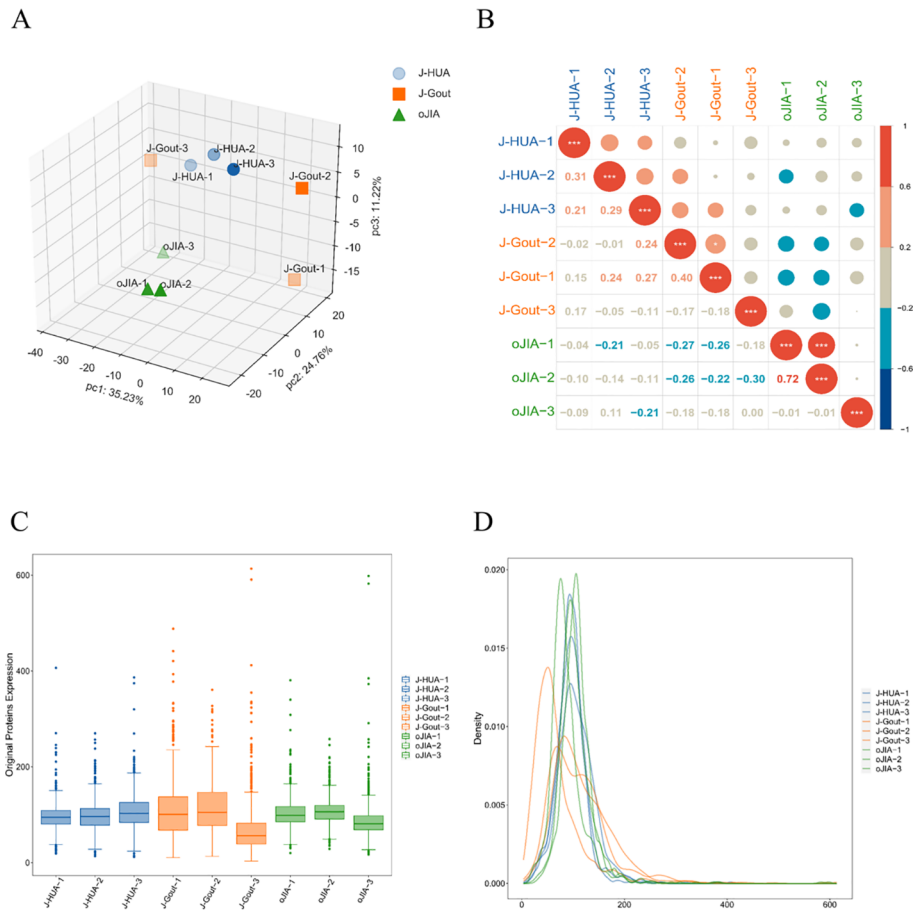

FIGURE 2
Quality control of proteomics data. **(A)** PCA. **(B)** Corrplot analysis. **(C)** Box plot analysis. **(D)** Density map analysis.

3.4.1 Screening and functional analysis of differentially expressed proteins in J-Gout vs. J-HUA

Proteins that were differentially expressed in J-Gout and J-HUA groups were identified according to the criteria of log2 | fold-change | ≥ 1.2 and $p < 0.05$. The volcano plot results showed that compared with the J-HUA, 13 and 75 proteins were upregulated and downregulated in J-Gout, respectively (Figure 3A). Upregulated proteins included histone H1.10 (H1-10) and heparin cofactor 2 (SERPIND1), and downregulated proteins included immunoglobulin kappa variable 1-17 (IGKV1-17) and immunoglobulin kappa variable 6-21 (IGKV6-21) (Table 2). Hierarchical clustering analysis was performed to reveal the dynamic profiles of differentially expressed proteins in the two groups (Figure 3B). Bioinformatic analysis indicated that the differentially expressed proteins were significantly involved in "immune response", "Fc epsilon RI signaling pathway", "B cell receptor signaling pathway" and "neutrophil extracellular trap formation" (Figures 3C, D).

3.4.2 Screening and functional analysis of differentially expressed proteins in J-Gout vs. oJIA

Proteins that were differentially expressed in J-Gout and oJIA groups were identified according to the criteria of log2 | fold-change | ≥ 1.2 and $p < 0.05$. The volcano plot results showed that compared with the oJIA, 20 proteins were upregulated, while 101 were downregulated in J-Gout (Figure 4A). Upregulated proteins included histone H1–10 and spondin-1 (SPON1), and downregulated proteins included immunoglobulin lambda variable 3-25 (IGLV3-25) and immunoglobulin lambda variable 3-1 (IGLV3-1) (Table 3). Hierarchical clustering analysis was performed to reveal the dynamic profiles of differentially expressed proteins in the two groups (Figure 4B). Bioinformatic analysis indicated that the differentially expressed proteins were significantly involved in "immune response", "Fc epsilon RI signaling pathway", "B cell receptor signaling pathway" and "primary immunodeficiency" (Figures 4C, D).

10.3389/fendo.2025.1460218

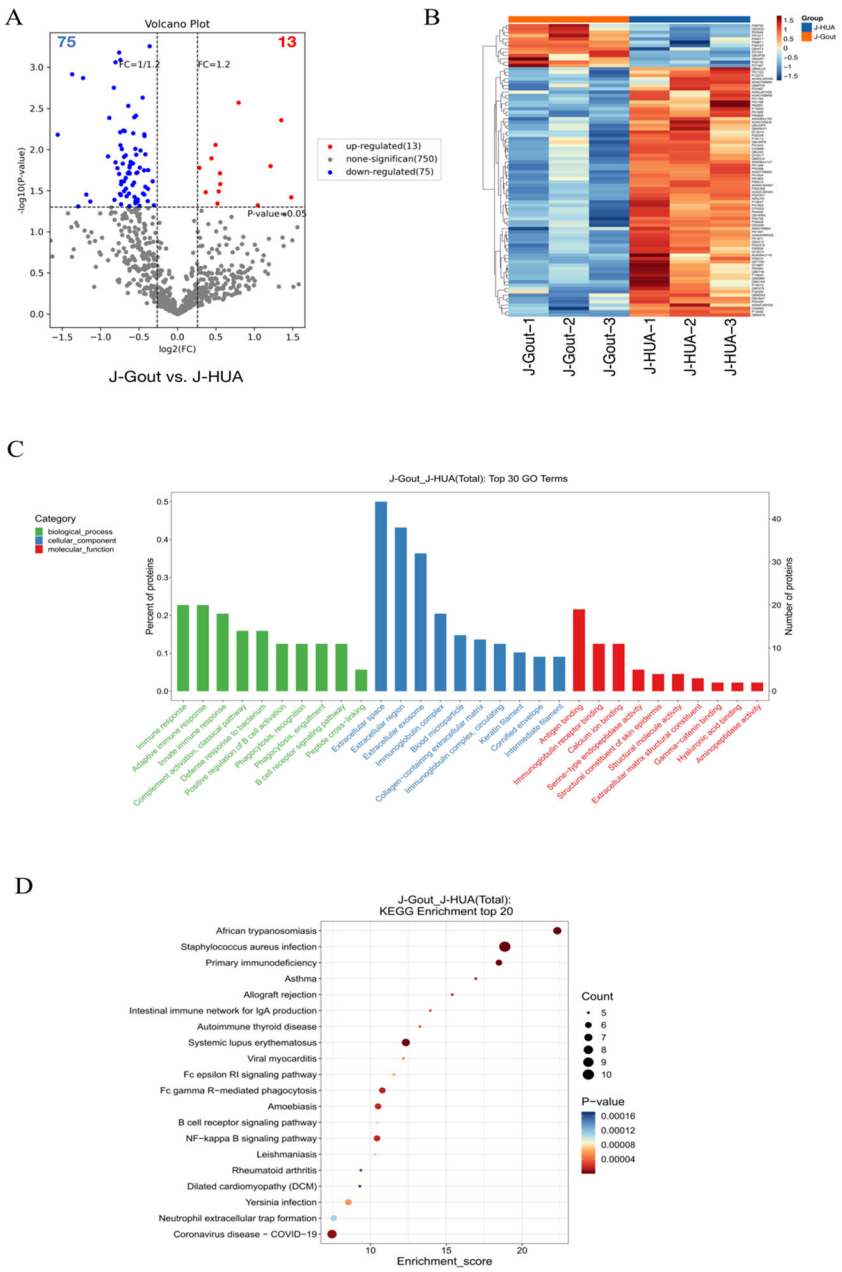

FIGURE 3
Screening and functional analysis of differentially expressed proteins in J-Gout vs. J-HUA. **(A)** Volcano plots. **(B)** Hierarchical clustering analysis. In the color bar, red represents upregulated expression, and blue represents downregulated expression. **(C)** GO analysis. **(D)** KEGG pathway analysis.

3.4.3 Screening and functional analysis of differentially expressed proteins in J-Gout vs. J-HUA and J-Gout vs. oJIA

A total of 166 differentially expressed proteins were identified when examining the combination of J-Gout vs. J-HUA and J-Gout vs. oJIA according to the criteria of log2 | fold-change | ≥ 1.2 and $p < 0.05$ (Figure 5A). Upregulated expression proteins included SPON1 and H1-10, and downregulated expression proteins included immunoglobulin lambda variable 10-54 (IGLV10-54) and IGKV1-17 (Table 4). Hierarchical clustering analysis was performed to reveal the dynamic profiles of differentially expressed proteins in the three groups (Figure 5B). Bioinformatic analysis indicated that the differentially expressed proteins were significantly involved in “immune response”, “Fc epsilon RI signaling pathway”, “B cell receptor signaling pathway”, “NF-kappa B signaling pathway” and “primary immunodeficiency” (Figures 5C, D).

3.4.4 Screening of differentially expressed proteins in the intersection between J-Gout vs. J-HUA and J-Gout vs. oJIA

A total of 43 differentially expressed proteins were identified in J-Gout based on the intersection of J-Gout vs. J-HUA and J-Gout vs.

TABLE 2 The differentially expressed proteins in J-Gout vs. J-HUA.

Accession number	Gene name	Description	J-Gout/J-HUA FC	*P* value
Q92522	H1-10	Histone H1.10	2.788711474	0.038
P05546	SERPIND1	Heparin cofactor 2	2.545981773	0.004
Q9UPZ9	CILK1	Serine/threonine-protein kinase ICK	2.31308222	0.016
O95497	VNN1	Pantetheinase	2.062615101	0.047
P01031	C5	Complement C5	1.733464956	0.003
P01599	IGKV1-17	Immunoglobulin kappa variable 1-17	0.339959225	0.007
A0A0C4DH24	IGKV6-21	Immunoglobulin kappa variable 6-21	0.386996904	0.001
A0A075B6K0	IGLV3-16	Immunoglobulin lambda variable 3-16	0.408347928	0.049
P12035	KRT3	Keratin, type II cytoskeletal 3	0.426857143	0.001
P16112	ACAN	Aggrecan core protein	0.43933518	0.035

Gray represents upregulated proteins, and white represents downregulated proteins.

oJIA (Figure 6A). The cluster heatmap shows the most highly expressed proteins as red and the proteins expressed in low levels in J-Gout as blue (Figure 6B). With the criteria of ≥ 2 unique peptides, 6 proteins were found to be uniquely highly expressed in J-Gout, including H1-10, CILK1, SERPIND1, pantetheinase (VNN1), dipeptidyl peptidase 4 (DPP4), and proprotein convertase subtilisin/kexin type 6 (PCSK6) (Table 5).

The above experimental results indicate that based on proteomic analysis, we screened significant differentially expressed proteins in juvenile gout.

3.5 Verification of DPP4 and SERPIND1 concentrations and correlation analysis with clinical indicators

ELISA results showed that the concentrations of DPP4 in serum-derived exosomes were 57.77 ± 43.82 pg/ml, 38.91 ± 14.12 pg/ml, and 32.53 ± 10.32 pg/ml in the J-Gout, J-HUA and oJIA groups, respectively (Figure 7A). The concentrations of serum-derived exosomal SERPIND1 were 10.26 ± 6.14 ng/ml, 8.21 ± 2.36 ng/ml, and 6.70 ± 1.85 ng/ml in the J-Gout, J-HUA and oJIA groups, respectively (Figure 7B). Both protein concentrations were highest in J-Gout and lowest in oJIA. Although the differences observed were not statistically significant, they were consistent with trends in proteomics.

The correlation between DPP4 and SERPIND1 expression levels and clinical indicators (CRP and ESR) was assessed. The results indicated that the DPP4 and SERPIND1 expression levels were positively correlated with CRP and ESR in serum-derived exosomes. The observed differences were statistically significant. (Figure 8). The expression levels of DPP4 and SERPIND1 did not correlate with age, sex, white blood cell count, neutrophil count, platelets, hemoglobin, serum uric acid level, RF and CCP. The results further verified that the differentially expressed proteins we selected were clinically significant.

4 Discussion

Exosomes can transfer bioactive lipids, nucleic acids, and proteins, to regulate gene expression and coordinate a broad spectrum of biological processes. Exosomes may become biomarkers for disease and potential candidates for disease therapy (16, 17). The advanced analytical approach of combining proteomics and bioinformatics analyses is currently used for discovering potential biomarkers for disease diagnosis and treatment. Because serum-derived exosomes are closely related to the pathogenesis of inflammation, there has been a recent increase in proteomic studies of exosomes for different rheumatic diseases (18, 19).

With changes in lifestyle, the proportion of J-Gout gradually increases, and there is a tendency for a younger age of onset, which can have a more significant impact on quality of life (20). The discussion of risk factors and clinical features is inadequate, and there are currently no guidelines for the management of J-Gout. JIA is an acquired autoinflammatory disease characterized by unexplained arthritis with onset before the age of 16 years, which can also present clinically with redness, pain, and limited mobility of the joints. The appearance of J-Gout is sometimes difficult to distinguish from other forms of JIA (21). Exosomes are essential mediators of intercellular communication and are involved in many processes. In our study, we used TMT proteomics technology to comprehensively analyze the protein composition of serum-derived exosomes in J-Gout, J-HUA and oJIA patients, and used bioinformatics to further explored the function of differentially abundant proteins in J-Gout.

The results showed that 88 differentially expressed proteins (13 upregulated and 75 downregulated) were found in J-Gout exosomes when compared with J-HUA exosomes. When compared with oJIA exosomes, 121 differentially expressed proteins (20 upregulated and 101 downregulated) were found in J-Gout exosomes. To comprehensively analyze the funcions of the differentially expressed proteins in J-Gout, 166 differentially expressed proteins were screened in J-Gout based on the combination of J-Gout vs. J-HUA and J-Gout

10.3389/fendo.2025.1460218

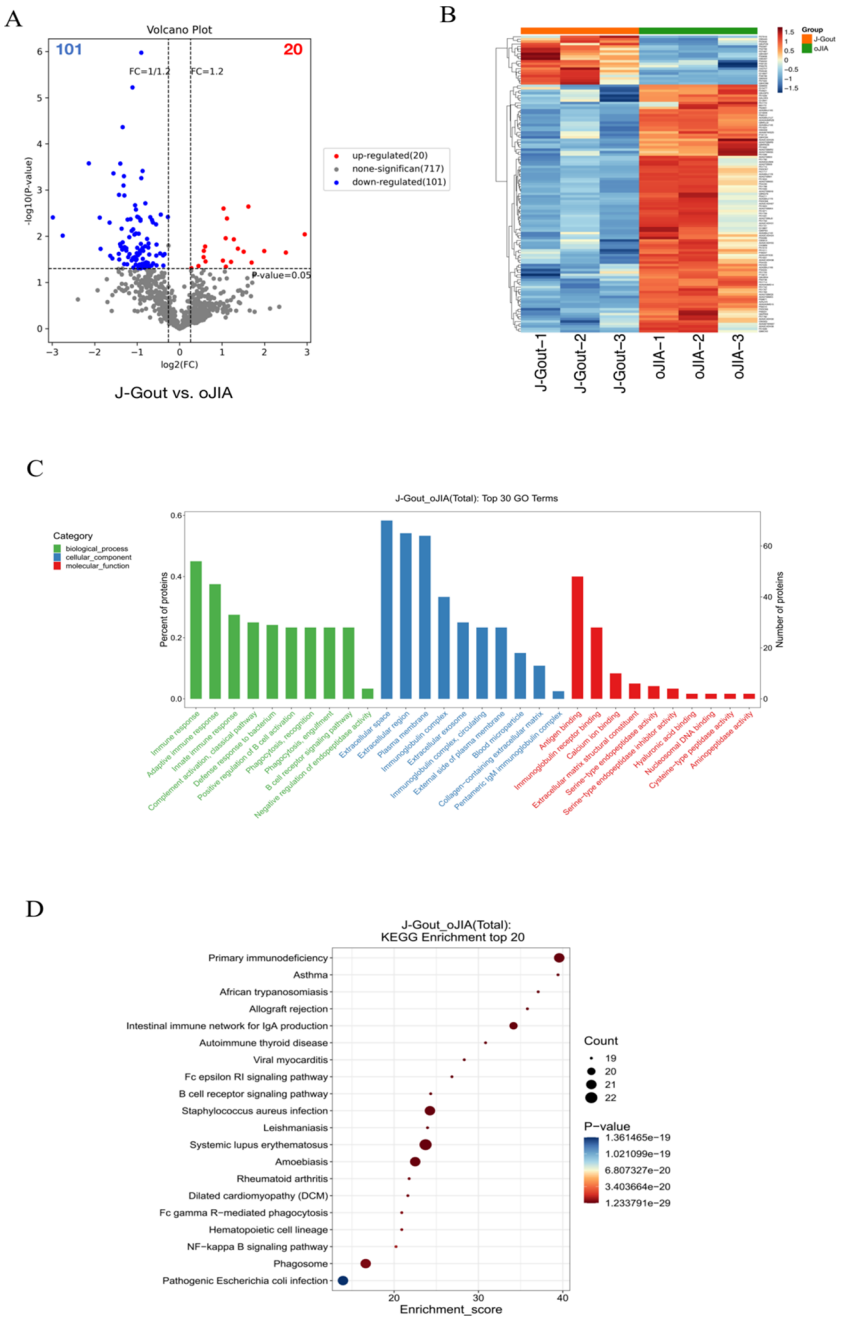

FIGURE 4
Screening and functional analysis of differentially expressed proteins in J-Gout vs. oJIA. **(A)** Volcano plots. **(B)** Hierarchical clustering analysis. In the color bar, red represents upregulated expression, and blue represents downregulated expression. **(C)** GO analysis. **(D)** KEGG pathway analysis.

vs. oJIA. The bioinformatics functional analysis of the differentially expressed proteins indicated that they were mainly enriched in "immune response", "NF-kappa B signaling pathway", "Fc epsilon RI signaling pathway" and "B cell receptor signaling pathway". Previous studies revealed that macrophage phagocytosis of MSU is a key step in the pathogenesis of gout. MSU phagocytosis triggers NF-κB translocation to induce the expression and secretion of proinflammatory cytokines, such as IL-8, TNF-α and monocyte chemotactic protein-1 (MCP-1), which initiates the inflammatory response (22). By constructing murine models of gouty arthritis and observing joint swelling, synovial tissue edema, and inflammatory cell infiltration in mice, Cheng found that PAL attenuated MSU-induced gouty arthritis inflammation, indicating that Sirt1 alleviates M1 macrophage polarization and inflammation in gouty arthritis by inhibiting the MAPK/NF-κB/AP-1 pathway and activating the Nrf2/HO-1 pathway. Thus, activating Sirt1 may provide a new therapeutic target for gouty arthritis (23). In addition to its involvement in IgE-mediated antigen presentation, Fc ε RI also induces the transcription of cytokine genes by activating multiple signaling pathways. Fc epsilon RI signaling plays an important role in the pathogenesis of autoimmune

10.3389/fendo.2025.1460218

TABLE 3 Differentially expressed proteins in J-Gout vs. oJIA.

Accession number	Gene name	Description	J-Gout/oJIA FC	*P* value
Q92522	H1-10	Histone H1.10	7.694672131	0.009
Q9HCB6	SPON1	Spondin-1	5.661495063	0.022
P07305	H1-0	Histone H1.0	3.97469459	0.021
P28799	GRN	Progranulin	3.231152993	0.037
P05546	SERPIND1	Heparin cofactor 2	3.071464268	0.002
P01717	IGLV3-25	Immunoglobulin lambda variable 3-25	0.126243958	0.004
P01715	IGLV3-1	Immunoglobulin lambda variable 3-1	0.14797546	0.010
A0A0A0MS15	IGHV3-49	Immunoglobulin heavy variable 3-49	0.227100271	0.000
P01763	IGHV3-48	Immunoglobulin heavy variable 3-48	0.271468144	0.004
A0A075B6I4	IGLV10-54	Immunoglobulin lambda variable 10-54	0.275268817	0.019

Gray represents upregulated proteins, and white represents downregulated proteins.

allergic diseases, involving the activation of mast cells and the release of inflammatory mediators (24). NF-kappa B may be activated downstream of Fc epsilon RI signaling and thus participate in inflammatory responses. For example, mast cell activation may promote cytokine production and exacerbate inflammation through the NF-kappa B pathway. Fc epsilon RI-activated mast cells release cytokines such as TNF-α, which may further activate the inflammatory response through NF-kappa B and form a positive feedback loop. A study detected 256 unique extrachromosomal circular DNA elements (eccDNAs) in gout patients in the acute phase and found that these eccDNA genes were highly associated with immune and inflammatory responses, including the T-cell receptor, Fc ε RI and JAK-STAT signaling pathways (25). The hypothetical molecular mechanisms proposed above may provide therapeutic insights for J-Gout.

The uniquely expressed proteins in J-Gout were further screened based on the intersection of differentially expressed proteins in J-Gout vs. J-HUA and J-Gout vs. oJIA. The results showed that 6 proteins were uniquely highly expressed in J-Gout, of which SERPIND1 and DPP4 might be worthy of further study. ELISA results showed that the concentrations of SERPIND1 and DPP4 proteins in serum exosomes were highest in J-Gout and lowest in oJIA, which is consistent with the trend observed in the proteomics results. SERPIND1 is a thrombin inhibitor that restrains thrombin activity by interacting with heparin during the inflammatory response and affects the coagulation cascade. SERPIND1 can be cleaved by neutrophil elastase to promote neutrophil chemotaxis in acute inflammatory responses and also promote the release of leukocyte chemokines inducing those involved in angiogenesis. Guo's study demonstrated that NF-κB could regulate SERPIND1 through the PI3K/AKT signaling pathway, thereby mediating cell migration, invasion, proliferation, apoptosis, and cell cycle regulation (26). Previous studies have shown that the pathogenesis of gout is closely related to the production of inflammatory factors in the acute inflammatory response. SERPIND1 acts as an inhibitor of thrombin and may reduce the release of inflammatory mediators by inhibiting thrombin. Thrombin can activate protease-activated receptors (PARs), thereby promoting the production of inflammatory factors, such as 1L-6 and IL-1β, while inhibition of thrombin may reduce the levels of these inflammatory factors and downregulate the expression of 1L-6 and IL-1β. In a gastric mucosal injury study, downregulation of SERPIND1 was associated with a decrease in inflammatory cytokines IL-6 and IL-1β, while expression of protective factors (eg, PGE2, SOD) was upregulated, suggesting that it may act through dual mechanisms (coagulation inhibition and anti-inflammation) (27). Alternatively, activation of the inflammasome often involves the action of coagulation factors and proteases. Thrombin activates the NLRP3 inflammasome, while SERPIND1 as a thrombin inhibitor may indirectly inhibit inflammasome activity by blocking this process, thereby reducing the release of pyroptosis-related factors (eg, caspase-1, IL-1β). DPP4 is expressed in many types of immune cells, and increasing research has focused on the potential role of DPP4 in autoimmune rheumatism. Both gout and diabetes mellitus type 2 (T2DM) are associated with HUA, and insulin resistance caused by HUA may be one of the causes involved in the pathogenesis. Previous studies showed that using antidiabetic agents reduced the risk of gout (28). Some novel antidiabetic agents, such as dipeptidyl peptidase-4 inhibition (DPP4I), reduced UA levels in patients with T2DM and had additional benefits for gout (29). These results indicated that DPP4 expression is closely related to the pathogenesis of gout. Our study also had an interesting finding that the DPP4 and SERPIND1 expression levels were positively correlated with CRP and ESR in serum-derived exosomes. Gout initially manifests as acute inflammatory arthritis, the activation of the NLRP3 inflammasome triggered by uric acid is considered a key pathogenic mechanism in the acute inflammatory response of gout, which leads to the production of proinflammatory cytokines, including interleukin-1β (IL-1β) and IL-18 (30, 31). Kim found that gout patients showed a higher expression of CXCL12 and proinflammatory cytokines, including IL-1β and IL-18, than members of the control group. Therefore, chemokine CXCL12 and its receptor CXCR4 might be considered to be potent therapeutic targets in uric acid-induced NLRP3 inflammasome activation in gout patients (32). Previous studies clarified that pharmacological inhibition of NLRP3 inflammasome assembly and activation may also be a promising approach for gouty arthritis treatment. Targeting NLRP3 through

10.3389/fendo.2025.1460218

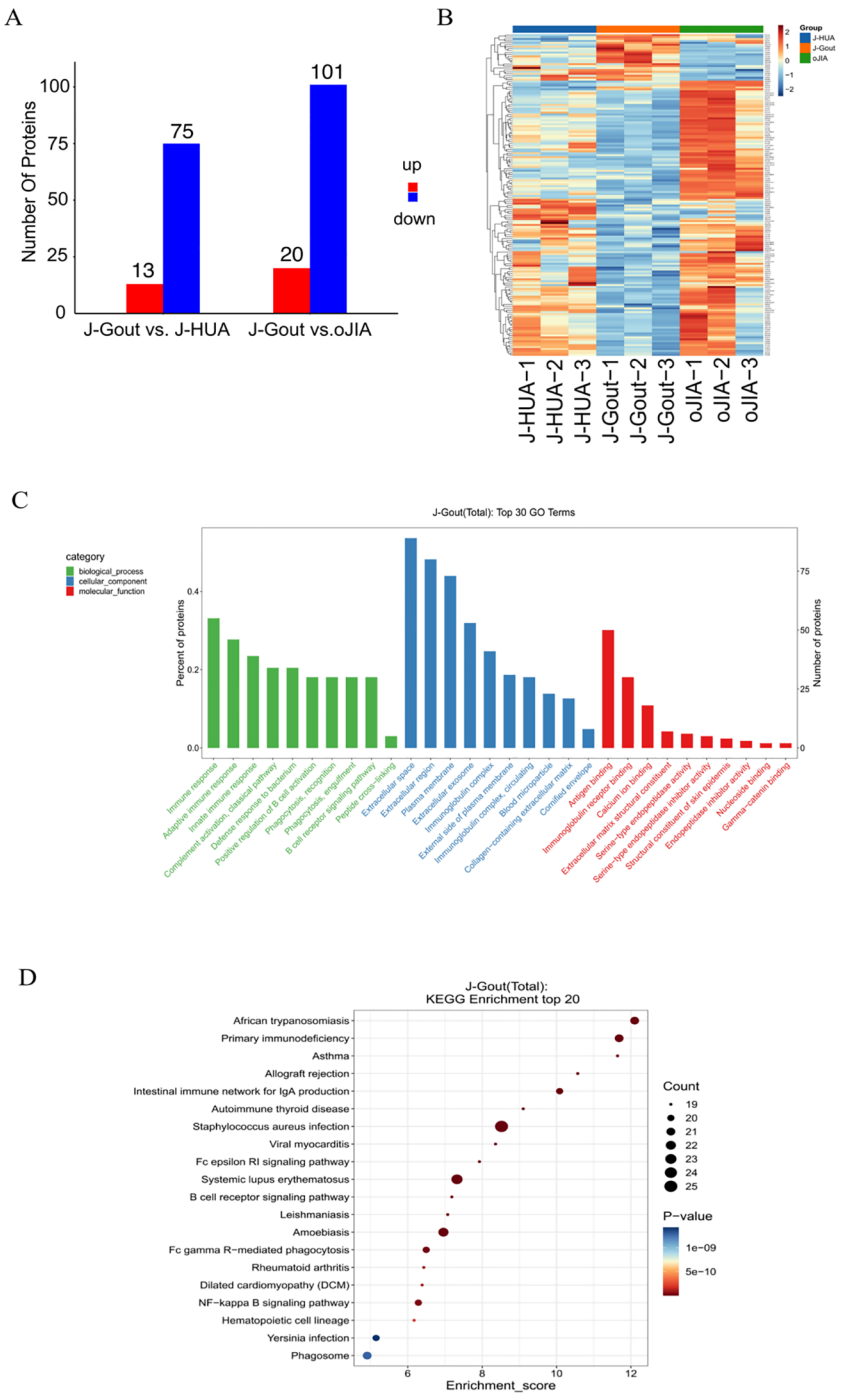

FIGURE 5
Screening and functional analysis of differentially expressed proteins in J-Gout vs. J-HUA and J-Gout vs. oJIA. **(A)** The number of differentially expressed proteins (J-Gout vs. J-HUA, J-Gout vs. oJIA). **(B)** Hierarchical clustering analysis of the three groups. In the color bar, red represents upregulated expression, and blue represents downregulated expression. **(C)** GO analysis. **(D)** KEGG pathway analysis.

potentially effective drugs such as natural products, novel compounds, and non-coding RNAs (ncRNAs) for the treatment of mouse models of MSU-induced gouty arthritis may be important for the treatment of gouty arthritis (33). Therefore, SERPIND1 and DPP4 may participate in the occurrence and development of J-Gout.

There are some limitations in our study. Firstly, assessment of the basic demographic data of the subjects revealed significant differences in age and sex among the three groups. While the younger age of oJIA patients than J-Gout patients is consistent with the clinical characteristics of oJIA having a younger age of onset, the sample size

10.3389/fendo.2025.1460218

TABLE 4 Differentially expressed proteins in J-Gout vs. J-HUA and J-Gout vs. oJIA.

Accession number	Gene name	Description	J-Gout/J-HUA FC	J-Gout/oJIA FC
Q9HCB6	SPON1	Spondin-1	2.626963351	5.661495063
Q92522	H1-10	Histone H1.10	2.788711474	7.694672131
P28799	GRN	Progranulin	1.78803681	3.231152993
Q9UPZ9	CILK1	Serine/threonine-protein kinase ICK	2.31308222	2.587675578
P05546	SERPIND1	Heparin cofactor 2	2.545981773	3.071464268
A0A075B6I4	IGLV10-54	Immunoglobulin lambda variable 10-54	0.456327986	0.275268817
P01599	IGKV1-17	Immunoglobulin kappa variable 1-17	0.339959225	0.403386755
A0A0C4DH24	IGKV6-21	Immunoglobulin kappa variable 6-21	0.386996904	0.439859245
A0A0B4J1X5	IGHV3-74	Immunoglobulin heavy variable 3-74	0.617647059	0.378823529
P16112	ACAN	Aggrecan core protein	0.43933518	0.418690602

Gray represents upregulated proteins, and white represents downregulated proteins.

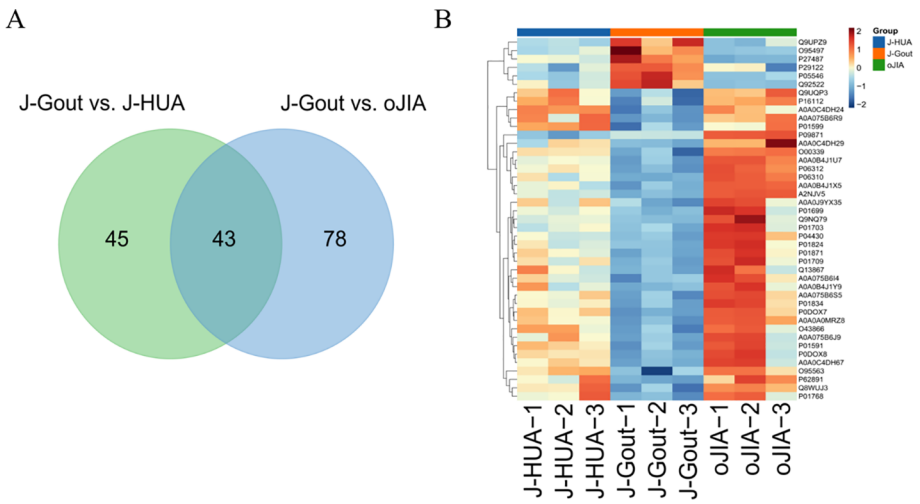

FIGURE 6
Screening of differentially expressed proteins in the intersection between J-Gout vs. J-HUA and J-Gout vs. oJIA. **(A)** Venn diagram analysis of J-Gout vs. J-HUA and J-Gout vs. oJIA. **(B)** Hierarchical clustering of the three groups.

TABLE 5 Proteins uniquely highly expressed in J-Gout.

Protein name	Abundance								
	J-Gout			J-HUA			oJIA		
H1-10	275.9	314	161.1	130.4	42.2	96.7	30.4	36.9	30.3
CILK1	211.9	137.6	221.6	83.1	89.2	74.6	63.3	54.3	103.1
SERPIND1	208.2	235.9	170.5	79.6	63.6	98.2	60.4	60.6	79.1
VNN1	200.9	114.1	133	62.6	69.4	85.2	49.6	52.8	55.5
DPP4	145.1	118.2	107.6	87.9	85.4	79.1	54	58.5	58.7
PCSK6	137.4	137.8	128.2	99.4	80.8	106	110.2	111.2	75

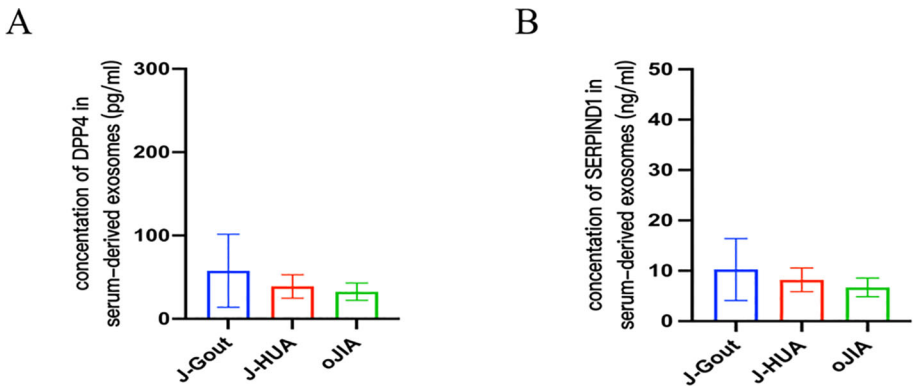

FIGURE 7
Verification of DPP4 and SERPIND1 protein expression by ELISA. **(A)** The level of DPP4 in serum-derived exosomes. **(B)** The level of SERPIND1 in serum-derived exosomes. (**A, B**, bars = mean ± standard error).

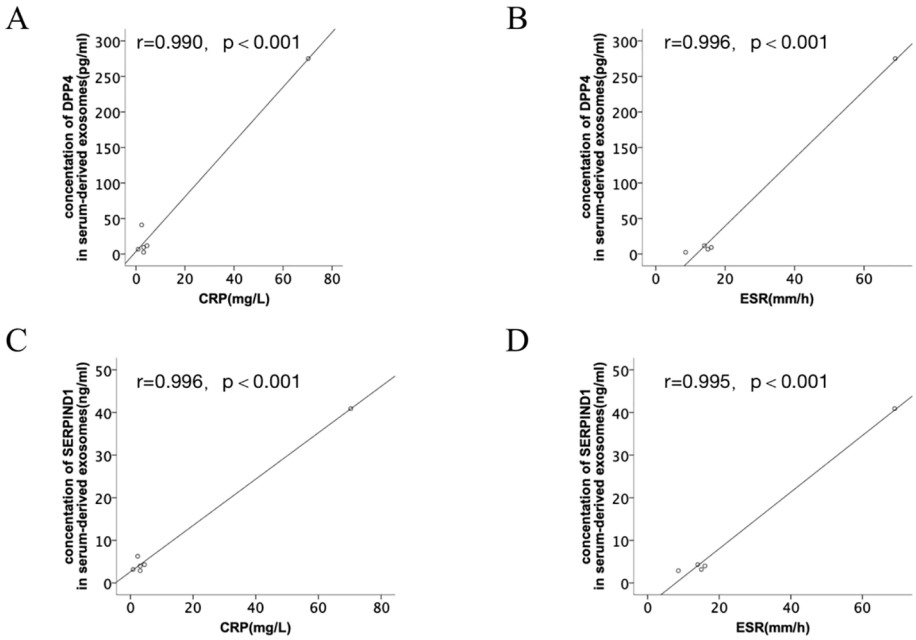

FIGURE 8
Correlation analysis between the differentially expressed proteins and clinical indicators. **(A, B)** Correlation analysis between DPP4 expression levels and clinical indicators (CRP and ESR). **(C, D)** Correlation analysis between SERPIND1 expression levels and clinical indicators (CRP and ESR).

was relatively small in our study. Secondly, because the study population was children, on the one hand due to ethical restrictions, and on the other hand, the small number of pediatric patients willing to enter the study resulted in the lack of healthy control group data in this study and the lack of female patients in the J-Gout group, although gout was more common in boys than in girls, we should further expand the sample size and conduct multicenter recruitment to obtain more objective results. Thirdly, the function of uniquely highly expressed proteins should be verified *in vivo* and *in vitro* to explore the significance of these proteins in greater depth.

In conclusion, the protein profiles of serum-derived exosomes in J-Gout were significantly different from those in J-HUA and oJIA. Some possible mechanisms were proposed. DPP4 and SERPIND1 were uniquely highly expressed in J-Gout. The highly expressed differential proteins in serum-derived exosomes are closely related to their function, which may be of great value in

identifying potential biomarkers and further exploring the molecular mechanism of J-gout.

Data availability statement

The datasets presented in this study can be found in online repositories. The names of the repository/repositories and accession number(s) can be found in the article/supplementary material.

Ethics statement

The studies involving humans were approved by The Ethics Committee of the Guangdong Second Provincial General Hospital (2019-QNJJ-17-02). The studies were conducted in accordance with the local legislation and institutional requirements. Written informed consent for participation in this study was provided by the participants' legal guardians/next of kin.

Author contributions

ZJ: Writing – original draft, Writing – review & editing. SZ: Formal Analysis, Methodology, Writing – review & editing. LL: Software, Visualization, Writing – review & editing. LH: Conceptualization, Investigation, Writing – review & editing. SS: Methodology, Visualization, Writing – review & editing. ZH: Validation, Writing – review & editing. YHe: Investigation, Software, Writing – review & editing. XP: Writing – review & editing. TL: Funding acquisition, Supervision, Writing – review & editing. YHu: Funding acquisition, Validation, Writing – review & editing.

Funding

The author(s) declare that financial support was received for the research and/or publication of this article. This study was supported by Science and Technology Projects in Guangzhou, China (No. 202102020127, No. 202102080321, No. 2023A03J0259, No. 2023A03J0260); The 3D printing research project of Guangdong Second Provincial General Hospital (No. 3D-A2021002).

Acknowledgments

We sincerely thank the researchers and participants in the study.

Conflict of interest

The authors declare that the research was conducted in the absence of any commercial or financial relationships that could be construed as a potential conflict of interest.

Publisher's note

References

1. Dalbeth N, Choi HK, Joosten LAB, Khanna PP, Matsuo H, Perez-Ruiz F, et al. Gout. *Nat Rev Dis Primers*. (2019) 5:69. doi: 10.1038/s41572-019-0115-y

2. Chen-Xu M, Yokose C, Rai SK, Pillinger MH, Choi HK. Contemporary prevalence of gout and hyperuricemia in the United States and decadal trends: the national health and nutrition examination survey, 2007–2016. *Arthritis Rheumatol (Hoboken NJ)*. (2019) 71:991–9. doi: 10.1002/art.40807

3. Chen S-Y, Shen M-L. Juvenile gout in Taiwan associated with family history and overweight. *J Rheumatol*. (2007) 34:2308–11. Available at online: https://www.jrheum.org/content/jrheum/34/11/2308.full.pdf.

4. Rao J, Ye P, Lu J, Chen B, Li N, Zhang H, et al. Prevalence and related factors of hyperuricaemia in Chinese children and adolescents: a pooled analysis of 11 population-based studies. *Ann Med*. (2022) 54:1608–15. doi: 10.1080/07853890.2022.2083670

5. Zheng S, Lee PY, Huang Y, Deng W, Huang Z, Huang Q, et al. Clinical characteristics of juvenile gout and treatment response to febuxostat. *Ann Rheum Dis*. (2022) 81:599–600. doi: 10.1136/annrheumdis-2021-221762

6. Sezer M, Aydın F, Kurt T, Tekgöz N, Tekin ZE, Karagöl C, et al. Prediction of inactive disease and relapse in oligoarticular juvenile idiopathic arthritis. *Modern Rheumatol*. (2021) 31:1025–30. doi: 10.1080/14397595.2020.1836788

7. Rodríguez-Muguruza S, Altuna-Coy A, Castro-Oreiro S, Poveda-Elices MJ, Fontova-Garrofé R, Chacón MR. A Serum Biomarker Panel of exomiR-451a, exomiR-25-3p and Soluble TWEAK for Early Diagnosis of Rheumatoid Arthritis. *Front Immunol*. (2021) 12:790880. doi: 10.3389/fimmu.2021.790880

8. Zhang Y, Bi J, Huang J, Tang Y, Du S, Li P. Exosome: A review of its classification, isolation techniques, storage, diagnostic and targeted therapy applications. *Int J Nanomed*. (2020) 15:6917–34. doi: 10.2147/IJN.S264498

9. Zhang L, Qin Z, Sun H, Chen X, Dong J, Shen S, et al. Nanoenzyme engineered neutrophil-derived exosomes attenuate joint injury in advanced rheumatoid arthritis via regulating inflammatory environment. *Bioact Mater*. (2022) 18:1–14. doi: 10.1016/j.bioactmat.2022.02.017

10. Yoo J, Lee SK, Lim M, Sheen D, Choi EH, Kim SA. Exosomal amyloid A and lymphatic vessel endothelial hyaluronic acid receptor-1 proteins are associated with disease activity in rheumatoid arthritis. *Arthritis Res Ther*. (2017) 19:119. doi: 10.1186/s13075-017-1334-9

11. Ying Y, Chen Y, Zhang S, Huang H, Zou R, Li X, et al. Investigation of serum biomarkers in primary gout patients using iTRAQ-based screening. *Clin Exp Rheumatol*. (2018) 36:791–7. Available online at: https://www.clinexprheumatol.org/article.asp?a=12366.

12. Huang Y, Liu Y, Huang Q, Sun S, Ji Z, Huang L, et al. TMT-based quantitative proteomics analysis of synovial fluid-derived exosomes in inflammatory arthritis. *Front Immunol*. (2022) 13:800902. doi: 10.3389/fimmu.2022.800902

13. Neogi T, Jansen TLTA, Dalbeth N, Fransen J, Schumacher HR, Berendsen D, et al. Gout classification criteria: an American College of Rheumatology/European League Against Rheumatism collaborative initiative. *Ann Rheum Dis*. (2015) 74:1789–98. doi: 10.1136/annrheumdis-2015-208237

14. Chen G, Cheng J, Yu H, Huang X, Bao H, Qin L, et al. Quantitative proteomics by iTRAQ-PRM based reveals the new characterization for gout. *Proteome Sci*. (2021) 19:12. doi: 10.1186/s12953-021-00180-0

15. Petty RE, Southwood TR, Manners P, Baum J, Glass DN, Goldenberg J, et al. International League of Associations for Rheumatology classification of juvenile idiopathic arthritis: second revision, Edmonton, 2001. *J Rheumatol*. (2004) 31:390–2. Available online at: https://www.jrheum.org/content/31/2/390.long.

16. Cortez MA, Calin GA. MicroRNA identification in plasma and serum: a new tool to diagnose and monitor diseases. *Expert Opin Biol Ther*. (2009) 9:703–11. doi: 10.1517/14712590902932889

17. Montecalvo A, Larregina AT, Shufesky WJ, Stolz DB, Sullivan MLG, Karlsson JM, et al. Mechanism of transfer of functional microRNAs between mouse dendritic cells via exosomes. *Blood*. (2012) 119:756–66. doi: 10.1182/blood-2011-02-338004

18. Hejrati A, Hasani B, Esmaili M, Bashash D, Tavakolinia N, Zafari P. Role of exosome in autoimmunity, with a particular emphasis on rheumatoid arthritis. *Int J Rheum Dis*. (2021) 24:159–69. doi: 10.1111/1756-185X.14021

19. Tsuno H, Arito M, Suematsu N, Sato T, Hashimoto A, Matsui T, et al. A proteomic analysis of serum-derived exosomes in rheumatoid arthritis. *BMC Rheumatol*. (2018) 2:35. doi: 10.1186/s41927-018-0041-8

20. Ito S, Torii T, Nakajima A, Iijima T, Murano H, Horiuchi H, et al. Prevalence of gout and asymptomatic hyperuricemia in the pediatric population: a cross-sectional study of a Japanese health insurance database. *BMC Pediatr*. (2020) 20:481. doi: 10.1186/s12887-020-02379-0

21. Prakken B, Albani S, Martini A. Juvenile idiopathic arthritis. *Lancet*. (2011) 377:2138–49. doi: 10.1016/S0140-6736(11)60244-4

22. Qadri M, Jay GD, Zhang LX, Wong W, Reginato AM, Sun C, et al. Recombinant human proteoglycan-4 reduces phagocytosis of urate crystals and downstream nuclear factor kappa B and inflammasome activation and production of cytokines and chemokines in human and murine macrophages. *Arthritis Res Ther*. (2018) 20:192. doi: 10.1186/s13075-018-1693-x

23. Cheng J-J, Ma X-D, Ai G-X, Yu QX, Chen XY, Yan F, et al. Palmatine protects against MSU-induced gouty arthritis via regulating the NF-κB/NLRP3 and nrf2 pathways. *Drug Des Devel Ther*. (2022) 16:2119–32. doi: 10.2147/DDDT.S356307

24. Isaifan D, Crovella S, Soubra L, Al-Nesf M, Steinhoff M. Fc epsilon RI-neuroimmune interplay in pruritus triggered by particulate matter in atopic dermatitis patients. *Int J Mol Sci*. (2023) 24(24):11851. doi: 10.3390/ijms241411851

25. Pang J, Pan X, Lin L, Li L, Yuan S, Han P, et al. Characterization of plasma extrachromosomal circular DNA in gouty arthritis. *Front Genet*. (2022) 13:859513. doi: 10.3389/fgene.2022.859513

26. Guo Q, Zhu L, Wang C, Wang S, Nie X, Liu J, et al. SERPIND1 affects the Malignant biological behavior of epithelial ovarian cancer via the PI3K/AKT pathway: A mechanistic study. *Front Oncol*. (2019) 9:954. doi: 10.3389/fonc.2019.00954

27. Wang F, Yuan C, Deng R, Liu Y. Multi-omics analysis reveals the pre-protective mechanism of Dendrobium flexicaule polysaccharide against alcohol-induced gastric mucosal injury. *Int J Biol Macromol*. (2025) 291:139191. doi: 10.1016/j.ijbiomac.2024.139191

28. Zhou J, Liu X, Chou OH-I, Li L, Lee S, Wong WT, et al. Lower risk of gout in sodium glucose cotransporter 2 (SGLT2) inhibitors versus dipeptidyl peptidase-4 (DPP4) inhibitors in type-2 diabetes. *Rheumatol (Oxford)*. (2022) 62(4):1501–10. doi: 10.1093/eurheartj/ehac544.2681

29. Yamagishi S-I, Ishibashi Y, Ojima A, Sugiura T, Matsui T. Linagliptin, a xanthine-based dipeptidyl peptidase-4 inhibitor, decreases serum uric acid levels in type 2 diabetic patients partly by suppressing xanthine oxidase activity. *Int J Cardiol*. (2014) 176:550–2. doi: 10.1016/j.ijcard.2014.07.023

30. So AK, Martinon F. Inflammation in gout: mechanisms and therapeutic targets. *Nat Rev Rheumatol*. (2017) 13:639–47. doi: 10.1038/nrrheum.2017.155

31. Kim S-K. The mechanism of the NLRP3 inflammasome activation and pathogenic implication in the pathogenesis of gout. *J Rheum Dis*. (2022) 29:140–53. doi: 10.4078/jrd.2022.29.3.140

32. Kim S-K, Choe J-Y, Park K-Y. CXCL12 and CXCR4 as novel biomarkers in uric acid-induced inflammation and patients with gouty arthritis. *Biomedicines*. (2023) 11(3):649. doi: 10.3390/biomedicines11030649

33. Liu Y-R, Wang J-Q, Li J. Role of NLRP3 in the pathogenesis and treatment of gout arthritis. *Front Immunol*. (2023) 14:1137822. doi: 10.3389/fimmu.2023.1137822

frontiers | Frontiers in Endocrinology

TYPE Original Research
PUBLISHED 20 May 2025
DOI 10.3389/fendo.2025.1506664

OPEN ACCESS

EDITED BY
Åke Sjöholm,
Gävle Hospital, Sweden

REVIEWED BY
Grzegorz K. Jakubiak,
Medical University of Silesia, Poland
Deniz Gezer,
Mersin City Hospital, Türkiye

*CORRESPONDENCE
Xijie Yu
xijieyu@scu.edu.cn
He He
hehe@wchscu.cn

RECEIVED 08 October 2024
ACCEPTED 29 April 2025
PUBLISHED 20 May 2025

CITATION
Wang X, Zhang M, Liu Z, Li C, Li Y, Huang H, He H and Yu X (2025) Biological variation in serum thyroid, iron metabolism, and plasma bone metabolism biomarkers in patients with type 2 diabetes mellitus. *Front. Endocrinol.* 16:1506664. doi: 10.3389/fendo.2025.1506664

Biological variation in serum thyroid, iron metabolism, and plasma bone metabolism biomarkers in patients with type 2 diabetes mellitus

Xia Wang[1], Mei Zhang[1], Zhi Liu[1], Chuan Li[2], Yujue Li[3], Hengjian Huang[1], He He[1]* and Xijie Yu[4]*

[1]Department of Laboratory Medicine, West China Hospital, Sichuan University, Chengdu, China, [2]Department of Thoracic Surgery, West China Hospital, Sichuan University, Chengdu, China, [3]Department of Nuclear Medicine, Sichuan Provincial People's Hospital, School of Medicine, University of Electronic Science and Technology of China, Chengdu, China, [4]Department of Endocrinology and Metabolism, Laboratory of Endocrinology and Metabolism, Rare Disease Center, West China Hospital, Sichuan University, Chengdu, China

Objectives: Variability in biomarkers is crucial for clinical decision-making in individuals with type 2 diabetes mellitus (T2DM). The biological variation (BV) of biomarkers associated with thyroid function, iron metabolism, and bone metabolism may show population-specific differences. This study aims to evaluate the biological variation of sixteen biomarkers in T2DM patients and compare these with variations observed in a healthy population.

Methods: Twenty-four T2DM patients, aged 43 to 67 and in stable condition, were enrolled. Blood samples were collected biweekly for three months. Analysis of variance models were used to assess the BV, including within-subject BV (CV_I), between-subject BV (CV_G), analytical variation, reference change value (RCV), index of individuality (II), the number of samples required for steady-state set points (NHSP), and analytical performance specifications for all biomarkers.

Results: Females exhibited lower CV_I estimates for thyroid-stimulating hormone, parathyroid hormone, and phosphate compared to males. No significant differences in CV_I estimates were observed between T2DM patients and healthy individuals across the study. However, the CV_G estimates for cortisol and iron were significantly lower in T2DM patients compared to the healthy individuals.

Conclusions: BV data is critical for the precise interpretation of serial biomarker level changes in T2DM patients. It is deemed reasonable to use RCVs for four bone metabolism markers and five thyroid biomarkers, derived from a healthy population, as a reference for monitoring T2DM patients.

KEYWORDS

biological variation, type 2 diabetes mellitus, thyroid, iron, biomarker

Introduction

Type 2 Diabetes mellitus (T2DM) is a prevalent health issue that has significantly grown over the past few decades, becoming a significant challenge to public health worldwide (1). There are strong associations between diabetes mellitus and numerous concurrent health issues, such as osteoporosis, thyroid dysfunction, and abnormalities in iron metabolism (2–4). Biomarkers can be used for diagnosis, risk stratification, and management of complications in patients with T2DM. Therefore, it is important to accurately interpret variations in these biomarker results, which are influenced by biological variation (BV) (5, 6).

Biomarker variation refers to the fluctuation of an analyte around a homeostatic set point (HSP) and encompasses both individual and analytical variations (7). While improvements in analytical techniques and testing processes can reduce analytical variation, individual variability is likely influenced by specific populations and may differ across various epidemiological studies (8). Most studies on BV focus on healthy populations, with few examining individuals with T2DM. Previous studies have explored BV in conditions such as kidney transplantation, chronic liver disease, and heart failure (6, 9, 10), revealing that BV data from healthy individuals often differs from those in unhealthy populations. Consequently, our study aims to investigate the BV of an expanded set of biomarkers in patients with T2DM.

Biomarkers for thyroid function are essential in diagnosing and managing thyroid-related disorders. T2DM can lead to a decrease in thyroid-stimulating hormone (TSH) levels and impair the transformation of thyroxine (T4) to triiodothyronine (T3) in the peripheral tissues (11). There are individual variations in thyroid hormones related to factors such as age, circadian rhythms, and hypothyroidism (12–14), but there are no data on BV in patients with T2DM. Similarly, patients with T2DM frequently experience disturbances in bone and mineral metabolism (15). Common measurands of bone metabolism include calcium (Ca), phosphate (PHOS) and parathyroid hormone (PTH), and 25-hydroxyvitamin D [25(OH)D]. Moreover, high iron is a risk factor for T2DM (16), and biomarkers are used to assess iron homeostasis. We included four common metrics, serum iron, transferrin saturation (TSAT), unsaturated iron-binding capacity (UIBC), and total iron-binding capacity (TIBC), and the variability of these metrics in patients with T2DM was not known previously.

We analysed BV data for sixteen serum/plasma biomarkers, including four related to bone metabolism, four to iron metabolism, five thyroid biomarkers, and three additional hormones in patients with T2DM. These data were used to determine the reference change value (RCV), the number of samples needed for steady-state set point (NHSP), and the analytical performance specifications (APS). Ultimately, we compared these results with previously published data from healthy populations.

Materials and methods

Participants and samples

Patients with T2DM were enrolled in the study following an eligibility assessment based on specific inclusion and exclusion criteria. The inclusion criteria were as follows: First, male and female participants aged 18 to 70 were eligible; secondly, participants diagnosed with T2DM without complications for at least three months, according to the American Diabetes Association guidelines published in 2015; thirdly, participants needed to have been on a stable diabetes medication regimen for at least 3 months prior to enrolment; fourthly, participants had to be capable of understanding the study requirements and providing written informed consent. The exclusion criteria included: firstly, individuals treated with insulin, vitamin D supplements, or medications that affect thyroid function; secondly, participants with severe, uncontrolled comorbid conditions within the last three months; thirdly, participants with severe psychological disorders that may interfere with their ability to comply with study procedures; and fourthly, women who were pregnant, breastfeeding, or planning to become pregnant during the study period. This study received approval from the Institutional Ethical Review Board of the West China Hospital of Sichuan University (No. 20201079). Each participant voluntarily signed an informed consent form after being informed about the content and purpose of the study.

Fasting venous blood samples were collected (BD Vacutainer®, New Jersey, USA) biweekly between 8:30 a.m. and 9:30 a.m., a total of six times. Plasma tubes were centrifuged within 45 min at 3000 g for 10 min at 4°C, while serum tubes were centrifuged at 22°C. Serum and plasma were then stored at −80°C until analysis.

Analytical methods

Quantitative determination of serum TSH, T3, free triiodothyronine (FT3), T4, free thyroxine (FT4), cortisol (CORT), insulin (INS), C-peptide (C-P), plasma intact PTH, and 25(OH)D was performed using the Roche Cobas e601 (Roche, Basle, Switzerland) with immunoassay electrochemiluminescence reagents and calibrators. The assays for TSH, T3, T4, and CORT were conducted utilising first-generation reagents, whereas FT3 and FT4 assays used third-generation reagents. INS, C-P, and intact PTH tests employed second-generation reagents. Serum PHOS, iron, Ca, and UIBC were analysed using Roche Cobas 8000 (Roche, Basle, Switzerland). Total iron-binding capacity (TIBC) is calculated as the sum of Serum Iron and UIBC, and TSAT is determined by the ratio of serum iron to TIBC. All samples were measured in duplicate in a single run.

Data analysis

To obtain analytical variation (CV_A) and within-subject biological variation (CV_I) estimates, data were analysed using standard ANOVA or CV-ANOVA. The CV-ANOVA method is based on the CV transformation, which normalises the data for each individual by dividing by the mean value of each individual (17). The CV_G estimates were calculated by a standard nested ANOVA after identifying outliers between subjects with Reed's criterion and the Dixon-q test2 (18). Outliers from replicates and within-subject were excluded using the Bartlett test and the Cochran test. The Shapiro-Wilk test was used to analyse data normality, and log-transformation was applied to non-normally distributed data. The steady state of subjects was assessed by linear regression of six pooled mean group sample concentrations for each biomarker (19). Subjects were considered to be in a steady state when the 95% confidence interval (CI) of the regression line's slope included zero. Mean values and BV estimates were calculated for the entire study population and separately for women and men. The 95% CI for BV estimates was calculated using Miller's formula (20). Differences in mean values and BV estimates between subgroups were considered significant if the 95% CI did not overlap. The CV_I and CV_G values for the entire study population were applied to APS using the criteria: $CV = 0.5CV_I$; $B = 0.25\ (CV_I^2 + CV_G^2)^{0.5}$; total allowable error (TE) = 1.65CV + B. The RCV, index of individuality (II), and the NHSP were calculated for each measurand according to the following formula:

$$RCV\% = 100\% \times (\exp(\pm\sqrt{2} \times Z \times \sqrt{CV_{I,ln}^2 + CV_{A,ln}^2}) - 1)$$

$$CV_{A,ln} = [\ln(CV_A^2 + 1)]^{0.5}$$

$$CV_{I,ln} = [ln(CV_I^2 + 1)]^{0.5}$$

$$II = \sqrt{CV_I^2 + CV_A^2}/$$

$$NHSP = \left(Z \times \sqrt{CV_I^2 + CV_A^2}/D\right)^2$$

The Z factor was set at 1.96, indicating a two-sided change and a 95% probability. The D values represented deviations of 10%, 15%, and 20% from the true HSP (21).

For normally distributed data with equal variances, use mean ± SD and T-tests. Otherwise, use median and Kruskal-Wallis tests.

Results

Twenty-four patients diagnosed with T2DM (11 men and 13 women), aged 43–69 years, were included in this study. We collected the medical and medication histories of each participant, including metformin, glimepiride, miglitol, gliclazide, and acarbose. All participants were non-smokers and non-alcohol drinkers. Of the 24 participants, 20 completed all six collections, and four completed four collections; the mean number of blood samples per participant was 5.7. Baseline characteristics and the concentrations of sixteen biomarkers for all participants, as well as for the men and women subgroups, are summarised in Table 1. All subjects showed no systematic changes in the concentrations of these biomarkers during the follow-up, as confirmed by linear regression (Supplementary Table S1). Reference intervals for each measurand are summarised in Supplementary Table S1, and all measurements fell within these defined ranges. Details about the outliers are provided in Supplementary Table S2. The median and 95% CI of eight hormones for each individual, grouped by sex, are shown in Supplementary Figure S1. The remaining eight measurements (including four for bone metabolism and four for iron metabolism biomarkers) are shown in Supplementary Figure S2.

No statistically significant differences were observed in the concentrations of TSH, C-P, PTH, 25(OH)D, Ca, iron, UIBC, and TSAT between genders. However, significant intersexual disparities were identified in the levels of FT3, FT4, T3, T4, CORT, INS, and TIBC, with males exhibiting markedly higher levels than those exhibited by females ($P < 0.05$). The only exception was the mean serum concentration of PHOS, which was significantly elevated in women compared to men ($P < 0.05$).

The results for CV_A, CV_I, and CV_G, along with their 95% CIs, for sixteen biomarkers are displayed in Table 2. The BV components of CV_I and CV_G based on healthy populations from the European Federation of Clinical Chemistry and Laboratory Medicine Biological Variation Database (EFLM BVD) are also presented (22). The reliability of the CV_I estimates was confirmed by SD_A/SD_I ratios, according to the recommendations of Røraas et al. (23), with all biomarkers demonstrating ratios below the threshold of 1.0. According to the 95% CI, CV_I estimates for TSH, PTH, and PHOS calculated for females were lower than those derived for males. For the entire study population, CORT and iron CV_G estimates were significantly lower than those reported by the EFLM BVD, whereas the overall CV_I estimates were similar between patients with T2DM and healthy individuals.

TABLE 1 Baseline characteristics and concentrations of sixteen biomarkers for patients with T2DM, grouped by sex.

Sort	All participants	Males	Females	P value[a]
Number of participants	24	11	13	–
Total number of results	136	62	74	–
Total number of samples	272	124	148	
Age, year	55 (7)	54 (15)	56 (11)	0.64
BMI	55 (12.5)	54.5 (10)	56.0 (13.8)	0.64
FPG, mmol/l	6.52 (2.67)	4.98 (1.05)	5.11 (0.91)	0.39
HbA1C, %	6.5 (1.7)	6.85 (2.43)	6.3 (1.0)	0.09
TSH, mIU/L	2.18 (2.03)	1.94 (1.82)	2.5 (2.2)	0.32
FT3, pmol/l	4.41 ± 0.46	4.69 ± 0.49	4.18 ± 0.3	<0.001
FT4, pmol/l	15.9 ± 1.84	16.45 ± 1.65	15.45 ± 1.88	0.01
T3, nmol/l	1.54 ± 0.23	1.6 ± 0.27	1.5 ± 0.18	0.015
T4, nmol/l	93.93 (18.81)	96.03 (18.81)	90.8 (23.42)	0.005
CORT, nmol/l	287.88 ± 77.17	314.0 ± 67.73	264.49 ± 77.82	<0.001
INS, uU/ml	6.11 (3.6)	6.57 (3.73)	6.33 ± 2.7	0.02
C-P, nmol/l	0.63 ± 0.15 (0.15)	0.65 ± 0.13 (0.19)	0.62 ± 0.17	0.31
PTH, pmol/l	4.92 (1.02)	4.92 (2.03)	5.31 ± 1.56	0.31
25 (OH)D, nmol/l	62.29 (26.97)	63.75 (29.19)	61.89 (16.26)	0.89
Ca, mmol/l	2.35 ± 0.07	2.34 ± 0.09	2.35 ± 0.07	0.45
PHOS, mmol/l	1.16 ± 0.13	1.12 ± 0.21	1.17 ± 0.1	<0.001
Iron, umol/l	16.6 (5.24)	17.1 (5.07)	16.48 (6.01)	0.07
UIBC, umol/l	37.07 ± 6.34	37.09 ± 7.83	35.64 ± 6.42	0.38
TSAT, %	31.92 (8.96)	32.3 (9.09)	30.78 (10.13)	0.32
TIBC, umol/l	53.56 ± 6.38	54.71 ± 7.48	52.52 ± 6.65	0.04

[a]The P value represents the comparison between males and females.
CI, confidence interval; FPG, Fasting Plasma Glucose; TSH, thyroid stimulating hormone; FT3, free triiodothyronine; FT4, free thyroxine; T3, triiodothyronine; T4, thyroxine; CORT, cortisol; INS, insulin; C-P, c-peptide; PTH, parathyroid hormone; 25 (OH)D, 25-hydroxyvitamin D; Ca, calcium; PHOS, phosphorus; UIBC, unsaturated iron-binding capacity; TSAT, transferrin saturation; TIBC, total iron-binding capacity.

Table 3 presents the RCV, II, and NHSP values for each biomarker. The APS were derived from the CV_I and CV_G of sixteen measurands for all participants. For INS, the NHSP could be estimated with 95% probability using eight samples if the D values were set at 15%. The II values for five thyroid hormones, INS, C-P, 25(OH)D, and TIBC, were <0.6, whereas the II estimates for iron, TSAT, and Ca were >1.4.

Discussion

Currently, BV data from healthy individuals are widely used in clinical settings for many common measurands. To ensure the reliability of these data, the EFLM Biovariation Working Group published the BV Critical Appraisal Checklist (BIVAC) (24). According to the study criteria for BV data, this study provides the first-ever BV estimates and RCV for sixteen biomarkers in patients with T2DM, assessing whether differences between measurements and HSP are clinically relevant.

Thyroid hormones are crucial endocrine regulators influenced by multiple factors, including genetics, environment, disease status, and circadian rhythm (25). To date, BV studies on thyroid hormones have predominantly focused on healthy populations, with only a few examining patients with hypothyroidism or pregnant women (26, 27). Moreover, the sampling interval must be considered when studying BV in thyroid hormone (28). There are long-term BV studies of thyroid hormones and short-term BV studies that lasted one year and 24 h, respectively (14, 29). In this study, the CV_I and CV_G estimates for TSH, FT3, and FT4 in patients with T2DM are similar to those reported in the European Biological Variation Study, which is also a mid-term study (30). Meanwhile, patients with T2DM exhibited comparable CV_I, CV_G, and RCV estimates to those from another study focusing on the elderly population (31). In clinical practice, using the TSH

10.3389/fendo.2025.1506664

TABLE 2 Biological variation estimates of CV_A, CV_I, and CV_G, with 95% CIs, for sixteen biomarkers and compared against the EFLM BV database.

Biomarker	Sort	CV_A, % (95% CI)	CV_I, % (95% CI)	CV_G, % (95% CI)	SD_A/SD_I	CV_I, % (95% CI) EFLM BV database	CV_G, % (95% CI) EFLM BV database
TSH, mIU/L	All articipants	1.6 (1.4-1.7)	18.2 (16.0-21.1)	42.9 (33.4-60.2)	0.1	17.9 (14.7-29.3)	36.1 (23.9-48.4)
	male		21.9 (18.2-27.4)	41.7 (29.2-73.2)			
	female		15.2 (12.9-18.6)	44.7 (32.0-73.7)			
FT3, pmol/l	All participants	1.2 (1.1-1.3)	4.5 (4.0-5.2)	9.5 (7.4-13.3)	0.3	5.1 (4.7-7.9)	8.1 (8.0-22.5)
	male		4.3 (3.6-5.3)	9.1 (6.3-15.9)			
	female		4.8 (4.1-5.8)	5.6 (4.0-9.3)			
FT4, pmol/l	All participants	2.6 (2.4-2.8)	5.3 (4.6-6.1)	10.4 (8.1-14.6)	0.5	4.8 (4.6-9.5)	8.0 (7.5-12.1)
	male		5.4 (4.5-6.7)	8.6 (6.0-15.1)			
	female		5.1 (4.4-6.3)	11.3 (8.1-18.7)			
T3, nmol/l	All participants	3.9 (3.6-4.3)	6.2 (5.4-7.1)	13.6 (10.6-19.1)	0.6	6.2 (5.1-10.4)	11.1 (4.4-20.4)
	male		6.2 (5.2-7.7)	16.3 (11.4-28.6)			
	female		6.2 (5.2-7.5)	10.2 (7.3-16.9)			
T4, nmol/l	All participants	1.7 (1.5-1.8)	5.8 (5.1-6.7)	15.1 (11.7-21.1)	0.3	6.4 (4.9-7.4)	11.8 (11.0-12.2)
	male		5.2 (4.4-6.6)	15.0 (10.5-26.4)			
	female		6.3 (5.3-7.6)	14.5 (10.4-24.0)			
CORT, nmol/l	All participants	2.4 (2.2-2.6)	19.4 (17.2-22.6)	18.8 (14.6-26.6)	0.1	16.1 (15.5-26.6)	33.6 (28.8-53.1)
	male		16.0 (13.5-20.2)	15.1 (10.5-26.4)			
	female		22.9 (19.3-28.1)	19.3 (13.7-32.7)			
INS, uU/ml	All participants	3.4 (3.1-3.7)	20.7 (18.3-23.9)	36.5 (28.3-51.1)	0.2	25.4 (21.1-37.1)	33.5 (31.5-81.8)
	male		19.1 (16.0-23.8)	36.1 (25.2-63.4)			
	female		22.5 (19.1-27.5)	37.5 (26.9-61.9)			
C-P, nmol/l	All participants	1.1 (1.0-1.2)	11.4 (10.1-13.3)	21.5 (16.6-30.4)	0.1	–	–
	male		12.0 (10.0-15.2)	16.7 (11.5-30.6)			
	female		10.9 (9.2-13.3)	25.2 (18.0-41.5)			
PTH, pmol/l	All participants	2.5 (2.3-2.8)	18.4 (16.3-21.2)	26.3 (20.5-36.9)	0.1	14.7 (11.3-25.9)	28.9 (21.8-43.3)
	male		21.9 (18.4-27.2)	27.4 (19.2-48.2)			
	female		15.2 (12.9-18.6)	26.1 (18.7-43.1)			
25 (OH)D, mol/l	All participants	2.7 (2.5-3.0)	6.9 (6.1-8.0)	23.7 (18.3-33.6)	0.4	6.8 (1.8-12.8)	30.1 (23.0-64.3)
	male		6.3 (5.2-7.8)	23.6 (16.5-41.5)			
	female		7.4 (6.2-9.0)	24.8 (17.6-42.1)			
Ca, mmol/l	All participants	0.8 (0.8-0.9)	2.1 (1.9-2.5)	1.6 (1.2-2.2)	0.4	1.8 (0.8-2.3)	2.7 (1.6-4.1)
	male		2.0 (1.7-2.5)	1.3 (0.9-2.2)			
	female		2.3 (1.9-2.7)	1.9 (1.4-3.1)			
PHOS, mmol/l	All participants	1.2 (1.2-1.4)	7.8 (6.9-9.0)	8.4 (6.5-11.8)	0.2	7.7 (5.7-8.3)	10.7 (7.9-17.4)
	male		10.1 (8.5-12.6)	8.8 (6.2-15.5)			
	female		5.6 (4.8-6.9)	6.4 (4.6-10.6)			
Iron, umol/l	All participants	2.2 (2.0-2.4)	19.1 (16.9-22.0)	9.7 (7.5-13.6)	0.1	27.6 (19.8-30.3)	26.7 (25.1-32.3)
	male		17.6 (14.8-21.9)	9.8 (6.9-17.2)			

(Continued)

TABLE 2 Continued

Biomarker	Sort	CV_A, % (95% CI)	CV_I, % (95% CI)	CV_G, % (95% CI)	SD_A/SD_I	CV_I, % (95% CI) EFLM BV database	CV_G, % (95% CI) EFLM BV database
	female		20.5 (17.4-24.9)	9.1 (6.5-15.0)			
UIBC, umol/l	All participants	1.3 (1.2-1.4)	10.1 (8.9-11.6)	14.7 (11.4-20.8)	0.1	–	–
	male		9.3 (7.8-11.7)	14.9 (10.2-27.2)			
	female		10.6 (9.1-13.1)	15.1 (10.8-24.9)			
TSAT, %	All participants	1.4 (1.3-1.5)	18.3 (16.2-21.2)	12.0 (9.3-17.0)	0.1	–	–
	male		17.1 (14.2-21.4)	13.0 (9.0-23.8)			
	female		18.8 (16.0-23.0)	11.2 (8.0-18.4)			
TIBC, umol/l	All participants	1.4 (1.3-1.5)	6.1 (5.4-7.1)	11.0 (8.5-15.6)	0.2	–	–
	male		4.6 (3.9-5.8)	9.9 (6.8-18.0)			
	female		6.8 (5.7-8.2)	11.1 (8.0-18.3)			

CV_A, analytical variation; within-subject biological variation (CV_I), between-subject biological variation (CV_G); CI, confidence interval; SD_A/SD_I, ratio between analytical (SD_A) and within-subject variance (SD_I); TSH, thyroid stimulating hormone; FT3, free triiodothyronine; FT4, free thyroxine; T3, triiodothyronine; T4, thyroxine; CORT, cortisol; INS, insulin; C-P, c-peptide; PTH, parathyroid hormone; 25 (OH)D, 25-hydroxyvitamin D; Ca, calcium; PHOS, phosphorus; UIBC, unsaturated iron-binding capacity; TSAT, transferrin saturation; TIBC, total iron-binding capacity.

RCV estimates (65.8%) from this study, an individual's serum TSH concentration, initially measured at 2.0 mIU/L, could naturally rise to 3.3 mIU/L without any pathological cause, ascribed to the combined effects of biological and analytical variability. All five analytes used to assess thyroid function showed low II values (<0.6), indicating high individuality; similar findings were reported in a meta-analysis of BV in thyroid-related measures (32).

As another important endocrine hormone, CORT exhibits a more pronounced circadian rhythm than that of thyroid hormones and is affected by multiple factors, including season, disease, and sex

TABLE 3 Analytical performance specification and NHSP for sixteen biomarkers based on biological variation estimates.

Biomarker			NHSP			APS derived from present study		
	RCV, % (Decrease; Increase)	II, %	10%	15%	20%	Imprecision, %	B, %	TE, %
TSH, mIU/L	-39.7; 65.8	0.42	13	6	3	9.11	11.66	26.69
FT3, pmol/l	-12.1; 13.8	0.49	1	1	1	2.26	2.63	6.36
FT4, pmol/l	-14.9; 17.6	0.56	1	1	1	2.63	2.91	7.24
T3, nmol/l	-18.3; 22.3	0.53	2	1	1	3.08	3.74	8.81
T4, nmol/l	-15.3; 18.0	0.4	1	1	1	2.88	4.03	8.78
CORT, nmol/l	-41.8; 71.8	1.04	15	7	4	9.72	6.76	22.8
INS, uU/ml	-44.1; 78.74	0.58	17	8	4	10.37	10.49	27.6
C-P, nmol/l	-27.1; 37.3	0.53	5	2	1	5.71	6.08	15.49
PTH, pmol/l	-40.2; 67.1	0.71	13	6	3	9.21	8.03	23.22
25(OH)D, nmol/l	-18.4; 22.6	0.31	2	1	1	3.43	6.17	11.83
Ca, mmol/l	-6.1; 6.5	1.43	1	1	1	1.07	0.67	2.43
PHOS, mmol/l	-19.6; 24.5	0.94	2	1	1	3.92	2.87	9.34
Iron, umol/l	-41.2; 70.3	1.98	14	6	4	9.57	5.37	21.16
UIBC, umol/l	-24.5; 32.4	0.69	4	2	1	5.04	4.46	12.76
TSAT, %	-39.8; 66.2	1.53	13	6	3	9.17	5.48	20.61
TIBC, umol/l	-15.9; 18.9	0.57	2	1	1	3.06	3.15	8.2

RCV, reference change value; NHSP, number of samples required to homeostatic set point; APS: analytical performance specification; TSH, thyroid stimulating hormone; FT3, free triiodothyronine; FT4, free thyroxine; T3, triiodothyronine; T4, thyroxine; CORT, cortisol; INS, insulin; C-P, c-peptide; PTH, parathyroid hormone; 25(OH)D, 25-hydroxyvitamin D; Ca, calcium; PHOS, phosphorus; UIBC, unsaturated iron-binding capacity; TSAT, transferrin saturation; TIBC, total iron-binding capacity.

(33). Compared to the EuBIVAS BV estimates for morning serum CORT in healthy populations, patients with T2DM showed higher CV_I. However, similar CV_G values were observed in subgroups of men and women older than 50 years (34). Unlike other measurands, INS and C-P are integral to the pathology of T2DM patients, where insufficient INS secretion or INS resistance can lead to the development of the disease. Unfortunately, no BV meta-analysis results for C-peptide were available in the EFLM BVD. Dittadi R et al. (35) provided estimates of CV_G and CV_I for serum C-peptide in healthy individuals, which were higher than those found in this study; however, their data lacked corresponding confidence intervals for both CV_G and CV_I. The EuBIVAS reported a higher CV_I estimate than what was observed in our study (36), a discrepancy that may be attributed to differences in health status among the study populations.

Parathyroid hormone and vitamin D are crucial regulators of Ca and PHOS and are widely used in diagnosing and treating bone metabolism disorders (37). This study analysed total 25(OH)D and intact PTH levels in plasma. Total 25(OH)D primarily comprises 25-hydroxyvitamin D_3 [$25(OH)D_3$], with its active form being 1,25-hydroxyvitamin D [$1,25(OH)_2D$]. The plasma concentration of 25 (OH)D varied up to 6–7 times among participants and was affected by factors such as diet, season, and genetics, and it does not remain constant over time (38). Consequently, Cavalier E et al. suggested that any APS derived from BV estimates may not be suitable for this parameter (39). However, in this study, the patients were in a stable state, and the CV_I and CV_G did not exhibit any significant differences compared to those in healthy individuals. The fluctuation in 25(OH)D concentration also affects PTH secretion, thereby influencing calcium and phosphorus homeostasis (38). Similar to 25(OH)D, PTH exists in multiple forms. Second-generation PTH assays measure not only the full-length, biologically active PTH 1–84 but also large C-terminal PTH fragments, which tend to accumulate in patients with chronic kidney disease. Corte Z and Venta R (40) assessed the BV estimates of PTH in haemodialysis patients and healthy individuals using the same analytical method employed in our study. Our CV_I estimates for PTH were higher than those reported for healthy subjects in their study, as indicated by the mostly non-overlapping 95% CI of CV_I. However, BV estimates for PTH, Ca, and PHOS in this study were consistent with the meta-analysis results reported by EFLM BVD. A high II for Ca, exceeding 1.4, suggests a low degree of individual variation, implying that population-based reference intervals are expected to have good diagnostic sensitivity.

Here, we present the BV estimates for four markers used in the diagnosis of anaemia and iron metabolism. To date, the EFLM BV database includes fifteen studies on BV data for iron assays, with CV_I values ranging from 1.3 to 38.4%. This variation is largely attributed to differences in study duration. Iron overload or deficiency can lead to metabolic disorders (41), making it crucial to evaluate BV values for iron metabolic markers in such conditions. Unfortunately, only two studies have reported BV data for TSAT and TIBC. The CV_I estimates for TSAT were 25.9% and 38.2% (8, 42), which were higher than the 18.3% observed in patients with T2DM. This indicates a need for more studies to meet clinical requirements for interpreting iron metabolism biomarkers.

Overall, the BV data obtained from patients with T2DM in this study contribute to enriching the BV database, which is still under development. The BV data are essential for accurately interpreting changes in serially detected biomarker levels in patients with T2DM. The index of individuality (> 1.4) for Ca, iron, and TSAT indicates that the reference intervals are likely to exhibit good diagnostic sensitivity. The RCV, derived from BV data, is considered an optimal approach for monitoring patients with chronic conditions (43). Our findings show that BV data for these four bone metabolism analytes and five thyroid biomarkers in T2DM patients are similar to those in healthy individuals. This finding supports the rationale for applying RCVs developed using BV data from healthy individuals to patients with T2DM who are in a stable condition. It is worth noting that CV_A in this study was derived from repeated samples. Laboratories should estimate RCVs based on their specific conditions. Furthermore, a more precise analysis of BV is needed, as hormonal analytes are influenced by rhythms and seasons. This study mainly focused on patients over 50 years old, with only three patients between 40 and 50 years of age, highlighting a gap in BV assessment for younger patients. Future research should address these aspects.

Data availability statement

The original contributions presented in the study are included in the article/Supplementary Material. Further inquiries can be directed to the corresponding author/s.

Ethics statement

The studies involving humans were approved by Institutional Ethical Review Board of the West China Hospital of Sichuan University. The studies were conducted in accordance with the local legislation and institutional requirements. The participants provided their written informed consent to participate in this study.

Author contributions

XW: Data curation, Writing – original draft. MZ: Visualization, Writing – review & editing. ZL: Visualization, Writing – review & editing. CL: Writing – review & editing, Funding acquisition. YL: Funding acquisition, Writing – review & editing. HJH: Writing – review & editing, Project administration, Supervision. HH: Project administration, Supervision, Writing – review & editing. XY: Project administration, Supervision, Writing – review & editing.

Funding

The author(s) declare that financial support was received for the research and/or publication of this article. This study was supported

by the Department of Science and Technology, Sichuan Province, grant number: 2025ZNSFSC1619, and the National Natural Science Foundation of China, grant number: 82300987.

Acknowledgments

We express our gratitude to the department of Clinical Biochemistry and Laboratory Medicine of West China Hospital of Sichuan University and the blood collection staff for their support and willingness to spend valuable time with us to complete the study.

Conflict of interest

The authors declare that the research was conducted in the absence of any commercial or financial relationships that could be construed as a potential conflict of interest.

Generative AI statement

The author(s) declare that no Generative AI was used in the creation of this manuscript.

Publisher's note

Supplementary material

The Supplementary Material for this article can be found online at: https://www.frontiersin.org/articles/10.3389/fendo.2025.1506664/full#supplementary-material

SUPPLEMENTARY FIGURE 1
The median values and 95% CIs of thyroid biomarkers, CORT, INS, and C-P for each participant according to sex. CI, confidence interval; TSH, thyroid stimulating hormone; FT3, free triiodothyronine; FT4, free thyroxine; T3, triiodothyronine; T4, thyroxine; CORT, cortisol; INS, insulin; C-P, c-peptide.

SUPPLEMENTARY FIGURE 2
The median values and 95% CIs of bone metabolism and iron metabolism biomarkers for each participant according to sex. CI, confidence interval; PTH, parathyroid hormone; 25(OH)D, 25-hydroxyvitamin D; Ca, calcium; PHOS, phosphorus; UIBC, unsaturated iron-binding capacity; TSAT, transferrin saturation; TIBC, total iron-binding capacity.

References

1. Tomic D, Shaw JE, Magliano DJ. The burden and risks of emerging complications of diabetes mellitus. *Nat Rev Endocrinol.* (2022) 18:525–39. doi: 10.1038/s41574-022-00690-7

2. Biondi B, Kahaly GJ, Robertson RP. Thyroid dysfunction and diabetes mellitus: two closely associated disorders. *Endocr Rev.* (2019) 40:789–824. doi: 10.1210/er.2018-00163

3. Khosla S, Samakkarnthai P, Monroe DG, Farr JN. Update on the pathogenesis and treatment of skeletal fragility in type 2 diabetes mellitus. *Nat Rev Endocrinol.* (2021) 17:685–97. doi: 10.1038/s41574-021-00555-5

4. Miao R, Fang X, Zhang Y, Wei J, Zhang Y, Tian J. Iron metabolism and ferroptosis in type 2 diabetes mellitus and complications: mechanisms and therapeutic opportunities. *Cell Death Dis.* (2023) 14:186. doi: 10.1038/s41419-023-05708-0

5. Fraser CG, Harris EK. Generation and application of data on biological variation in clinical chemistry. *Crit Rev Clin Lab Sci.* (1989) 27:409–37. doi: 10.3109/10408368909106595

6. Meijers WC, van der Velde AR, Muller Kobold AC, Dijck-Brouwer J, Wu AH, Jaffe A, et al. Variability of biomarkers in patients with chronic heart failure and healthy controls. *Eur J Heart Fail.* (2017) 19:357–65. doi: 10.1002/ejhf.669

7. Flatland B, Baral RM, Freeman KP. Current and emerging concepts in biological and analytical variation applied in clinical practice. *J Vet Intern Med.* (2020) 34:2691–700. doi: 10.1111/jvim.15929

8. Thyagarajan B, Howard AG, Durazo-Arvizu R, Eckfeldt JH, Gellman MD, Kim RS, et al. Analytical and biological variability in biomarker measurement in the hispanic community health study/study of latinos. *Clin Chim Acta.* (2016) 463:129–37. doi: 10.1016/j.cca.2016.10.019

9. Trapé J, Botargues JM, Porta F, Ricós C, Badal JM, Salinas R, et al. Reference change value for alpha-fetoprotein and its application in early detection of hepatocellular carcinoma in patients with hepatic disease. *Clin Chem.* (2003) 49:1209–11. doi: 10.1373/49.7.1209

10. Biosca C, Ricós C, Lauzurica R, Petersen PH. Biological variation at long-term renal post-transplantation. *Clin Chim Acta.* (2006) 368:188–91. doi: 10.1016/j.cca.2005.12.018

11. Kalra S, Aggarwal S, Khandelwal D. Thyroid dysfunction and type 2 diabetes mellitus: screening strategies and implications for management. *Diabetes Ther.* (2019) 10:2035–44. doi: 10.1007/s13300-019-00700-4

12. Karmisholt J, Andersen S, Laurberg P. Analytical goals for thyroid function tests when monitoring patients with untreated subclinical hypothyroidism. *Scand J Clin Lab Invest.* (2010) 70:264–8. doi: 10.3109/00365511003782778

13. Oladipo O, Nenninger DA, Parvin CA, Dietzen DJ. Intraindividual variability of thyroid function tests in a pediatric population. *Clin Chim Acta.* (2010) 411:1143–5. doi: 10.1016/j.cca.2010.03.030

14. Zhang Y, He DH, Jiang SN, Wang HL, Xu XH, Kong LR. Biological Variation of Thyroid Function Biomarkers over 24 hours. *Clin Chim Acta.* (2021) 523:519–24. doi: 10.1016/j.cca.2021.11.007

15. Sanches CP, Vianna AGD, Barreto FC. The impact of type 2 diabetes on bone metabolism. *Diabetol Metab Syndr.* (2017) 9:85. doi: 10.1186/s13098-017-0278-1

16. Harrison AV, Lorenzo FR, McClain DA. Iron and the pathophysiology of diabetes. *Annu Rev Physiol.* (2023) 85:339–62. doi: 10.1146/annurev-physiol-022522-102832

17. Røraas T, Støve B, Petersen PH, Sandberg S. Biological variation: the effect of different distributions on estimated within-person variation and reference change values. *Clin Chem.* (2016) 62:725–36. doi: 10.1373/clinchem.2015.252296

18. Dixon WJ. Processing data for outliers. *Biometrics.* (1953) 9:74–89. doi: 10.2307/3001634

19. Ceriotti F, Díaz-Garzón Marco J, Fernández-Calle P, Maregnani A, Aarsand AK, Coskun A, et al. The european biological variation study (Eubivas): weekly biological variation of cardiac troponin I estimated by the use of two different high-sensitivity cardiac troponin I assays. *Clin Chem Lab Med.* (2020) 58:1741–7. doi: 10.1515/cclm-2019-1182

20. Edward Miller G. Asymptotic test statistics for coefficients of variation. *Commun Stat - Theory Methods.* (1991) 20:3351–63. doi: 10.1080/03610929108830707

21. Young DS. Biological variation: from principles to practice. Callum G. Fraser. Washington, dc: aacc press, 2001, 151 pp., $38.00 ($30.00 aacc members). Isbn 1-890883-49-2. *Clin Chem.* (2002) 48:395–. doi: 10.1093/clinchem/48.2.395a

22. Aarsand AK, Fernandez-Calle P, Webster C, Coskun A, Gonzales-Lao E, Diaz-Garzon J, et al. The EFLM biological variation database . Available online at: https://biologicalvariation.eu/ (Accessed August 4, 2024).

23. Røraas T, Petersen PH, Sandberg S. Confidence intervals and power calculations for within-person biological variation: effect of analytical imprecision, number of

replicates, number of samples, and number of individuals. *Clin Chem*. (2012) 58:1306–13. doi: 10.1373/clinchem.2012.187781

24. Aarsand AK, Røraas T, Fernandez-Calle P, Ricos C, Díaz-Garzón J, Jonker N, et al. The biological variation data critical appraisal checklist: A standard for evaluating studies on biological variation. *Clin Chem*. (2018) 64:501–14. doi: 10.1373/clinchem.2017.281808

25. Gauthier BR, Sola-García A, Cáliz-Molina M, Lorenzo PI, Cobo-Vuilleumier N, Capilla-González V, et al. Thyroid hormones in diabetes, cancer, and aging. *Aging Cell*. (2020) 19:e13260. doi: 10.1111/acel.13260

26. Browning MC, Bennet WM, Kirkaldy AJ, Jung RT. Intra-individual variation of thyroxin, triiodothyronine, and thyrotropin in treated hypothyroid patients: implications for monitoring replacement therapy. *Clin Chem*. (1988) 34:696–9. doi: 10.1093/clinchem/34.4.696

27. Hölzel WG, Deschner W. Intra-individual variation of serum thyroxin and triiodothyronine in pregnancy. *Clin Chem*. (1988) 34:2063–5. doi: 10.1093/clinchem/34.10.2063

28. Andersen S, Riis J, Karmisholt JS, Andersen SL. On the importance of sampling interval in studies of biological variation in thyroid function. *Clin Chem Lab Med*. (2023) 61:e112–e4. doi: 10.1515/cclm-2022-1130

29. Karmisholt J, Andersen S, Laurberg P. Variation in thyroid function tests in patients with stable untreated subclinical hypothyroidism. *Thyroid*. (2008) 18:303–8. doi: 10.1089/thy.2007.0241

30. Bottani M, Aarsand AK, Banfi G, Locatelli M, Coşkun A, Díaz-Garzón J, et al. European biological variation study (Eubivas): within- and between-subject biological variation estimates for serum thyroid biomarkers based on weekly samplings from 91 healthy participants. *Clin Chem Lab Med*. (2022) 60:523–32. doi: 10.1515/cclm-2020-1885

31. Riis J, Westergaard L, Karmisholt J, Andersen SL, Andersen S. Biological variation in thyroid function tests in older adults and clinical implications. *Clin Endocrinol (Oxf)*. (2023) 99:598–605. doi: 10.1111/cen.14973

32. Fernández-Calle P, Díaz-Garzón J, Bartlett W, Sandberg S, Braga F, Beatriz B, et al. Biological variation estimates of thyroid related measurands - meta-analysis of bivac compliant studies. *Clin Chem Lab Med*. (2022) 60:483–93. doi: 10.1515/cclm-2021-0904

33. Gamble KL, Berry R, Frank SJ, Young ME. Circadian clock control of endocrine factors. *Nat Rev Endocrinol*. (2014) 10:466–75. doi: 10.1038/nrendo.2014.78

34. Carobene A, Guerra E, Marqués-García F, Boned B, Locatelli M, Coşkun A, et al. Biological variation of morning serum cortisol: updated estimates from the european biological variation study (Eubivas) and meta-analysis. *Clin Chim Acta*. (2020) 509:268–72. doi: 10.1016/j.cca.2020.06.038

35. Dittadi R, Gelisio P, Rossi L, Frigato F, Gion M. Biological variability evaluation and comparison of three different methods for C-peptide measurement. *Clin Chem Lab Med*. (2008) 46:1480–2. doi: 10.1515/cclm.2008.285

36. Carobene A, Lao EG, Simon M, Locatelli M, Coşkun A, Díaz-Garzón J, et al. Biological variation of serum insulin: updated estimates from the european biological variation study (Eubivas) and meta-analysis. *Clin Chem Lab Med*. (2022) 60:518–22. doi: 10.1515/cclm-2020-1490

37. Tebben PJ, Singh RJ, Kumar R. Vitamin D-mediated hypercalcemia: mechanisms, diagnosis, and treatment. *Endocr Rev*. (2016) 37:521–47. doi: 10.1210/er.2016-1070

38. Krall EA, Sahyoun N, Tannenbaum S, Dallal GE, Dawson-Hughes B. Effect of vitamin D intake on seasonal variations in parathyroid hormone secretion in postmenopausal women. *N Engl J Med*. (1989) 321:1777–83. doi: 10.1056/nejm198912283212602

39. Cavalier E, Fraser CG, Bhattoa HP, Heijboer AC, Makris K, Ulmer CZ, et al. Analytical performance specifications for 25-hydroxyvitamin D examinations. *Nutrients*. (2021) 13(2):431. doi: 10.3390/nu13020431

40. Corte Z, Venta R. Biological variation of metabolic cardiovascular risk factors in haemodialysis patients and healthy individuals. *Ann Transl Med*. (2020) 8:281. doi: 10.21037/atm.2020.03.26

41. Galy B, Conrad M, Muckenthaler M. Mechanisms controlling cellular and systemic iron homeostasis. *Nat Rev Mol Cell Biol*. (2024) 25:133–55. doi: 10.1038/s41580-023-00648-1

42. Van Wyck DB, Alcorn H Jr., Gupta R. Analytical and biological variation in measures of anemia and iron status in patients treated with maintenance hemodialysis. *Am J Kidney Dis*. (2010) 56:540–6. doi: 10.1053/j.ajkd.2010.05.009

43. Bugdayci G, Oguzman H, Arattan HY, Sasmaz G. The use of reference change values in clinical laboratories. *Clin Lab*. (2015) 61:251–7. doi: 10.7754/clin.lab.2014.140906

frontiers | Frontiers in Endocrinology

TYPE Original Research
PUBLISHED 30 July 2025
DOI 10.3389/fendo.2025.1555082

OPEN ACCESS

EDITED BY
Darko Stefanovski,
University of Pennsylvania, United States

REVIEWED BY
Xiaozhu Liu,
Capital Medical University, China
Yong Sun,
Xuzhou Medical University, China

*CORRESPONDENCE
Youfen Fan
13906683613@163.com
Sida Xu
nbeyxusida@126.com

†These authors have contributed equally to this work

RECEIVED 03 January 2025
ACCEPTED 15 July 2025
PUBLISHED 30 July 2025

CITATION
Lou J, Xiang Z, Zhu X, Song J, Cui S, Li J, Jin G, Huang N, Fan Y and Xu S (2025) Association between serum glucose potassium ratio and short- and long-term all-cause mortality in patients with sepsis admitted to the intensive care unit: a retrospective analysis based on the MIMIC-IV database. *Front. Endocrinol.* 16:1555082. doi: 10.3389/fendo.2025.1555082

Association between serum glucose potassium ratio and short- and long-term all-cause mortality in patients with sepsis admitted to the intensive care unit: a retrospective analysis based on the MIMIC-IV database

Jiaqi Lou[1†], Ziyi Xiang[2†], Xiaoyu Zhu[3†], Jingyao Song[4], Shengyong Cui[1], Jiliang Li[1], Guoying Jin[1], Neng Huang[1], Youfen Fan[1*] and Sida Xu[1*]

[1]Burn Department, Ningbo No. 2 Hospital, Ningbo, Zhejiang, China, [2]Institute of Pathology, Faculty of Medicine, University of Bonn, Bonn, Germany, [3]Health Science Center, Ningbo University, Ningbo, Zhejiang, China, [4]School of Mental Health, Wenzhou Medical University, Wenzhou, Zhejiang, China

Background: The glucose potassium ratio (GPR) is emerging as a biomarker for predicting clinical outcomes in various conditions. However, its value in sepsis patients admitted to the intensive care unit (ICU) remains unclear. Prior studies have shown conflicting results, with some indicating GPR's potential as an early warning indicator of metabolic decompensation in septic patients, while others found no significant association. The current study addresses these inconsistencies by conducting the first large-scale, systematic validation of GPR in ICU sepsis patients.

Methods: This retrospective cohort study used patient records from the MIMIC-IV database to examine outcomes in sepsis patients. The primary outcomes were hospital and ICU mortality at 30, 60, and 90 days. The correlation between GPR and these outcomes was evaluated using Kaplan-Meier survival analysis, Cox regression models, and restricted cubic spline (RCS) regression analysis. Sensitivity analyses, including Propensity Score Matching (PSM) and E-value Quantification and Subgroup analyses, were performed to assess the robustness of the findings.

Results: The study included 9,108 patients with sepsis. Kaplan-Meier survival curves indicated progressively worsening survival probabilities from Q1 to Q4 for both hospital and ICU mortality across all time points. Cox analysis revealed that patients in the highest GPR quartile (Q4) had a significantly increased risk of mortality compared to those in the lowest quartile (Q1). A nonlinear relationship between GPR and mortality was identified, with a critical threshold at GPR=30. Subgroup analysis showed that the effect size and direction were consistent across different subgroups. Sensitivity analyses, including E-value quantification and propensity score matching, supported the robustness of our findings.

Conclusion: This study demonstrates that higher GPR levels strongly predict increased short- and long-term mortality risk in ICU-admitted sepsis patients.

The composite nature of GPR, reflecting both hyperglycemia and hypokalemia, offers incremental prognostic value beyond single metabolic parameter. A critical threshold effect was observed at GPR=30, where risk substantially increased. This consistent association across patient subgroups positions GPR as a promising biomarker for identifying high-risk sepsis patients, warranting prospective validation.

KEYWORDS

intensive care unit, MIMIC, mortality, sepsis, glucose potassium ratio, long term, Cox regression

1 Background

Sepsis, a life-threatening organ dysfunction stemming from a dysregulated host response to infection, poses a significant challenge in intensive care units (ICUs) across the globe. Despite advancements in medical care, it remains one of the leading causes of morbidity and mortality, impacting millions annually and resulting in substantial healthcare expenditures (1). The pathophysiology of sepsis is intricate, characterized by a cascade of inflammatory responses that lead to widespread cellular and metabolic abnormalities. Notably, alterations in glucose and potassium homeostasis are critical metabolic disruptions that affect cellular function and systemic homeostasis. Hyperglycemia is frequently observed in septic patients, often attributed to stress-induced hypermetabolism and insulin resistance (2). This metabolic state intensifies oxidative stress and inflammation, further compromising immune function and organ performance. Conversely, potassium imbalances, such as hypokalemia, are common due to factors like increased renal excretion and intracellular shifts caused by insulin therapy or catecholamine surges (3). These electrolyte disturbances can lead to severe complications, including cardiac arrhythmias and muscle weakness (4), thereby worsening the clinical trajectory of sepsis. In recent years, there has been a pressing need to identify reliable prognostic markers to enhance the prediction of sepsis outcomes. While markers like procalcitonin, C-reactive protein, and lactate have shown promise (5), they primarily reflect inflammatory or perfusion-related aspects. Consequently, the identification of novel prognostic biomarkers that capture the complex metabolic imbalances in sepsis remains a crucial research priority.

The serum glucose-potassium ratio (GPR) has emerged as a promising biomarker that reflects the dynamic interplay between glucose and potassium homeostasis, which is often disrupted in various pathological states. Its clinical utility has been recognized in conditions such as diabetic ketoacidosis (6), myocardial infarction (7), and heart failure (8), where it offers a composite view of metabolic derangements that singular parameters fail to capture. In these conditions, an altered GPR has been associated with increased morbidity and mortality, suggesting its potential as a prognostic tool. For instance, studies in myocardial infarction patients have demonstrated a correlation between a high GPR and adverse cardiovascular events, indicating that this biomarker could enhance risk stratification and guide treatment decisions (9, 10). However, research on the application of GPR in sepsis remains limited and has yielded mixed results. Some studies suggest that a high GPR correlates with increased mortality rates and worsened clinical outcomes in sepsis patients, positing that the ratio could serve as an early warning of metabolic decompensation (11, 12). In contrast, a study by Güler et al. (13) found no significant predictive relationship between the glucose-to-potassium ratio and mortality risk in sepsis or septic shock patients admitted to the emergency intensive care unit. These discrepancies may stem from variations in study design, patient populations, or analytical methods. Furthermore, the lack of standardized thresholds and guidelines for interpreting GPR in sepsis complicates its clinical application. Thus, the current understanding of GPR's relevance to sepsis is limited, underscoring the need for comprehensive evaluations and validation in larger, well-characterized cohorts to establish its potential as a reliable prognostic indicator.

In this context, the MIMIC-IV database serves as a rich repository of de-identified health-related data from thousands of ICU admissions (14), offering a unique opportunity to comprehensively investigate the clinical parameters of sepsis. The database is publicly accessible via the MIMIC-IV platform and contains extensive datasets, including vital signs, laboratory results, and clinical outcomes, which facilitate large-scale retrospective analyses (15). This study aims to explore the association between

Abbreviations: ICU, Intensive Care Units; TG, Triglyceride; HDL-C, High-Density Lipoprotein Cholesterol; BMI, Body Mass Index; MIMIC-IV, Medical Information Mart for Intensive Care IV; SOFA, Sequential Organ Failure Assessment; RCS, Restricted Cubic Splines; COPD, Chronic Obstructive Pulmonary Disease; CKD, Chronic Kidney Disease; HR, Hazard Risk; CI, Confidence Interval; HF, Heart Failure; HT, Hypertension; DM2, Diabetes Mellitus type 2; OASIS, Oxford Acute Severity of Illness Score; SAPS II, Simplified Acute Physiology Score II; WBC, White Blood Cell; Rbc, Red Blood Cell; RDW, Red blood cell Distribution Width. AKI, Acute Kidney Injury; CRRT, Continuous Renal Replacement Therapy; HLP, Hyperlipidemia; TB, Tuberculosis; ARF, acute renal failure; MT, Malignant Tumor; MI, Myocardial Infarction.

the serum glucose-potassium ratio and short- and long-term all-cause mortality in ICU-admitted sepsis patients using the MIMIC-IV database. By examining this relationship, we aim to enhance the understanding of metabolic markers in sepsis and potentially identify a novel prognostic indicator that can improve risk stratification and inform treatment strategies for critically ill patients.

2 Methods

2.1 Data source and study design

We conducted a retrospective cohort study utilizing data from the MIMIC-IV database (version 2.2), which is developed and maintained by the Massachusetts Institute of Technology (MIT) and Beth Israel Deaconess Medical Center (BIDMC) (15). This database comprises two in-house systems: a customized hospital-wide electronic health record (EHR) and an ICU-specific clinical information system, encompassing data from 2008 to 2024. One of the authors (JQ L) completed the necessary authentication process and passed the Collaborative Institutional Training Initiative examination (authentication number 60691748) to access the database. Relevant variables were extracted, and patient data were de-identified to ensure privacy. Given the study's retrospective nature and the anonymized patient data, the Human Research Ethics Committee of Ningbo No.2 Hospital waived the requirement for informed consent.

2.2 Participants

The study encompassed all sepsis patients from the MIMIC-IV v2.2 database. Sepsis was defined according to the Sepsis 3.0 criteria, which were jointly established by the American Society for Critical Care Medicine (SCCM) and the European Society for Critical Care Medicine (ESICM). Patient data were extracted using PostgreSQL. The inclusion criteria were sepsis patients aged 18 and above who were admitted to the ICU for the first time. The following exclusion criteria were applied: (1) patients under 18 years old; (2) ICU stay shorter than 48 hours; (3) patients with recurrent sepsis (only their initial ICU admission was considered); and (4) insufficient data, such as missing records for serum glucose and potassium (Figure 1).

2.3 Research procedures and definitions

Data extraction from MIMIC-IV was performed using Structured Query Language (SQL) via Navicat Premium. The extracted data encompassed a comprehensive set of variables, including patient demographics (age, height, weight, gender, insurance, race, marital status), medical history (hypertension, type 2 diabetes, heart failure, myocardial infarction, malignant tumors, chronic renal failure, cirrhosis, hepatitis, tuberculosis, pneumonia, chronic obstructive pulmonary disease, hyperlipidemia, etc.), and initial laboratory test results (white blood cell count, red blood cell count, neutrophil count, lymphocyte count, platelet count, hemoglobin, mean corpuscular volume, hematocrit, albumin, globulin, total protein, sodium, potassium, calcium, chloride, blood glucose, GPR, anion gap, blood pH, lactate, free calcium, thrombin time, fibrinogen, partial thromboplastin time, international normalized ratio, bilirubin, ALT, AST, urea nitrogen, creatinine, troponin, urine protein, creatine kinase, creatine kinase isoenzyme, N-terminal B-type natriuretic peptide precursor). Special treatments (mechanical ventilation and CRRT), clinical scores (SOFA score, APACHE III score, SAPS II, Oasis score, Charlson Comorbidity Index, SIRS score, GCS score), and clinical outcomes (length of hospital stay, in-hospital mortality, ICU stay, ICU mortality) were also recorded. The 30-day, 60-day, and 90-day mortality rates were calculated. During data cleaning, predictors with more than 30% missing data were excluded. The serum glucose-potassium ratio (GPR) was calculated using the first recorded serum glucose and potassium measurements obtained within 24 hours of ICU admission, based on the formula: GPR = serum glucose (mg/dL)/serum potassium (mmol/L) (16).

2.4 Outcomes and measures

The primary outcomes of this study were hospital mortality and ICU mortality at 30-day, 60-day and 90-day.

2.5 Statistical analysis

Continuous variables were presented as mean ± standard deviation or median (interquartile range), while categorical variables were reported as frequency and percentage. Data conforming to a normal distribution were analyzed through the t-test or analysis of variance (ANOVA).

For data not following a normal distribution, the Mann-Whitney U test or Kruskal-Wallis test was employed (17, 18). Kaplan-Meier survival analysis was utilized to assess the incidence of endpoint events across different GPR levels, with differences evaluated through the log-rank test. Kaplan-Meier curves offer a visual comparison of survival differences between groups or conditions and do not require prior assumptions about data distribution (19), so it was relatively flexible in use.

The Cox proportional hazards model was utilized to calculate the hazard ratio (HR) and 95% confidence interval (CI) between the GPR and the endpoint. This model, taking survival outcome and survival time as dependent variables, enabled simultaneous analysis of multiple factors affecting survival and analysis of the data with censored survival time, and did not necessitate the estimation of the survival distribution type (20). The GPR was analyzed both as a continuous variable and by quartiles. Cox proportional hazards models were constructed in three sequential tiers: Model 1 (univariate); Model 2 (adjusted for demographics: age, sex, height, weight, insurance, marital status, race); Model 3 (further adjusted for laboratory/clinical covariates: WBC, RBC, RDW, albumin, chloride, ALT, AST, comorbidities [hypertension, diabetes, heart

failure, etc.], treatments [CRRT], and severity scores [SOFA, SAPS II, etc.]).

Restricted cubic splines (RCS) used 4 knots placed at the 5th, 35th, 65th, and 95th percentiles. Nonlinearity was tested via the significance of the second spline term. The GPR was incorporated as either a continuous or ordered variable into the model, with the first quartile of the GPR serving as the reference group. The quartile level was used for the calculation of the P-value of the trend. RCS was a non-parametric flexible fitting method that models survival curves by transforming survival times into piecewise functions at individual nodes (21) and can accommodate various types of survival time distributions without excessive assumptions.

Subgroup analyses (22) were conducted to explore potential differences across various subgroups based on age (≤ 70 years and > 70 years), sex, BMI (<27.4 kg/m², 27.4-31.2 kg/m², ≥31.2 kg/m²), age, sex, BMI, hypertension, type 2 diabetes, heart failure, CKD, stroke, AKI, CRRT, and mechanical ventilation, to evaluate the consistency of the GPR's prognostic value for the primary outcomes. Cox models were also adopted in subgroup analyses to adjust for all variables in the patient's baseline information.

Sensitivity analyses included: (1) E-values to quantify unmeasured confounding. To evaluate the potential impact of unmeasured confounding on the association between GPR and mortality outcomes, we also calculated E-values using the formula: E-value = RR + √(RR*(RR-1)), where RR is the hazard ratio (HR) derived from Cox regression models. This approach helped assess the robustness of our findings against unmeasured confounding.; (2) Propensity score matching (PSM) (22)). To further assess the robustness of our findings and address potential confounding factors, we conducted a propensity score matching (PSM) analysis. This method helps to reduce selection bias by balancing the distribution of observed covariates between the exposure groups (high GPR group and low GPR group). We defined the high GPR group as patients with GPR above the mean value and the low GPR group as patients with GPR below the mean value. The nearest-neighbor matching method was used to match each patient in the high GPR group with two patients in the low GPR group (1:2 matching), with a caliper width of 0.2 standard errors. Categorical variables were converted into dummy variables for the analysis. For example, marital status was categorized as divorced (1) versus others (0), married (1) versus others (0), and so on. The matching process aimed to create a more balanced comparison group by controlling for key variables such as age, sex, and SOFA score, which are known to influence outcomes in sepsis patients. In the PSM analysis, the balance assessment focuses on comparing the distribution of covariates between the treatment (high GPR) and control (low GPR) groups. The goal of balance assessment is to ensure that these groups are comparable in terms of key covariates, which is crucial for reducing selection bias and enhancing the validity of the study. It is important to note that different outcome variables do not influence the results of balance assessment, as the assessment is solely concerned with the distribution of covariates. Thus, our selection of covariates for balance assessment is based on their potential confounding effects on the relationship between GPR and hospital mortality. This approach ensures that the matched groups are balanced in terms of key covariates, providing a solid foundation for the subsequent analysis of the association between GPR and hospital mortality. After matching, we repeated the Cox regression analysis to assess the association between GPR and hospital mortality. The primary outcome was the all-cause mortality at 30-day, 60-day, and 90-day. The balance of covariates before and after matching was assessed using standardized bias and t-tests. A standardized bias of less than 10% and a p-value greater than 0.05 for the t-tests indicated successful matching. Additionally, a common support test was performed to ensure that the propensity scores of the treatment and control groups overlapped sufficiently, minimizing potential biases.

Data processing and analysis were carried out via R version 4.3.0, along with Zstats v1.0 (www.zstats.net), with statistical significance set at P<0.05 for two-tailed tests. The primary analyses utilized the following packages: Data management and transformation were conducted using dplyr and tidyr. Survival analyses including Kaplan-Meier curves, log-rank tests (via survdiff()), and univariate/multivariate Cox proportional hazards regression (via coxph()) were implemented with the survival package. Nonlinear relationships were assessed through RCS using the rms package, with knots placement and trend significance testing performed via rcs() and anova() functions. Subgroup analyses were streamlined using purrr for iterative modeling and broom for result standardization. E-value analysis was also conducted in R, utilizing packages survival for Cox regression and EValue for E-value calculation. The PSM was performed using the MatchIt package in R, which allows for various matching algorithms, including nearest neighbor, optimal, and full matching. Visualizations were generated with ggplot2 and enhanced using survminer for survival plots. For missing values in the data, the multiple imputation method of the random forest was used to interpolate the missing value data (through the R package "mice"). Features with missing values exceeding 50% were removed before interpolation.

3 Results

Among the adult patients in the MIMIC-IV database, a total of 22,517 subjects met the eligibility criteria. From the database, 148 prognostic factors were initially extracted. Following data cleaning, 80 predictors with over 30% missing data were excluded. In the end, 68 forecast factors were included in the model.

3.1 Characteristics of included patients

A total of 9,108 people were included in the study, of which 2,272 (24.95%) were in GPR quantile 1 (Q1) group (GPR ≤ 6.67), 2,282 (25.05%) people were in quantile 2 group (6.67 < GPR≤ 25.71), 2,277 people were in quantile 3 group (25.71 < GPR ≤ 40.81), and 2,277 people in quantile 4 group, accounting for 25.00% (GPR > 40.81). IQR is 15.09. The average GPR of all patients was 35.55 ± 16.49. Upon stratification into these four categories, the distribution of each variable across the groups was analyzed. All baseline data are presented in Table 1 and Supplementary Table 1.

10.3389/fendo.2025.1555082

TABLE 1 Summary of characteristics that are statistically different of the study population.

Variables	Total (n = 9,108)	Q1 (n = 2,272)	Q2 (n = 2,282)	Q3 (n = 2,277)	Q4 (n = 2,277)	Statistic	*P*
Characteristics							
Age (year)	71.61 ± 14.73	72.07 ± 14.94	71.52 ± 14.98	71.95 ± 14.52	70.91 ± 14.45	F=2.91	**0.033**
Weight (kg)	79.16 ± 23.62	77.69 ± 23.65	77.85 ± 23.39	78.96 ± 22.97	82.15 ± 24.17	F=17.45	**<0.001**
Gender (n(%))						χ^2=13.82	**0.003**
F	4038 (44.33)	944 (41.55)	993 (43.51)	1046 (45.94)	1055 (46.33)		
M	5070 (55.67)	1328 (58.45)	1289 (56.49)	1231 (54.06)	1222 (53.67)		
Marital Status, n(%)						χ^2=51.12	**<0.001**
Divorced	644 (7.07)	165 (7.26)	163 (7.14)	168 (7.38)	148 (6.50)		
Married	3801 (41.73)	944 (41.55)	960 (42.07)	937 (41.15)	960 (42.16)		
NA	1017 (11.17)	200 (8.80)	229 (10.04)	264 (11.59)	324 (14.23)		
Single	2127 (23.35)	573 (25.22)	564 (24.72)	497 (21.83)	493 (21.65)		
Widowed	1519 (16.68)	390 (17.17)	366 (16.04)	411 (18.05)	352 (15.46)		
Laboratory parameters							
WBC ($\times10^9$/L)	13.76 ± 12.36	13.37 ± 13.52	13.08 ± 11.54	13.72 ± 9.73	14.88 ± 14.11	F=9.27	**<0.001**
RBC ($\times10^{12}$/L)	3.42 ± 0.70	3.32 ± 0.68	3.38 ± 0.66	3.46 ± 0.71	3.51 ± 0.73	F=35.03	**<0.001**
Hemoglobin (g/dL)	10.23 ± 1.97	9.93 ± 1.90	10.15 ± 1.86	10.36 ± 2.01	10.47 ± 2.07	F=34.01	**<0.001**
RDW (%)	16.00 ± 2.51	16.48 ± 2.63	15.96 ± 2.47	15.88 ± 2.50	15.67 ± 2.36	F=43.44	**<0.001**
Hematocrit (%)	31.29 ± 5.92	30.60 ± 5.83	30.95 ± 5.52	31.60 ± 6.01	32.02 ± 6.19	F=26.51	**<0.001**
Albumin (g/L)	2.91 ± 0.65	2.86 ± 0.65	2.89 ± 0.64	2.96 ± 0.67	2.93 ± 0.65	F=4.76	**0.003**
Sodium (mmol/L)	138.56 ± 5.76	137.62 ± 5.44	138.56 ± 5.55	138.81 ± 5.43	139.24 ± 6.44	F=32.59	**<0.001**
Potassium (mmol/L)	4.26 ± 0.64	4.60 ± 0.68	4.25 ± 0.58	4.14 ± 0.57	4.06 ± 0.59	F=344.80	**<0.001**
Chlorine (mmol/L)	104.06 ± 7.03	103.48 ± 6.87	104.42 ± 6.73	104.20 ± 6.74	104.12 ± 7.69	F=7.51	**<0.001**
Glucose (mmol/L)	148.62 ± 64.05	96.47 ± 18.25	122.39 ± 17.48	148.66 ± 23.13	226.90 ± 75.54	F=4205.85	**<0.001**
Anion gap (mmol/L)	15.73 ± 4.61	15.99 ± 4.95	14.97 ± 4.21	15.33 ± 4.21	16.65 ± 4.85	F=60.36	**<0.001**
pH	7.35 ± 0.09	7.34 ± 0.09	7.36 ± 0.08	7.36 ± 0.08	7.35 ± 0.10	F=32.84	**<0.001**
PCO_2 (mmHg)	41.76 ± 11.39	42.69 ± 12.88	41.85 ± 10.96	41.51 ± 11.13	41.13 ± 10.57	F=5.78	**<0.001**
PO_2 (mmHg)	118.76 ± 71.09	113.39 ± 72.25	122.64 ± 73.70	121.03 ± 69.82	117.69 ± 68.65	F=5.45	**<0.001**
Free calcium (mmol/L)	1.10 ± 0.11	1.11 ± 0.11	1.11 ± 0.10	1.10 ± 0.10	1.10 ± 0.11	F=3.67	**0.012**
PT (s)	18.31 ± 10.24	19.64 ± 11.10	17.67 ± 8.72	17.64 ± 9.14	18.31 ± 11.56	F=17.03	**<0.001**
Fibrinogen (mg/dL)	310.32 ± 187.88	287.49 ± 173.05	291.86 ± 171.25	335.99 ± 201.95	330.48 ± 201.03	F=11.33	**<0.001**
PPT (s)	40.89 ± 20.28	40.87 ± 17.61	39.63 ± 18.68	40.39 ± 20.54	42.65 ± 23.60	F=8.20	**<0.001**
INR	1.68 ± 0.99	1.82 ± 1.12	1.62 ± 0.86	1.63 ± 0.97	1.66 ± 1.00	F=18.18	**<0.001**
Total bilirubin (mg/dL)	2.79 ± 5.88	3.67 ± 6.79	2.78 ± 5.87	2.84 ± 6.08	1.92 ± 4.47	F=22.47	**<0.001**
Direct bilirubin (mg/dL)	4.24 ± 5.73	5.05 ± 6.18	4.33 ± 5.84	4.09 ± 5.52	3.29 ± 5.12	F=2.88	**0.035**
Indirect bilirubin (mg/dL)	2.22 ± 2.85	2.65 ± 3.45	2.45 ± 2.83	1.85 ± 2.32	1.86 ± 2.46	F=3.36	**0.019**
ALT (U/L)	167.94 ± 596.01	186.59 ± 784.00	134.50 ± 479.30	140.58 ± 452.44	205.54 ± 597.57	F=5.00	**0.002**
AST (U/L)	302.91 ± 1065.00	349.66 ± 1235.43	253.35 ± 858.19	234.05 ± 758.68	366.35 ± 1273.72	F=5.79	**<0.001**
Urea nitrogen (mmol/L)	35.33 ± 25.42	39.73 ± 27.33	32.31 ± 24.14	32.67 ± 23.03	36.64 ± 26.23	F=44.41	**<0.001**

(Continued)

TABLE 1 Continued

Variables	Total (n = 9,108)	Q1 (n = 2,272)	Q2 (n = 2,282)	Q3 (n = 2,277)	Q4 (n = 2,277)	Statistic	*P*
Laboratory parameters							
Creatinine (mg/dL)	1.77 ± 1.60	2.17 ± 1.96	1.57 ± 1.39	1.61 ± 1.47	1.74 ± 1.42	F=70.06	**<0.001**
LDH (U/L)	715.76 ± 1616.90	828.65 ± 2105.51	633.76 ± 1211.17	563.17 ± 1040.05	829.50 ± 1828.93	F=7.34	**<0.001**
CKMB (U/L)	21.15 ± 52.72	14.24 ± 34.27	17.83 ± 48.56	21.76 ± 51.27	28.24 ± 65.76	F=12.94	**<0.001**
Troponint (μg/L)	0.75 ± 2.38	0.39 ± 1.15	0.61 ± 1.71	0.71 ± 2.06	1.14 ± 3.43	F=16.66	**<0.001**
NT-proBNP (pmol/L)	10065.50 ± 12234.37	11888.63 ± 12317.15	8313.65 ± 10569.28	9541.94 ± 12367.29	10538.55 ± 13343.72	F=2.69	**0.045**
Treatment							
CRRT (n(%))						χ^2=18.04	**<0.001**
No	8297 (91.10)	2026 (89.17)	2112 (92.55)	2091 (91.83)	2068 (90.82)		
Yes	811 (8.90)	246 (10.83)	170 (7.45)	186 (8.17)	209 (9.18)		
Ventilation (hours)	101.88 ± 145.10	91.36 ± 144.60	99.46 ± 141.63	108.83 ± 152.51	107.59 ± 140.66	F=5.94	**<0.001**
Comorbidity							
Hypertension (n(%))						χ^2=41.33	**<0.001**
No	5615 (61.65)	1526 (67.17)	1394 (61.09)	1350 (59.29)	1345 (59.07)		
Yes	3493 (38.35)	746 (32.83)	888 (38.91)	927 (40.71)	932 (40.93)		
Type 2 diabetes mellitus (n(%))						χ^2=640.05	**<0.001**
No	6235 (68.46)	1760 (77.46)	1787 (78.31)	1599 (70.22)	1089 (47.83)		
Yes	2873 (31.54)	512 (22.54)	495 (21.69)	678 (29.78)	1188 (52.17)		
Myocardial infarct (n(%))						χ^2=50.89	**<0.001**
No	8397 (92.19)	2139 (94.15)	2130 (93.34)	2104 (92.40)	2024 (88.89)		
Yes	711 (7.81)	133 (5.85)	152 (6.66)	173 (7.60)	253 (11.11)		
Malignant tumor (n(%))						χ^2=35.32	**<0.001**
No	7061 (77.53)	1719 (75.66)	1720 (75.37)	1758 (77.21)	1864 (81.86)		
Yes	2047 (22.47)	553 (24.34)	562 (24.63)	519 (22.79)	413 (18.14)		
Chronic kidney diseases (n(%))						χ^2=17.68	**<0.001**
No	6884 (75.58)	1663 (73.20)	1776 (77.83)	1753 (76.99)	1692 (74.31)		
Yes	2224 (24.42)	609 (26.80)	506 (22.17)	524 (23.01)	585 (25.69)		
Acute renal failure (n(%))						χ^2=27.54	**<0.001**
No	4374 (48.02)	1011 (44.50)	1188 (52.06)	1106 (48.57)	1069 (46.95)		
Yes	4734 (51.98)	1261 (55.50)	1094 (47.94)	1171 (51.43)	1208 (53.05)		
Cirrhosis (n(%))						χ^2=42.28	**<0.001**
No	7998 (87.81)	1934 (85.12)	1979 (86.72)	2009 (88.23)	2076 (91.17)		
Yes	1110 (12.19)	338 (14.88)	303 (13.28)	268 (11.77)	201 (8.83)		
Stroke (n(%))						χ^2=25.50	**<0.001**
No	8138 (89.35)	2068 (91.02)	2054 (90.01)	2043 (89.72)	1973 (86.65)		
Yes	970 (10.65)	204 (8.98)	228 (9.99)	234 (10.28)	304 (13.35)		

(Continued)

TABLE 1 Continued

Variables	Total (n = 9,108)	Q1 (n = 2,272)	Q2 (n = 2,282)	Q3 (n = 2,277)	Q4 (n = 2,277)	Statistic	*P*
Comorbidity							
Hyperlipidemia, (n(%))						χ^2=37.19	**<0.001**
No	6215 (68.24)	1628 (71.65)	1572 (68.89)	1570 (68.95)	1445 (63.46)		
Yes	2893 (31.76)	644 (28.35)	710 (31.11)	707 (31.05)	832 (36.54)		
Acute kidney injury stage (n(%))						χ^2=34.38	**<0.001**
1	1403 (18.94)	356 (19.63)	347 (18.89)	353 (18.76)	347 (18.51)		
2	3087 (41.67)	666 (36.71)	835 (45.45)	810 (43.04)	776 (41.39)		
3	2918 (39.39)	792 (43.66)	655 (35.66)	719 (38.20)	752 (40.11)		
Scoring systems							
SOFA score (score)	6.77 ± 3.90	7.15 ± 4.08	6.23 ± 3.65	6.52 ± 3.74	7.18 ± 4.02	F=33.60	**<0.001**
APSIII score (score)	58.48 ± 23.59	60.89 ± 24.31	53.75 ± 21.65	56.23 ± 21.93	63.08 ± 25.13	F=76.14	**<0.001**
SAPSII score (score)	45.83 ± 14.75	47.50 ± 15.57	43.74 ± 13.71	44.94 ± 14.03	47.14 ± 15.28	F=34.07	**<0.001**
OASIS, score (score)	36.09 ± 8.90	36.05 ± 8.95	35.07 ± 8.57	35.91 ± 8.70	37.32 ± 9.24	F=24.98	**<0.001**
GCS score (score)	13.06 ± 3.18	13.12 ± 3.08	13.23 ± 2.90	13.07 ± 3.15	12.84 ± 3.53	F=6.07	**<0.001**
Charlson score (score)	6.53 ± 2.81	6.69 ± 2.81	6.42 ± 2.76	6.42 ± 2.79	6.59 ± 2.87	F=5.23	**<0.001**
SIRS score (score)						χ^2=110.42	**<0.001**
0	60 (0.66)	18 (0.79)	19 (0.83)	13 (0.57)	10 (0.44)		
1	637 (6.99)	188 (8.27)	187 (8.19)	145 (6.37)	117 (5.14)		
2	2302 (25.27)	655 (28.83)	629 (27.56)	549 (24.11)	469 (20.60)		
3	3837 (42.13)	916 (40.32)	939 (41.15)	993 (43.61)	989 (43.43)		
4	2272 (24.95)	495 (21.79)	508 (22.26)	577 (25.34)	692 (30.39)		

Continuous variables are expressed as the median and interquartile range. Counting data are presented as numbers and percentages. The medical condition was defined based on the ICD-9 code. WBC, white blood cell; RBC, red blood cell; RDW, red blood cell distribution width; PCO_2, partial pressure of carbon dioxide; PO_2, partial pressure of oxygen; LD, Lactate Dehydrogenase; PT, prothrombin time; PTT, partial thromboplastin time; INR, international normalized ratio; ALT, alanine aminotransferase; AST, aspartate aminotransferas; CKMB, creatine kinase-MB; BCK, blood ketone; NT-proBNP, N-terminal pro-brain natriuretic peptide; CRRT, continuous renal replacement therapy; COPD, chronic obstructive pulmonary disease; OASIS, oxford acute severity of illness score; SASPII, simplified acute physiology score II; SOFA, sequential organ failure assessment; CNS, central nervous system; GCS, Glasgow Coma Scale; SIRS, Systemic Inflammatory Response Syndrome; F, ANOVA; χ^2, Chi-square test; SD, standard deviation.
Bold red font indicates p-values with statistical significance.

Patients in Q1 were older and had lower body weight than those in the other groups, and there were differences in sex and marital status among the four groups. WBC, RBC, platelet, hemoglobin, hematocrit, albumin, sodium, glucose, anion gap, fibrinogen, PPT, ALT, CK, CKMB were also higher in Q4 group than in Q1 group, but RDW, potassium, hematocrit and bilirubin were lower than Q1 group. There was no significant difference in height, insurance, languages, CRRT days, ventilation, COPD, heart failure, hepatitis, tuberculosis and pneumonia (P>0.05) (Table 1).

3.2 Kaplan-Meier survival curve analysis

Kaplan-Meier curves (Figure 2) demonstrated worsening survival probabilities from Q1 to Q4 for both hospital and ICU mortality at 30-day, 60-day, and 90-day intervals (log-rank test, all P < 0.001). Specifically, a total of 9,108 people were included in the study, of which 2,272 (24.95%) were in GPR quantile 1 (Q1) group (GPR ≤ 6.67), 2,282 (25.05%) people were in quantile 2 group (6.67 < GPR≤ 25.71), 2,277 people were in quantile 3 group (25.71 < GPR ≤ 40.81), and 2,277 people in quantile 4 group, accounting for 25.00% (GPR > 40.81).

3.3 Cox regression models for all-cause mortality (in hospital and ICU)

In the Cox regression analysis, a higher GPR was positively correlated with increased mortality rates in both the ICU and hospital settings among critically ill patients with sepsis. When the GPR was analyzed as a continuous variable, it was independently associated with a higher risk of hospital mortality both at 30-day, 60-day and 90-day (All P < 0.05). Patients in Q4 had a 15–20% higher risk of mortality compared to Q1 across all time

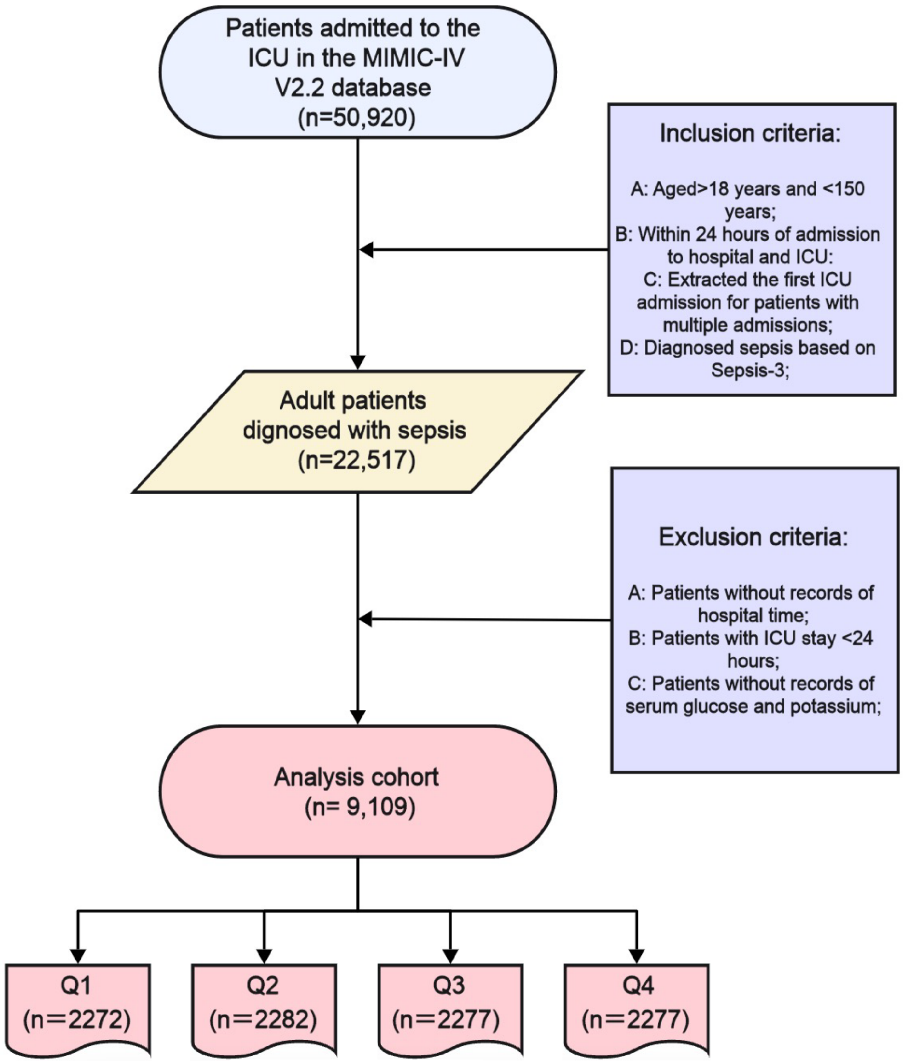

FIGURE 1
Selection of the study population from the MIMIC-IV database.

points. At 60-day, when categorized into quartiles, Model 1 revealed that the risk of hospital mortality for Q4 were 19% higher than for Q1 (HR 1.19 [95% CI 1.08 to 1.31], P < 0.001), Model 2 revealed that the risk of hospital mortality for Q4 were 18% higher than for Q1 (HR 1.18 [95% CI 1.03 to 1.35], P < 0.001). At 90-day, when categorized into quartiles, Model 1 revealed that the risk of hospital mortality for Q4 were 20% higher than for Q1 (HR 1.20 [95% CI 1.09 to 1.32], P < 0.001), Model 2 revealed that the risk of hospital mortality for Q4 were 15% higher than for Q1 (HR 1.15 [95% CI 1.01 to 1.32], P = 0.037). The differences in Model 3 results compared to Models 1 and 2 are likely due to the additional adjustment for confounding variables such as WBC, RBC, RDW, albumin, chloride, ALT, etc.

For ICU mortality, the GPR, when used as a continuous variable, was significantly associated with an elevated risk of ICU death in Models 1, 2 and 3 (All P < 0.001). Furthermore, when the GPR was categorized into quartiles, at 30-day, Model 1 demonstrated that the risk of ICU mortality for Q4 was 1.13 times that of Q1 (HR 1.13 [95% CI 1.01 to 1.26], P < 0.001). At 60-day, Model 1 demonstrated that the risk of ICU mortality for Q4 was 1.23 times that of Q1 (HR 1.23 [95% CI 1.10 to 1.37], P < 0.001), Model 2 demonstrated that the risk of ICU mortality for Q4 was 1.21 times that of Q1 (HR 1.04 [95% CI 1.01 to 1.41], P = 0.015) (Table 2).

3.4 RCS regression models for all-cause mortality (in hospital and ICU)

We subsequently employed the RCS regression models to elucidate the risk and discovered a nonlinear association between the GPR and mortality. Figures 3 and 4 illustrate the results of the univariate and multivariate analyses regarding the relationship between the GPR and in-hospital, In-ICU mortality in three time points, respectively.

Figures 3A, B present the findings of the univariate and multivariate analyses concerning the association between the GPR and hospital mortality on 30-day, respectively. Before adjusting for

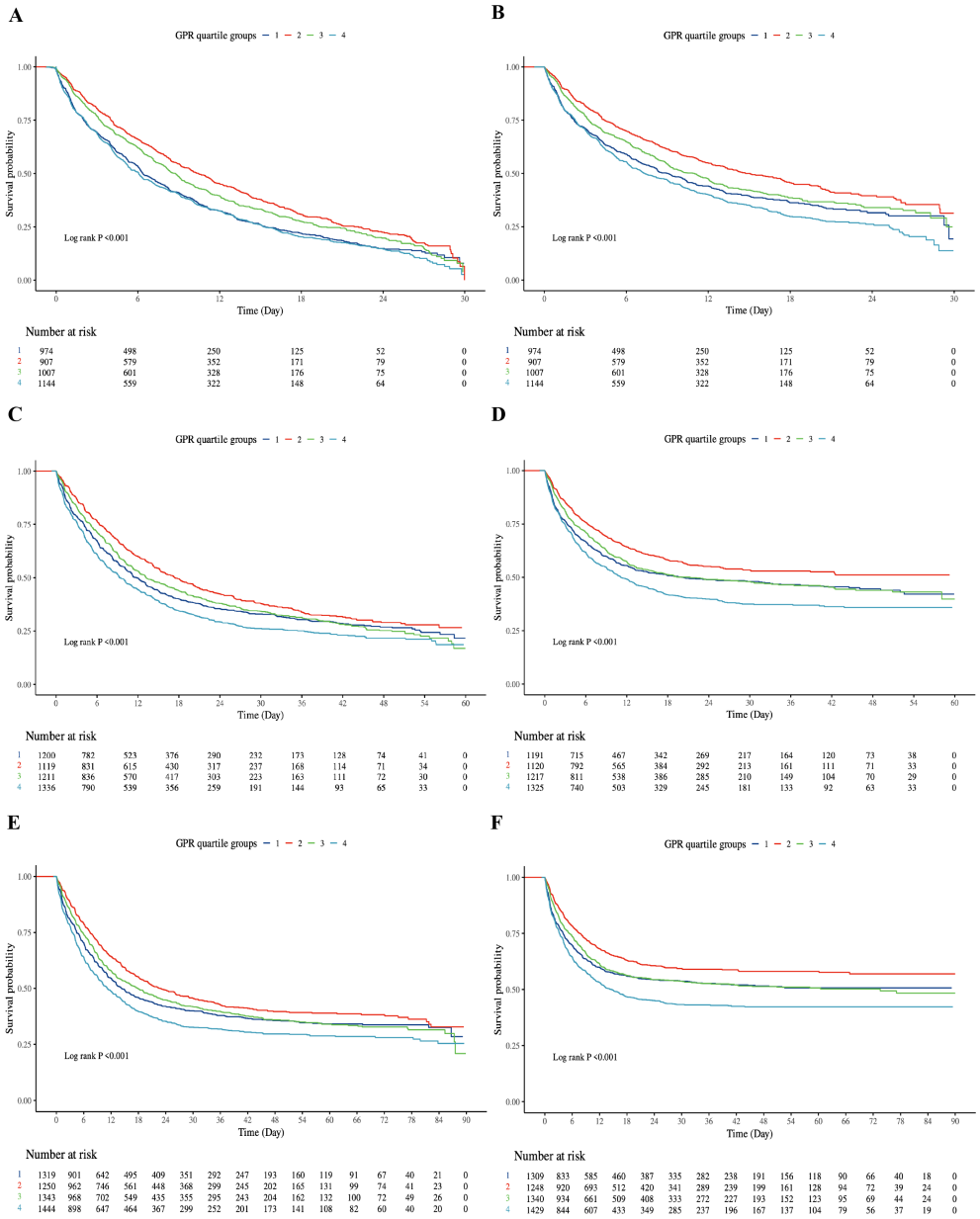

FIGURE 2
Kaplan-Meier survival curve of cumulative survival rate during hospitalization and ICU for groups. **(A)**: Kaplan-Meier survival curve of cumulative survival rate during hospitalization for groups at 30-day. **(B)**: Kaplan-Meier survival curve of cumulative survival rate during ICU for groups at 30-day. **(C)** Kaplan-Meier survival curve of cumulative survival rate during hospitalization for groups at 60-day. **(D)** Kaplan-Meier survival curve of cumulative survival rate during ICU for groups at 60-day. **(E)** Kaplan-Meier survival curve of cumulative survival rate during hospitalization for groups at 90-day. **(F)** Kaplan-Meier survival curve of cumulative survival rate during ICU for groups at 90-day. X-axis: Time (Days); Y-axis: Survival Probability. Log-rank test, all $P < 0.001$. Q1: dark blue; Q2: red; Q3: green; Q4: light blue.

30-day in-hospital mortality, the p-value for the overall effect was < 0.001, and the p-value for the nonlinear effect was also < 0.001. Following adjustment, all p-values were less than 0.05. Similarly, nonlinear associations were observed for 60-day (Figures 3C, D) and 90-day (Figures 3E, F) in-hospital mortality, both before and after adjustment for relevant factors.

For ICU mortality, on 30-day mortality (Figures 4A, B), the unadjusted p value for the overall effect was less than 0.001, the p value for the nonlinear effect was less than 0.001, and all adjusted p values were greater than 0.05. The unadjusted p value was less than 0.001 for the overall effect and less than 0.001 for the nonlinear effect on 60-day mortality (Figures 4C, D). The adjusted p value was 0.007 for the overall effect and 0.004 for the nonlinear effect. Finally, on 90-day mortality (Figures 4E, F), the unadjusted p value was less than 0.001 for the overall effect and less than 0.001 for the nonlinear effect. After adjustment, the p value of overall effect was 0.014, and the p value of nonlinear effect was 0.01. Figures 3 and 4 demonstrate that the inflection point in both multifactorial models is about 30.

10.3389/fendo.2025.1555082

TABLE 2 The association between GPR groups and in-hospital and ICU mortality at 30-day, 60-day and 90-day.

Exposure	Model 1		Model 2		Model 3	
	HR (95% CI)	*P*-value	HR (95% CI)	*P*-value	HR (95% CI)	*P*-value
In-hospital mortality						
At 30-day						
GPR as continuous	1.01 (1.01 ~ 1.01)	**<0.001**	1.01 (1.01 ~ 1.01)	**0.012**	1.01 (1.01 ~ 1.01)	**0.012**
Q1	1.00 (Reference)		1.00 (Reference)		1.00 (Reference)	
Q2	0.73 (0.65 ~ 0.81)	**<0.001**	0.79 (0.68 ~ 0.91)	**0.002**	0.87 (0.70 ~ 1.08)	**0.200**
Q3	0.82 (0.74 ~ 0.91)	**<0.001**	0.81 (0.70 ~ 0.93)	**0.004**	0.80 (0.64 ~ 0.99)	**0.042**
Q4	1.05 (0.95 ~ 1.15)	0.370	0.99 (0.86 ~ 1.13)	0.838	0.99 (0.80 ~ 1.22)	0.916
At 60-day						
GPR as continuous	1.01 (1.01 ~ 1.01)	**<0.001**	1.01 (1.01 ~ 1.01)	**<0.001**	1.01 (1.01 ~ 1.01)	**0.012**
Q1	1.00 (Reference)		1.00 (Reference)		1.00 (Reference)	
Q2	0.81 (0.73 ~ 0.90)	**<0.001**	0.92 (0.80 ~ 1.07)	0.270	0.91 (0.74 ~ 1.13)	0.397
Q3	0.94 (0.85 ~ 1.04)	0.214	0.98 (0.85 ~ 1.13)	0.795	0.92 (0.75 ~ 1.13)	0.433
Q4	1.19 (1.08 ~ 1.31)	**<0.001**	1.18 (1.03 ~ 1.35)	**0.015**	1.14 (0.93 ~ 1.41)	0.202
At 90-day						
GPR as continuous	1.01 (1.01 ~ 1.01)	**<0.001**	1.01 (1.01 ~ 1.01)	**<0.001**	1.01 (1.01 ~ 1.01)	**0.012**
Q1	1.00 (Reference)		1.00 (Reference)		1.00 (Reference)	
Q2	0.81 (0.73 ~ 0.90)	**<0.001**	0.90 (0.78 ~ 1.03)	0.135	0.87 (0.70 ~ 1.07)	0.173
Q3	0.93 (0.85 ~ 1.03)	0.182	0.96 (0.83 ~ 1.10)	0.523	0.91 (0.74 ~ 1.12)	0.355
Q4	1.20 (1.09 ~ 1.32)	**<0.001**	1.15 (1.01 ~ 1.32)	**0.037**	1.10 (0.90 ~ 1.35)	0.351
ICU mortality						
At 30-day						
GPR as continuous	1.01 (1.01 ~ 1.01)	**<0.001**	1.01 (1.01 ~ 1.01)	**<0.001**	1.01 (1.01 ~ 1.01)	**<0.001**
Q1	1.00 (Reference)		1.00 (Reference)		1.00 (Reference)	
Q2	0.72 (0.63 ~ 0.81)	**<0.001**	0.81 (0.69 ~ 0.96)	**0.017**	0.73 (0.65 ~ 0.81)	**<0.001**
Q3	0.87 (0.78 ~ 0.98)	**0.024**	0.85 (0.72 ~ 1.00)	0.052	0.82 (0.74 ~ 0.91)	**<0.001**
Q4	1.13 (1.01 ~ 1.26)	**0.027**	1.07 (0.91 ~ 1.24)	0.425	1.05 (0.95 ~ 1.15)	0.370
At 60-day						
GPR as continuous	1.01 (1.01 ~ 1.01)	**<0.001**	1.01 (1.01 ~ 1.01)	**<0.001**	1.01 (1.01 ~ 1.01)	**0.012**
Q1	1.00 (Reference)		1.00 (Reference)		1.00 (Reference)	
Q2	0.76 (0.67 ~ 0.86)	**<0.001**	0.89 (0.76 ~ 1.06)	0.190	0.73 (0.65 ~ 0.81)	**<0.001**
Q3	0.93 (0.83 ~ 1.05)	0.255	0.96 (0.82 ~ 1.13)	0.618	0.82 (0.74 ~ 0.91)	**<0.001**
Q4	1.23 (1.10 ~ 1.37)	**<0.001**	1.21 (1.04 ~ 1.41)	**0.015**	1.05 (0.95 ~ 1.15)	0.370
At 90-day						
GPR as continuous	1.01 (1.01 ~ 1.01)	**<0.001**	1.01 (1.01 ~ 1.01)	**<0.001**	1.01 (1.01 ~ 1.01)	**0.012**
Q1	1.00 (Reference)		1.00 (Reference)		1.00 (Reference)	
Q2	0.76 (0.67 ~ 0.86)	**<0.001**	0.88 (0.75 ~ 1.04)	0.148	0.73 (0.65 ~ 0.81)	**<0.001**

(Continued)

TABLE 2 Continued

Exposure	Model 1		Model 2		Model 3	
	HR (95% CI)	*P*-value	HR (95% CI)	*P*-value	HR (95% CI)	*P*-value
ICU mortality						
Q3	0.95 (0.84 ~ 1.06)	0.353	0.95 (0.81 ~ 1.11)	0.515	0.82 (0.74 ~ 0.91)	**<0.001**
Q4	1.26 (1.13 ~ 1.40)	**<0.001**	1.20 (1.03 ~ 1.40)	**0.018**	1.05 (0.95 ~ 1.15)	0.370

*GPR: Q1 (Quartile 1; GPR ≤ 6.67, n=436), Q2 (Quartile 2; 6.67 < GPR ≤ 25.71), Q3 (Quartile 3; 25.71 < GPR ≤ 40.81) and Q4 (Quartile 4; GPR > 40.81). HR: hazard ratio; CI: confidential interval.
Model 1: Cox univariate analysis.
Model 2: Adjusted for age, gender, height, weight, insurance, marital status and race.
Model 3: Adjusted for age, gender, height, weight, insurance, marital status and race, WBC, RBC, RDW, albumin, chloride, ALT, AST, Hypertension, Type 2 diabetes mellitus, heart failure, malignant tumor, chronic kidney disease, acute renal failure, stroke, hyperlipidemia, chronic obstructive pulmonary disease, SIRS, CRRT, Oxford acute severity of illness score, Simplified acute physiology score II, Sequential organ failure assessment, Central nervous system, Glasgow coma scale.
Bold red font indicates p-values with statistical significance.

3.5 Subgroup analysis

In subgroup analyses, the directionality of the effect estimates in subgroups was consistent with the overall outcomes. Subgroup analyses were stratified by age, sex, BMI, hypertension, type 2 diabetes, heart failure, CKD, stroke, AKI, CRRT, and mechanical ventilation.

The directional trends in the effect estimates for in-hospital mortality (Figure 5A) in almost subgroups were consistent with the overall outcomes before adjustment for covariates. Similarly, almost all subgroups were consistent with the overall outcome of ICU mortality (Figure 5B). In addition, there was an interaction between mechanical ventilation subgroup parameters ($P < 0.01$ for interaction). After adjustment for covariates, the directionality of the effect estimates in in-hospital and ICU mortality was consistent with the overall outcome in almost all subgroups except AKI and the subgroups with CRRT and no mechanical ventilation. There was no interaction between GPR and age, gender, BMI, hypertension, type 2 diabetes, heart failure, CKD, shock and mechanical ventilation (all P for interaction >0.05).

3.6 Sensitivity analyses

The E-values for the association between GPR and mortality outcomes at different time points are as follows: For ICU mortality, the E-values are 1.60 (30-day, HR=1.13), 1.79 (60-day, HR=1.23), and 1.85 (90-day, HR=1.26). For in-hospital mortality, the E-values are 1.11 (30-day, HR=1.05), 1.66 (60-day, HR=1.19), and 1.68 (90-day, HR=1.20). An E-value of 1.60 for 30-day ICU mortality implies that an unmeasured confounder would need to be associated with both the exposure and outcome by at least 1.60-fold to fully explain the observed association. Similarly, higher E-values for other time points indicate the minimum association strength required for potential unmeasured confounders to explain the observed results.

The common support test results confirmed that the propensity scores of the high GPR and low GPR groups had sufficient overlap. The kernel density plots showed that the density lines for the two groups were closely aligned both before and after matching, indicating a large common support region. The histograms further demonstrated that most observations were within the common support range, ensuring minimal sample loss during the matching process. This confirmed the reliability of the matching process and the comparability of the matched groups. The balance assessment figures demonstrate that after PSM, the bias for all covariates was reduced to below 10%, and the t-tests showed no significant differences between the groups ($p > 0.05$). This indicates that the matching process successfully balanced the covariates between the high and low GPR groups. The kernel density and histogram figures show that the propensity scores of the two groups had sufficient overlap both before and after matching. After matching, the density lines and histogram bars for the two groups were closely aligned, indicating a large common support region and minimal loss of samples. This ensures that the matched groups are comparable and the results are reliable. These visualizations provide additional evidence of the effectiveness of the PSM method in reducing bias and enhancing the comparability of the groups, thereby strengthening the validity of the study findings. (Supplementary Table 2, Figures 6, 7).

4 Discussion

This study examines the association between GPR and short- and long-term all-cause mortality in ICU-admitted sepsis patients using the MIMIC-IV database. With a large sample and extensive confounder adjustment, the results show a significant link between higher GPR and increased mortality risk in both hospital and ICU settings over 90 days. The nonlinear relationship identified by restricted cubic spline regression, with an inflection point at GPR 30, adds depth to GPR's prognostic potential. Our study is the first large-scale validation of GPR in ICU sepsis patients, addressing inconsistencies in prior literature (13, 23). The composite GPR captures synergistic metabolic dysregulation (hyperglycemia + hypokalemia), explaining its incremental prognostic value over isolated markers. The U-shaped association—lower risk in Q2/Q3 vs. Q1—may reflect protective effects of moderate metabolic stress, whereas extremes (Q1: hypokalemia; Q4: severe dysregulation) drive mortality. The former is likely to exacerbate cardiac instability, while the latter's extreme dysregulation overrides compensatory mechanisms. This aligns with the RCS-identified threshold (GPR=30), beyond which mortality risk escalates

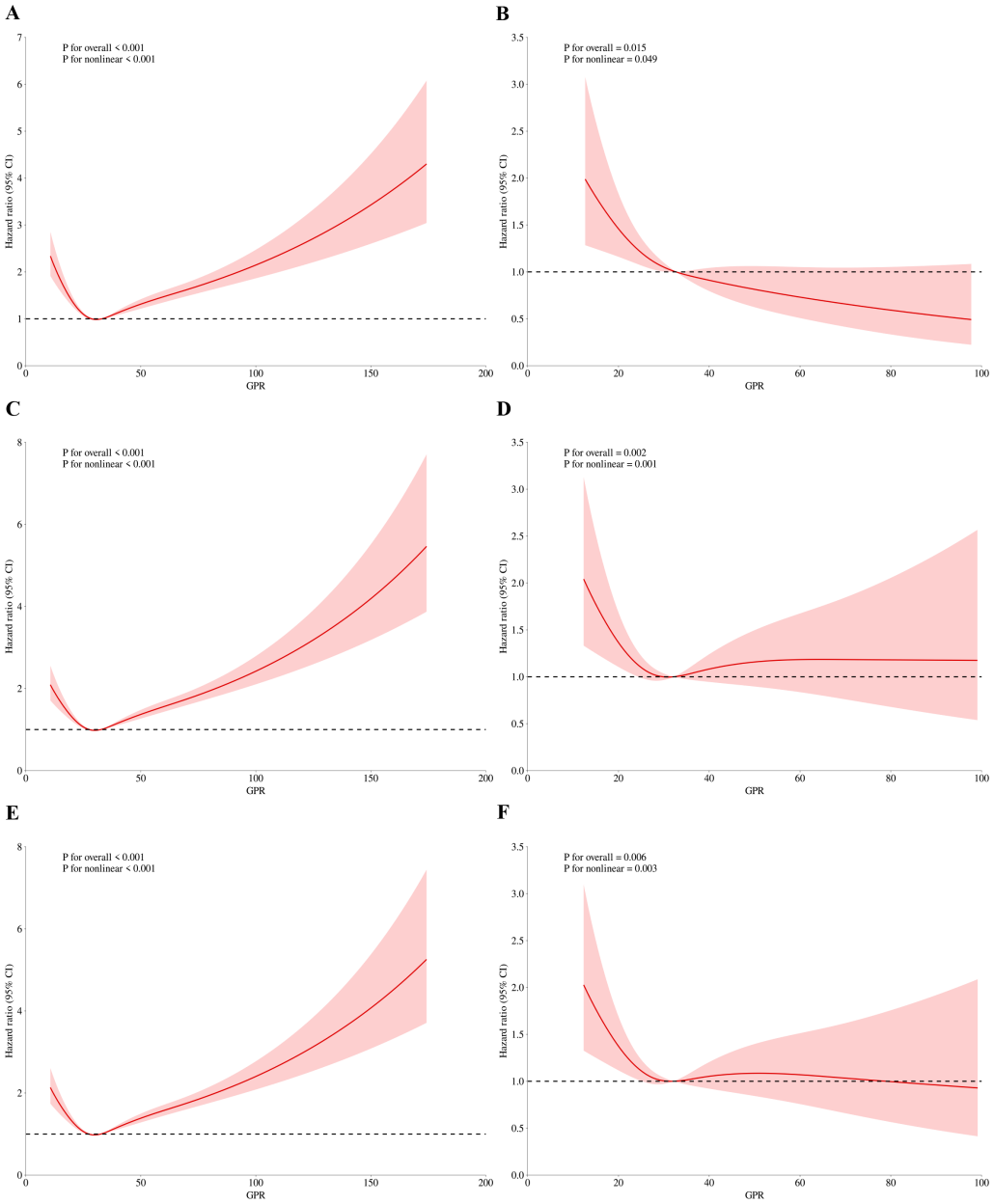

FIGURE 3
RCS regression for GPR and in-hospital mortality. **(A)** Univariate analysis at 30-day (P for overall effect <0.001; P for nonlinearity <0.001). **(B)** Multivariate analysis at 30-day (P for overall effect <0.001; P for nonlinearity <0.001). **(C)** Univariate analysis at 60-day (P for overall effect <0.001; P for nonlinearity <0.001). **(D)** Multivariate analysis at 60-day (P for overall effect 0.007; P for nonlinearity 0.004). **(E)** Univariate analysis at 90-day (P for overall effect <0.001; P for nonlinearity <0.001). **(F)** Multivariate analysis at 90-day (P for overall effect 0.014; P for nonlinearity 0.010).

sharply. Sensitivity analyses including E-value quantification and propensity score matching further reinforced the robustness of our primary findings. The E-values (1.60–1.85 for ICU mortality) indicate that unmeasured confounders would need strong associations to nullify our results, while PSM confirmed the mortality gradient across quartiles in matched cohorts. These findings underscore GPR's utility as a prognostic indicator in critically ill septic patients.

This study underscores that GPR, when evaluated both as a continuous variable and within categorized quartiles, stands out as a predictive marker for mortality in septic patients requiring intensive care. In particular, patients belonging to the highest GPR quartile (Q4) consistently demonstrated notably higher mortality rates compared to those in the lowest quartile (Q1) across all measured intervals (30, 60, and 90 days) and settings (hospital and ICU), as shown by Hazard Ratios (HRs) that reflected increased risk. These findings highlight the GPR's potential as an independent prognostic indicator beyond traditional physiological and biochemical markers often used in ICU settings. While our study offers novel insights into the prognostic role of GPR in sepsis, it builds upon a modest body of prior research investigating GPR in various medical contexts. In non-septic conditions, such as myocardial infarction

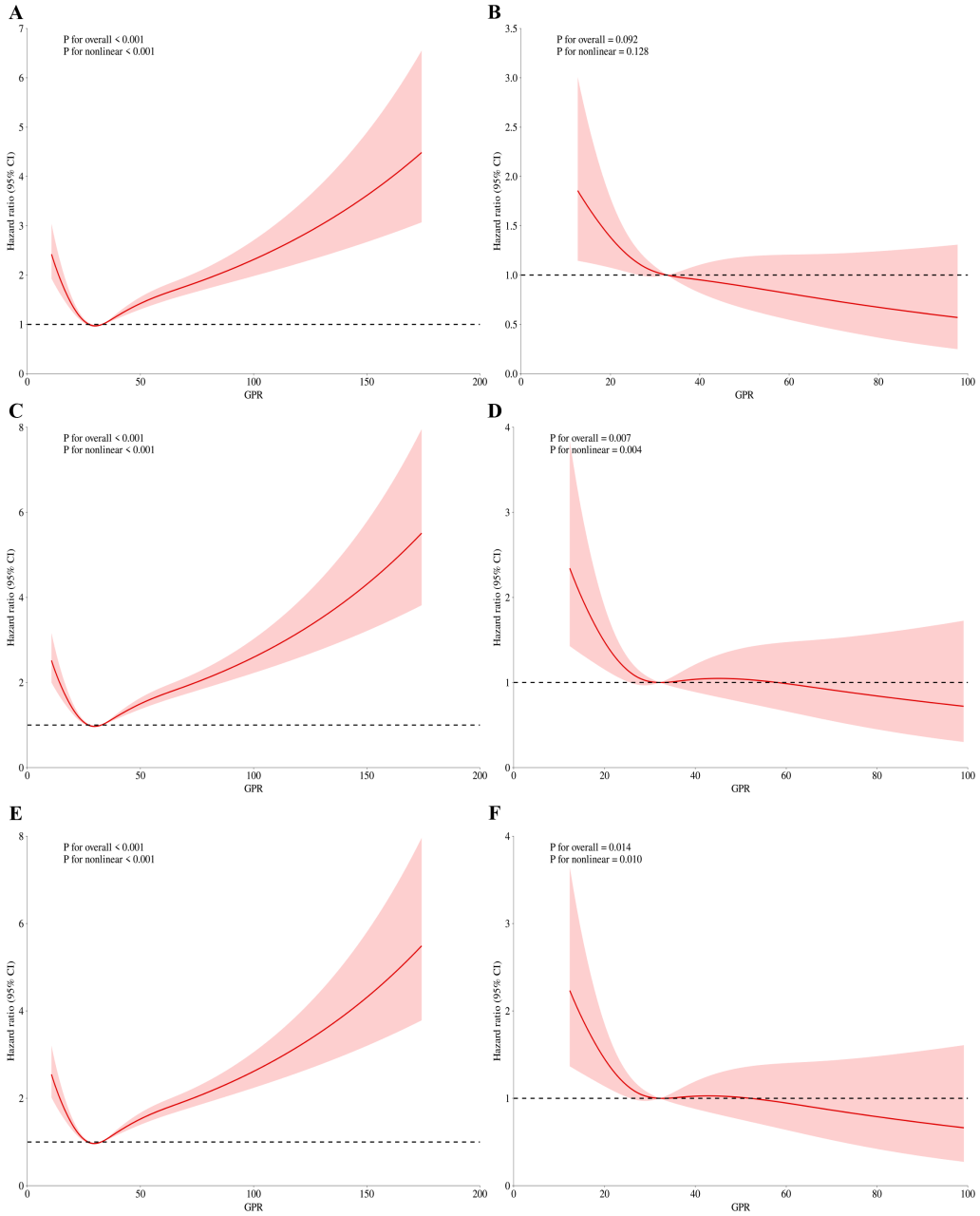

FIGURE 4
RCS regression for GPR and mortality during ICU admission. **(A)** Univariate analysis at 30-day (P for overall effect <0.001; P for nonlinearity <0.001). **(B)** Multivariate analysis at 30-day (P for overall effect <0.001; P for nonlinearity <0.001). **(C)** Univariate analysis at 60-day (P for overall effect <0.001; P for nonlinearity <0.001). **(D)** Multivariate analysis at 60-day (P for overall effect 0.007; P for nonlinearity 0.004). **(E)** Univariate analysis at 90-day (P for overall effect <0.001; P for nonlinearity <0.001). **(F)** Multivariate analysis at 90-day (P for overall effect 0.014; P for nonlinearity 0.010).

(7) and heart failure (6), elevated GPRs have also demonstrated correlations with increased morbidity and mortality, signifying its broad potential as a marker of metabolic imbalance. In ischemic stroke patients, a study (24) found that GPR was positively correlated with 30-day mortality, and the relationship between them was linear. In a multicenter retrospective cohort study (25), baseline GPR serum was found to be an independent predictor of all-cause mortality within 12 months in patients with acute and subacute ischemic stroke, and the study by Zhang et al. (26) also reached a similar conclusion. Chen et al. (27) found that high GPR was an independent risk factor for in-hospital mortality in patients with Acute type A aortic dissection (ATAAD). Serum GPR was observed in 146 patients. In cases of severe traumatic brain injury is substantially associated with trauma severity and 30-day mortality (28), and a similar association has been observed in patients with traumatic brain injury undergoing emergency craniotomy (29). Similarly, another study (30) observed a significant relationship between serum GPR and admission injury severity and the 6-month prognosis acute traumatic Spinal cord injurypatients. A high GFR correlated with Hunt and Kosnik grade and was also observed in

10.3389/fendo.2025.1555082

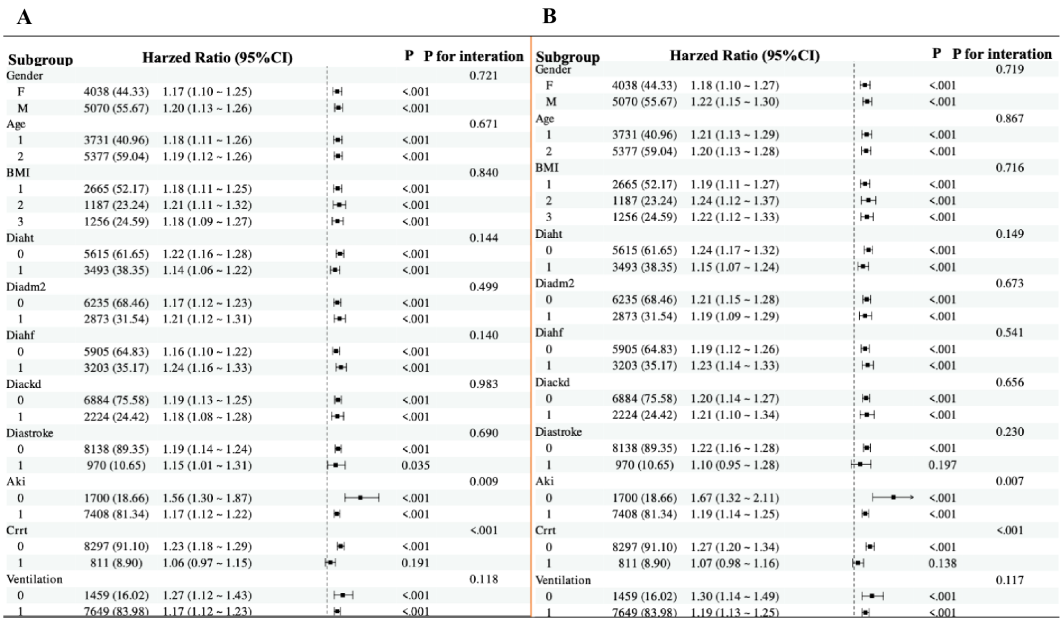

FIGURE 5
Forest plots for subgroup analyses of the association between GPR and mortality. **(A)** Subgroup analysis of the association between GPR and in-hospital mortality after covariate adjustment. **(B)** Subgroup analysis of the association between GPR and ICU mortality after covariate adjustment. For both plots, hazard ratios (HRs) and 95% confidence intervals (CIs) are shown. The analysis includes subgroups based on age (≤70 years and >70 years), sex, BMI (<27.4 kg/m^2, 27.4–31.2 kg/m^2, ≥31.2 kg/m^2), hypertension, type 2 diabetes, heart failure, CKD, stroke, AKI, CRRT, and mechanical ventilation. The P value for interaction is provided for each subgroup analysis.

patients with aneurysmal subarachnoid hemorrhage at admission Glasgow Outcome Scale score at discharge (31, 32). The predictive value between GPR and adverse clinical outcomes was also preliminarily verified in patients with acute intracerebral hemorrhage. In a retrospective study (33), it was observed that the predictive efficacy of GRF for the diagnosis of massive pulmonary embolism and non-massive pulmonary embolism in ICU patients was higher than that of D-dimer. However, another study based on ICU patients (34) found that the mortality of patients with isolated blunt abdominal trauma was highly correlated with GFR, and the sensitivity and specificity of GRF were both higher than 70%. Such studies provide a contextual backdrop where the dysregulation of glucose and potassium levels has been similarly implicated in adverse outcomes, suggesting a possible cross-pathophysiological utility of the GPR. However, existing literature on GPR specifically within sepsis is relatively scant, and the findings have been inconclusive due to significant methodological variances and population differences.

The GPR in sepsis reflects intricate metabolic dysregulations that accompany the systemic inflammatory response characteristic of this condition. Understanding the potential pathological mechanisms that lead to changes in both glucose and potassium levels can provide valuable insights into the prognostic value and clinical significance of GPR in sepsis. In sepsis, hyperglycemia is a frequent occurrence due to a combination of increased hepatic glucose production and impaired peripheral glucose utilization. Stress-induced hormonal responses (35), including the release of cortisol, catecholamines, glucagon, and pro-inflammatory cytokines (36), like tumor necrosis factor-alpha and interleukins, stimulate hepatic gluconeogenesis and glycogenolysis. This hypermetabolic state is compounded by insulin resistance, which limits glucose uptake by peripheral tissues, further elevating blood glucose levels (37). The pathological mechanism of hyperglycemia in sepsis can exacerbate the disease's course through a variety of pathways. Elevated glucose levels contribute to oxidative stress by generating advanced glycation end products (AGEs) (38), which promote inflammation and tissue injury. Hyperglycemia also impairs neutrophil function (39), thereby weakening the host immune response and increasing susceptibility to infections. Furthermore, it is associated with endothelial dysfunction (40, 41), facilitating microvascular thrombosis and impaired tissue perfusion, which can deteriorate organ function. Clinically, the presence of hyperglycemia in sepsis patients has been linked to worse outcomes, including increased mortality rates, prolonged ICU stay, and higher incidences of multi-organ failure (42). This underlines the importance of close glycemic control in critical care settings, although the potential benefits must be weighed against the risks of hypoglycemia. Potassium imbalances, notably hypokalemia, are also common in sepsis and can stem from several factors. These include intracellular shifts of potassium driven by insulin administration (43) (used therapeutically to control hyperglycemia), beta-adrenergic stimulation, and metabolic alkalosis, as well as increased renal losses due to activation of the renin-angiotensin-aldosterone system and nephrotoxic effects of medications or the sepsis itself. Alternatively, hyperkalemia can occur, particularly in cases of acute kidney injury or significant cellular lysis (44). The clinical consequences of potassium imbalances are profound. Hypokalemia may lead to arrhythmias,

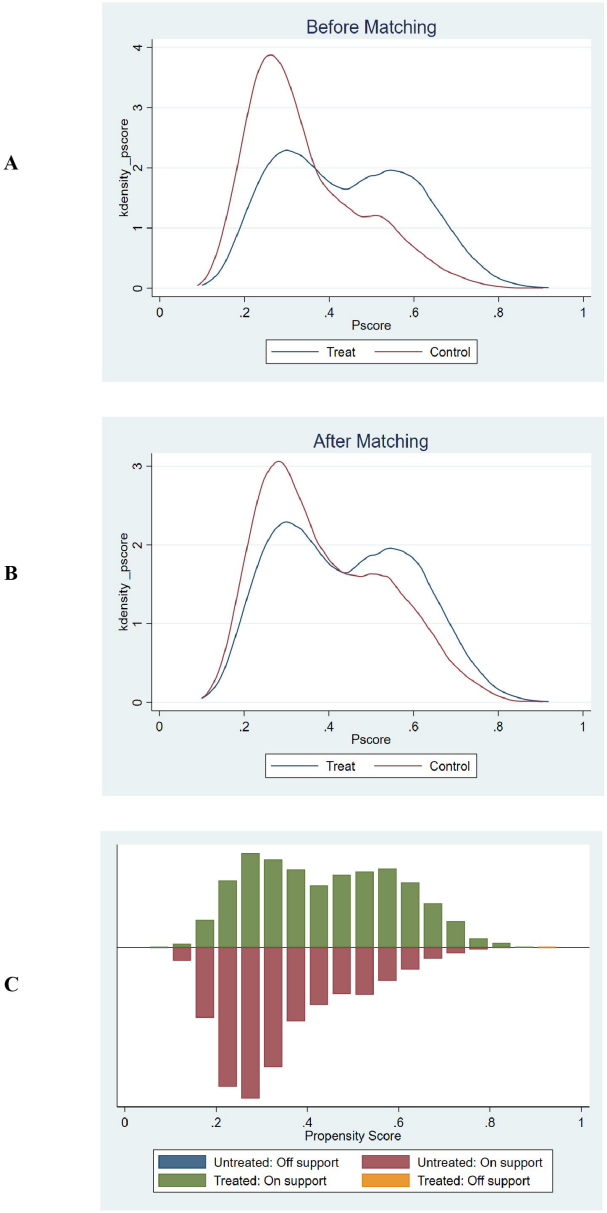

FIGURE 6
Propensity score matching and common support assessment regarding in-hospital mortality. **(A)** Kernel Density Estimation Before Matching: Displays the kernel density estimates of propensity scores for the treatment group (blue line) and control group (red line) prior to matching. The overlapping regions between the two curves indicate the initial common support area. Before matching, the density curves show some overlap, but there are also areas where the propensity scores of the treatment and control groups do not align closely, suggesting a limited common support region. **(B)** Kernel Density Estimation After Matching: Shows the kernel density estimates of propensity scores for the treatment group (blue line) and control group (red line) following matching. After matching, the density curves of the two groups are closely aligned across a wider range of propensity scores. This close alignment demonstrates an expanded common support region, indicating that the matching process has effectively balanced the distribution of propensity scores between the treatment and control groups. **(C)** Histogram of Common Support: Presents a histogram displaying the distribution of propensity scores for both the treatment and control groups. The green bars represent the treated observations within the common support range, the red bars represent the untreated observations within the common support range, the blue bar represents untreated observations outside the support, and the orange bar represents treated observations outside the support. The majority of observations fall within the common support range (indicated by the green and red bars), which means that only a minimal number of samples were excluded during the matching process. This ensures that the matched groups are highly comparable and reduces the potential for bias in the subsequent analysis.

muscle weakness, and respiratory failure, while hyperkalemia can precipitate potentially fatal cardiac arrhythmias (45). Potassium levels are critical for the function of cells, particularly in excitable tissues such as nerves and muscles, including the heart, implicating disturbances in significant morbidity in septic patients (46).

The ratio of serum glucose to potassium, or GPR, synthesizes the metabolic derangements of these two crucial solutes into a single metric. While each component on its own provides insight into specific pathophysiological processes, the GPR captures the overarching metabolic stress within the body (47). A high GPR

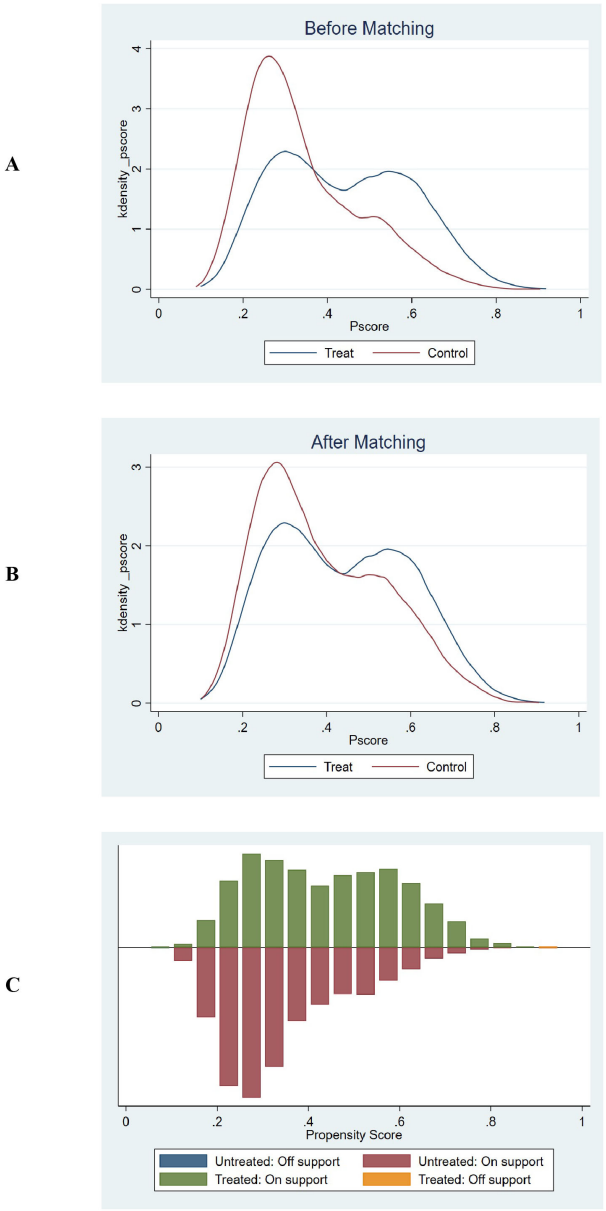

FIGURE 7
Propensity score matching and common support assessment regarding in-ICU mortality. **(A)** Kernel Density Estimation Before Matching: Displays the kernel density estimates of propensity scores for the treatment group (blue line) and control group (red line) prior to matching. The overlapping regions between the two curves indicate the initial common support area. Before matching, the density curves show some overlap, but there are also areas where the propensity scores of the treatment and control groups do not align closely, suggesting a limited common support region. **(B)** Kernel Density Estimation After Matching: Shows the kernel density estimates of propensity scores for the treatment group (blue line) and control group (red line) following matching. After matching, the density curves of the two groups are closely aligned across a wider range of propensity scores. This close alignment demonstrates an expanded common support region, indicating that the matching process has effectively balanced the distribution of propensity scores between the treatment and control groups. **(C)** Histogram of Common Support: Presents a histogram displaying the distribution of propensity scores for both the treatment and control groups. The green bars represent the treated observations within the common support range, the red bars represent the untreated observations within the common support range, the blue bar represents untreated observations outside the support, and the orange bar represents treated observations outside the support. The majority of observations fall within the common support range (indicated by the green and red bars), which means that only a minimal number of samples were excluded during the matching process. This ensures that the matched groups are highly comparable and reduces the potential for bias in the subsequent analysis.

may indicate a metabolic milieu marked by severe insulin resistance, profound stress response, and possibly inadequate compensatory mechanisms for electrolyte maintenance (48). This composite biomarker might therefore reflect a higher severity of systemic physiological derangement, correlating with worse clinical outcomes. Integrating glucose and potassium levels into a single ratio could afford a fuller picture of the metabolic state in sepsis compared to evaluating each element in isolation. In clinical practice, monitoring the GPR in sepsis patients could potentially aid in identifying patients at higher risk of adverse outcomes,

offering opportunities for early intervention and more tailored therapeutic strategies. However, understanding the precise interplay and optimizing clinical use of GPR necessitate further research exploring the dynamic interrelations between glucose and potassium metabolisms in the progression of sepsis.

The E-values calculated for the association between GPR and mortality outcomes provide additional insight into the robustness of our findings against unmeasured confounding. For instance, an E-value of 1.60 for 30-day ICU mortality implies that an unmeasured confounder would need to be associated with both the exposure and outcome by at least 1.60-fold to fully explain the observed association. Similarly, the propensity score matching (PSM) analysis confirmed the consistency of our findings, further strengthening the validity of the observed association between GPR and mortality in sepsis patients.

This study's contribution to the field is highlighted by its significant dataset derived from the MIMIC-IV database, encompassing a variety of demographic and clinical variables not previously analyzed in this combination. By confirming the prognostic relevance of GPR across a diverse ICU population, our findings suggest this biomarker could play a critical role in advancing sepsis management protocols, potentially guiding therapeutic decisions to mitigate mortality risks more effectively. Future research should focus on prospective validation of GPR thresholds and exploration of GPR dynamics over the course of sepsis to better understand its prognostic implications. By identifying patients at high risk of poor outcomes early in their treatment course, clinicians could tailor more aggressive monitoring and intervention strategies, which might include tighter glucose control, more frequent electrolyte assessments, or enhanced cardiovascular monitoring. Such an approach could lead to better resource allocation in high-intensity care environments and possibly improve patient outcomes by preemptively managing predicted complications.

This study also has limitations. The MIMIC-IV database consists largely of data from patients at a single tertiary care center, potentially limiting the generalizability of findings to other settings with different demographics, socioeconomic backgrounds, or healthcare systems (49). This can result in a population that is not fully representative of broader, more diverse sepsis populations worldwide. The demographic composition within the database may not sufficiently capture the variability across different ethnic and racial groups, which can affect disease presentation and responses to treatment, potentially skewing results and interpretations. Although the study includes adjustments for factors such as age and comorbidities, the inherent diversity in these variables may not be fully comparable across different demographic groups (50), implicating variations in baseline mortality risk that might confound the association between GPR and outcomes. In addition, as a retrospective study, it is subject to inherent biases such as selection bias and information bias (51). Decisions regarding data extraction and the variables included can introduce unintended biases that might impact the overall interpretation of findings. Despite efforts to adjust for numerous confounders, it is possible that not all relevant factors were considered or measured accurately, leading to residual confounding. Factors such as medication usage, nutritional status, or patient management differences might not be fully accounted for. The timing of GPR measurement relative to the onset of sepsis or the clinical course has not been standardized (52), potentially impacting its reliability as a consistent prognostic tool. The variation in when glucose and potassium levels are recorded can introduce discrepancies in how the GPR is calculated and interpreted. What's more, a notable limitation is the potential for missing data, as not all patients may have fully recorded laboratory measurements or clinical outcomes. The study relied on multiple imputation methods to address missing data, which may introduce bias if assumptions about missingness are incorrect (53). The dataset may lack comprehensive longitudinal data necessary to explore causal relationships over time, limiting insights into how changes in GPR might reflect disease progression or response to interventions. Certain clinical variables crucial for understanding individual patient conditions, such as specific dietary intake, detailed medication histories, and underlying genetic predispositions (54, 55), may not be captured in the database, affecting the depth of analysis. Given the nature of the database as an aggregation of EMR from clinical practice, the quality and precision of recorded data can be variable. This variability may affect the accuracy of the input data, especially laboratory measurements, and the resulting analysis (56, 57). Notably, the lack of data on treatment interventions such as insulin therapy and fluid resuscitation represent a key limitation, as these factors can significantly influence patient outcomes and may confound the relationship between GPR and mortality (58, 59).

As a path forward, prospective studies evaluating GPR longitudinally across different stages of sepsis, and within broader and more varied populations, could validate our findings. Investigations might also focus on optimal intervention strategies for patients identified as high-risk by their GPR, possibly examining the impact of targeted therapies aimed at normalizing glucose and potassium homeostasis (60). Furthermore, establishing standardized GPR thresholds and developing clinical guidelines for their use could facilitate more widespread integration of GPR into ICU protocols. Limitations of our study, such as its retrospective nature and reliance on a single database, should also be addressed in future studies to enhance generalizability (61). Additionally, detailed longitudinal data collection could enable a better understanding of the causal pathways potentially involved in the links between GPR and sepsis outcomes.

5 Conclusion

In summary, the serum glucose-potassium ratio emerges from our investigation as a promising biomarker of mortality risk in sepsis, warranting further exploration and validation in future clinical research endeavors. By enhancing our understanding and application of GPR, healthcare practitioners may improve prognostic accuracy and patient outcomes in the challenging realm of sepsis management.

Data availability statement

The datasets presented in this study can be found in online repositories. The names of the repository/repositories and accession number(s) can be found in the article/Supplementary Material.

Ethics statement

This study adhered to the principles outlined in the Declaration of Helsinki. Furthermore, it is important to note that the MIMIC-IV database received approval from the Massachusetts Institute of Technology and the Beth Israel Deaconess Medical Center. The copies of the datasets used in this study are available from the MIMIC database. Due to the retrospective nature of the study, the need of informed consent was waived by the Human Research Ethics Committee of Ningbo No.2 Hospital. The studies were conducted in accordance with the local legislation and institutional requirements. Written informed consent for participation in this study was provided by the participants' legal guardians/next of kin.

Author contributions

JQL: Conceptualization, Data curation, Formal analysis, Funding acquisition, Investigation, Methodology, Project administration, Resources, Software, Supervision, Validation, Visualization, Writing – original draft, Writing – review & editing. ZX: Conceptualization, Data curation, Formal analysis, Funding acquisition, Investigation, Methodology, Project administration, Resources, Software, Supervision, Validation, Visualization, Writing – original draft, Writing – review & editing. XZ: Conceptualization, Data curation, Formal analysis, Funding acquisition, Investigation, Methodology, Project administration, Resources, Software, Supervision, Validation, Visualization, Writing – original draft, Writing – review & editing. JS: Conceptualization, Data curation, Formal analysis, Funding acquisition, Investigation, Methodology, Project administration, Resources, Software, Supervision, Validation, Visualization, Writing – original draft, Writing – review & editing. SC: Conceptualization, Data curation, Formal analysis, Funding acquisition, Investigation, Methodology, Project administration, Resources, Software, Supervision, Validation, Visualization, Writing – original draft, Writing – review & editing. JLL: Conceptualization, Data curation, Formal analysis, Funding acquisition, Investigation, Methodology, Project administration, Resources, Software, Supervision, Validation, Visualization, Writing – original draft, Writing – review & editing. GJ: Conceptualization, Data curation, Formal analysis, Funding acquisition, Investigation, Methodology, Project administration, Resources, Software, Supervision, Validation, Visualization, Writing – original draft, Writing – review & editing. NH: Conceptualization, Data curation, Formal analysis, Funding acquisition, Investigation, Methodology, Project administration, Resources, Software, Supervision, Validation, Visualization, Writing – original draft, Writing – review & editing. YF: Conceptualization, Data curation, Formal analysis, Funding acquisition, Investigation, Methodology, Project administration, Resources, Software, Supervision, Validation, Visualization, Writing – original draft, Writing – review & editing. SX: Conceptualization, Data curation, Formal analysis, Funding acquisition, Investigation, Methodology, Project administration, Resources, Software, Supervision, Validation, Visualization, Writing – original draft, Writing – review & editing.

Funding

The author(s) declare that financial support was received for the research and/or publication of this article. This work was supported by the HwaMei Research Foundation of Ningbo No.2 Hospital (Grant No.2022HMKY48 and No.2023HMZD07), Medical Scientific Research Foundation of Zhejiang Province (Grant No.2021KY1004, No.2023RC081 and No.2025KY1395), the Project of NINGBO Leading Medical & Health Discipline (Project No.2022-F17), the Ningbo Top Medical and Health Research Program (No.2023030615) the Zhejiang Clinovation Pride (CXTD202502004), Research and development of efficient hemostatic materials (2024001), the Zhu Xiu Shan Talent Project of Ningbo No.2 Hospital (No.2023HMYQ25) and Ningbo Health Youth Technical Backbone Talent Development Program (No.2024RC-QN-02). Funders played no role in the study design, execution, or manuscript writing.

Conflict of interest

The authors declare that the research was conducted in the absence of any commercial or financial relationships that could be construed as a potential conflict of interest.

Generative AI statement

The author(s) declare that no Generative AI was used in the creation of this manuscript.

Publisher's note

Supplementary material

The Supplementary Material for this article can be found online at: https://www.frontiersin.org/articles/10.3389/fendo.2025.1555082/full#supplementary-material

References

1. Qian H, Shang W, Zhang S, Pan X, Huang S, Li H, et al. Trends and predictions of maternal sepsis and other maternal infections among women of childbearing age: a systematic analysis for the global burden of disease study 2019. *Front Public Health*. (2024) 12:1428271. doi: 10.3389/fpubh.2024.1428271

2. Cheng S, Li Y, Sun X, Liu Z, Guo L, Wu J, et al. The impact of glucose metabolism on inflammatory processes in sepsis-induced acute lung injury. *Front Immunol*. (2024) 15:1508985. doi: 10.3389/fimmu.2024.1508985

3. Li J, Nie M, Lu Z, Wang Y, Shen X. Efficacy of compound sodium acetate Ringer's solution in early fluid resuscitation for children with septic shock: a preliminary retrospective cohort study. *BMC Pediatr*. (2024) 24:708. doi: 10.1186/s12887-024-05184-1

4. Lou J, Xiang Z, Zhu X, Fan Y, Song J, Cui S, et al. A retrospective study utilized MIMIC-IV database to explore the potential association between triglyceride-glucose index and mortality in critically ill patients with sepsis. *Sci Rep*. (2024) 14:24081. doi: 10.1038/s41598-024-75050-8

5. Liu S, Yang T, Jiang Q, Zhang L, Shi X, Liu X, et al. Lactate and lactylation in sepsis: A comprehensive review. *J Inflammation Res*. (2024) 17:4405–17. doi: 10.2147/JIR.S459185

6. Khan AA, Ata F, Yousaf Z, Aljafar MS, Seijari MN, Matarneh A, et al. A retrospective study on comparison of clinical characteristics and outcomes of diabetic ketoacidosis patients with and without acute pancreatitis. *Sci Rep*. (2023) 13:4347. doi: 10.1038/s41598-023-31465-3

7. Won P, Craig J, Choe D, Collier Z, Gillenwater TJ, Yenikomshian HA. Blood glucose control in the burn intensive care unit: A narrative review of literature. *Burns: J Int Soc Burn Injuries*. (2023) 49:1788–95. doi: 10.1016/j.burns.2023.06.002

8. Shan L, Zheng K, Dai W, Hao P, Wang Y. J-shaped association between serum glucose potassium ratio and prognosis in heart failure with preserved ejection fraction with stronger predictive value in non-diabetic patients. *Sci Rep*. (2024) 14:29965. doi: 10.1038/s41598-024-81289-y

9. Gao H, Xiang Q, Li J, Yu M, Lan Y, Ba J, et al. Clinical analysis of the serum muscle enzyme spectrum of patients with newly diagnosed Sheehan's syndrome. *Medicine*. (2022) 101:e30834. doi: 10.1097/MD.0000000000030834

10. Hagerman A, Schorer R, Putzu A, Keli-Barcelos G, Licker M. Cardioprotective effects of glucose-insulin-potassium infusion in patients undergoing cardiac surgery: A systematic review and meta-analysis. *Semin Thorac Cardiovasc Surg*. (2024) 36:167–81. doi: 10.1053/j.semtcvs.2022.11.002

11. Cheng NC, Tai HC, Chang SC, Chang CH, Lai HS. Necrotizing fasciitis in patients with diabetes mellitus: clinical characteristics and risk factors for mortality. *BMC Infect Dis*. (2015) 15:417. doi: 10.1186/s12879-015-1144-0

12. Koyuncu S, Sipahioglu H, Bol O, İlik HKZ, Dilci A, Elmaağaç M, et al. The evaluation of different treatment approaches in patients with earthquake-related crush syndrome. *Cureus*. (2023) 15:e47194. doi: 10.7759/cureus.47194

13. Güler S, Demirtaş E, Üçöz Kocaşaban D, Sarıhan MB, Esen E, Ata MA, et al. Evaluation of the predictive value of the glucose-to-potassium ratio in predicting in-hospital mortality of patients with sepsis and septic shock. Untersuchung des prädiktiven Werts des Glukose-Kalium-Quotienten für die Vorhersage der Krankenhausmortalität bei Patienten mit Sepsis und septischem Schock. *Medizinische Klinik Intensivmedizin und Notfallmedizin*. (2025). doi: 10.1007/s00063-024-01244-7

14. Monard C, Tebib N, Trächsel B, Kelevina T, Schneider AG. Comparison of methods to normalize urine output in critically ill patients: a multicenter cohort study. *Crit Care (Lond Engl)*. (2024) 28:425. doi: 10.1186/s13054-024-05200-x

15. Seckel MA. Sepsis best practices: Definitions, guidelines, and updates. *Nursing*. (2024) 54:31–9. doi: 10.1097/NSG.0000000000000010

16. Liu Y, Qiu T, Fu Z, Wang K, Zheng H, Li M, et al. Systemic immune-inflammation index and serum glucose-potassium ratio predict poor prognosis in patients with spontaneous cerebral hemorrhage: An observational study. *Medicine*. (2024) 103:e39041. doi: 10.1097/MD.0000000000039041

17. Lange S, Lange R, Tabibi E, Hitschold T, Müller VI, Naumann G. Comparison of vaginal pessaries to standard care or pelvic floor muscle training for treating postpartum urinary incontinence: a pragmatic randomized controlled trial. *Geburtshilfe und Frauenheilkunde*. (2024) 84:246–55. doi: 10.1055/a-2243-3784

18. Tramonti Fantozzi MP, Ceccarelli L, Petri D, De Vita E, Agostini A, Colombatto P, et al. Hepatitis C epidemiology and treatment outcomes in Italy: Impact of the DAA era and the COVID-19 pandemic. *J Viral hepatitis*. (2024) 31:623–32. doi: 10.1111/jvh.13983

19. Rebernick RJ, Bell HN, Wakeam E. Survival analyses: A statistical review for surgeons. *Semin Thorac Cardiovasc Surg*. (2022) 34:1388–94. doi: 10.1053/j.semtcvs.2022.01.001

20. Liu C, Deng L, Lin S, Liu T, Ren J, Shi J, et al. Enteral nutrition support in patients with cancer: association of short-term prognosis and medical costs with inflammation. *Supportive Care Cancer*. (2024) 33:50. doi: 10.1007/s00520-024-09085-y

21. Dai T, Liu M, Bao D, Manor B, Zhou J. Transcranial direct current stimulation alleviates the pain severity in people suffering from knee osteoarthritis: a systematic review and meta-analysis. *Pain Rep*. (2024) 10:e1215. doi: 10.1097/PR9.0000000000001215

22. Pu Y, Xing N, Wang Y, Wang H, Xu J, Li X. Differential impact of TyG and TyG-BMI indices on short- and long-term mortality in critically ill ischemic stroke patients. *BMC Cardiovasc Disord*. (2024) 24:754. doi: 10.1186/s12872-024-04450-5

23. Demir FA, Ersoy İ, Yılmaz AŞ, Taylan G, Kaya EE, Aydın E, et al. Serum glucose-potassium ratio predicts inhospital mortality in patients admitted to coronary care unit. *Rev da Associacao Med Bras (1992)*. (2024) 70:e20240508. doi: 10.1590/1806-9282.20240508

24. Lu Y, Ma X, Zhou X, Wang Y. The association between serum glucose to potassium ratio on admission and short-term mortality in ischemic stroke patients. *Sci Rep*. (2022) 12:8233. doi: 10.1038/s41598-022-12393-0

25. Alamri FF, Almarghalani DA, Alraddadi EA, Alharbi A, Algarni HS, Mulla OM, et al. The utility of serum glucose potassium ratio as a predictive factor for haemorrhagic transformation, stroke recurrence, and mortality among ischemic stroke patients. *Saudi Pharm J*. (2024) 32:102082. doi: 10.1016/j.jsps.2024.102082

26. Zhang Q, Huang Z, Chen S, Yan E, Zhang X, Su M, et al. Association between the serum glucose-to-potassium ratio and clinical outcomes in ischemic stroke patients after endovascular thrombectomy. *Front Neurol*. (2024) 15:1463365. doi: 10.3389/fneur.2024.1463365

27. Chen Y, Peng Y, Zhang X, Liao X, Lin J, Chen L, et al. The blood glucose-potassium ratio at admission predicts in-hospital mortality in patients with acute type A aortic dissection. *Sci Rep*. (2023) 13:15707. doi: 10.1038/s41598-023-42827-2

28. Zhou J, Yang CS, Shen LJ, Lv QW, Xu QC. Usefulness of serum glucose and potassium ratio as a predictor for 30-day death among patients with severe traumatic brain injury. *Clin Chim Acta*. (2020) 506:166–71. doi: 10.1016/j.cca.2020.03.039

29. Zhou H, Tang Y, Li Y, Zhu T. Serum glucose-potassium ratio predicts prognosis of traumatic brain injury in patients undergoing emergency craniotomy: A retrospective study. *Asian J Surg*. (2023) 46:2958–9. doi: 10.1016/j.asjsur.2023.02.034

30. Zhou W, Liu Y, Wang Z, Mao Z, Li M. Serum glucose/potassium ratio as a clinical risk factor for predicting the severity and prognosis of acute traumatic spinal cord injury. *BMC Musculoskeletal Disord*. (2023) 24:870. doi: 10.1186/s12891-023-07013-5

31. Fujiki Y, Matano F, Mizunari T, Murai Y, Tateyama K, Koketsu K, et al. Serum glucose/potassium ratio as a clinical risk factor for aneurysmal subarachnoid hemorrhage. *J Neurosurg*. (2018) 129:870–5. doi: 10.3171/2017.5.JNS162799

32. Matano F, Fujiki Y, Mizunari T, Koketsu K, Tamaki T, Murai Y, et al. Serum glucose and potassium ratio as risk factors for cerebral vasospasm after aneurysmal subarachnoid hemorrhage. *J Stroke Cerebrova Dis*. (2019) 28:1951–7. doi: 10.1016/j.jstrokecerebrovasdis.2019.03.041

33. Boyuk F. The predictor potential role of the glucose to potassium ratio in the diagnostic differentiation of massive and non-massive pulmonary embolism. *Clin Appl thrombosis/hemostasis*. (2022) 28:10760296221076146. doi: 10.1177/10760296221076146

34. Katipoğlu B, Demirtaş E. Assessment of serum glucose potassium ratio as a predictor for morbidity and mortality of blunt abdominal trauma. Künt Abdominal Travma Hastalarında Serum Glikoz Potasyum Oranının Morbidite Ve Mortalite İçin Bir Öngörücü Olarak Değerlendirilmesi. *Ulusal travma ve acil cerrahi dergisi = Turkish J Trauma Emergency Surg: TJTES*. (2022) 28:134–9. doi: 10.14744/tjtes.2020.88945

35. Wasyluk W, Wasyluk M, Zwolak A. Sepsis as a pan-endocrine illness-endocrine disorders in septic patients. *J Clin Med*. (2021) 10:2075. doi: 10.3390/jcm10102075

36. Maas MB, Lizza BD, Kim M, Abbott SM, Gendy M, Reid KJ, et al. Stress-induced behavioral quiescence and abnormal rest-activity rhythms during critical illness. *Crit Care Med*. (2020) 48:862–71. doi: 10.1097/CCM.0000000000004334

37. Miyauchi H, Fujioka K, Okubo S, Nishida K, Ashina M, Ikuta T, et al. Insulin therapy for hyperglycemia in neonatal sepsis using a preterm mouse model. *Pediatr Int*. (2020) 62:581–6. doi: 10.1111/ped.14126

38. Yi H, Duan Y, Song R, Zhou Y, Cui Y, Liu C, et al. Activation of glucagon-like peptide-1 receptor in microglia exerts protective effects against sepsis-induced encephalopathy via attenuating endoplasmic reticulum stress-associated inflammation and apoptosis in a mouse model of sepsis. *Exp Neurol*. (2023) 363:114348. doi: 10.1016/j.expneurol.2023.114348

39. Fan W, Wang C, Xu K, Liang H, Chi Q. Ccl5+ Macrophages drive pro-inflammatory responses and neutrophil recruitment in sepsis-associated acute kidney injury. *Int Immunopharmacol*. (2024) 143:113339. doi: 10.1016/j.intimp.2024.113339

40. Yang X, Pu X, Xu Y, Zhao J, Fang X, Cui J, et al. A novel prognosis evaluation indicator of patients with sepsis created by integrating six microfluidic-based neutrophil chemotactic migration parameters. *Talanta*. (2025) 281:126801. doi: 10.1016/j.talanta.2024.126801

41. Binny R, Kotsanas D, Buttery J, Korman T, Tan K. Is neutrophil to lymphocyte ratio an accurate predictor of neonatal sepsis in premature infants? *Early Hum Dev*. (2025) 200:106147. doi: 10.1016/j.earlhumdev.2024.106147

42. Guo Y, Qiu Y, Xue T, Yan P, Zhao W, Wang M, et al. Association between admission baseline blood potassium levels and all-cause mortality in patients with acute

kidney injury combined with sepsis: A retrospective cohort study. *PLoS One*. (2024) 19: e0309764. doi: 10.1371/journal.pone.0309764

43. Yu J, Fu Y, Zhang N, Gao J, Zhang Z, Jiang X, et al. Extracellular histones promote TWIK2-dependent potassium efflux and associated NLRP3 activation in alveolar macrophages during sepsis-induced lung injury. *Inflammation Res*. (2024) 73:1137–55. doi: 10.1007/s00011-024-01888-3

44. Contrera Rolón N, Cantos J, Huespe I, Prado E, Bratti GI, Schreck C, et al. Fractional excretion of sodium and potassium and urinary strong ion difference in the evaluation of persistent AKI in sepsis. *Medicina Intensiva*. (2024) 49(1):1–7. doi:10.1016/j.medine.2024.02.003

45. Luo W, Xiong L, Wang J, Li C, Zhang S. Development and performance evaluation of a clinical prediction model for sepsis risk in burn patients. *Medicine*. (2024) 103:e40709. doi: 10.1097/MD.0000000000040709

46. Bouadma L, Mankikian S, Darmon M, Argaud L, Vinclair C, Siami S, et al. Influence of dyskalemia at admission and early dyskalemia correction on survival and cardiac events of critically ill patients. *Crit Care (Lond Engl)*. (2019) 23:415. doi: 10.1186/s13054-019-2679-z

47. López A, Varela JJ, Cid MM, Couñago M, Gago N. Hydroelectrolytic and infectious complications in one year of parenteral nutrition in critical care. Complicaciones hidroelectrolíticas e infecciosas en un año de nutrición parenteral en cuidados críticos. *Rev Espanola Anestesiol y Reanimacion*. (2018) 65:373–9. doi: 10.1016/j.redar.2018.03.002

48. Zhang JL, Chen YT, Chen GD, Wang T, Zhang JX, Zeng QY. Glucose-insulin-potassium alleviates intestinal mucosal barrier injuries involving decreased expression of uncoupling protein 2 and NLR family-pyrin domain-containing 3 inflammasome in polymicrobial sepsis. *BioMed Res Int*. (2017) 2017:4702067. doi: 10.1155/2017/4702067

49. Duan W, Yang F, Ling H, Li Q, Dai X. Association between lactate to hematocrit ratio and 30-day all-cause mortality in patients with sepsis: a retrospective analysis of the Medical Information Mart for Intensive Care IV database. *Front Med*. (2024) 11:1422883. doi: 10.3389/fmed.2024.1422883

50. Shi Y, Hu Y, Xu GM, Ke Y. Development and validation of a predictive model for pulmonary infection risk in patients with traumatic brain injury in the ICU: a retrospective cohort study based on MIMIC-IV. *BMJ Open Respir Res*. (2024) 11: e002263. doi: 10.1136/bmjresp-2023-002263

51. Zhang Y, Zhou C, Huang Z, Ye X. Study of cuffless blood pressure estimation method based on multiple physiological parameters. *Physiol Measurement*. (2021) 42. doi: 10.1088/1361-6579/abf889

52. Simons PIHG, Simons N, Stehouwer CDA, Schalkwijk CG, Schaper NC, Brouwers MCGJ. Association of common gene variants in glucokinase regulatory protein with cardiorenal disease: A systematic review and meta-analysis. *PLoS One*. (2018) 42(5):e0206174. doi: 10.1371/journal.pone.0206174

53. Luo J, Huang S, Lan L, Yang S, Cao T, Yin J, et al. EMR-LIP: A lightweight framework for standardizing the preprocessing of longitudinal irregular data in electronic medical records. *Comput Methods Programs Biomed*. (2025) 259:108521. doi: 10.1016/j.cmpb.2024.108521

54. Russell SL, Penunuri G, Condon C. Diverse genetic conflicts mediated by molecular mimicry and computational approaches to detect them. *Semin Cell Dev Biol*. (2025) 165:1–12. doi: 10.1016/j.semcdb.2024.07.001

55. Gu D, Huang S. Letter to the editor on 'Aspirin is associated with improved outcomes in patients with sepsis-induced myocardial injury: An analysis of the MIMIC-IV database'. *J Clin Anesth*. (2025) 100:111683. doi: 10.1016/j.jclinane.2024.111683

56. Park YJ, Bae J, Yoo JK, Ahn SH, Park SY, Kim YS, et al. Effects of NF-κB inhibitor on sepsis depend on the severity and phase of the animal sepsis model. *J Personal Med*. (2024) 14:645. doi: 10.3390/jpm14060645

57. Alcamo AM, Becker AE, Barren GJ, Hayes K, Pennington JW, Curley MAQ, et al. Diagnostic identification of acute brain dysfunction in pediatric sepsis and septic shock in the electronic health record: A comparison of four definitions in a reference dataset. *Pediatr Crit Care Med*. (2024) 25(8):740–7. doi: 10.1097/PCC.0000000000003529

58. Pérez-Tome JC, Parrón-Carreño T, Castaño-Fernández AB, Nievas-Soriano BJ, Castro-Luna G. Sepsis mortality prediction with Machine Learning Tecniques. *Med Intensiva (Engl Ed*. (2024) 48(10):584–593. doi: 10.1016/j.medine.2024.05.009

59. Yang B, Niu K, Zhu Y, Zheng X, Li T, Wang Z, et al. Effects of ondansetron exposure during ICU stay on outcomes of critically ill patients with sepsis: a cohort study. *Front Cell Infect Microbiol*. (2023) 13:1256382. doi: 10.3389/fcimb.2023.1256382

60. Yu X, Xin Q, Hao Y, Zhang J, Ma T. An early warning model for predicting major adverse kidney events within 30 days in sepsis patients. *Front Med (Lausanne)*. (2024) 10:1327036. doi: 10.3389/fmed.2023.1327036

61. Fang Y, Xiong B, Shang X, Yang F, Yin Y, Sun Z, et al. Triglyceride-glucose index predicts sepsis-associated acute kidney injury and length of stay in sepsis: A MIMIC-IV cohort study. *Heliyon*. (2024) 10:e29257. doi: 10.1016/j.heliyon.2024.e29257

frontiers | Frontiers in Endocrinology

TYPE Original Research
PUBLISHED 02 September 2025
DOI 10.3389/fendo.2025.1570332

OPEN ACCESS

EDITED BY
Darko Stefanovski,
University of Pennsylvania, United States

REVIEWED BY
Yuriy L. Orlov,
I.M. Sechenov First Moscow State Medical University, Russia
Xuchu Duan,
Nantong University, China

*CORRESPONDENCE
Ya Wang
wangya@yangtzeu.edu.cn
Jie Tan
tanjie@yangtzeu.edu.cn
Yaling Sun
339081132@qq.com

†These authors have contributed equally to this work

RECEIVED 03 February 2025
ACCEPTED 18 August 2025
PUBLISHED 02 September 2025

CITATION
Ke D, He X, Li W, Wu H, Sun Y, Tan J and Wang Y (2025) The biological and immunological significance of the estrogen-related gene IER3 in diabetes.
Front. Endocrinol. 16:1570332.
doi: 10.3389/fendo.2025.1570332

The biological and immunological significance of the estrogen-related gene IER3 in diabetes

Da Ke[1†], Xian He[1†], Wenzhe Li[1†], Hongyan Wu[1], Yaling Sun[2*], Jie Tan[3*] and Ya Wang[1,2*]

[1]Department of Endocrinology, The First Affiliated Hospital of Yangtze University, Jingzhou First People's Hospital, Jingzhou, Hubei, China, [2]Department of Hubei Provincial Clinical Research Center for Personalized Diagnosis and Treatment of Cancer, The First Affiliated Hospital of Yangtze University, Jingzhou First People's Hospital, Jingzhou, Hubei, China, [3]Department of Hematology, The First Affiliated Hospital of Yangtze University, Jingzhou First People's Hospital, Jingzhou, Hubei, China

Background: Diabetes Mellitus (DM) is a complex metabolic disorder characterized by hyperglycemia, primarily arising from insufficient insulin secretion or the development of insulin resistance. Estrogen plays a significant role in regulating the occurrence and progression of DM. This study aims to investigate the role of estrogen-related genes in diabetes, focusing on identifying potential biomarkers and therapeutic targets for the disease.

Methods: We initially obtained gene expression datasets related to type 2 diabetes mellitus (T2DM) from the GEO database. A systematic and coherent series of methodologies was then implemented in a structured manner. First, Principal Component Analysis (PCA) was employed for preliminary data exploration and dimensionality reduction. Next, we identified Differentially Expressed Genes (DEGs). Subsequently, we conducted Weighted Gene Co-expression Network Analysis (WGCNA) to uncover gene modules associated with DM. This was followed by Gene Ontology (GO) and Kyoto Encyclopedia of Genes and Genomes (KEGG) enrichment analyses to explore the biological functions and pathways associated with the identified genes. To enhance the precision of biomarker identification, we applied three distinct machine learning algorithms, including Least Absolute Shrinkage and Selection Operator (LASSO), Support Vector Machine-Recursive Feature Elimination (SVM-RFE), and Random Forest (RF), for further refined selection. This comprehensive approach ultimately identified the estrogen-related gene IER3 as a promising biomarker for DM. Furthermore, correlation analyses focusing on immune cell infiltration were conducted to clarify the immunological role of IER3 in DM.

Results: Our findings revealed a significant downregulation of IER3 in DM patients, accompanied by an AUC value of 0.723 in the diagnostic curve ROC, indicating its considerable diagnostic and prognostic potential for DM. Furthermore, the expression levels of IER3 exhibited a strong correlation with variations in the proportions of diverse immune cell types, suggesting that it may play a pivotal role in the immunoregulatory mechanisms underlying DM.

10.3389/fendo.2025.1570332

Conclusion: In conclusion, our findings reveal that the estrogen-related gene IER3 is significantly downregulated in patients with DM, highlighting its potential as a diagnostic and prognostic marker for the disease. Therefore, IER3 may serve as a promising biomarker and therapeutic target for DM.

KEYWORDS

diabetes mellitus, glycometabolism, estrogen, bioinformatics analysis, machine learning, IER3

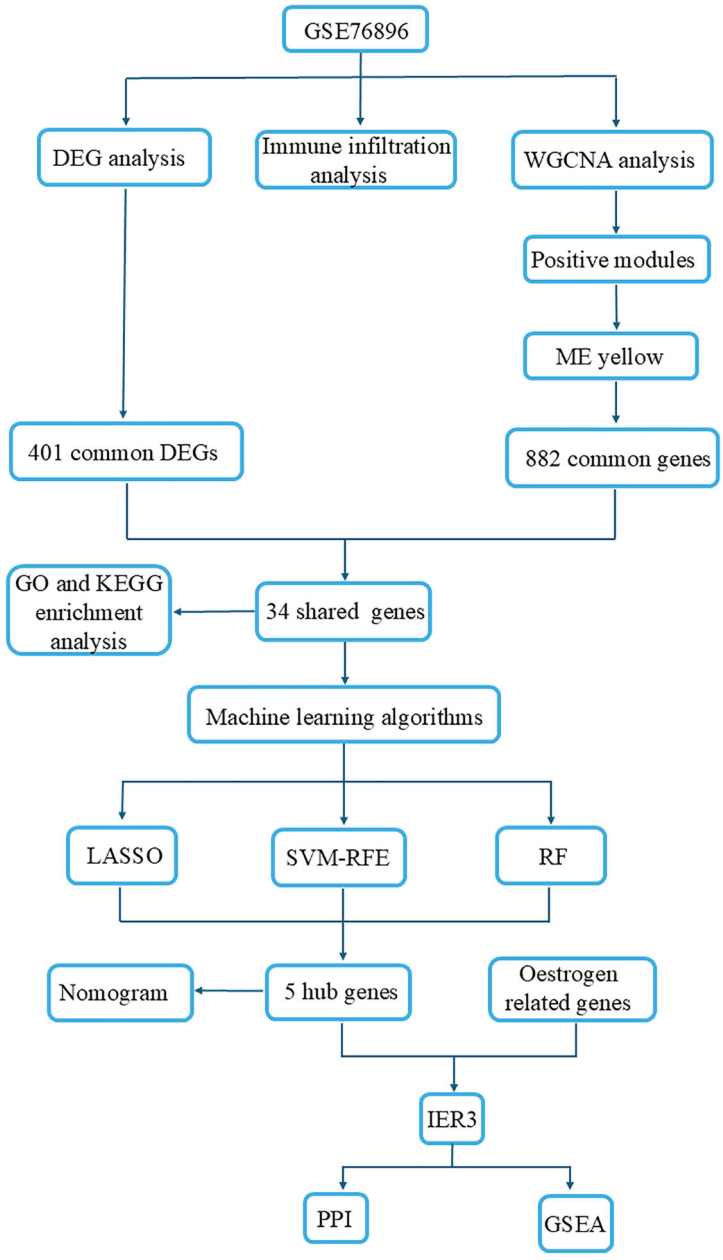

GRAPHICAL ABSTRACT

1 Introduction

Diabetes mellitus (DM) is characterized by hyperglycemia and encompasses several types, primarily type 1 diabetes mellitus (T1DM), type 2 diabetes mellitus (T2DM), and gestational diabetes mellitus (GDM). The primary pathological mechanisms underlying DM involve either inadequate insulin secretion or the presence of insulin resistance, resulting in sustained elevations in blood glucose levels (1, 2). This hyperglycemic state not only disrupts systemic metabolism but also inflicts damage to multiple organs and systems. Chronic hyperglycemia is a contributing factor to both microvascular and macrovascular complications, leading to conditions such as diabetic retinopathy, diabetic nephropathy, diabetic neuropathy, alongside a variety of gynecological malignancies (3, 4). Furthermore, individuals with DM demonstrate a markedly higher incidence of cardiovascular diseases, contributing to a cardiovascular mortality rate that exceeds that of individuals without DM (5, 6). Preventive strategies for DM emphasize the importance of managing established risk factors, including obesity, hypertension, and unhealthy dietary habits, while also promoting public awareness of DM through health policies designed to enhance early screening rates. Notably, early intervention in T2DM has been shown to effectively delay or prevent the onset of the disease.

Estrogens, a class of steroid hormones predominantly secreted by the ovaries, include estradiol (E2), estrone (E1), and estriol (E3). These hormones play a crucial role in the development of the female reproductive system, the manifestation of secondary sexual characteristics, and a multitude of physiological functions (7). Recent advancements in understanding of estrogen signaling mechanisms have yielded a more nuanced perspective on their roles in various physiological processes. Within the female reproductive system, estrogens are primarily responsible for promoting the development and maturation of ovarian follicles, sustaining endometrial proliferation, and facilitating ovulation. Additionally, estrogens have garnered considerable attention for their protective effects on bone health, as they help maintain bone density by promoting bone matrix synthesis and inhibiting bone resorption, thereby effectively reducing the risk of osteoporosis in postmenopausal women (8). Furthermore, estrogens exert significant influences on cognitive function, mood regulation, and neuroprotection, with clinical studies suggesting their positive impact on slowing the progression of Alzheimer's disease (9).

It is essential to highlight the significant role that estrogens play in DM. At certain concentrations, elevated estrogen levels can enhance insulin sensitivity, thereby reducing the risk of developing DM (10). Specifically, estrogens exert their effects by binding to specific receptors and activating signaling pathways such as PI3K/Akt and MAPK, which subsequently influence both insulin secretion and action (11). This interaction ultimately modulates the onset and progression of DM (12, 13). Given the intricate interplay between estrogens and DM, alongside the current gaps in understanding their molecular mechanisms and pathological interactions, recent advancements in biotechnology offer valuable tools for exploring the underlying mechanisms linking these two factors.

This study utilizes a comprehensive bioinformatics approach combined with machine learning techniques to investigate the shared genes and associated signaling pathways linking estrogens and DM. By elucidating the specific pathogenic mechanisms of estrogen-related genes in the context of DM, this research offers valuable data support and identifies potential breakthroughs for more targeted and effective prevention and treatment strategies for DM.

2 Materials and methods

2.1 Data acquisition and preprocessing

Graphical Abstract illustrates the workflow of this study. The gene expression dataset for DM was sourced from the GEO database (https://www.ncbi.nlm.nih.gov/geo/) using "diabetes" as the search term. We applied filtering criteria including "DataSets Database" and "Homo sapiens" to refine the dataset. Specimens related to "methylation," "diabetic nephropathy," and "non-pancreatic tissues" were excluded from consideration. Ultimately, we selected sequencing data from the T2DM group and the normal pancreatic tissue group for further analysis. Based on the aforementioned selection criteria, GSE76896 was identified as the discovery cohort, comprising a total of 206 samples, including 117 from the normal group, 55 from the T2DM group, while 34 samples from the impaired glucose tolerance group were excluded.

2.2 Principal component analysis

To reduce dimensionality and facilitate the visualization of sample clustering, PCA was conducted on the original dataset, with all preprocessing executed utilizing the "affy" package in R (14). Probes were converted to gene symbols based on the GPL570 platform (Affymetrix Human Genome U133 Plus 2.0 Array). PCA serves as a dimensionality reduction technique that applies orthogonal transformation to reconfigure the data into a new coordinate system, thereby maximizing variance along these new axes. This approach preserves the most significant features of the data and enables visualization of the distribution of high-dimensional data across the first two principal components.

2.3 Identification of differentially expressed genes in DM

We utilized the "Limma" package in R to identify DEGs within the GSE76896 dataset. The criteria for DEG selection were established as an adjusted p-value of <0.05 and a log-fold change (logFC) of ≥ 0.70. Additionally, we constructed a volcano plot to visually depict the statistical significance and magnitude of expression changes

associated with these DEGs. This approach enables researchers to effectively identify target genes that exhibit significant upregulation or downregulation under disease conditions.

2.4 Weighted gene co-expression network analysis and module gene identification

We employed the R package "WGCNA" to identify biologically meaningful co-expression gene modules and to explore the relationship between gene networks and disease (15). Initially, the top 10,000 genes with the highest variance were selected for further analysis. Subsequently, the "pickSoft Threshold" function was utilized to determine the optimal soft thresholding power (β), which ranges from 1 to 20, in order to construct a scale-free network. The average connectivity R^2 threshold was set at 0.85. Following this, the adjacency matrix was transformed into a Topological Overlap Matrix (TOM) to evaluate gene ratios and dissimilarity. In the fourth step, hierarchical clustering and the dynamic tree cut function were applied to delineate and identify co-expression modules. These modules were then merged based on analogous expression patterns for further analysis, with the parameters "minModuleSize" and "deepSplit" set to 150 and 2, respectively. In the fifth step, we examined the correlation between modules and disease by calculating Gene Significance (GS) and Module Membership (MM). Genes within the modules that exhibited the strongest correlation with the disease were selected for further investigation. Finally, we conducted an intersection analysis between the DEGs and the genes identified through WGCNA, which yielded a set of 34 common genes. We visualized these shared genes using clustering heatmaps generated by the "ggplot2" and "pheatmap" R packages (16). This step aims to identify co-expression modules that are significantly associated with DM, thereby providing a candidate set of genes for subsequent functional enrichment analysis and machine learning screening.

2.5 Functional enrichment analysis

To further investigate the biological functions and signaling pathway characteristics of diabetes-related genes, as well as to elucidate their potential molecular mechanisms, we conducted functional enrichment analysis using the "clusterProfiler" and "ggplot2" R packages. This approach facilitated an efficient evaluation and visualization of gene functionality. In the Gene Ontology (GO) analysis, genes were categorized into three main functional categories: Biological Process (BP), Cellular Component (CC), and Molecular Function (MF). This categorization enhances our comprehension of the roles of genes across various biological dimensions. Additionally, Kyoto Encyclopedia of Genes and Genomes (KEGG) pathway enrichment analysis offers a systematic framework for investigating gene functions, particularly concerning cellular signaling and metabolic pathways. To ensure the statistical significance of the analysis results, we established a cutoff criterion for p-values and q-values at 0.05.

2.6 Machine learning approaches for identifying candidate biomarkers

To accurately identify candidate biomarkers associated DM from extensive genomic datasets, we employed machine learning methodologies. These algorithms have gained prominence in the field of bioinformatics due to their robust capabilities for handling complex datasets (17). They are capable of extracting critical information from gene expression data and identifying the genes that are most pertinent to specific disease states. By leveraging machine learning techniques, we can more effectively manage high-dimensional data, uncover nonlinear relationships, and filter potential biomarkers. This approach enhances predictive accuracy and addresses challenges that frequently confound traditional statistical methods. Consequently, machine learning was used in this study to further refine candidate genes with the aim of discovering novel biomarkers for DM. We employed three widely recognized machine learning algorithms to further refine the selection of candidate biomarkers: Least Absolute Shrinkage and Selection Operator (LASSO) (18), Support Vector Machine-Recursive Feature Elimination (SVM-RFE) (19), and Random Forest (RF) (20). LASSO is a regularized regression technique that applies an L1 penalty to shrink the coefficients of less informative variables to zero, thus facilitating simultaneous variable selection and regularization. SVM-RFE is a backward feature elimination method based on support vector machines, which recursively eliminates features with the lowest ranking weights to identify the subset that optimally separates the classes. RF, an ensemble learning approach based on decision trees, trains each tree on a bootstrap sample and a subset of features, allowing for the assessment of feature importance via the mean decrease in impurity. These three algorithms collectively enhance the feature selection process: LASSO prioritizes sparsity, SVM-RFE focuses on margin-based discrimination, and RF utilizes ensemble-based ranking. This complementary synergy significantly bolsters the robustness and reliability of the selected biomarkers. Candidate genes identified through the intersection of these algorithms were considered highly reliable for subsequent analysis.

2.7 Expression analysis and diagnostic evaluation of candidate genes for DM

To further verify the diagnostic efficacy of candidate genes and construct a clinically applicable risk assessment model, the "ggplot2" package was utilized to assess the expression levels of candidate biomarkers in both control and DM groups, with a significance threshold set at $p < 0.05$. A Nomogram was constructed using the "rms" package, wherein "Points" represent the scores assigned to the candidate genes, and the "Total Score" denotes the cumulative score across all the aforementioned genes. To evaluate the diagnostic accuracy of the candidate biomarkers, the area under the receiver operating characteristic (ROC) curve (AUC) was calculated using the "pROC" package.

2.8 Identification of candidate biomarkers

Candidate genes related to estrogen were retrieved from the NCBI (National Center for Biotechnology Information, https://www.ncbi.nlm.nih.gov/gene) database using the search terms "oestrogen" and "Homo sapiens". These estrogen-related genes were subsequently intersected with genes linked to DM, with selection criteria requiring an AUC ≥ 0.7 for further analysis. After screening and identifying five candidate genes, we conducted a comprehensive evaluation of each and determined that IER3 exhibits the highest research value for the following reasons:A. Estrogen linkage: Previous studies have demonstrated that OHT, a related compound, stimulates IER3 expression in an estrogen receptor-dependent manner (21). In contrast, other genes, including LRRK2, have not shown a similar association.B. Immune modulation: IER3 is a well-established immunoregulatory gene. For instance, induction of IER3 protects macrophages from LPS-induced apoptosis and inhibits NF-κB activity (22). This function in modulating inflammation is directly relevant to diabetes, which is characterized by chronic immune dysregulation.C. Metabolic inflammation: IER3 plays a crucial role in mediating metabolic and immune crosstalk in obesity. Mice deficient in IER3 exhibit reduced adipose inflammation and improved insulin sensitivity under high-fat diet conditions (23). This demonstrates that IER3 plays a significant role in regulating the interface between metabolism and immune responses.

2.9 Gene set enrichment analysis

The Pearson correlation coefficients between IER3 and all other genes were calculated using the cor.test function in R. Following this calculation, all genes were ranked in descending order according to their correlation with the target gene. This ranked gene list was then utilized for GSEA to determine whether gene sets exhibiting a strong correlation with the target gene are enriched in specific biological pathways or functional modules. The primary objective of this analysis was to identify the gene sets that demonstrated significant correlations with the target gene and to elucidate the biological implications of these gene sets.

2.10 Construction of protein-protein interaction network

To further elucidate the functions and mechanisms of IER3 in biological processes associated with DM, this study utilized the STRING network data platform (https://string-db.org) to identify protein associations and construct a PPI network. By establishing a specified required confidence threshold of 0.400, we ensured that only high-confidence interactions were included in the network, thereby facilitating the identification of key proteins closely related to the function of IER3. The establishment of this network enhances our understanding of the molecular mechanisms underlying the role of IER3 in DM, as well as the associated signaling pathways and biological processes in which it may be involved. Through this systematic approach, we are able to delineate the critical role of IER3 in the pathophysiology of DM and propose potential molecular targets for future therapeutic strategies. To explore the correlations between IER3 and key genes in the PI3K/Akt and MAPK signaling pathways in DM, we utilized gene expression data from public databases. We identified core genes in the PI3K/Akt pathway, including PIK3CA, PIK3CB, PIK3CD, PIK3R1, AKT1, AKT2, and AKT3, as well as key genes in the MAPK pathway, such as MAPK3, MAPK8, MAPK9, MAPK14, MAP2K1, MAP2K2, and MAP3K4. Following this, we performed a correlation analysis to assess the expression relationships between IER3 and these genes in DM samples. The results were visualized using a heat map to facilitate interpretation of the correlations.

2.11 Immuno-infiltration analysis

To attain a deeper insight into the cellular composition and functional alterations within the immune system in the context of DM, this study employed the CIBERSORT algorithm for a comprehensive analysis of immune cell infiltration. CIBERSORT is a deconvolution algorithm that leverages gene expression data to identify the relative abundances of 22 distinct immune cell types, estimating their proportions in heterogeneous cell samples based on a training set derived from established gene expression profiles characteristic of known immune cells (24). The "CIBERSORT" package was employed in our analysis to further elucidate the differences in immune cell proportions between DM patients and healthy control groups, as well as to explore potential correlations between these variations and the immune responses and inflammatory processes associated with DM.

To effectively present the analysis results visually, we applied R packages such as "ggplot2," "corrplot," and "vioplot" to effectively illustrate the distribution and interrelationships of various immune cell types across the two groups. Furthermore, Spearman correlation analysis was conducted to assess the association between immune cells and the candidate biomarker IER3, evaluating the impact of IER3 expression levels on the immune cell ratios. This segment of the research not only deepens our understanding of the role of immune cells in the pathological processes of DM, but also provides empirical support for the potential use of IER3 as a key biomarker. Consequently, it offers new insights and viable targets for the diagnosis, treatment, and prognostic evaluation of DM.

2.12 Statistical analysis

Statistical analyses were conducted utilizing R software (version 4.4.1), and the Wilcoxon and T-tests were employed to compare differences between the T2DM group and the control group. A p-value of less than 0.05 was considered statistically significant.

3 Results

3.1 Identification of DEGs in DM

The results of PCA reveal a notable trend of separation between DM patients and the normal population within the PCA space (Figure 1A). While some overlapping regions are observed, the overall clustering characteristics of the data points from the two groups demonstrate marked differences. These findings indicate that PCA effectively captures the principal variance patterns within the dataset and partially elucidates the differences between the two groups.

In the GSE76896 dataset, we identified a total of 401 DEGs, comprising 177 upregulated and 224 downregulated genes (Supplementary Table 1). The volcano plot (Figure 1B) visually illustrates the expression changes and statistical significance of these genes, with orange and green dots representing genes that are significantly upregulated or downregulated in the DM group, respectively. The black dots at the center of the plot indicate genes with no significant changes in expression. Our results reveal that the expression of the IER3 gene is significantly decreased in DM patients compared to the control group, whereas the SLC26A4 and ELFN1 genes exhibit significant upregulation. These key DEGs identified in DM lay the groundwork for further functional analysis.

3.2 WGCNA and module gene identification in DM

To identify the gene modules most closely associated with DM, we conducted a WGCNA. The optimal soft threshold for GSE76896 was determined to be 6 (Figure 1C). A total of 14 distinct modules were then identified, among which the MEyellow module demonstrated the strongest negative correlation with DM (correlation coefficient = -0.38, p = 8e-05) (Figures 1D, E) (Supplementary Table 2), encompassing 882 genes. We subsequently intersected the DEGs with the genes selected through WGCNA, resulting in a set of 34 shared genes associated with DM (Figure 1F) (Supplementary Table 3). A clustering heatmap for these 34 DM-related genes was generated using the "ggplot2" and "pheatmap" R packages (Figure 1G).

3.3 GO enrichment analysis and KEGG pathway analysis

To further explore the biological functions of the identified DM-related genes and to uncover potential key signaling pathways involved, we conducted GO enrichment analysis (Figures 2A–C) and KEGG pathway analysis (Figure 2D). The top ten enriched BPs included intracellular signal transduction, cell activation, leukocyte activation, inflammatory response, regulation of signaling receptor activity, myeloid leukocyte activation, response to molecule of bacterial origin, regulation of leukocyte chemotaxis, nitric-oxide synthase biosynthetic process, and regulation of nitric-oxide synthase biosynthetic process. Notably, the enrichment of nitric oxide synthase biosynthetic process regulation aligns with emerging evidence linking endothelial dysfunction to DM (25). In this context, impaired NO bioavailability contributes to vascular complications (26). The top ten enriched CC were identified as extracellular region, endomembrane system, extracellular space, organelle membrane, secretory vesicle, cytoplasmic vesicle membrane, vesicle membrane, secretory granule, receptor complex, and plasma membrane receptor complex. CC analysis highlighted significant extracellular space and secretory vesicles, indicating dysregulated paracrine signaling. For instance, extracellular vesicles derived from β cells can serve as a medium for intercellular communication within the pancreatic microenvironment in type 1 DM and participate in immune regulation (27). Furthermore, the top ten enriched MF included receptor ligand activity, receptor regulator activity, signaling receptor binding, co-receptor binding, growth factor activity, cytokine activity, G protein-coupled receptor binding, molecular function regulator, enzyme activator activity, and ion channel binding. Additionally, Ion channel binding may be associated with potassium channel mutations that lead to insufficient insulin secretion in response to glucose levels (28). Following this, in terms of KEGG pathways, the top ten pathways identified were the NOD-like receptor signaling pathway, TNF signaling pathway, IL - 17 signaling pathway, Rheumatoid arthritis, Viral protein interaction with cytokine and cytokine receptor, AGE-RAGE signaling pathway in diabetic complications, NF-kappa B signaling pathway, Kaposi sarcoma-associated herpesvirus infection, Chemokine signaling pathway, and Legionellosis. Notably, these findings of the GO classification and KEGG pathway analysis reveal the functional characteristics of DM-related genes at the molecular biological and signaling transduction levels, particularly in relation to immune responses, signal transduction, and metabolic regulation, thereby providing crucial insights into the molecular pathophysiological mechanisms underlying the onset of DM.

3.4 Identification of candidate biomarkers for DM through machine learning

To further refine the identification of key genes associated with DM, we identified 34 common genes by intersecting 401 DEGs with 882 genes selected through WGCNA. Subsequently, we utilized three machine learning algorithms to screen for potential candidate biomarkers based on these 34 common genes. In the GSE76896 dataset, the LASSO regression identified eight genes (Figures 3A, B), whereas the SVM-RFE algorithm extracted 20 genes with the lowest root mean square error (RMSE) (Figure 3C). Additionally, the RF classifier ranked the top 20 genes according to their importance (Supplementary Table 4, Figures 3D, E). By intersecting the results obtained from these three methods, we ultimately identified five candidate biomarkers for DM, including ALDH1A3, MIOS-DT, MELTF-AS1, LRRK2, and IER3 (Figure 3F).

10.3389/fendo.2025.1570332

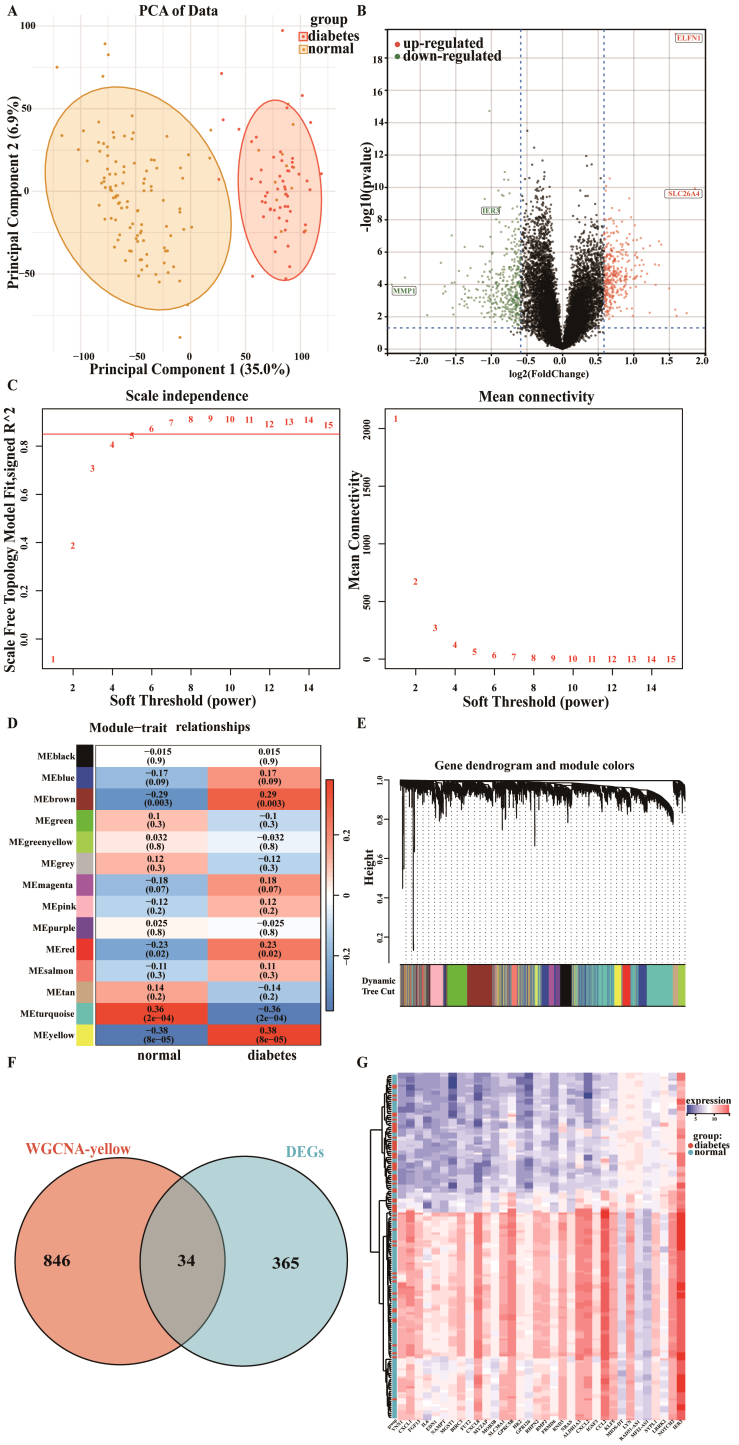

FIGURE 1
Exploratory analysis of gene expression in DM. **(A)** Principal Component Analysis (PCA). **(B)** A volcano plot illustrating all differentially expressed genes (DEGs). **(C)** Determination of the optimal soft threshold. **(D)** Heatmap depicting the relationship between gene modules and clinical traits. **(E)** Gene cluster tree of co-expressed genes. **(F)** Venn diagram demonstrates the intersection of common genes identified through Weighted Gene Co-expression Network Analysis (WGCNA) and DEGs. **(G)** Cluster heatmap based on all DEGs.

3.5 Risk stratification of candidate biomarkers for DM

We subsequently constructed a nomogram (Figures 4A, B) based on the above five identified candidate biomarkers for DM, which translates the relative expression levels of each gene into a specific score ranging from 0 to 100. By aggregating the individual gene scores to obtain a total score, we can effectively evaluate the overall risk of an individual developing DM. Specifically, a higher total score correlates with an increased risk of DM occurrence. This

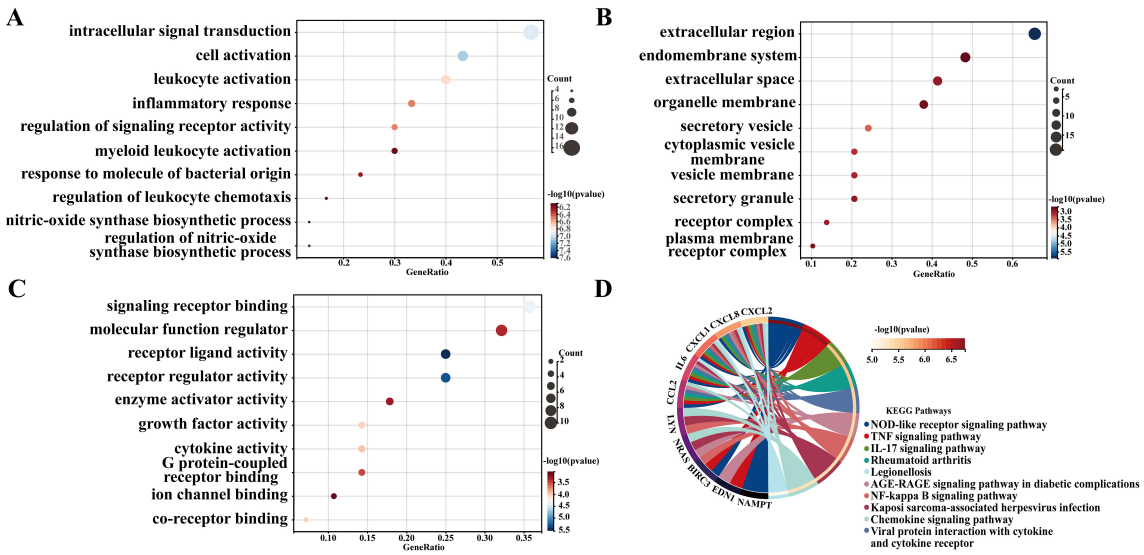

FIGURE 2
GO and KEGG analyses of diabetes-related genes. **(A–C)** Gene Ontology (GO) categories for Biological Processes (BP), Cellular Components (CC), and Molecular Functions (MF). The top 10 categories of BP, CC and MF are shown. **(D)** Kyoto Encyclopedia of Genes and Genomes (KEGG) enrichment analysis.

methodology not only furnishes clinicians with a robust tool for risk stratification of patients but also holds significant predictive value for the prognosis of DM.

Furthermore, we evaluated the diagnostic performance of each gene as a biomarker for DM through ROC curve analysis (Figure 4C). The resulting AUC values were as follows: ALDH1A3 (AUC: 0.627), MIOS-DT (AUC: 0.742), MELTF-AS1 (AUC: 0.694), and LRRK2 (AUC: 0.764), and IER3 (AUC: 0.723). These findings not only enhance our understanding of the molecular mechanisms underlying the onset of DM but also provide valuable biomarkers for prospective clinical applications in the prevention and treatment of DM.

3.6 Significance of estrogen-related gene IER3 as a diagnostic and prognostic marker for DM

In this study, we identified the estrogen-related genes and intersected them with the five candidate genes for DM that previously identified through machine learning techniques. We specifically focused on genes exhibiting an AUC value of ≥0.7, ultimately determining IER3 as a key biomarker for DM (Figures 4D, E). ROC curve analysis revealed that IER3 achieved an AUC value of 0.723, with a 95% confidence interval ranging from 0.636 to 0.811. This finding suggests that IER3 demonstrates both accurate and satisfactory diagnostic and prognostic value for DM. Furthermore, the ROC curve revealed sensitivity and specificity values for IER3 of 0.8205 and 0.7636, respectively. These performance metrics further underscore the significant role of IER3 as an effective biomarker for DM, highlighting its potential clinical utility. To further evaluate the accuracy of the candidate biomarkers, we employed the GSE72377 dataset for verification and ROC curve analysis revealed that IER3 exhibits significant diagnostic value, with an AUC value of 0.703 (Figure 4F). As shown in Figure 4G, a significant negative correlation was observed between the expression levels of IER3 and ESR1 (R =- 0.39, P = 1.5e-07). The trend line, along with the 95% confidence interval, is represented in gray. These findings offer evidence suggesting a potential association between IER3 and estrogen signaling pathways.

3.7 PPI network analysis of IER3 in DM

PPI network analysis serves as a crucial tool for elucidating gene functions and their biological roles. To further investigate the role of the IER3 gene in DM more comprehensively, we constructed a PPI network centered on IER3 utilizing the STRING database (Figure 5A). This network not only illustrates the direct and indirect interactions between IER3 and its interactive genes but also offers valuable insights into the strength and sources of evidence supporting these interactions.

Using this high-throughput analytical approach, we successfully identified the protein nodes that are closely associated with IER3, specifically DUSP5, PHLDA1, ADCYAP1, PPP2R5C, PPP2R5B, MAPK1, MCL1, MAPK3, RELA, and PPP2CA. These protein nodes are depicted in the network with varying colors and line styles, effectively illustrating the positioning of IER3 within the network and its potential influence on other biomolecules. The identification of these interacting proteins provides valuable insights into the potential roles of IER3 in the pathological processes of DM, thereby enhancing our understanding of the

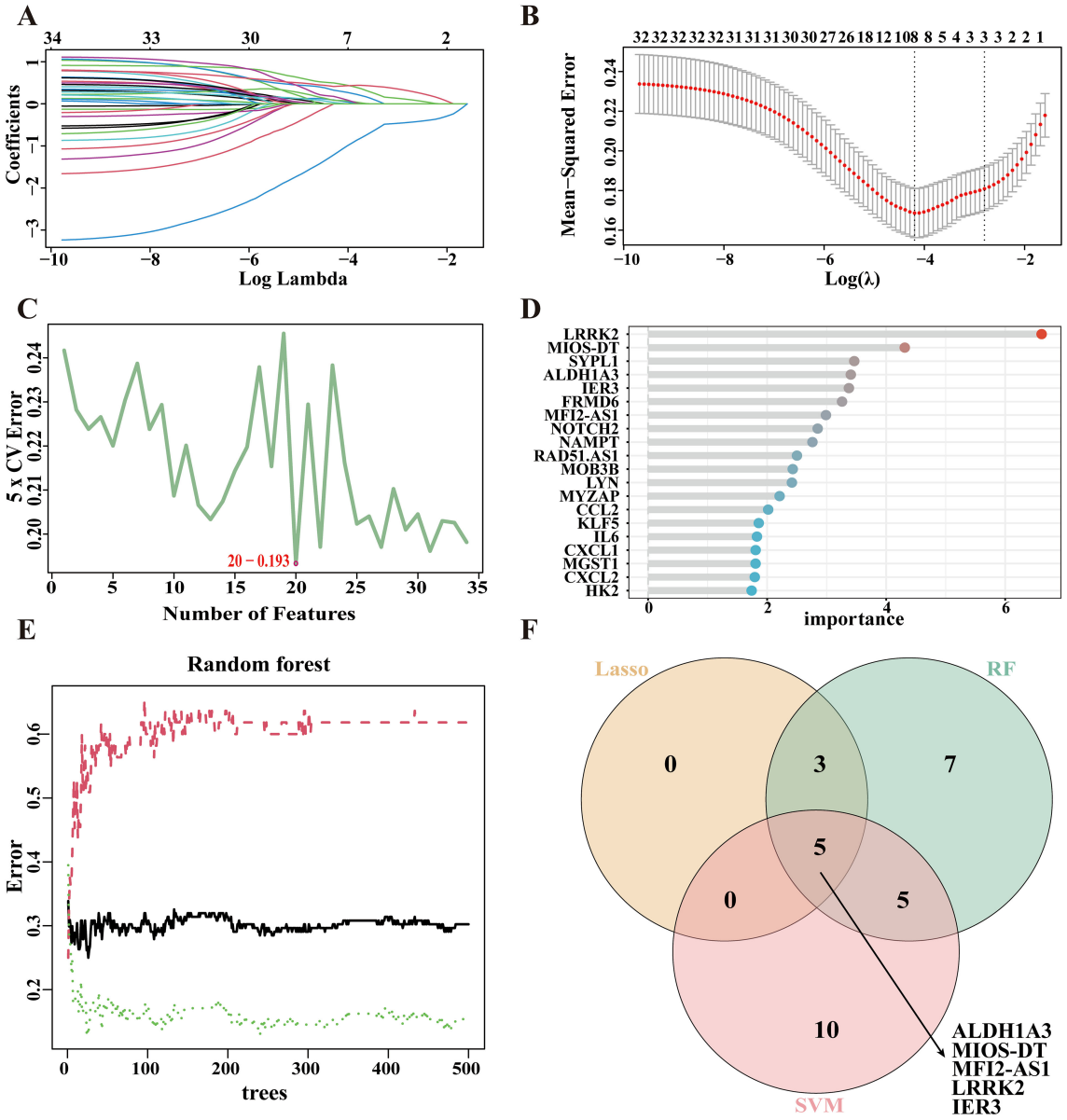

FIGURE 3
Machine learning in the screening of candidate biomarkers. **(A, B)** Based on the Lasso regression algorithm, 8 genes corresponding to the lowest binominal deviation were identified as the most appropriate for diabetes mellitus (DM) diagnosis. **(C)** The top 20 genes were selected based on Support Vector Machine Recursive Feature Elimination (SVM-RFE) with the lowest error rates and highest accuracy for DM classification. **(D, E)** The top 20 genes were selected and ranked according to the importance scores derived from the random forest algorithm applied to DM. **(F)** A Venn diagram showing the intersected genes identified by the three machine learning algorithms in DM.

molecular pathways through which IER3 is involved in the progression of DM. The heatmap illustrates significant correlations between IER3 and genes involved in the PI3K/Akt and MAPK signaling pathways associated with diabetes (Figure 5B). In the PI3K/Akt pathway, both PIK3CA and PIK3CB exhibit strong positive correlations with IER3. Within the MAPK pathway, MAP2K1 shows a positive correlation with IER3, while MAP3K4 reveals a negative correlation. These findings suggest that IER3 may play a role in the pathogenesis of diabetes through its interactions with specific genes in these pathways.

3.8 Functional enrichment of IER3

To further elucidate the functions of genes and their underlying biological mechanisms, we conducted GSEA enrichment analysis to identify differentially expressed genes between the low and high expression groups of IER3 (Figure 5C). In the GO enrichment analysis, the most significantly activated biological process identified was axoneme assembly, followed by processes such as microtubule bundle formation, host interaction, non-motile cilium assembly, and positive regulation of canonical NF-κB signaling.

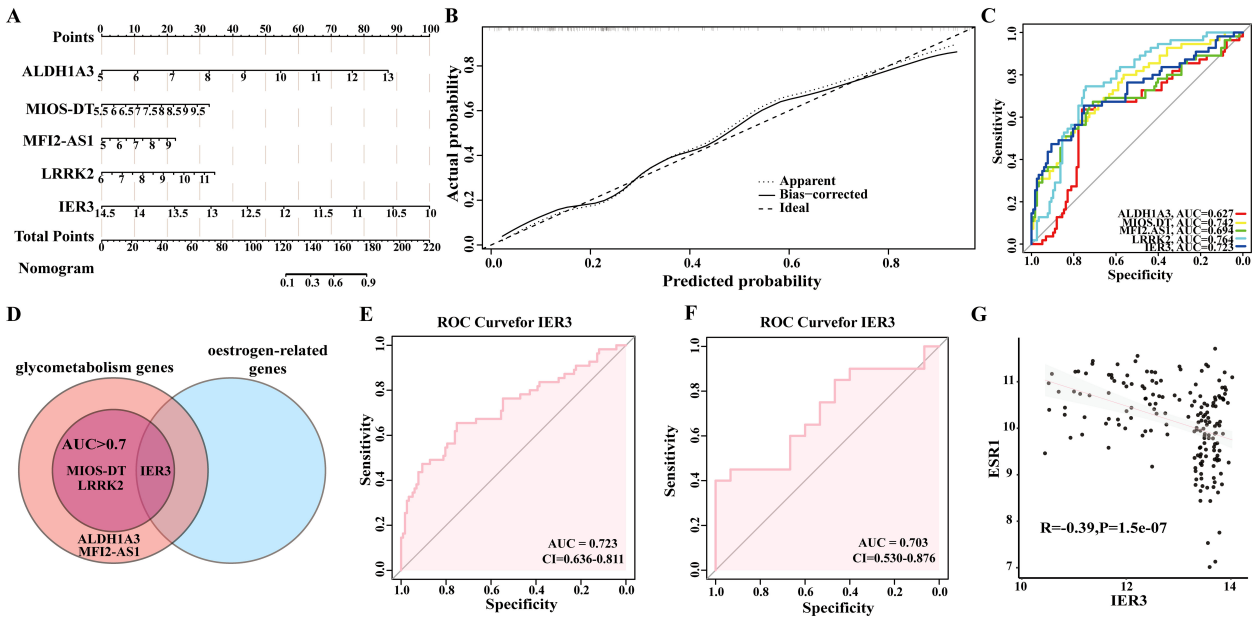

FIGURE 4
Analysis of IER3 as a candidate biomarker for DM. **(A, B)** Nomogram construction based on five shared genes identified in discovery datasets. **(C)** The Receiver Operating Characteristic (ROC) curve for the shared genes in discovery datasets. **(D)** IER3 was identified as a candidate biomarker. **(E, F)** The ROC curve of IER3 in the GSE76896 and GSE72377 datasets. **(G)** The correlation between IER3 and ESR1 in diabetes.

Additionally, the top five KEGG pathways identified included the Escherichia ESPG to microtubule RHOA signaling pathway, the SARS-CoV-2 spike protein to ANGII/AT1R/NOX2 signaling pathway, the IL - 2-JAK-STAT signaling pathway, kinetochore microtubule attachment, and microtubule depolymerization (Figure 5D). These findings indicate that IER3 may be involved in various complex biological processes related to DM, including infection, cardiovascular diseases, immune regulation, cellular dynamics, and cytoskeletal remodeling.

3.9 Immune cell infiltration analysis

In this study, we conducted a comprehensive analysis of the cellular composition and functional alterations of the immune system in the context of DM. Utilizing the CIBERSORT algorithm, we performed a detailed comparison of immune cell proportions between the DM group and normal controls (Figure 6A). Our findings revealed significant differences in the proportions of various immune cell types between the two groups, which may be closely related to the immune response and inflammatory processes associated with DM. Specifically, the proportions of naive B cells, monocytes, M0 macrophages, and activated dendritic cells were significantly elevated in the DM group compared to the control group. Conversely, the proportions of CD8 + T cells and follicular helper T cells markedly decreased in the DM group. To further investigate the activation states of different immune cells in DM, we constructed heatmaps to analyze the gene expression patterns of various cell types (Figure 6B) and visualized the proportions of different immune cell types (Figure 6C). The results indicated that the distribution of multiple immune cell types in the DM group differed significantly from that of the normal group, thereby reinforcing the role of immune cells in the pathology of DM. An in-depth analysis through correlation heatmaps illustrated the relationships among various immune cell types, revealing a notably high degree of similarity between different T cell subtypes, such as resting CD4 memory T cells and CD8+ T cells (Figure 6D). This observation suggests potential functional synergy among these cells. Overall, the correlation analyses underscore the intricate interactions and regulatory mechanisms of diverse immune cells in the context of DM.

To further explore the influence of IER3 on the proportions of the aforementioned immune cells, we stratified the DM group into two subgroups based on high and low expression levels of IER3 (Figure 6E). The results revealed that the proportions of naive B cells, regulatory T cells (Tregs), activated dendritic cells, and neutrophils were significantly elevated in the high IER3 expression group compared to those in the low expression group. Conversely, the proportions of CD8+ T cells and follicular helper T cells were markedly reduced in the high IER3 expression group. Notably, consistent trends were observed in the proportions of naive B cells, CD8+ T cells, follicular helper T cells, and activated dendritic cells across both comparisons of immune cell proportions. These findings strongly suggest that IER3 plays a pivotal role in modulating the immune microenvironment, thereby influencing the progression of DM. The elevated expression of IER3 appears to

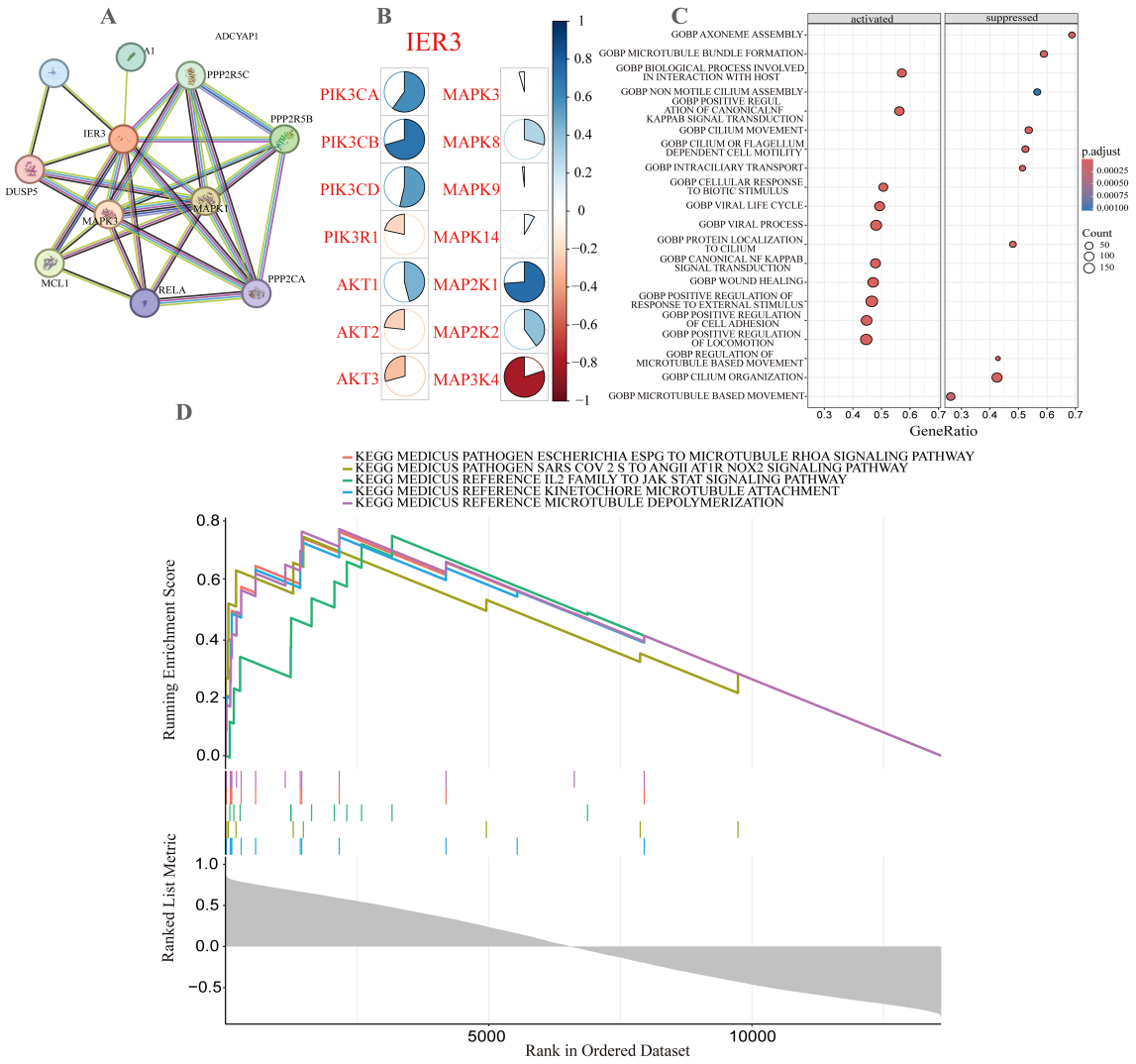

FIGURE 5
PPI network and functional enrichment analysis of IER3 in DM. **(A)** The network of interacting genes associated with IER3. The circles represent the query proteins and their corresponding first shell interactors in the network. The color and number of edges indicate the source and quantity of supporting evidence, respectively. **(B)** Correlation heatmap of IER3 with genes involved in the PI3K/Akt and MAPK signaling pathways. **(C)** Gene Set Enrichment Analysis (GSEA) illustrating pathway enrichment across the ordered gene dataset. **(D)** KEGG analysis of the activated and repressed biological processes.

be associated with enhanced immune cell activation and increased inflammatory responses. This segment of the research not only underscores the significance of immune cells in the pathological processes of DM but also provides additional empirical evidence for IER3 as a potential biomarker, opening new avenues for the diagnosis, treatment, and prognostic evaluation of DM.

Collectively, these results demonstrate significant changes in immune cell composition under DM conditions, and IER3 is not only closely correlated with variations in immune cell proportions but also plays a crucial role in the immunoregulatory mechanisms underlying DM. These findings underscore the considerable research value of IER3 in elucidating the immunological basis of DM and suggest its potential as a biomarker for future therapeutic strategies.

4 Discussion

DM is characterized as a complex metabolic disorder syndrome, distinguished by hyperglycemia, insulin resistance, and hyperinsulinemia, making it one of the most prevalent chronic metabolic diseases globally (29). This condition significantly affects individuals' overall quality of life (30). Estrogen plays a crucial protective role in the pathogenesis of DM by enhancing both insulin sensitivity and secretion, thereby contributing to the maintenance of stable blood glucose levels (31). Nevertheless, postmenopausal women frequently experience increased insulin resistance and a heightened risk of developing DM due to declining estrogen levels (11, 32). Research has demonstrated that estrogen can regulate pancreatic beta cell function (33), facilitate glucose uptake and

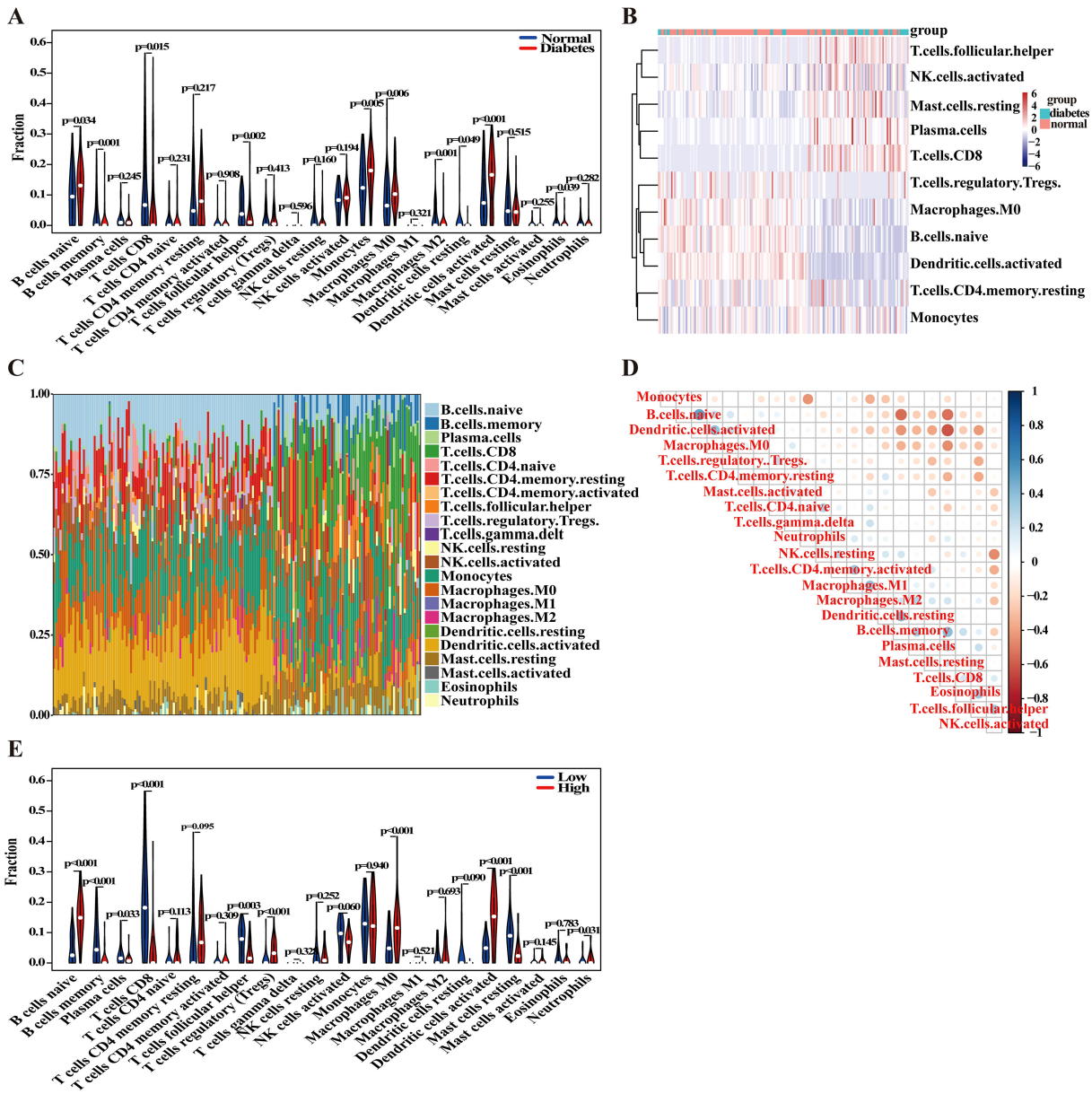

FIGURE 6
Analysis of immune cell infiltration. **(A)** The boxplot comparing the proportion of immune cells between DM and control groups. **(B)** Comparative heatmap depicting immune cell gene expression in DM and control groups. **(C)** The bar plot visualizing the proportion of infiltrating immune cells in different samples. **(D)** Correlation heatmap representing associations between various immune cell types. **(E)** The boxplot comparing the proportions of immune cells in high and low IER3 expression groups.

utilization, and reduce cellular apoptosis, all of which are critical for preventing and controlling the onset and progression of DM (34). This regulatory effect of estrogen is particularly vital for women's health.

This study employs a comprehensive approach that integrates bioinformatics methods with machine learning techniques to explore the shared genes and associated signaling pathways related to DM and estrogen. It specifically highlights the potential role of the estrogen-related gene IER3 in DM. The findings reveal a significant downregulation of IER3 in DM patients, and it appears to affect the progression of DM through the regulation of glucose metabolism, immune responses, and inflammatory pathways, suggesting that IER3 may play a pivotal role in the pathological processes linking DM and estrogen. Furthermore, the construction of a diagnostic ROC curve based on IER3 gene expression demonstrates both accurate and satisfactory diagnostic and prognostic value of IER3 for DM. Notably, the study reveals significant changes in immune cell composition under DM conditions, and IER3 is not only closely correlated with variations in the proportions of various immune cells, but also plays a crucial role in the immunoregulatory mechanisms underlying DM. Through an in-depth analysis of IER3 and its associated signaling pathways, this research underscores the unique value of the estrogen-related gene IER3 as a potential biomarker and

therapeutic target for DM. Collectively, our study lays the groundwork for future investigations into the molecular mechanisms underlying the pathogenesis of DM, while also providing more molecular evidence and therapeutic strategies for its diagnosis and treatment.

IER3 plays a crucial role in regulating cell apoptosis and the heterogeneity of immune cells (35). Research indicates that macrophages are key contributors to obesity-related inflammation, particularly through the transition of adipose tissue macrophages from alternatively activated macrophages (AAM) to classically activated macrophages (CAM), a process that is significant in the context of obesity-associated inflammation (36, 37). The high expression of IER3 in macrophages may facilitate this transformation, thereby promoting the onset of obesity-related inflammation and enhancing insulin sensitivity in murine models (38). Additionally, IER3 is extensively implicated in vital biological processes such as cell proliferation, differentiation, and apoptosis, with its expression regulated by various transcription factors, including NF-κB, p53, SP1, AP1, vitamin D3 receptor (VD3R), and retinoic acid receptors (RAR/RXR) (39, 40). Furthermore, studies have highlighted the prognostic value of IER3 in several pathological conditions, including pancreatic cancer, hepatocellular carcinoma, and acute kidney injury (41–44).

Estrogen plays a pivotal regulatory role in the onset and progression of DM, particularly among female patients, where fluctuations in estrogen levels may directly affect insulin sensitivity and glucose metabolism (45). This study posits that IER3 may serve as an intermediary between DM and estrogen, thereby establishing a critical connection between the two. The expression of the IER3 gene is modulated by various factors, with estrogen emerging as a significant regulator that may influence the development of DM through its impact on IER3 expression. Furthermore, our findings indicate a significant negative correlation between the expression levels of IER3 and ESR1, suggesting a potential association between IER3 and estrogen signaling pathways. Additionally, studies have shown that IER3 exhibits a dose-dependent response to 17β-estradiol stimulation in MCF - 7 (BUS) cells, with its expression being upregulated in conjunction with cyclin D1 and its mutants (46). These findings collectively underscore the potential regulatory role of estrogen on IER3 and highlight the importance for further investigation into this gene and its associated pathways. Such investigations will enhance our understanding of the pathological mechanisms underlying DM and may offer novel therapeutic targets for clinical intervention.

In addition to its involvement in glucose metabolism and estrogen levels, the IER3 gene may also participate in the immune regulatory mechanisms associated with DM by modulating immune system functionality. Recently, the interplay between immune responses and DM has garnered significant attention (47). Research has indicated that the chronic inflammatory state characteristic of DM is closely linked to the aberrant activation of immune cells (48, 49). The dysregulation of immune cell subset proportions constitutes a critical pathological hallmark within the immune microenvironment of DM. Significant elevations in the proportions of naive B cells, monocytes, M0 macrophages, and activated dendritic cells (DCs) were observed in the DM patients. Research has demonstrated that in insulin-dependent DM, activated DCs play a crucial role in autoimmune pathogenesis by presenting β-cell-derived autoantigens to naive autoreactive Th0 lymphocytes (50). This antigen presentation facilitates the differentiation of Th0 cells into pro-inflammatory effector T cells, which subsequently initiate β-cell apoptosis through cytotoxic mechanisms. The resulting impairment of insulin biosynthesis in pancreatic islets constitutes a key pathogenic mechanism in disease progression, with DC-mediated antigen presentation serving as a pivotal initiating event in the autoimmune destruction of β-cells. Monocytes also contribute significantly to the vascular complications associated with DM. In the diabetic environment, monocytes are recruited to the vascular wall, leading to a rapid release of inflammatory cytokines such as IL - 1β and TNF-α, which accelerate the progression of atherosclerotic lesions and plaque instability (51). Our study revealed significant reductions in $CD8^+$ T cells and follicular helper T cells among DM patients. As primary cytotoxic lymphocytes, the depletion of $CD8^+$ T cells may be linked to functional exhaustion characterized by PD - 1 upregulation and metabolic dysregulation manifested by glycolytic inhibition and mitochondrial dysfunction. Consequently, this depletion diminishes their capacity to eliminate aberrant cells in target tissues (52, 53). Furthermore, follicular helper T cells play a pivotal role in maintaining immune tolerance and regulating B-cell antibody production, with their diminished frequency potentially predisposing to aberrant humoral immune responses (54). This pathological process may exacerbate β-cell dysfunction through disrupting local T-B cell interactions within pancreatic islets and impairing antigen-specific immunomodulation. Collectively, the imbalance of immune cell repertoires in DM is not merely a passive epiphenomenon, it likely drives metabolic derangements, islet dysfunction, and chronic inflammation via mechanisms involving immunometabolic decoupling, dysregulated cytokine release, and impaired local immune regulation. These findings underscore the centrality of immune cell dyshomeostasis in elucidating the pathophysiological progression of DM. Our findings indicate a strong correlation between IER3 expression and alterations in the proportions of immune cells, particularly in patients with DM, suggesting that dysregulation of the immune system may exacerbate the progression of DM by influencing the activation states of immune cells. Therefore, IER3 may be pivotal in regulating the chronic inflammatory response associated with DM through its impact on immune system functionality. Several studies have highlighted the significant role of IER3 in immune cells, potentially modulating the release of cytokines, the activation of immune cells, and their migration, thereby affecting systemic inflammatory responses (55).

This study elucidates the potential biological and immunological significance of IER3 in DM by employing an integrated approach that combines bioinformatics and machine learning techniques. However, it remains in its preliminary stages and has certain limitations. The molecular mechanisms that link IER3 to estrogen signaling pathways, specifically the PI3K/Akt and MAPK cascades, along with their interactions with immune regulation, require experimental validation. Moreover, the causal relationship between IER3 downregulation and the progression of DM necessitates verification through longitudinal studies and interventional models. Future research should strive to diversify data sources by incorporating a wide range of sample data from DM patients across various ethnicities

and regions, thereby enhancing the reliability and generalizability of the findings. Furthermore, it is essential to clarify the relationship between IER3 and different types of DM, such as type 1 diabetes and gestational diabetes, in order to further deepen and broaden the scope of the research. Therefore, such future efforts have the potential to substantially enhance the applicability of IER3 in the treatment of DM.

5 Conclusion

In this study, we conducted a thorough investigation focusing on the role of the estrogen-related gene IER3 in the context of DM. Our findings reveal a significant downregulation of IER3 in DM patients, with an AUC value of 0.723 on the diagnostic ROC curve, indicating its considerable diagnostic and prognostic potential for DM. Furthermore, IER3 acts as a critical link between DM and estrogen, influencing the progression of DM through its regulatory effects on glucose metabolism, immune responses, and inflammatory pathways. Notably, our study uncovers significant alterations in immune cell composition under DM conditions. IER3 is not only closely correlated with variations in the proportions of diverse immune cell types but also plays a crucial role in the immunoregulatory mechanisms underlying DM. Through an in-depth analysis of IER3 and its associated signaling pathways, this research emphasizes the unique value of the estrogen-related gene IER3 as a potential biomarker and therapeutic target for DM.

Conclusively, these findings offer valuable insights into the biological and immunological significance of IER3. Monitoring its expression could facilitate the identification of high-risk populations, and its significance in the early diagnosis and prognostic evaluation of DM should not be underestimated. Consequently, extensive research on IER3 and its related signaling pathways opens new avenues for the development of innovative diagnostic tools and therapeutic strategies for the prevention and management of DM. Future investigations should explore the modulation of IER3 expression through pharmacological or gene-editing techniques, aiming to establish new treatment strategies for DM and provide essential evidence for personalized therapy. We anticipate that further exploration in this field will facilitate advancements in relevant technologies and their practical applications, ultimately enhancing the quality of life and health outcomes for individuals affected by DM.

Data availability statement

The datasets presented in this study can be found in online repositories. The names of the repository/repositories and accession number(s) can be found in the article/Supplementary Material.

Ethics statement

This study was approved by the Medical Ethics Committee of the First People's Hospital of Jingzhou and complied with medical ethics requirements. The studies were conducted in accordance with the local legislation and institutional requirements. Written informed consent for participation was not required from the participants or the participants' legal guardians/next of kin in accordance with the national legislation and institutional requirements.

Author contributions

DK: Visualization, Conceptualization, Writing – original draft. XH: Writing – original draft. WL: Visualization, Project administration, Software, Writing – review & editing. HW: Investigation, Methodology, Writing – review & editing. YS: Project administration, Supervision, Writing – review & editing. JT: Conceptualization, Software, Writing – review & editing. YW: Resources, Supervision, Data curation, Writing – review & editing.

Funding

The author(s) declare financial support was received for the research and/or publication of this article. This work was supported by grants from the Yangtze University Science and Technology Aid to Tibet Medical Talent Training Program Project (grant no. 2023YZ08).

Conflict of interest

The authors declare that the research was conducted without any commercial or financial relationships that could be perceived as a potential conflict of interest.

Generative AI statement

The author(s) declare that no Generative AI was used in the creation of this manuscript.

Any alternative text (alt text) provided alongside figures in this article has been generated by Frontiers with the support of artificial intelligence and reasonable efforts have been made to ensure accuracy, including review by the authors wherever possible. If you identify any issues, please contact us.

Publisher's note

Supplementary material

The Supplementary Material for this article can be found online at: https://www.frontiersin.org/articles/10.3389/fendo.2025.1570332/full#supplementary-material

References

1. Yaribeygi H, Sathyapalan T, Atkin SL, Sahebkar A. Molecular mechanisms linking oxidative stress and diabetes mellitus. *Oxid Med Cell Longevity*. (2020) 2020. doi: 10.1155/2020/8609213

2. Galicia-Garcia U, Benito-Vicente A, Jebari S, Larrea-Sebal A, Siddiqi H, Uribe KB, et al. Pathophysiology of type 2 diabetes mellitus. *Int J Mol Sci*. (2020) 21:17. doi: 10.3390/ijms21176275

3. Wang Y, Zeng X, Tan J, Xu Y, Yi C. Diabetes mellitus and endometrial carcinoma: risk factors and etiological links. *Medicine*. (2022) 101:34. doi: 10.1097/md.0000000000030299

4. Li W, Ke D, Xu Y, Wang Y, Wang Q, Tan J, et al. The immunological and prognostic significance of the diabetes mellitus-related gene wfs1 in endometrial cancer. *Front Immunol*. (2024) 15:1464421. doi: 10.3389/fimmu.2024.1464421

5. Sousa RAL, Improta-Caria AC, Souza BSF. Exercise-linked irisin: consequences on mental and cardiovascular health in type 2 diabetes. *Int J Mol Sci*. (2021) 22:4. doi: 10.3390/ijms22042199

6. Mansour A, Mousa M, Abdelmannan D, Tay G, Hassoun A, Alsafar H. Microvascular and macrovascular complications of type 2 diabetes mellitus: exome wide association analyses. *Front Endocrinol*. (2023) 14:1143067. doi: 10.3389/fendo.2023.1143067

7. Simpson ER. Sources of estrogen and their importance. *J Steroid Biochem Mol Biol*. (2003) 86:3–5. doi: 10.1016/s0960-0760(03)00360-1

8. Pacifici R. Estrogen deficiency, T cells and bone loss. *Cell Immunol*. (2008) 252:1–2. doi: 10.1016/j.cellimm.2007.06.008

9. Maioli S, Leander K, Nilsson P, Nalvarte I. Estrogen receptors and the aging brain. *Essays in biochemistry*. (2021) 65:6. doi: 10.1042/ebc20200162

10. Yan H, Yang W, Zhou F, Li X, Pan Q, Shen Z, et al. Estrogen improves insulin sensitivity and suppresses gluconeogenesis via the transcription factor foxo1. *Diabetes*. (2019) 68:2. doi: 10.2337/db18-0638

11. Gessler CJ, Halsted JA, Stetson RP. Effect of estrogenic substance on the blood sugar of female diabetics after the menopause. *J Clin Invest*. (1939) 18:6. doi: 10.1172/jci101087

12. Abu Aqel Y, Alnesf A, Aigha II, Islam Z, Kolatkar PR, Teo A, et al. Glucokinase (Gck) in diabetes: from molecular mechanisms to disease pathogenesis. *Cell Mol Biol Lett*. (2024) 29:1. doi: 10.1186/s11658-024-00640-3

13. De Paoli M, Zakharia A, Werstuck GH. The role of estrogen in insulin resistance: A review of clinical and preclinical data. *Am J Pathol*. (2021) 191:9. doi: 10.1016/j.ajpath.2021.05.011

14. Gautier L, Cope L, Bolstad BM, Irizarry RA. Affy–analysis of affymetrix genechip data at the probe level. *Bioinf (Oxford England)*. (2004) 20:3. doi: 10.1093/bioinformatics/btg405

15. Langfelder P, Horvath S. Wgcna: an R package for weighted correlation network analysis. *BMC Bioinf*. (2008) 9:559. doi: 10.1186/1471-2105-9-559

16. Wu T, Hu E, Xu S, Chen M, Guo P, Dai Z, et al. Clusterprofiler 4.0: A universal enrichment tool for interpreting omics data. *Innovation (Cambridge (Mass))*. (2021) 2:3. doi: 10.1016/j.xinn.2021.100141

17. Binson VA, Thomas S, Subramoniam M, Arun J, Naveen S, Madhu S. A review of machine learning algorithms for biomedical applications. *Ann Biomed Eng*. (2024) 52:5. doi: 10.1007/s10439-024-03459-3

18. Tibshirani R. Regression shrinkage and selection via the lasso. *J R Stat Soc*. (2018) 58:1. doi: 10.1111/j.2517-6161.1996.tb02080.x

19. Lin X, Li C, Zhang Y, Su B, Fan M, Wei H. Selecting feature subsets based on svm-rfe and the overlapping ratio with applications in bioinformatics. *Molecules*. (2017) 23:1. doi: 10.3390/molecules23010052

20. Blanchet L, Vitale R, van Vorstenbosch R, Stavropoulos G, Pender J, Jonkers D, et al. Constructing bi-plots for random forest: tutorial. *Analytica chimica Acta*. (2020) 1131:669–75. doi: 10.1016/j.aca.2020.06.043

21. Semlali A, Oliva J, Badia E, Pons M, Duchesne MJ. Immediate early gene X - 1 (Iex-1), a hydroxytamoxifen regulated gene with increased stimulation in mcf-7 derived resistant breast cancer cells. *J Steroid Biochem Mol Biol*. (2004) 88:3. doi: 10.1016/j.jsbmb.2003.12.005

22. Schott J, Reitter S, Philipp J, Haneke K, Schafer H, Stoecklin G. Translational regulation of specific mrnas controls feedback inhibition and survival during macrophage activation. *PLoS Genet*. (2014) 10:6. doi: 10.1371/journal.pgen.1004368

23. Shahid M, Javed AA, Chandra D, Ramsey HE, Shah D, Khan MF, et al. Iex-1 deficiency induces browning of white adipose tissue and resists diet-induced obesity. *Sci Rep*. (2016) 6. doi: 10.1038/srep24135

24. Chen B, Khodadoust MS, Liu CL, Newman AM, Alizadeh AA. Profiling tumor infiltrating immune cells with cibersort. *Methods Mol Biol (Clifton NJ)*. (2018) 243-259:1711. doi: 10.1007/978-1-4939-7493-1_12

25. Goncalves JS, Seica RM, Laranjinha J, Lourenco CF. Impairment of neurovascular coupling in the hippocampus due to decreased nitric oxide bioavailability supports early cognitive dysfunction in type 2 diabetic rats. *Free Radic Biol Med*. (2022) 193. doi: 10.1016/j.freeradbiomed.2022.11.009

26. Masha A, Dinatale S, Allasia S, Martina V. Role of the decreased nitric oxide bioavailability in the vascular complications of diabetes mellitus. *Curr Pharm Biotechnol*. (2011) 12:9. doi: 10.2174/138920111798281054

27. Dekkers MC, Pu X, Enciso-Martinez A, Zaldumbide A. Beta-cell-derived extracellular vesicles: mediators of intercellular communication in the islet microenvironment in type 1 diabetes. *Cells*. (2024) 13:23. doi: 10.3390/cells13231996

28. Zhang J, Juhl CR, Hylten-Cavallius L, Salling-Olsen M, Linneberg A, Holst JJ, et al. Gain-of-function mutation in the voltage-gated potassium channel gene kcnq1 and glucose-stimulated hypoinsulinemia - case report. *BMC endocrine Disord*. (2020) 20:1. doi: 10.1186/s12902-020-0513-x

29. Saeedi P, Petersohn I, Salpea P, Malanda B, Karuranga S, Unwin N, et al. Global and regional diabetes prevalence estimates for 2019 and projections for 2030 and 2045: results from the international diabetes federation diabetes atlas, 9(Th) edition. *Diabetes Res Clin Pract*. (2019) 157. doi: 10.1016/j.diabres.2019.107843

30. Zimmet P, Alberti KG, Shaw J. Global and societal implications of the diabetes epidemic. *Nature*. (2001) 414:6865. doi: 10.1038/414782a

31. Brown LM, Clegg DJ. Central effects of estradiol in the regulation of food intake, body weight, and adiposity. *J Steroid Biochem Mol Biol*. (2010) 122:1–3. doi: 10.1016/j.jsbmb.2009.12.005

32. Lovejoy JC, Champagne CM, de Jonge L, Xie H, Smith SR. Increased visceral fat and decreased energy expenditure during the menopausal transition. *Int J Obes*. (2008) .32:6. doi: 10.1038/ijo.2008.25

33. Tiano JP, Mauvais-Jarvis F. Importance of oestrogen receptors to preserve functional B-cell mass in diabetes. *Nat Rev Endocrinol*. (2012) 8:6. doi: 10.1038/nrendo.2011.242

34. Zhu L, Brown WC, Cai Q, Krust A, Chambon P, McGuinness OP, et al. Estrogen Treatment after Ovariectomy Protects against Fatty Liver and May Improve Pathway-Selective Insulin Resistance. *Diabetes*. (2013) 62:2. doi: 10.2337/db11-1718

35. Shen L, Guo J, Santos-Berrios C, Wu MX. Distinct domains for anti- and pro-apoptotic activities of iex-1. *J Biol Chem*. (2006) 281:22. doi: 10.1074/jbc.M600054200

36. Li X, Ren Y, Chang K, Wu W, Griffiths HR, Lu S, et al. Adipose tissue macrophages as potential targets for obesity and metabolic diseases. *Front Immunol*. (2023) 14:1153915. doi: 10.3389/fimmu.2023.1153915

37. Lumeng CN, Bodzin JL, Saltiel AR. Obesity induces a phenotypic switch in adipose tissue macrophage polarization. *J Clin Invest*. (2007) 117:1. doi: 10.1172/jci29881

38. Abu-Rustum N, Yashar C, Arend R, Barber E, Bradley K, Brooks R, et al. Uterine neoplasms, version 1.2023, nccn clinical practice guidelines in oncology. *J Natl Compr Cancer Network*. (2023) 21:2. doi: 10.6004/jnccn.2023.0006

39. Arlt A, Schäfer H. Role of the immediate early response 3 (Ier3) gene in cellular stress response, inflammation and tumorigenesis. *Eur J Cell Biol*. (2011) 90:6–7. doi: 10.1016/j.ejcb.2010.10.002

40. Huang YH, Wu JY, Zhang Y, Wu MX. Synergistic and opposing regulation of the stress-responsive gene iex-1 by P53, C-myc, and multiple nf-kappab/rel complexes. *Oncogene*. (2002) 21:44. doi: 10.1038/sj.onc.1205854

41. Molejon MI, Iovanna JL. Ier3 in pancreatic carcinogenesis. *Oncotarget*. (2015) 6:18. doi: 10.18632/oncotarget.4588

42. Garcia MN, Grasso D, Lopez-Millan MB, Hamidi T, Loncle C, Tomasini R, et al. Ier3 supports krasg12d-dependent pancreatic cancer development by sustaining erk1/2 phosphorylation. *J Clin Invest*. (2014) 124:11. doi: 10.1172/jci76037

43. Wang Q, Liu Y, Zhang Y, Zhang S, Zhao M, Peng Z, et al. Characterization of macrophages in ischemia-reperfusion injury-induced acute kidney injury based on single-cell rna-seq and bulk rna-seq analysis. *Int Immunopharmacol*. (2024) 130. doi: 10.1016/j.intimp.2024.111754

44. Liu S, Qiu J, He G, He W, Liu C, Cai D, et al. Trail promotes hepatocellular carcinoma apoptosis and inhibits proliferation and migration via interacting with ier3. *Cancer Cell Int*. (2021) 21:1. doi: 10.1186/s12935-020-01724-8

45. Bian C, Bai B, Gao Q, Li S, Zhao Y. 17β-estradiol regulates glucose metabolism and insulin secretion in rat islet B Cells through gper and akt/mtor/glut2 pathway. *Front Endocrinol*. (2019) 10:531. doi: 10.3389/fendo.2019.00531

46. Yang C, Trent S, Ionescu-Tiba V, Lan L, Shioda T, Sgroi D, et al. Identification of cyclin D1- and estrogen-regulated genes contributing to breast carcinogenesis and progression. *Cancer Res*. (2006) 66:24. doi: 10.1158/0008-5472.Can-06-1645

47. Tsalamandris S, Antonopoulos AS, Oikonomou E, Papamikroulis GA, Vogiatzi G, Papaioannou S, et al. The role of inflammation in diabetes: current concepts and future perspectives. *Eur Cardiol*. (2019) 14:1. doi: 10.15420/ecr.2018.33.1

48. Alexander M, Cho E, Gliozheni E, Salem Y, Cheung J, Ichii H. Pathology of diabetes-induced immune dysfunction. *Int J Mol Sci*. (2024) 25:13. doi: 10.3390/ijms25137105

49. Berbudi A, Rahmadika N, Tjahjadi AI, Ruslami R. Type 2 diabetes and its impact on the immune system. *Curr Diabetes Rev*. (2020) 16:5. doi: 10.2174/1573399815666191024085838

50. Mbongue JC, Nieves HA, Torrez TW, Langridge WH. The role of dendritic cell maturation in the induction of insulin-dependent diabetes mellitus. *Front Immunol*. (2017) 8:327. doi: 10.3389/fimmu.2017.00327

51. Kanter JE, Hsu CC, Bornfeldt KE. Monocytes and macrophages as protagonists in vascular complications of diabetes. *Front Cardiovasc Med*. (2020) 7:10. doi: 10.3389/fcvm.2020.00010

52. Yi HS, Kim SY, Kim JT, Lee YS, Moon JS, Kim M, et al. T-cell senescence contributes to abnormal glucose homeostasis in humans and mice. *Cell Death Dis*. (2019) 10:3. doi: 10.1038/s41419-019-1494-4

53. Callender LA, Carroll EC, Garrod-Ketchley C, Schroth J, Bystrom J, Berryman V, et al. Altered nutrient uptake causes mitochondrial dysfunction in senescent cd8(+) emra T cells during type 2 diabetes. *Front Aging*. (2021) 2:681428. doi: 10.3389/fragi.2021.681428

54. Vinuesa CG, Linterman MA, Yu D, MacLennan IC. Follicular helper T cells. *Annu Rev Immunol*. (2016) 34:335–68. doi: 10.1146/annurev-immunol-041015-055605

55. Hong S, Zhou W, Fang B, Lu W, Loro E, Damle M, et al. Dissociation of muscle insulin sensitivity from exercise endurance in mice by hdac3 depletion. *Nat Med*. (2017) 23:2. doi: 10.1038/nm.4245

frontiers | Frontiers in Endocrinology

TYPE Original Research
PUBLISHED 22 September 2025
DOI 10.3389/fendo.2025.1555277

OPEN ACCESS

EDITED BY
Sijung Yun,
Predictiv Care, Inc., United States

REVIEWED BY
Geng-dong Chen,
Foshan Women and Children Hospital, China
Satyajit Kulkarni,
Gujarat Ayurved University, India

*CORRESPONDENCE
Li Li
ZZSYLiLi@163.com
Gang Tian
Gang_tian@yeah.net
Xiaona Tian
2312890919@qq.com

†These authors have contributed equally to this work and share first authorship

RECEIVED 04 January 2025
ACCEPTED 28 August 2025
PUBLISHED 22 September 2025

CITATION
Zhang F, Hua Q, You X, Shi F, Zhou Y, Xu X, Tian X, Tian G and Li L (2025) The association between gestational hypothyroidism in pregnant women with preeclampsia, maternal liver function indicators, and neonatal birth weight: a study in Chinese pregnant women. *Front. Endocrinol.* 16:1555277. doi: 10.3389/fendo.2025.1555277

The association between gestational hypothyroidism in pregnant women with preeclampsia, maternal liver function indicators, and neonatal birth weight: a study in Chinese pregnant women

Fang Zhang[1†], Qing Hua[1†], Xiaoyan You[1], Fenglian Shi[1], Yadan Zhou[1], Xia Xu[2], Xiaona Tian[1*], Gang Tian[3*] and Li Li[1*]

[1]Department of Obstetrics, Zhengzhou Central Hospital Affiliated to Zhengzhou University, Zhengzhou, China, [2]Institute of Trauma and Metabolism, Zhengzhou Central Hospital Affiliated to Zhengzhou University, Zhengzhou, China, [3]Henan Province Hypertension Precision Prevention and Control Engineering Research Center, Henan Provincial People's Hospital, Zhengzhou University People's Hospital, Zhengzhou, Henan, China

Birth weight serves as a critical indicator of neonatal survival. Preeclampsia represents a serious complication during pregnancy and is closely associated with gestational hypothyroidism (GHT), both of which severely affect neonatal birth weight. Preeclampsia and hypothyroidism during pregnancy are usually accompanied by abnormalities of maternal liver function, which frequently leads to adverse pregnancy outcomes including low birth weight (LBW). This retrospective study utilized data from 420 cases of patients with preeclampsia who underwent prenatal examinations and delivery at department of Obstetrics. The association between preeclampsia combined with GHT in pregnancy, maternal liver function and neonatal birth weight was estimated using generalized linear model (GLM), and the potential partial mediating effects of maternal liver function were assessed through mediating models. Among pregnant women with preeclampsia, 11.0% had GHT, and the median (interquartile range) birth weight of all neonates was 2990.0 (2541.3, 3368.8) grams. Neonates born to pregnant women who had preeclampsia combine with GHT showed a higher incidence of LBW (χ^2=22.13, P< 0.001), exhibited a significantly lower birth weight compared to those born to women with preeclampsia alone (β=-258.53;95%CI:-398.56, -118.50). Additionally, maternal alanine aminotransferase (ALT) levels were found to partially mediate this association (indirect effect:-50.85, 95%CI:-101.07, -15.07). The findings of this study indicate that compared with pregnant women with preeclampsia alone, neonates born to pregnant women suffering from preeclampsia combined with

GHT have significantly lower birth weights, with maternal ALT levels acting as a potential partial mediator in this association. These results provide an important reference for clinicians to monitor thyroid and liver function in patients with preeclampsia.

KEYWORDS

birth weight, preeclampsia, gestational hypothyroidism, liver function, mediating model

Introduction

Neonatal birth weight is determined by maternal health, the placenta, and the fetus' own growth potential, and serving as a critical indicator of neonatal survival (1, 2). Low birth weight (LBW), defined as a birth weight of less than 2500 grams(g), is considered an important factor in neonatal mortality (3, 4). Studies have demonstrated that LBW increases the risk of future cardiovascular morbidity and is associated with an elevated risk of future hypertension in pregnancy (5, 6).

Preeclampsia is a serious complication of pregnancy with hypertension and proteinuria as the main clinical manifestations, and is one of the leading causes of maternal and neonatal mortality (7, 8). Preeclampsia can cause a series of serious obstetric complications, including preterm labor and placental abruption, as well as fetal complications such as fetal respiratory distress, intrauterine growth restriction, oligohydramnios, and stillbirth (9). There is increasing evidence suggests that preeclampsia is closely associated with maternal hypertension, cardiovascular disease, and dementia (10–12). Mechanistically, placental dysfunction induced by preeclampsia profoundly impacts on fetal development, with studies confirming it as an important predictor of neonatal birth weigh (13–15). The thyroid gland is involved in endocrine regulation and plays a crucial role in maternal and fetal development during pregnancy (16). Studies have confirmed the correlation between thyroid dysfunction and preeclampsia, and the prevalence of hypothyroidism in pregnant women with preeclampsia is significantly increased (17–19). Currently, hypothyroidism has become a common complication of preeclampsia, leading to adverse pregnancy outcomes, including LBW, and severely affecting neonatal birth weight and even future growth and development (20).

Preeclampsia and hypothyroidism during pregnancy are closely associated with alterations in liver function. Preeclampsia causes impaired liver function, which has been identified as the third most important predictor after hypertension and proteinuria (21, 22). Simultaneously, hypothyroidism, which is characterized by a feedback increase in thyroid-stimulating hormone (TSH) as a biochemical marker, interacts with hepatic function metabolically (23, 24). Experimental evidence has been presented that hepatic dysfunction in pregnant mice predisposes to placental dysfunction, which results in lower birth weights in newborn mice (25). Population-based studies have also confirmed that pregnant women with abnormal liver function are associated with adverse birth outcomes, such as preterm labor, LBW, intrauterine stillbirth, and fetal respiratory distress (26). Several scholars have investigated the mechanisms underlying the association of preeclampsia and hypothyroidism in pregnancy with LBW, including placental dysfunction in preeclampsia, maternal nutritional deficiencies associated with pregnancy, and maternal thyroid hormone levels (27–29). In conclusion, the mechanism by which preeclampsia combined with hypothyroidism affects neonatal birth weight is multifactorial. But there are currently limited studies exploring the mediating role of liver function as an important factor in the relationship between preeclampsia combined with hypothyroidism and birth weight. As shown in some studies, maternal liver function status is associated with fetal growth and development during pregnancy. Conducting research on the association between liver function indicators and birth weight can provide a basis for early risk monitoring strategies.

Therefore, the objective of this study was to explore the association between preeclampsia in conjunction with gestational hypothyroidism, maternal liver function, and neonatal birth weight. Additionally, the study aimed to explore whether maternal liver function serves as a potential mediating factor in the association between preeclampsia combined with gestational hypothyroidism and neonatal birth weight. This investigation seeks to address existing gaps in the literature regarding the underlying mechanisms and to offer insights for future related studies.

Materials and methods

Study design and population

This study was a retrospective study, and 554 cases who underwent prenatal examinations and deliveries at department of Obstetrics, Zhengzhou Central Hospital Affiliated to Zhengzhou from January 2021 to September 2023 were selected as the study subjects. According to the following inclusion criteria, 482 cases diagnosed with preeclampsia were initially included, and then 62 cases were excluded according to the exclusion criteria, 420 cases of preeclampsia patients were ultimately included in this study, and the median gestational age at diagnosis of preeclampsia

(interquartile range) was 35.4(32.5, 37.3) weeks. Among these, 46 cases were complicated by hypothyroidism, and the median gestational age at diagnosis of hypothyroidism (interquartile range) was 32.2(27.0, 36.0) weeks.

The inclusion criteria were as follows: (1) fulfillment of the diagnostic criteria for preeclampsia; (2) maternal age ≥ 18 years; (3) gestational age ≥ 24 weeks; (4) singleton pregnancy; (5) absence of a history of substance abuse, smoking, or alcohol consumption among the pregnant women.

The exclusion criteria were as follows: (1) pregnant individuals with other complications, such as gestational diabetes or hypertension, as well as those with underlying medical conditions prior to pregnancy (e.g., thyroid disorders, chronic hypertension, heart disease, liver or biliary diseases, or renal diseases); (2) patients lacking relevant information, such as those with incomplete or missing neonatal birth weight and liver function indicators; (3) individuals who conceived through assisted reproductive technology.

The diagnostic criteria for preeclampsia were based on the "Diagnosis and treatment of hypertension and preeclampsia in pregnancy: a clinical practice guideline in China (2020)" issued by the Obstetrics and Gynecology Branch of the Chinese Medical Association. Specifically, preeclampsia is diagnosed when, after 20 weeks of gestation, a pregnant woman exhibits a systolic blood pressure of ≥140 mmHg and/or a diastolic blood pressure of ≥90 mmHg, accompanied by at least one of the following: (1) a 24-hour urinary protein quantification of ≥0.3 g, or a urinary protein-to-creatinine ratio of ≥0.3, or a random urinary protein result of ≥(+); (2) the absence of proteinuria but the presence of any one of the following organ or system involvements, including abnormalities affecting vital organs such as the heart, lungs, liver, and kidneys, or alterations in the hematological, gastrointestinal, or neurological systems, as well as involvement of the placenta and fetus (30).

The diagnostic criteria for hypothyroidism during pregnancy refer to the revised "Guideline on diagnosis and management of thyroid diseases during pregnancy and postpartum (2nd edition)" by the Chinese Medical Association, which stipulates that serum thyroid-stimulating hormone (TSH) levels exceed the upper limit of the pregnancy-specific reference range, while serum free thyroxine (FT4) levels fall below the lower limit of the specific reference range. Combined with the types of kits and fully automated chemiluminescent immunoassay analyzers used in this study, the guideline recommended reference ranges for TSH and FT4 were as follows: in early pregnancy, TSH 0.05~3.55 mIU/L, FT49.01~15.89 pmol/L; in mid-pregnancy, TSH 0.21~3.31 mIU/L, FT4 6.62~13.51 pmol/L; in late pregnancy, TSH 0.43~3.71 mIU/L, FT4 6.42~10.75 pmol/L (31).

Ethical compliance statement for human participant research

All study participants provided written informed consent, and this study received approved from the Ethics Committee of Zhengzhou Central Hospital Affiliated to Zhengzhou (No. ZXYY202470). All methods were performed in accordance with the relevant guidelines and regulations of the Declaration of Helsinki.

Variables and definitions

Measurement of serum liver function indicators

In this study, we collected the levels of liver function indicators from subjects during their hospitalization. Based on previous research, this study selected indicators closely related to liver function, primarily including alanine aminotransferase (ALT 7-40U/L), aspartate aminotransferase (AST 13-35U/L), alkaline phosphatase (ALP 50-135U/L), total bilirubin (TBIL 0-21μmol/L), total protein (TP 60-80g/L), and albumin (Alb 35-55g/L). A volume of 5 mL of fasting antecubital venous blood was collected, and serum was separated by centrifugation at 4000 rpm for 5 minutes. All biochemical analyses were performed using an AU5800 fully automated biochemistry analyzer (Beckman Coulter, USA) with matched reagent kits. All reagents and instruments were subjected to quality control procedures.

Measurement of neonatal birth weight

Neonatal birth weight, measured in grams, was measured and recorded within one hour after birth. The data pertaining to birth weight for this investigation was sourced from medical records.

Measurement of covariates

Participants in this study were requested to complete a baseline questionnaire upon admission, which encompassed demographic characteristics of the pregnant women (age, ethnicity, residence, and educational level), history of cesarean delivery (yes/no), history of adverse pregnancy outcomes (yes/no), primiparity (yes/no), and family history of hypertension (yes/no). Participants self-reported their pre-pregnancy weight (kg) and their height was measured in a barefoot standing position using a medical height and weight measuring device (cm). Subsequently, pre-pregnancy body mass index (PBMI) was calculated using the standard formula BMI = weight (kg)/height (m^2). According to World Health Organization (WHO) standards, participants were classified into categories of underweight (BMI< 18.5 kg/m^2), normal weight (18.5 ≤ BMI ≤ 24.9 kg/m^2), overweight (25 ≤ BMI ≤ 29.9 kg/m^2), and obese (BMI ≥ 30 kg/m^2). During hospitalization, ultrasound was utilized to assess whether the fetus was experiencing growth restriction, and postpartum data on preterm birth (yes/no) and neonatal sex (male/female) were collected from medical records. The ultrasound diagnostic criteria for fetal growth restriction (FGR) were defined as an ultrasound-estimated fetal weight or abdominal circumference below the 10th percentile for the corresponding gestational age; preterm birth was defined as delivery occurring before 37 weeks of gestation.

Statistical analysis

Data analysis was conducted using SPSS 26.0 statistical software. Initially, descriptive analysis was performed, with categorical data expressed as N (%) and continuous data described using either $\bar{x} \pm s$ or M (IQR). For univariate analysis, given that birth weight exhibited a non-normal distribution, the Mann-Whitney U test or Kruskal-Wallis H test were employed to examine differences in birth weight among various characteristic groups. Spearman correlation analysis

was utilized to assess the relationship between liver function indicators (ALT/AST/ALP/TP/Alb/TBIL) and birth weight. Subsequently, a generalized linear model (GLM) was applied for multivariate analysis to evaluate the potential association between the presence of GHT, the levels of liver function indicators, and birth weight. Finally, the presence of GHT was treated as the independent variable, liver function indicators as mediating variables, and birth weight as the dependent variable. The mediation effect of liver function indicators was calculated using the SPSS Process macro, employing the bias-corrected Bootstrap method (with 5000 resamples) for validation. A p-value of<0.05 was considered statistically significant.

Results

Descriptive statistics

This study included a total of 420 pregnant women diagnosed with preeclampsia, among whom 46 (11.0%) also had concomitant hypothyroidism. The median age (interquartile range) was 31 (28, 34) years, with the majority of the participants (72.1%) aged between 25 and 35 years. The median neonatal birth weight (interquartile range) was 2990.0 (2541.3, 3368.8) grams. Preterm birth occurred in 111 participants (26.4%), while 24 (5.7%) were diagnosed with fetal growth restriction. Additionally, 15 participants were classified as underweight prior to pregnancy, 123 as overweight, and 52 as obese. Univariate analysis revealed that preterm birth (P<0.001), occurrence of fetal growth restriction during pregnancy (P<0.001), a pre-pregnancy BMI below 18.5 kg/m^2 (P=0.003), and the presence of GHT (P<0.001) were associated with lower birth weights of the neonates born to women with preeclampsia (Table 1).

Compared with pregnant women with preeclampsia alone, those with preeclampsia combined with GHT had higher rates of preterm delivery (39.1% vs. 24.9%), fetal growth restriction (17.4% vs. 4.3%) and LBW (50.0% vs. 19.3%), were more likely to be primiparous (73.9% vs. 58.6%), and obese (13.0% vs. 12.3%). From the perspective of liver function indicators, the levels of ALT (P<0.001) and AST (P=0.002) showed statistically significant differences between the two subgroups (Table 2).

Correlation between maternal liver function indicators and neonatal birth weight

Except for total bilirubin, the levels of other maternal liver function indicators showed significant correlations with neonatal

TABLE 1 The baseline characteristics of the included pregnant women.

Variable	N (%)	Birth weight (g)	*Z/H*	*P*
Age (Years)				
<25	23 (5.5)	2980.0 (2610.0, 3250.0)	2.65	0.449
25~35	303 (72.1)	3000.0 (2600.0, 3370.0)		
35~40	79 (18.8)	2825.0 (2325.0, 3350.0)		
≥40	15 (3.6)	3155.0 (2795.0, 3630.0)		
Fetal sex				
Male	223 (53.1)	3015.0 (2600.0, 3370.0)	-0.68	0.494
Female	197 (46.9)	2950.0 (2497.5, 3365.0)		
Ethnicity				
Han ethnicity	411 (97.9)	2990.0 (2550.0, 3365.0)	-0.65	0.513
Ethnic minorities	9 (2.1)	2890.0 (2120.0, 3485.0)		
Residence				
Urban area	349 (83.1)	2980.0 (2547.5, 3322.5)	-1.26	0.208
Rural area	71 (16.9)	3100.0 (2500.0, 3570.0)		
Education level				
Junior high school and below	41 (9.8)	3155.0 (2260.0, 3500.0)	2.11	0.550
High school and vocational secondary school	51 (12.1)	2980.0 (2450.0, 3305.0)		
Junior college	134 (31.9)	3032.5 (2660.0, 3415.0)		
Undergraduate and postgraduate degrees	194 (46.2)	2950.0 (2543.8, 3311.3)		

(Continued)

10.3389/fendo.2025.1555277

TABLE 1 Continued

Variable	N (%)	Birth weight (g)	*Z*/*H*	*P*
PTD				
No	309 (73.6)	3160.0 (2880.0, 3495.0)	-12.79	<0.001
Yes	111 (26.4)	2240.0 (1985.0, 2525.0)		
History of cesarean section				
No	319 (76.0)	3005.0 (2545.0, 3370.0)	-0.68	0.496
Yes	101 (24.0)	2965.0 (2522.5, 3315.0)		
History of adverse obstetric				
No	363 (86.4)	3010.0 (2570.0, 3370.0)	-1.66	0.098
Yes	57 (13.6)	2760.0 (2450.0, 3275.0)		
Primipara				
No	167 (39.8)	2950.0 (2495.0, 3370.0)	-1.06	0.288
Yes	253 (60.2)	3020.0 (2570.0, 3367.5)		
FGR				
No	396 (94.3)	3017.5 (2630.0, 3370.0)	-5.92	<0.001
Yes	24 (5.7)	2182.5 (1788.8, 2338.8)		
Family history of hypertension				
No	370 (88.1)	3002.5 (2548.8, 3370.0)	-1.28	0.201
Yes	50 (11.9)	2895.0 (2498.8, 3242.5)		
PBMI (kg/m^2)				
<18.5	15 (3.6)	2645.0 (2255.0, 3165.0)	13.77	0.003*
18.5~24.9	230 (54.7)	2950.0 (2392.5, 3280.0)		
25.0~29.9	123 (29.3)	3035.0 (2660.0, 3390.0)		
≥30	52 (12.4)	3180.0 (2808.8, 3613.8)		
PE&GHT				
No	374 (89.0)	3015.0 (2610.0, 3371.3)	-3.95	<0.001
Yes	46 (11.0)	2530.0 (2023.8, 3143.8)		

*P<0.05; PTD, Preterm delivery; FGR, Fetal growth restriction; PBMI, Pre-pregnancy body mass index; PE&GHT, Preeclampsia combined with gestational hypothyroidism.

birth weight. Specifically, ALT (r=-0.320) and AST (r=-0.234) levels exhibited negative correlations with neonatal birth weight, while ALP (r=0.193), TP (r=0.165), and ALB (r=0.177) displayed positive correlations with neonatal birth weight (Table 3).

Relationship between thyroid function, liver function indicators in pregnant women with preeclampsia, and neonatal birth weight

This study explored the relationship between the presence of GHT in preeclamptic pregnant women and their liver function indicators with neonatal birth weight through the construction of a GLM and the adjustment of control variables. The findings revealed that, without adjusting for other variables (Model 1), the neonatal birth weight of infants born to preeclamptic mothers with GHT was significantly lower compared to those born to mothers with uncomplicated preeclampsia [β = -351.36; 95% confidence interval (*CI*): -532.57, -170.15]. Furthermore, as levels of ALT (β = -2.18; 95% *CI*: -3.90, -0.47) and AST (β = -4.04; 95% *CI*: -7.06, 1.02) increased, neonatal birth weight correspondingly decreased, while an elevation in ALP levels (β=1.43; 95% *CI*: 0.53, 2.32) was associated with an increase in neonatal birth weight. Following adjustments for preterm birth, FGR, and PBMI (Model 2), the presence of GHT (β = -258.53; 95% *CI*: -398.56, -118.50), ALT (β = -1.88; 95% *CI*: -3.19, -0.56), and ALP (β=1.02; 95% *CI*: 0.33, 1.70) levels remained significantly associated with neonatal birth weight, whereas the association between AST levels (β = -1.34; 95% *CI*: -3.66, 0.98) and neonatal birth weight became statistically insignificant (Table 4).

10.3389/fendo.2025.1555277

TABLE 2 Comparison of baseline data between the preeclampsia group and the preeclampsia with hypothyroidism group.

Variable	Maternal status [n (%)/M (P_{25}, P_{75})]		χ^2 /Z	P
	PE&GHT	PE		
Age (Years)				
<25	0 (0.0)	23 (6.1)	-1.07	0.283
25~35	35 (76.1)	268 (71.7)		
35~40	7 (15.2)	72 (19.3)		
≥40	4 (8.7)	11 (2.9)		
Fetal sex				
Male	22 (47.8)	201 (53.7)	0.58	0.448
Female	24 (52.2)	173 (46.3)		
Ethnicity				
Han ethnicity	45 (97.8)	366 (97.9)	—	1.000
Ethnic minorities	1 (2.2)	8 (2.1)		
Residence				
Urban area	43 (93.5)	306 (81.8)	3.97	0.058
Rural area	3 (6.5)	68 (18.2)		
Education level				
Junior high school and below	6 (13.0)	35 (9.4)	-0.28	0.778
High school and vocational secondary school	6 (13.0)	45 (12.0)		
Junior college	10 (21.8)	124 (33.2)		
Undergraduate and postgraduate degrees	24 (52.2)	170 (45.4)		
PTD				
No	28 (60.9)	281 (75.1)	4.29	0.038*
Yes	18 (39.1)	93 (24.9)		
History of cesarean section				
No	37 (80.4)	282 (75.4)	0.57	0.451
Yes	9 (19.6)	92 (24.6)		
History of adverse obstetric				
No	39 (84.8)	324 (86.6)	0.12	0.730
Yes	7 (15.2)	50 (13.4)		
Primipara				
No	12 (26.1)	155 (41.4)	4.03	0.045*
Yes	34 (73.9)	219 (58.6)		
FGR				
No	38 (82.6)	358 (95.7)	10.75	0.001*
Yes	8 (17.4)	16 (4.3)		

(Continued)

TABLE 2 Continued

Variable	Maternal status [n (%)/M (P_{25}, P_{75})]		χ^2 /Z	P
	PE&GHT	PE		
Family history of hypertension				
No	43 (93.5)	327 (87.4)	1.43	0.232
Yes	3 (6.5)	47 (12.6)		
PBMI (kg/m^2)				
<18.5	1 (2.2)	14 (3.7)	-2.33	0.020*
18.5~24.9	32 (69.6)	198 (53.0)		
25.0~29.9	7 (15.2)	116 (31.0)		
≥30	6 (13.0)	46 (12.3)		
Neonatal birth weight status				
non-LBW	23 (50.0)	302 (80.7)	22.13	<0.001
LBW	23 (50.0)	72 (19.3)		
ALT (U/L)	23.5 (12.8,59.3)	13.0 (9.0,20.0)	-4.34	<0.001
AST (U/L)	36.5 (24.0,50.3)	26.0 (22.0,33.0)	-3.17	0.002*
ALP (U/L)	155.0 (120.3,193.8)	151.0 (123.0,189.3)	-0.22	0.823
TP (g/L)	56.0 (52.4,62.0)	58.1 (54.0,62.0)	-1.18	0.238
Alb (g/L)	30.1 (27.5,34.4)	31.1 (29.0,34.0)	-1.66	0.097
TBIL (μmol/L)	10.9 (8.3,14.8)	11.0 (9.1,13.3)	-0.16	0.870

*P<0.05; PE&GHT, Preeclampsia combined with gestational hypothyroidism; PTD, Preterm delivery; FGR, Fetal growth restriction; PBMI, Pre-pregnancy body mass index; LBW, low birth weight; ALT, Alanine Aminotransferase; AST, Aspartate Aminotransferase; ALP, Alkaline Phosphatase; TP, Total Protein; Alb, Albumin; TBIL, Total Bilirubin; BW, Birth Weight.

We also did some extra analysis after sorting out liver function indicators (normal or abnormal) and birth weight (low birth weight or non-low birth weight). Check out the Supplementary Table S1 and Supplementary Table S2 for more details.

Mediating effects of liver function indicators

Since there was no statistically significant difference in ALP levels between the preeclampsia group and the preeclampsia combined with GHT group, this study only included ALT, which was statistically significant in the multifactorial analysis, into a mediation model to investigate whether the factor partially mediate the relationship between preeclampsia in pregnant women with GHT and neonatal birth weight. The path coefficients are detailed in Table 5. The results indicate that pregnant women with preeclampsia combined with GHT exhibited higher ALT levels compared to those with preeclampsia alone (β'=23.19, P=0.002), which was associated with a negative impact on neonatal birth weight (β'=-271.18, P<0.001). Furthermore, ALT levels had a negative effect on neonatal birth weight (β'=-2.40, P<0.001. In

TABLE 3 Analysis of the correlation of maternal liver function indicators and neonatal birth weight.

Variables	ALT	AST	ALP	TP	ALB	TBIL	BW
ALT	1.000						
AST	0.589**	1.000					
ALP	0.111*	0.051	1.000				
TP	-0.038	-0.139**	0.077	1.000			
Alb	0.000	-0.181**	0.099*	0.790**	1.000		
TBIL	0.100*	0.118*	0.130**	0.067	0.127**	1.000	
BW	-0.320**	-0.234**	0.193**	0.165**	0.177**	0.089	1.000

* P<0.05, ** P<0.01. ALT, Alanine Aminotransferase; AST, Aspartate Aminotransferase; ALP, Alkaline Phosphatase; TP, Total Protein; Alb, Albumin; TBIL, Total Bilirubin; BW, Birth Weight.

10.3389/fendo.2025.1555277

TABLE 4 The results of generalized linear regression analyses of birth weight.

Variable	Model 1		Model 2	
	β (95%*CI*)	*P*	*β* (95%*CI*)	*P*
PE&GHT				
No (ref.)	—	—	—	—
Yes	-351.36 (-532.57, -170.15)	<0.001	-258.53 (-398.56, -118.50)	<0.001
ALT	-2.184 (-3.90, -0.47)	0.013*	-1.88 (-3.19, -0.56)	0.005*
AST	-4.04 (-7.06, 1.02)	0.009*	-1.34 (-3.66, 0.98)	0.256
ALP	1.43 (0.53, 2.32)	0.002*	1.02 (0.33, 1.70)	0.004*
TP	10.45 (-1.65, 22.56)	0.090	6.07 (-3.21, 15.34)	0.200
ALB	4.74 (-14.59, 24.07)	0.631	-0.45 (-15.24, 14.35)	0.953
PTD				
No (ref.)	—	—	—	—
Yes	—	—	-799.73 (-899.72, -699.75)	<0.001
FGR				
No (ref.)	—	—	—	—
Yes	—	—	-296.60 (-487.72, -105.49)	0.002*
PBMI (kg/m^2)				
<18.5	—	—	-177.45 (-408.54, 53.64)	0.132
18.5~24.9 (ref.)	—	—	—	—
25.0~29.9	—	—	93.69 (-4.30, 191.68)	0.061
≥30.0	—	—	310.39 (176.83, 443.96)	<0.001

*P<0.05. CI, confidence interval; PE&GHT: Preeclampsia combined with gestational hypothyroidism; ALT, Alanine Aminotransferase; AST, Aspartate Aminotransferase; ALP, Alkaline Phosphatase; TP, Total Protein; Alb, Albumin; PTD, Preterm delivery; FGR, Fetal growth restriction; PBMI, Pre-pregnancy body mass index; ref., Reference Group.
Model 1 was the unadjusted model; Model 2 adjusted for PTD, FGR and PBMI.

light of these path results, the study explored the mediating effect of ALT, as detailed in Table 6. The findings indicate that preeclampsia in conjunction with GHT may indirectly diminish neonatal birth weight by elevating maternal ALT levels. The mediating effect of ALT is quantified at -50.85 with a 95% Bootstrap confidence interval. The interval (95% *CI*) of [101.07, -15.07] does not encompass zero, indicating a substantial mediating effect that accounts for 15.5% of the total effect. The constructed mediation model is illustrated in Figure 1.

Discussions

This study explores the impact of gestational hypothyroidism and liver function indicators on neonatal birth weight in women with preeclampsia by constructing generalized linear models and mediation models, while also evaluates the potential mediating effects of liver function indicators. The results indicate that approximately 11.0% of the preeclamptic participants included in the study concurrently suffered from hypothyroidism. Neonates

TABLE 5 Path-coefficients of the mediating models.

Pathway	Standardized coefficients	Coefficients(β')	S.E.	*P*
PE&GHT→ALT	0.49	23.19	7.44	0.002
PE&GHT→BW	-0.42	-271.18	72.25	<0.001
ALT→BW	-0.18	-2.40	0.48	<0.001

Adjusting for preterm delivery, fetal growth restriction and pre-pregnancy body mass index.
S.E., Standard Error; PE&GHT, Preeclampsia combined with gestational hypothyroidism; ALT, Alanine Aminotransferase; BW, Birth Weight.

10.3389/fendo.2025.1555277

TABLE 6 Mediating effects of maternal alanine aminotransferase between preeclampsia with gestational hypothyroidism and birth weight.

Variable	Estimate	S.E.	Bootstrap 95%*CI*		Effect size (%)
			Lower	Upper	
Total effect	-327.52	73.79	-472.56	-182.48	100.0
Direct effect	-276.66	72.89	-419.94	-133.39	84.5
Indirect effect	-50.85	22.53	-101.07	-15.07	15.5

Adjusting for preterm delivery, fetal growth restriction and pre-pregnancy body mass index.
S.E., Standard Error; CI, Confidence Interval.

born to mothers with preeclampsia and hypothyroidism exhibited lower birth weights; specifically, higher levels of ALT in liver function indicators were associated with lower neonatal birth weights, whereas neonatal birth weight increased with rising ALP levels. Notably, after adjusting for covariates such as preterm birth, FGR, and PBMI, the relationship between AST levels and neonatal birth weight became statistically insignificant. Furthermore, the mediation model revealed that hypothyroidism can directly affect the neonatal birth weight of women with preeclampsia and can also indirectly influence neonatal birth weight through elevated ALT levels (mediating effect: -50.85; 95% *CI* = -101.07, -15.07).

Preeclampsia and gestational hypothyroidism are two common pregnancy complications that can have severe implications for the health of both the mother and the fetus, including miscarriage, preterm birth, fetal growth restriction, and low birth weight (32, 33). Preeclampsia can lead to maternal vascular constriction and reduced blood flow, thereby affecting the blood supply to the placenta and subsequently influencing the nutritional supply to the fetus (34). Particularly, preeclampsia is one of the significant causes of maternal and neonatal mortality, and once diagnosed, there are currently no effective treatment options available aside from the termination of pregnancy (34, 35). Similarly, during pregnancy, thyroid hormones can regulate various metabolic balances in pregnant women and are also involved in the formation and function of the placenta. In cases of hypothyroidism, the resulting deficiency of thyroid hormones may lead to placental dysfunction, causing fetal developmental abnormalities (36). It is worth noting that these two diseases often coexist and influence each other. Previous studies have indicated that hypothyroidism is significantly associated with an increased incidence of preeclampsia (37), and the prevalence of hypothyroidism among patients with preeclampsia is significantly higher than that in the general population (38). Additionally, further research has pointed out that hypothyroidism is correlated with the severity of preeclampsia (39). Therefore, the combination of preeclampsia and gestational hypothyroidism may pose greater risks to both the mother and the fetus. On the other hand, the birth weight of neonates is not only related to their survival rates but also has lasting implications for their physical growth, the development of various systems, and health issues in adulthood (40, 41). That's why we focused on investigating the effect of hypothyroidism in pregnant women with preeclampsia on neonatal birth weight. Our study findings indicate that neonates born to mothers with preeclampsia combined with hypothyroidism have lower birth weights compared to those born to mothers with preeclampsia alone, which is consistent with previous research results (42). This may indicate that when pregnant women experience preeclampsia in conjunction with hypothyroidism, it may have a more severe impact on the birth weight of the neonate.

Furthermore, our study further investigated the association between maternal liver function indicators and neonatal birth weight. Among pregnant women, the prevalence of liver diseases during pregnancy is approximately 3%, primarily manifested by abnormal changes in transaminases, bilirubin, and other related parameters (43). Pregnancy-related liver diseases are closely associated with fetal growth and development. Some pregnancy-specific liver diseases, such as acute fatty liver of pregnancy (AFLP) and intrahepatic cholestasis of pregnancy (ICP), may result in

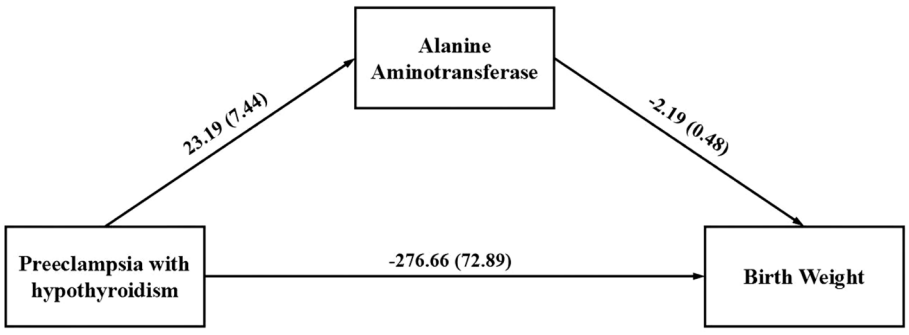

FIGURE 1
The mediation model examines the indirect correlation between gestational hypothyroidism in pregnant women with preeclampsia and neonatal birth weight through maternal alanine aminotransferase level.

maternal hepatic dysfunction, which can subsequently affect the placenta's ability to supply nutrients and oxygen to the fetus. This may lead to complications such as fetal intrauterine distress, preterm birth, and LBW, thereby posing risks to maternal and fetal safety (44). However, during pregnancy, the indicators related to liver function diagnosis do not change independently and may undergo physiological changes, which complicates the diagnosis of liver function in pregnant women. For instance, ALP levels may physiologically increase in the late stages of pregnancy due to placental production and fetal skeletal development. Conversely, albumin levels may decrease due to hemodilution. Nevertheless, when maternal transaminase and bilirubin levels increase, it is generally considered an abnormal phenomenon (45). Consistent with the findings of Sciarrone et, al (46), this study also indicates that maternal ALT levels are negatively correlated with neonatal birth weight. Elevated ALT levels typically indicate liver cell damage or liver dysfunction, which may lead to a decrease in the liver's synthetic capacity and subsequently affect fetal nutrition supply (47). Additionally, pro-inflammatory factors released due to liver damage can cross the placental barrier and inhibit fetal growth (48), ultimately resulting in reduced the neonatal birth weight (49). This study also found a positive correlation between maternal serum ALP levels and neonatal birth weight, which is consistent with previous research findings (50, 51). The variation in ALP levels is associated with gestational age; although elevated ALP levels are related to ICP (52), which may impair placental function, the increase in ALP during pregnancy is generally considered physiological. From another perspective, ALP is involved in the transport and metabolic processes within the placenta. Elevated ALP levels may reflect robust placental function, which is beneficial for fetal growth and development, thereby contributing to increased birth weight (53). Interestingly, after adjusting for covariates, the statistical significance between AST levels and neonatal birth weight dissipated. This may be attributed to the substantial influence of these covariates on neonatal birth weight, thereby obscuring the effect of AST levels. Additionally, there may be a high correlation between AST levels and the covariates, as indicated by the research conducted by Zhuang et al., which suggests that AST is an independent risk factor for preterm birth (54).

It is noteworthy that both preeclampsia and hypothyroidism can impair maternal liver function (35, 55), and that preeclampsia, hypothyroidism, and liver function all have an impact on neonatal birth weight. Therefore, we constructed a mediation model to explore whether preeclampsia combined with hypothyroidism could indirectly influence neonatal birth weight by altering liver function indicators. This investigation serves as an extension of our understanding of the impact of hypothyroidism on fetal development. The results of this study indicate that ALT levels partially mediate the relationship between preeclampsia combined with hypothyroidism and neonatal birth weight, that is, compared to pregnant women with preeclampsia alone, those with preeclampsia combined with hypothyroidism not only directly contribute to a reduction in neonatal birth weight but may also indirectly lower birth weight through increased ALT levels. Hypothyroidism is characterized by elevated serum TSH levels and decreased FT4 levels, leading to thyroid hormone deficiency, which plays a crucial role in hepatic cellular activity and liver metabolism. Thus, hypothyroidism may lead to hepatic dysfunction, commonly manifested as impaired lipid metabolism (56) and hepatic steatosis (57). Previous studies have primarily focused on the lipid metabolism of pregnant women with hypothyroidism and its impact on pregnancy outcomes (58). However, there is a paucity of research examining the effects of changes in liver function indicators caused by hypothyroidism on pregnancy outcomes. In fact, hypothyroidism can lead to abnormalities in serum liver enzymes. A study analyzing serum data from 10292 outpatient adults indicated a negative correlation between serum GGT and ALT concentrations and FT4 levels (59), suggesting that hypothyroidism may result in elevated concentrations of ALT and gamma-glutamyl transferase (GGT).

Certainly, this study has several limitations. Firstly, the scope of our investigation is not comprehensive enough, as it lacks details on factors such as the nutritional status of pregnant women and the treatment received during hospitalization, which may confound the relationship with neonatal birth weight. Secondly, given that this study employs an observational design, it cannot establish causal relationships, necessitating cautious interpretation of the findings. Thirdly, the study only included women with singleton live births, which may introduce selection bias; additionally, there is a lack of relevant data from normal pregnant women to serve as a control group. Fourthly, since the focus of research designs was on examining the effects of preeclampsia combined with or without hypothyroidism on maternal liver function and neonatal birth weight, the impact of the severity of preeclampsia on liver function and birth weight was overlooked. Consequently, some classification criteria lacked comprehensive data monitoring, making it impossible to conduct more in-depth exploratory research. Finally, there may exist a bidirectional relationship between thyroid function and liver function; this study only explored whether hypothyroidism could induce changes in liver function indicators that indirectly affect neonatal birth weight. Therefore, future research should consider conducting larger-scale prospective studies to gain a more comprehensive understanding of the intricate interplay between preeclampsia with hypothyroidism, liver function, and adverse pregnancy outcomes.

Conclusions

This study provides new insights by exploring the impact of hypothyroidism and liver function indicators in pregnant women with preeclampsia on neonatal birth weight. The findings support the notion that hypothyroidism adversely affects fetal development and suggest that maternal serum ALT levels may serve as a potential partial mediator linking preeclampsia combined with hypothyroidism and neonatal birth weight. Clinicians should

closely monitor thyroid and liver function in pregnant women with preeclampsia and implement appropriate interventions to improve neonatal birth weight and health outcomes.

Data availability statement

The raw data supporting the conclusions of this article will be made available by the authors, without undue reservation.

Ethics statement

All study participants provided written informed consent, and this study received approved from the Ethics Committee of Zhengzhou Central Hospital Affiliated to Zhengzhou (No. ZXYY202470). All methods were performed in accordance with the relevant guidelines and regulations of the Declaration of Helsinki. The studies were conducted in accordance with the local legislation and institutional requirements. The participants provided their written informed consent to participate in this study.

Author contributions

FZ: Conceptualization, Data curation, Investigation, Methodology, Writing – original draft. QH: Conceptualization, Data curation, Investigation, Methodology, Writing – original draft. XY: Conceptualization, Resources, Writing – original draft. FS: Methodology, Software, Writing – original draft. YZ: Project administration, Validation, Writing – original draft. XX: Validation, Visualization, Writing – original draft. XT: Supervision, Writing – review & editing. GT: Data curation, Formal Analysis, Writing – original draft. LL: Funding acquisition, Supervision, Writing – review & editing.

Funding

The author(s) declare that financial support was received for the research and/or publication of this article. This work was supported by the Henan Province Key Scientific Research Project Plan for Higher Education Institutions (24A320037).

Acknowledgments

We would like to express our gratitude to the pregnant women who took part in this project for providing us with comprehensive study data and Dr Tian Gang of Henan Provincial People's Hospital for his invaluable guidance in statistics.

Conflict of interest

The authors declare that the research was conducted in the absence of any commercial or financial relationships that could be construed as a potential conflict of interest.

Generative AI statement

The author(s) declare that no Generative AI was used in the creation of this manuscript.

Any alternative text (alt text) provided alongside figures in this article has been generated by Frontiers with the support of artificial intelligence and reasonable efforts have been made to ensure accuracy, including review by the authors wherever possible. If you identify any issues, please contact us.

Publisher's note

Supplementary material

The Supplementary Material for this article can be found online at: https://www.frontiersin.org/articles/10.3389/fendo.2025.1555277/full#supplementary-material

References

1. Svensson AC, Pawitan Y, Cnattingius S, Reilly M, Lichtenstein P. Familial aggregation of small-for-gestational-age births: the importance of fetal genetic effects. *Am J Obstet Gynecol.* (2006) 194:475–9. doi: 10.1016/j.ajog.2005.08.019

2. Basso O, Wilcox AJ, Weinberg CR. Birth weight and mortality: causality or confounding? *Am J Epidemiol.* (2006) 164:303–11. doi: 10.1093/aje/kwj237

3. McCormick MC. The contribution of low birth weight to infant mortality and childhood morbidity. *N Engl J Med.* (1985) 312:82–90. doi: 10.1056/NEJM198501103120204

4. McIntire DD, Bloom SL, Casey BM, Leveno KJ. Birth weight in relation to morbidity and mortality among newborn infants. *N Engl J Med.* (1999) 340:1234–8. doi: 10.1056/NEJM199904223401603

5. Osmond C, Barker DJ. Fetal, infant, and childhood growth are predictors of coronary heart disease, diabetes, and hypertension in adult men and women. *Environ Health Perspect.* (2000) 108:545–53. doi: 10.1289/ehp.00108s3545

6. Kurabayashi T, Mizunuma H, Kubota T, Nagai K, Hayashi K. Low birth weight and prematurity are associated with hypertensive disorder of pregnancy in later life: A cross-sectional study in Japan. *Am J Perinatol.* (2021) 38:1096–102. doi: 10.1055/s-0040-1705134

7. Shennan AH, Hurrell A. The evolving definition of preeclampsia. *BJOG.* (2021) 128:1383. doi: 10.1111/1471-0528.16632

8. Sibai B, Dekker G, Kupferminc M. Preeclampsia. *Lancet.* (2005) 365:785–99. doi: 10.1016/S0140-6736(05)17987-2

9. Bokslag A, van Weissenbruch M, Mol BW, de Groot CJ. Preeclampsia; short and long-term consequences for mother and neonate. *Early Hum Dev*. (2016) 102:47–50. doi: 10.1016/j.earlhumdev.2016.09.007

10. Phipps EA, Thadhani R, Benzing T, Karumanchi SA. Preeclampsia: pathogenesis, novel diagnostics and therapies. *Nat Rev Nephrol*. (2019) 15:275–89. doi: 10.1038/s41581-019-0119-6

11. Benschop L, Duvekot JJ, Roeters van Lennep JE. Future risk of cardiovascular disease risk factors and events in women after a hypertensive disorder of pregnancy. *Heart*. (2019) 105:1273–8. doi: 10.1136/heartjnl-2018-313453

12. Andolf EG, Sydsjö GC, Bladh MK, Berg G, Sharma S. Hypertensive disorders in pregnancy and later dementia: a Swedish National Register Study. *Acta Obstet Gynecol Scand*. (2017) 96:464–71. doi: 10.1111/aogs.13096

13. Odegard RA, Vatten LJ, Nilsen ST, Salvesen KA, Austgulen R. Preeclampsia and fetal growth. *Obstet Gynecol*. (2000) 96:950–5.

14. Li F, Wang T, Chen L, Zhang S, Chen L, Qin J, et al. Adverse pregnancy outcomes among mothers with hypertensive disorders in pregnancy: A meta-analysis of cohort studies. *Pregnancy Hypertens*. (2021) 24:107–17. doi: 10.1016/j.preghy.2021.03.001

15. Nakimuli A, Starling JE, Nakubulwa S, Namagembe I, Sekibubo M, Nakabembe E, et al. Relative impact of preeclampsia on birth weight in a low resource setting: A prospective cohort study. *Pregnancy Hypertens*. (2020) 21:1–6. doi: 10.1016/j.preghy.2020.04.002

16. Krassas GE, Poppe K, Glinoer D. Thyroid function and human reproductive health. *Endocr Rev*. (2010) 31:702–55. doi: 10.1210/er.2009-0041

17. Wang J, Gong XH, Peng T, Wu JN. Association of thyroid function during pregnancy with the risk of preeclampsia and gestational diabetes mellitus. *Endocr Pract*. (2021) 27:819–25. doi: 10.1016/j.eprac.2021.03.014

18. Khadir F, Rahimi Z, Vaisi-Raygani A, Shakiba E, Naseri R, et al. Gestational diabetes mellitus (GDM), hypothyroidism, and gene variants (Keap1 rs11085735) in patients with preeclampsia. *Rep Biochem Mol Biol*. (2022) 11:493–501. doi: 10.52547/rbmb.11.3.493

19. Lintula A, Keski-Nisula L, Sahlman H. Hypothyroidism and the increased risk of preeclampsia-interpretative factors? *Hypertens Pregnancy*. (2020) 39:411–7. doi: 10.1080/10641955.2020.1800030

20. Maraka S, Ospina NM, O'Keeffe DT, Espinosa De Ycaza AR, Gionfriddo MR, Erwin PJ, et al. Subclinical hypothyroidism in pregnancy: A systematic review and meta-analysis. *Thyroid*. (2016) 26:580–90. doi: 10.1089/thy.2015.0418

21. Abraham C, Kusheleva N. Management of preeclampsia and eclampsia: A simulation. *MedEdPORTAL*. (2019) 23:10832. doi: 10.15766/mep_2374-8265.10832

22. Thangaratinam S, Ismail K, Sharp S, Coomarasamy A, O'Mahony F, Khan KS, et al. TIPPS (Tests in Prediction of Preeclamsia's Severity) Review Group. Prioritisation of tests for the prediction of preeclampsia complications: a Delphi survey. *Hypertens Pregnancy*. (2007) 26:131–8. doi: 10.1080/10641950601148000

23. Vidal-Cevallos P, Murúa-Beltrán Gall S, Uribe M, Chávez-Tapia NC, et al. Understanding the relationship between nonalcoholic fatty liver disease and thyroid disease. *Int J Mol Sci*. (2022) 24:14605. doi: 10.3390/ijms241914605

24. Di Sessa A, Sambiase Sanseverino NC, De Simone RF, Marrapodi MM, Cirillo G, Umano GR, et al. Association between non-alcoholic fatty liver disease and subclinical hypothyroidism in children with obesity. *J Endocrinol Invest*. (2023) 46:1835–42. doi: 10.1007/s40618-023-02041-3

25. Kawakami T, Yoshimi M, Kadota Y, Inoue M, Sato M, Suzuki S. Prolonged endoplasmic reticulum stress alters placental morphology and causes low birth weight. *Toxicol Appl Pharmacol*. (2014) 275:134–44. doi: 10.1016/j.taap.2013.12.008

26. Jhirwal M, et al. Maternal and perinatal outcome in pregnancy complicated by intrahepatic cholestasis. *Cureus*. (2022) 14:e28512. doi: 10.7759/cureus.28512

27. Yu X, Yao Y, Wang D, Tang J, Lu J. Prediction of fetal growth restriction for fetal umbilical arterial/venous blood flow index evaluated by ultrasonic doppler under intelligent algorithm. *Comput Math Methods Med*. (2022) 2022:7451185. doi: 10.1155/2022/7451185

28. Devarshi PP, Grant RW, Ikonte CJ, Hazels Mitmesser S. Maternal omega-3 nutrition, placental transfer and fetal brain development in gestational diabetes and preeclampsia. *Nutrients*. (2019) 11:1107. doi: 10.3390/nu11051107

29. He X, Wang Y, Wu M, Wei J, Sun X, Wang A, et al. Secoisolariciresinol diglucoside improves ovarian reserve in aging mouse by inhibiting oxidative stress. *Front Mol Biosci*. (2022) 8:806412. doi: 10.3389/fmolb.2021.806412

30. Hypertensive Disorders in Pregnancy Subgroup, Chinese Society of Obstetrics and Gynecology, Chinese Medical Association. Diagnosis and treatment of hypertension and preeclampsia in pregnancy: a clinical practice guideline in China (2020). *Chin J Obstet Gynecol*. (2020) 55:227–38. doi: 10.3760/cma.j.cn112141-20200114-00039

31. Ad Hoc Writing Committee for Guidelines on diagnosis and management of thyroid diseases during pregnancy and postpartum, Chinese Society of Endocrinology, Chinese Medical Association and Chinese Society of Perinatology, Chinese Medical Association. Guideline on diagnosis and management of thyroid diseases during pregnancy and postpartum (2nd edition). *Chin J Endocrinol Metab*. (2019) 35:636–65.

32. Atamamen TF, Naing NN, Oyetunji JA, Wan-Arfah N. Systematic literature review on the neonatal outcome of preeclampsia. *Pan Afr Med J*. (2022) 41:82. doi: 10.11604/pamj.2022.41.82.31413

33. Korevaar TIM, Medici M, Visser TJ, Peeters RP. Thyroid disease in pregnancy: new insights in diagnosis and clinical management. *Nat Rev Endocrinol*. (2017) 13:610–22. doi: 10.1038/nrendo.2017.93

34. Rana S, Lemoine E, Granger JP, Karumanchi SA. Preeclampsia: pathophysiology, challenges, and perspectives. *Circ Res*. (2019) 124:1094–112. doi: 10.1161/CIRCRESAHA.118.313276

35. Dimitriadis E, et al. Preeclampsia. *Nat Rev Dis Primers*. (2023) 9:8. doi: 10.1038/s41572-023-00417-6

36. Adu-Gyamfi EA, Wang YX, Ding YB. The interplay between thyroid hormones and the placenta: a comprehensive review. *Biol Reprod*. (2020) 102:8–17. doi: 10.1093/biolre/ioz182

37. Lee SY, Cabral HJ, Aschengrau A, Pearce EN. Associations between maternal thyroid function in pregnancy and obstetric and perinatal outcomes. *J Clin Endocrinol Metab*. (2020) 105:e2015–23. doi: 10.1210/clinem/dgz275

38. Medjedovic E, Stanojevic M, Kurjak A, Begic E, Iglica A, Jonuzovic-Prosic S. Association between maternal thyroid function and risk of gestational hypertension and preeclampsia. *J Perinat Med*. (2022) 50:904–9. doi: 10.1515/jpm-2022-0121

39. Su X, Liu Y, Li G, Liu X, Huang S, Duan T, et al. Associations of hypothyroxinemia with risk of preeclampsia-eclampsia and gestational hypertension. *Front Endocrinol*. (2021) 12:777152. doi: 10.3389/fendo.2021.777152

40. Hack M, Flannery DJ, Schluchter M, Cartar L, Borawski E, Klein N. Outcomes in young adulthood for very-low-birth-weight infants. *N Engl J Med*. (2002) 346:149–57. doi: 10.1056/NEJMoa010856

41. Grillo MA, Mariani G, Ferraris JR. Prematurity and low birth weight in neonates as a risk factor for obesity, hypertension, and chronic kidney disease in pediatric and adult age. *Front Med*. (2022) 8:769734. doi: 10.3389/fmed.2021.769734

42. Liu CJ, Zheng YJ. Comparison of thyroid function and pregnancy outcomes in patients with severe preeclampsia complicated with hypothyroidism. *Med Sci J Cent South China*. (2017) 45:397–400.

43. Joshi D, James A, Quaglia A, Westbrook RH, Heneghan MA. Liver disease in pregnancy. *Lancet*. (2010) 375:594–605. doi: 10.1016/S0140-6736(09)61495-1

44. Terrault NA, Williamson C. Pregnancy-associated liver diseases. *Gastroenterology*. (2022) 163:97–117. doi: 10.1053/j.gastro.2022.01.060

45. Westbrook RH, Dusheiko G, Williamson C. Pregnancy and liver disease. *J Hepatol*. (2016) 64:933–45. doi: 10.1016/j.jhep.2015.11.030

46. Sciarrone SS, Ferrarese A, Bizzaro D, Volpato S, Maria Donato F, Invernizzi F, et al. Safe pregnancy after liver transplantation: Evidence from a multicenter Italian collaborative study. *Dig Liver Dis*. (2022) 54:669–75. doi: 10.1016/j.dld.2021.08.013

47. Vaughan OR, Rosario FJ, Powell TL, Jansson T. Regulation of placental amino acid transport and fetal growth. *Prog Mol Biol Transl Sci*. (2017) 145:217–51. doi: 10.1016/bs.pmbts.2016.12.008

48. Gomes J, Au F, Basak A, Cakmak S, Vincent R, Kumarathasan P, et al. Maternal blood biomarkers and adverse pregnancy outcomes: a systematic review and meta-analysis. *Crit Rev Toxicol*. (2019) 49:461–78. doi: 10.1080/10408444.2019.1629873

49. Li L, Chen YH, Yang YY, Cong L. Effect of intrahepatic cholestasis of pregnancy on neonatal birth weight: A meta-analysis. *J Clin Res Pediatr Endocrinol*. (2018) 10:38–43. doi: 10.4274/jcrpe.4930

50. Liu Y, Hou W, Meng X, Zhao W, Pan J, Tang J, et al. Early elevated alkaline phosphatase increases the risk of large-for-gestational-age birth weight in pregnant women with normal glucose tolerance. *Diabetes Res Clin Pract*. (2018) 141:209–16. doi: 10.1016/j.diabres.2018.04.024

51. Yarrington CD, Cantonwine DE, Seely EW, Mcelrath TF, Zera CA. The association of early unexplained elevated alanine aminotransferase with large-for-gestational-age birthweight. *Am J Obstet Gynecol*. (2016) 215:474.e1–e5. doi: 10.1016/j.ajog.2016.04.051

52. Monrose E, Bui A, Rosenbluth E, Dickstein D, Acheampong D, Sigel K, et al. Burden of future liver abnormalities in patients with intrahepatic cholestasis of pregnancy. *Am J Gastroenterol*. (2021) 116:568–75. doi: 10.14309/ajg.0000000000001132

53. Makris K, Mousa C, Cavalier E. Alkaline phosphatases: biochemistry, functions, and measurement. *Calcif Tissue Int*. (2023) 112:233–42. doi: 10.1007/s00223-022-01048-x

54. Zhuang X, Cui AM, Wang Q, Cheng XY, Shen Y, Cai WH, et al. Liver dysfunction during pregnancy and its association of with preterm birth in China: A prospective cohort study. *EBioMedicine*. (2017) 26:152–6. doi: 10.1016/j.ebiom.2017.11.014

55. Piantanida E, Ippolito S, Gallo D, Masiello E, Premoli P, Cusini C, et al. The interplay between thyroid and liver: implications for clinical practice. *J Endocrinol Invest*. (2020) 43:885–99. doi: 10.1007/s40618-020-01208-6

56. Sinha RA, Singh BK, Yen PM. Direct effects of thyroid hormones on hepatic lipid metabolism. *Nat Rev Endocrinol*. (2018) 14:259–69. doi: 10.1038/nrendo.2018.10

57. Hatziagelaki E, Paschou SA, Schön M, Psaltopoulou T, Roden M. NAFLD and thyroid function: pathophysiological and therapeutic considerations. *Trends Endocrinol Metab*. (2022) 33:755–68. doi: 10.1016/j.tem.2022.08.001

58. Qin Y, Wu Y, Zang H, Cong X, Shen Q, Chen L, et al. Lipid metabolism in pregnancy women with hypothyroidism and potential influence on pregnancy outcome. *J Lipids*. (2024) 2024:5589492. doi: 10.1155/2024/5589492

59. Targher G, Montagnana M, Salvagno G, Moghetti P, Zoppini G, Muggeo M, et al. Association between serum TSH, free T4 and serum liver enzyme activities in a large cohort of unselected outpatients. *Clin Endocrinol*. (2008) 68:481–4. doi: 10.1111/j.1365-2265.2007.03068.x

frontiers | Frontiers in Endocrinology

TYPE Original Research
PUBLISHED 15 October 2025
DOI 10.3389/fendo.2025.1557225

OPEN ACCESS

EDITED BY
Sijung Yun,
Predictiv Care, Inc., United States

REVIEWED BY
Dinakaran Vasudevan,
SKAN Research Trust, India
Pui-Ying Leong,
Chung Shan Medical University Hospital, Taiwan
Rupa Mazumder,
Noida Institute Of Engineering And Technology (Pharmacy Institute), India

*CORRESPONDENCE
Xiujuan Hou
houxiujuan2008@163.com

RECEIVED 08 January 2025
ACCEPTED 19 September 2025
PUBLISHED 15 October 2025

CITATION
Cao F, Yi W, Wu M, Gao A, Kang T and Hou X (2025) Characteristics of the gut microbiome of asymptomatic hyperuricemia.
Front. Endocrinol. 16:1557225.
doi: 10.3389/fendo.2025.1557225

Characteristics of the gut microbiome of asymptomatic hyperuricemia

Fengjiao Cao[1], Wenming Yi[1], Mengwei Wu[1], Ao Gao[1], Tianlun Kang[2] and Xiujuan Hou[2]*

[1]Department of Preventive Treatment of Disease, Dongfang Hospital, Beijing University of Chinese Medicine, Beijing, China, [2]Department of Rheumatology, Dongfang Hospital, Beijing University of Chinese Medicine, Beijing, China

Purpose: Asymptomatic hyperuricemia(AH) is characterized by elevated blood uric acid levels without symptoms,posing risks like gout, kidney stones, and cardiovascular diseases. This study aims to investigate the role of the gut microbiota in uric acid metabolism in AH.
Methods: Clinical data from 30 AH patients and 30 healthy controls were collected. Fecal microbiota genomic DNA was extracted, PCR amplified, library constructed, and sequenced. Bioinformatics and statistical analyses were conducted to study the gut microbiota of the two groups.
Results: The AH group exhibited significantly elevated levels of body mass index (BMI), Triglycerides (TG), Total Cholesterol (TC), as along with a history of smoking, hypertension, and fatty liver disease compared to the healthy group ($P < 0.05$). The overall richness and ecological diversity of gut microbiota in the AH group decreased, with differences in the distribution at the phylum and genus levels compared to the healthy group. Uric acid demonstrated significant correlations with various gut microbiota (e.g., Granulicatella), suggesting their potential as biomarkers for AH. Despite limitations such as a small sample size and lack of long-term follow-up, our findings provide new insights for the early diagnosis and personalized treatment of AH. Looking ahead, these discoveries may advance the clinical management of AH and the exploration of associated biomarkers.

KEYWORDS

asymptomatic hyperuricemia, gut microbiota, 16S rRNA sequencing, correlation study, clinical parameters

1 Introduction

Asymptomatic hyperuricemia(AH) is characterized by elevated levels of uric acid in the blood without clinical symptoms. Despite its increasing prevalence in adults, the potential health risks associated with this condition are often overlooked (1). AH is closely linked to the development of gout, kidney stones, and cardiovascular diseases (2), imposing significant economic burdens on healthcare systems. Current diagnostic and treatment

approaches primarily focus on symptomatic gout patients, while prevention and management of AH lack sufficient research and attention, highlighting the urgent need for further exploration and investigation in this field.

Recent research has indicated a potential significant role of the gut microbiota in metabolic disorders, including the regulation of uric acid metabolism (3, 4). The composition of the gut microbiota is closely associated with an individual's metabolic status, with certain microbes potentially impacting the synthesis and excretion of uric acid (5). This discovery has sparked scientific interest in exploring the connection between AH and the gut microbiota, suggesting a potential significant role of the gut microbiota in the development of hyperuricemia (6). Therefore, research focusing on the gut microbiota may unveil new pathophysiological insights into AH and offer novel avenues for intervention.

This study aims to explore the potential connection between gut microbiota characteristics and uric acid metabolism in patients with AH. The research methods include clinical data collection, DNA extraction and sequencing, microbiome data analysis, to elucidate how microbiota composition impacts the development and advancement of AH. This not only provides foundational data for mechanistic studies of AH but also offers potential biomarker support for future personalized treatment strategies.

Upon reviewing the background and existing research, it is evident that this study will provide a new perspective on the prevention and treatment of AH, particularly in the individualized intervention of the microbiome. This will offer a more scientific basis for clinical practice, ultimately reducing the incidence of AH and its related complications, thereby improving patients' quality of life.

2 Materials and methods

2.1 Study population

In the period from January to June 2023, we recruited 30 patients with AH at the Health Examination Center of Dongfang Hospital, Beijing University of Chinese Medicine. The diagnostic criteria for AH were defined as serum uric acid levels of > 7 mg/dL for males and > 6 mg/dL for females in two fasting tests on different dates under normal purine diet (7). Exclusion criteria for the AH patients included: a history of acute gouty arthritis, chronic tophaceous gout, chronic gouty arthritis, or uric acid nephropathy; the presence of severe cardiovascular, cerebrovascular, hepatic, renal, or hematopoietic system diseases; and secondary hyperuricemia due to other causes such as malignancy or renal disease. Additionally, we excluded individuals who had taken medications known to influence uric acid metabolism (e.g., aspirin, hydrochlorothiazide, probenecid) or those who had used antibiotics, probiotics, prebiotics, or synbiotics within the 3 months prior to enrollment. Pregnant or lactating women were also excluded. A parallel group of 30 age- and gender-matched healthy volunteers was recruited. These volunteers had no history of significant diseases or infections in the past 3 months and had likewise not used any antibiotics or probiotic supplements during that period.

Sample size estimation: The sample size was determined *a priori* using power analysis in G*Power 3.1, where based on pilot data from 5 asymptomatic hyperuricemia (AH) patients and 5 healthy controls, we estimated a Cohen's d effect size of 0.80 for α-diversity (Shannon index) differences; with a significance level (α) of 0.05 (two-tailed) and 80% statistical power, the minimum required sample was calculated as 22 participants per group, which was increased to 30/group to accommodate 20% potential attrition from DNA extraction/sequencing failures.

This study was conducted in accordance with the Helsinki Declaration and Good Clinical Practice guidelines. Approved by the Ethics Committee of Dongfang Hospital, Beijing University of Chinese Medicine (Approval No: JDF-IRB-2023051802), all participants provided written informed consent.

2.2 Clinical information

Patient consultation and physical examination data were collected, including patient ID, gender, age, height, weight, liver ultrasound results, medical history, smoking and alcohol consumption history. Body mass index (BMI) was calculated using the formula BMI = weight (kg)/height (m^2) based on the patient's height and weight information. Blood pressure was measured using a clinical electronic sphygmomanometer, with two seated blood pressure measurements taken 10 minutes apart and the average recorded. Hypertension was defined as systolic blood pressure ≥ 140 mmHg, diastolic blood pressure ≥ 90 mmHg, a history of hypertension, and/or current use of antihypertensive medication. Diabetes was defined as fasting blood glucose ≥ 7.1 mmol/l, a history of diabetes, and/or current use of antidiabetic medication. Smoking history referred to current or past smoking habits, while alcohol consumption history referred to the consumption of alcoholic beverages in the past year. Fatty liver was diagnosed based on abdominal ultrasound findings or a history of fatty liver disease. Additionally, 5ml of peripheral venous blood was collected from each patient after a 12-hour fast for laboratory testing, including routine blood parameters, blood biochemistry, renal and liver function parameters, and blood lipid analysis.

2.3 Specimen collection

Before sampling, instruct the participants to empty their bladders to prevent urine contamination of feces. Collect approximately 2g of freshly passed feces using a sterile spoon and place it in a 2 mL cryotube. Store the sample at -80 °C within 2 hours for sequencing.

2.4 DNA extraction and PCR amplification

In this study, genomic DNA of fecal gut microbiota was extracted using the CTAB method. Subsequently, DNA purity and concentration

were assessed by 1% agarose gel electrophoresis. An appropriate amount of fecal sample was diluted in sterile water to 1 ng/μl in a centrifuge tube. The highly variable V3V4 region of the bacterial 16S rRNA gene was selected for sequencing. Specific primers 341F (5'-CCTAYGGGRBGCASCAG-3') and 806R (5'-GGACTACNNGGG TATCTAAT-3') were used for PCR amplification of the V3 + V4 variable region. The amplification protocol involved using the diluted genomic DNA as a template, specific primers designed with specific barcodes, Phusion® High-Fidelity DNA polymerase enzyme, and Phusion® High-Fidelity PCR Master Mix with GC Buffer. Amplification of the V3 + V4 variable region was carried out using a Bio-rad T100 gradient PCR machine.

2.5 Purification and multiplexing of PCR products

After equalizing the concentrations of PCR products, they were thoroughly mixed and purified using a 2% agarose gel electrophoresis in 1xTAE buffer (Biowest, Spain). The target bands were recovered using the Universal DNA Purification Recovery Kit (TianGen, China).

2.6 Construction of libraries and sequencing on computers

Utilizing the NEB Next® Ultra DNA Library Prep Kit (Illumina, USA), libraries were constructed, followed by library quality assessment and qPCR quantification using the Agilent 5400 Bioanalyzer (Agilent Technologies, USA). Subsequently, qualified libraries were subjected to sequencing on the Illumina Novaseq 6000 PE250 platform (Illumina, USA).

2.7 Bioinformatics analysis

The analysis was conducted by following the "Atacama soil microbiome tutorial" of Qiime2docs along with customized program scripts (https://docs.qiime2.org/2019.1/).

Utilizing the QIIME2 dada2 plugin, all raw sequences underwent quality control, trimming, denoising, merging, and removal of chimeras to obtain the final feature sequences (amplicon sequence variants, ASVs). The ASV representative sequences were aligned to the pre-trained 13_8 version of the GREENGENES database at 99% similarity using the QIIME2 feature-classifier plugin (with the database trimmed to the V3V4 region based on the 341F/806R primers), resulting in a table of taxonomic classifications. Subsequently, the QIIME2 feature-table plugin was employed to eliminate all contaminant mitochondrial and chloroplast sequences. Various methods such as ANCOM, ANOVA, Kruskal-Wallis, LEfSe, and DESeq2 were employed to identify differential bacterial abundance between groups and samples. Subsequently, the QIIME2 core-diversity plugin was utilized to compute diversity matrices, including alpha diversity indices at the feature sequence level such as observed features, Chao1, Simpson, Shannon, and Faith's phylogenetic diversity, to assess the diversity within samples. Beta diversity indices, such as Bray Curtis, unweighted UniFrac, and weighted UniFrac, are utilized to assess differences in microbial community structures among samples. We employed Principal Coordinates Analysis (PCoA) and Partial Least-Squares Discrimination Analysis (PLS-DA) plots for visualization. To further understand the specific species contributing to inter-group microbial differences, bacteria with differential abundances between groups were identified using the Kruskal-Wallis test and Linear discriminant analysis Effect Size (LEfSe) based on species abundance tables. Spearman correlation coefficients were calculated between clinical phenotypes and microbial species, and a correlation heatmap was constructed to assess significant associations. Additionally, the functional composition of microbial communities was predicted using PICRUSt software. Unless stated otherwise, default parameters were utilized for the aforementioned analyses. (Sequencing service and data analysis service were provided by Wekemo Tech Group Co., Ltd. Shenzhen China.).

3 Result

3.1 The fundamental characteristics of the research subject.

The AH group and the healthy control group showed no significant differences in age and gender ($P > 0.05$). The AH group exhibited significantly higher levels of BMI, Serum Uric Acid (SUA), TG, and TC compared to the healthy control group ($P < 0.05$), while High-Density Lipoprotein Cholesterol (HDLC) levels were significantly lower in the AH group ($P < 0.05$). Differences in hypertension, fatty liver, and alcohol history were statistically significant ($P < 0.05$) (Table 1).

3.2 The characteristics of the distribution at the phylum and genus levels of gut microbiota in two groups.

By analyzing the feature table of Amplicon Sequence Variants (ASVs), the relative abundances of samples at different taxonomic levels including phylum, class, order, family, genus, and species were determined. The results were presented using stacked bar graphs. At the phylum level, the top 20 species were selected to compose the bar graph, as shown in Figure 1A. Both groups exhibited Firmicutes, Bacteroidota, Proteobacteria, Actinobacteria, and Euryarchaeota as dominant gut microbiota. Among the phyla with relatively higher proportions, the abundance of Euryarchaeota in the AH group was significantly lower compared to the other group (2.54% vs. 1.345%, P=0.019).

At the genus level, a bar graph was constructed using the top 20 ranked species, as shown in Figure 1B. The gut microbiota of the two groups exhibited differences at the genus level, with relatively higher abundances in the following genera for both groups: Bacteroides (20.40% vs 20.89%), Faecalibacterium (10.74% vs 12.98%), and Prevotella (8.01% vs 10.58%). In the AH group, Oscillospira (1.63%

10.3389/fendo.2025.1557225

TABLE 1 Comparison of baseline characteristics of the participants [(x ± s/n (%)].

Clinical data	Healthy group(*n*=30)	AH group(*n*=30)	*P-value*
Gender			0.79
Male = 1	17(56.7%)	18(60%)	
Female = 0	13(43.3%)	12(40%)	
Age(years)	38.03 ± 11.35	34.43 ± 9.65	0.19
BMI(kg/m^2)	23.36 ± 3.00	27.56 ± 4.71	0.00
SUA(mmol/L)	301 ± 67.00	462 ± 84.37	0.00
TC(mmol/L)	4.45 ± 0.75	4.96 ± 1.11	0.04
TG(mmol/L)	1.21 ± 0.61	1.97 ± 1.49	0.01
LDL-C(mmol/L)	2.80 ± 0.73	3.20 ± 0.96	0.07
HDL-C(mmol/L)	1.45± 0.34	1.21 ± 0.26	0.04
Fatty liver			
Yes = 1	5(16.7%)	19(63.3%)	0.00
No = 0	25(83.3%)	11(36.7%)	
Smoking history			
Yes = 1	6(20%)	13(43.3%)	0.52
No = 0	24(80%)	17(56.7%)	
Alcohol consumption history			
Yes = 1	6(20%)	19(63.3%)	0.00
No = 0	24(80%)	11(36.7%)	
Hypertension			
Yes = 1	2(6.7%)	11(36.7%)	0.01
No = 0	28(93.3%)	19(63.3%)	
Diabetes			
Yes = 1	4(13.3%)	10(33.3%)	0.07
No = 0	26(86.7%)	20(66.7%)	

vs 1.18%, p=0.035) and Methanomethylovorans (1.63% vs 0.65%, p=0.003) showed significantly lower abundance levels.

As shown in Figures 1C, D, the community heatmap illustrates the species abundance of the top 20 gut-dominant microbiota at the phylum and genus levels for two groups, revealing differences in gut microbiota composition between the groups.

3.3 Comparison of alpha diversity of gut microbiota

As shown in Figure 2A, the Chao1 index, Observed species index, Shannon index, and Simpson index of the AH group were lower than those of the healthy control group, but the differences were not statistically significant (P > 0.05). As depicted in Figure 2B below, the sequencing depth of the experimental samples gradually reached saturation with increasing sequencing efforts, indicating sufficient sequencing coverage to assess the diversity of the gut microbiota under study.

3.4 Comparison of beta diversity in gut microbiota

The PCoA analysis (Figure 3A) revealed differences in the gut microbiota community structure between the AH group and the healthy control group. Further confirmation of these differences was obtained through ANOSIM analysis, which indicated non-significant dissimilarities between the two groups (P=0.69). NMDS analysis results were consistent with the PCoA analysis (Figure 3B). Utilizing Partial Least Squares Discriminant Analysis (PLS-DA) (Figure 3C), the samples from the two groups were distinctly separated in the PLS-DA plot without overlap, with an

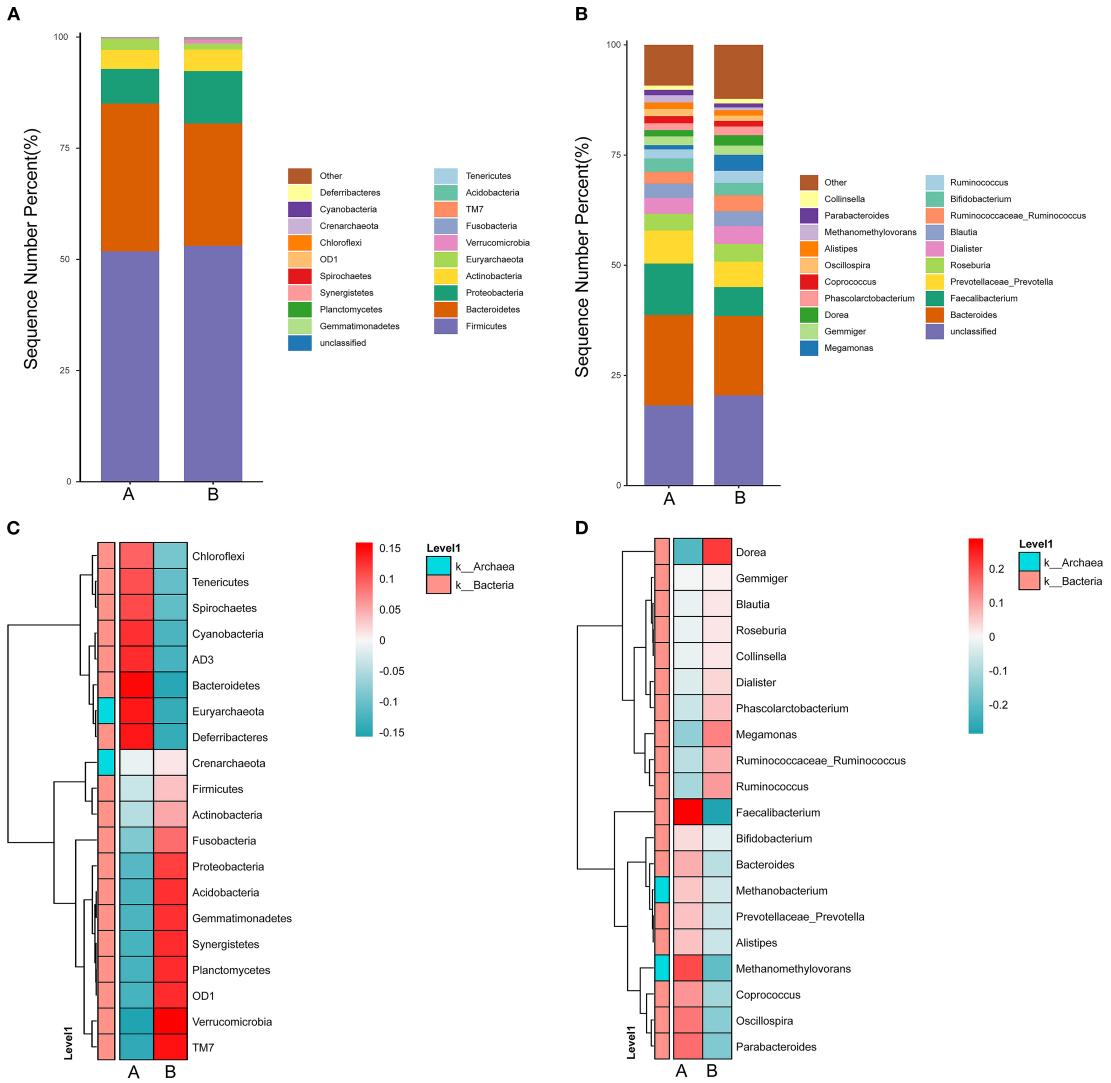

FIGURE 1
Characteristics of the distribution of gut microbiota at the phylum and genus levels in two groups. **(A)** displays the relative abundance of species at the phylum level, while **(B)** illustrates the relative abundance of species at the genus level. The x-axis represents the group names, and the y-axis (Sequence Number Percent%) indicates the proportion of sequences annotated at that level compared to the total annotated data, with the color sequence in the bar charts corresponding to the legend on the right. **(C)** represents a heatmap of species communities at the phylum level, and **(D)** shows a heatmap of species communities at the genus level. The x-axis denotes the group names, and the y-axis displays the phylum/genus-level taxonomic annotations. The clustering tree on the left clusters species based on similarity in abundance distribution. The middle heatmap represents the log10(absolute abundance) heatmap. Group A refers to the healthy group, while Group B refers to the AH group.

AUC value of 1 for both groups, indicating significant differences in gut microbiota composition between them. The Venn diagram (Figure 3D) visually displayed the shared and unique species compositions between the healthy and AH groups, showing 1140 shared ASVs and a differing number of ASVs, highlighting a quantitative difference in species between the two groups.

3.5 LEfSe analysis of divergent species

As shown in Figure 4, compared to the healthy group, the AH group exhibited higher relative abundance of g_Enhydrobacter, g_Dorea, g_Stenotrophomonas, and g_Acinetobacter ($P < 0.05$), while g_Sphingobium, g_Candidatus_Koribacter, p_Acidobacteria, g_Anaerostipes, g_Oscillospira, g_Methanomethylovorans, and p_Euryarchaeota showed lower relative abundance ($P < 0.05$).

3.6 Correlation analysis

The Spearman correlation analysis revealed a positive correlation between blood uric acid levels and the abundance of Enterococcaceae, Dorea, Bordetella, and Granulicatella ($P < 0.05$), and a negative correlation with Oxalobacter, Methanomethylovorans, Candidatus_Arthromitus, and Proteus ($P < 0.05$) (Figure 5). Additionally, clinical parameters such as BMI and blood lipid levels

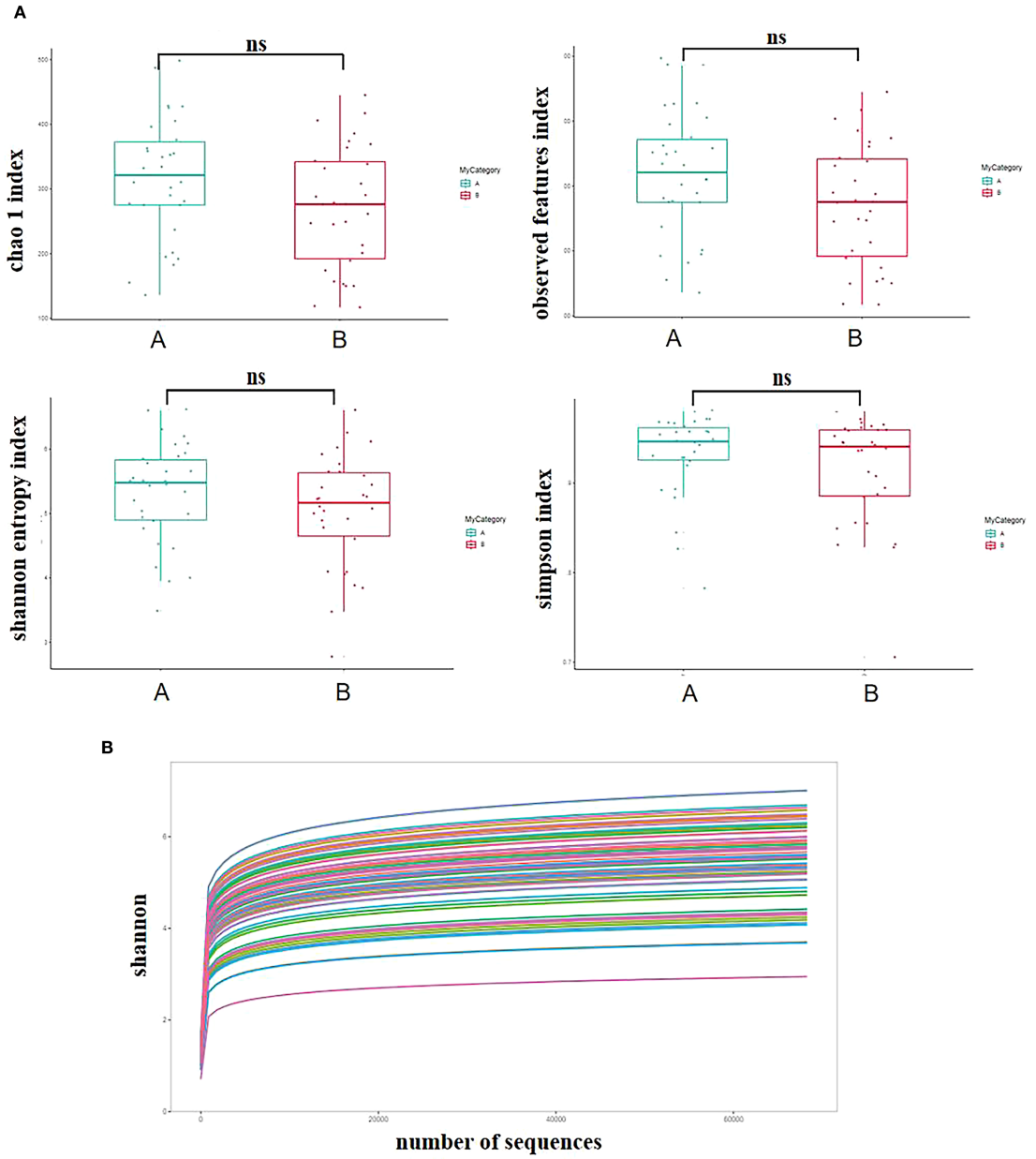

FIGURE 2
Comparison of alpha diversity in gut microbiota. **(A)** compares the alpha diversity (Chao1, Observed species, Shannon, Simpson) indices between the two groups; **(B)** the sampling depth on the x-axis and the Shannon index on the y-axis. "ns" indicates no statistical significance, Group A: healthy group, Group B: AH group.

showed significant correlations with the abundance of certain gut microbial species.

3.7 Analysis of inter-group differences in functionality

Based on PICRUSt2-predicted pathway annotations (MetaCyc database) and considering the grouping information, microbial community predicted functions were analyzed using ANOVA with Duncan and Dunn tests. As shown in Figure 6, the AH group exhibited downregulation of glycolysis V (Pyrococcus), 7-(3-amino-3-carboxypropyl)-wyosine biosynthesis, archaetidylinositol biosynthesis, CDP-archaeol biosynthesis, coenzyme B biosynthesis, mevalonate pathway II (archaea), phosphopantothenate biosynthesis III, and superpathway of methanogenesis, while L-tryptophan degradation IX was upregulated compared to the healthy group, with significant differences ($P < 0.05$).

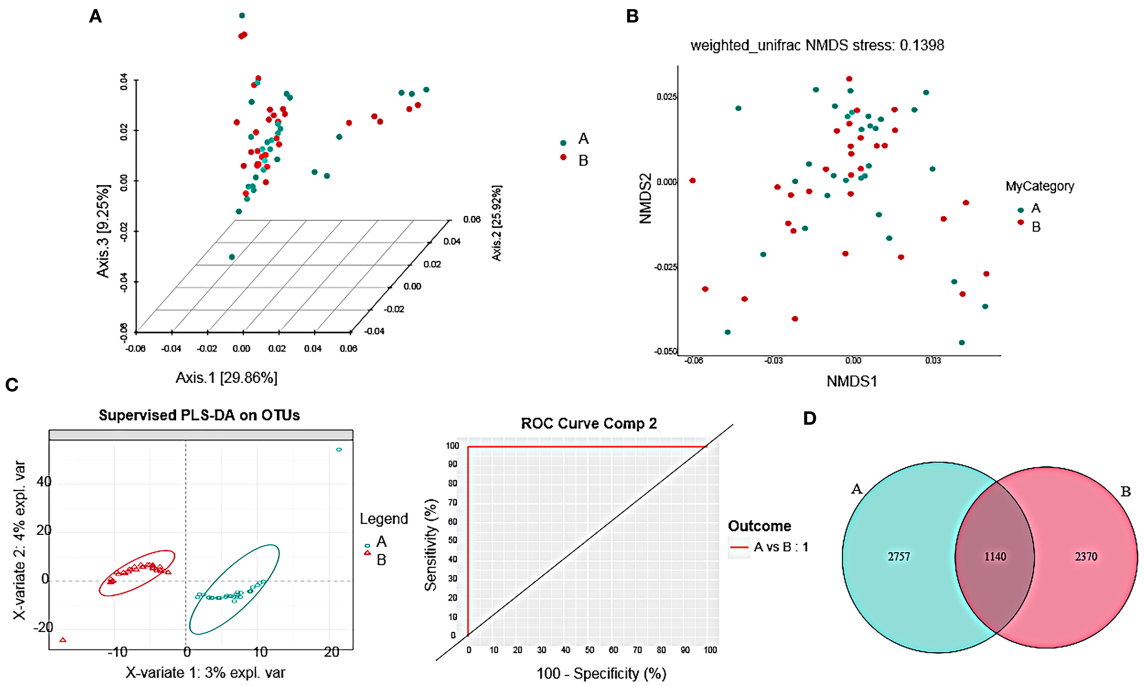

FIGURE 3
Comparison of beta diversity in gut microbiota. **(A)** Based on the 3D PCoA plot using weighted Unifrac, Axis 1 represents the first principal component contributing 29.86%, while Axis 2 represents the second principal component contributing 9.25%. **(B)** NMDS analysis was conducted using weighted Unifrac distances. Each point in the plot represents a sample, with different colors indicating different sample groups, and the distances between points represent the degree of microbial community differences. **(C)** PLS-DA coordinate plot where each point represents a sample, with points of the same color belonging to the same group; AUC curves of the regression model indicating the area under the curve for discriminant analysis of each group displayed on the right side of the plot. **(D)** Venn diagram showing Group A: healthy group, Group B: AH group.

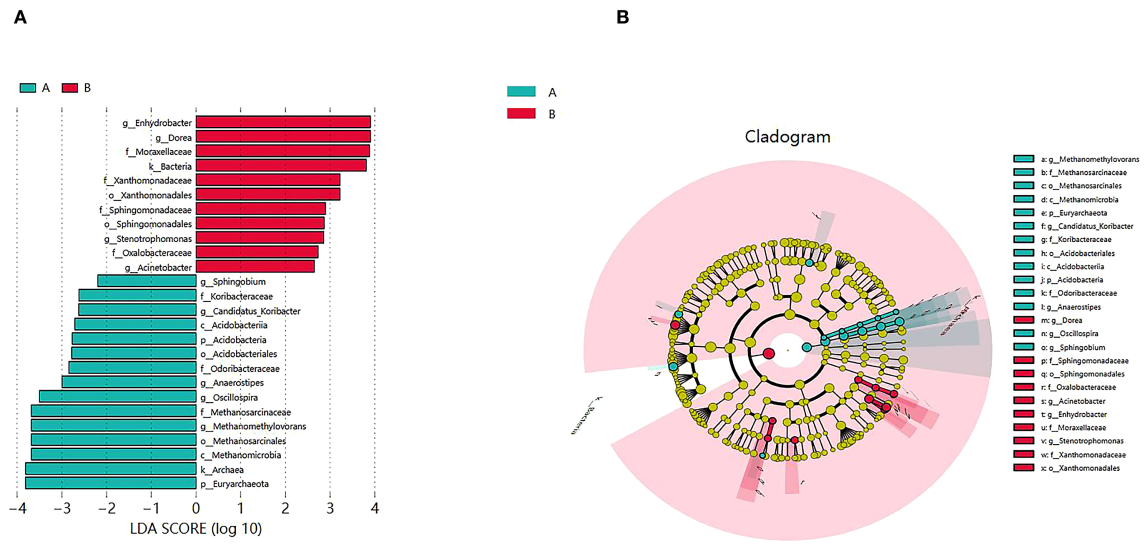

FIGURE 4
Analysis of differential species in the gut microbiota. **(A)** Each horizontal bar represents a species, with the length corresponding to the LDA value indicating the level of difference. The color of the bars indicates the microbial feature group to which the species belongs, reflecting its relatively higher abundance within that group. **(B)** In the cladogram, the layers from inner to outer represent different taxonomic levels such as phylum, class, order, family, and genus, with connecting lines indicating their hierarchical relationships. Each circular node represents a species, with yellow nodes indicating insignificant differences between groups, while non-yellow nodes represent species characteristic of a specific group (with significantly higher abundance within that group). Colored sectors highlight the taxonomic range of the characteristic microbes. Group A: healthy group, Group B: AH group.

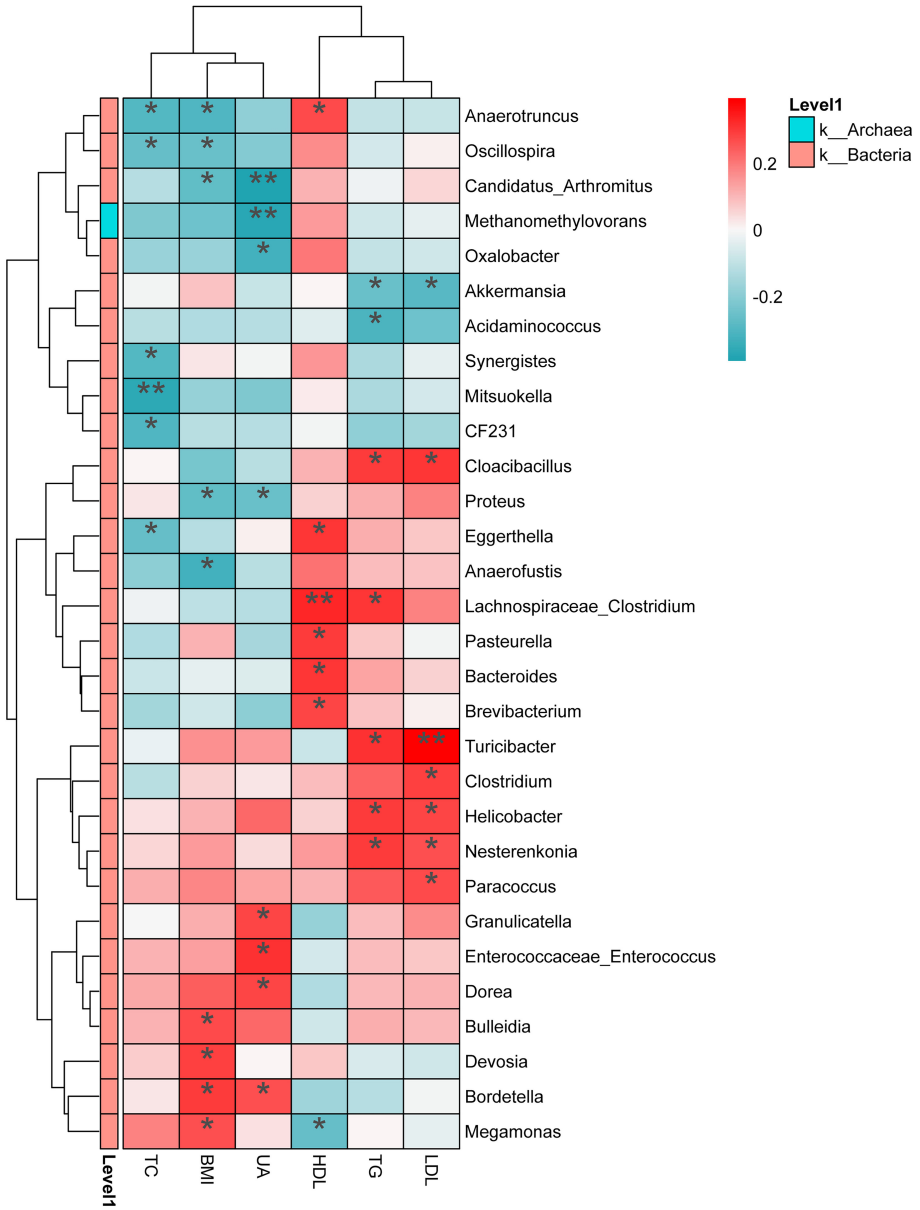

FIGURE 5
Heatmap illustrating the relationships between microbial species and clinical phenotypes in the study participants ($r \geq 0.3$). The X-axis represents clinical phenotypes (including BMI, TC, TG, LDL-C, UA, HDL-C), while the Y-axis indicates the corresponding species (at the genus level). The color bar on the far left denotes the phylum classification, with different colors representing different r values. The legend on the far right shows the color intervals corresponding to r values and the phylum names. *P < 0.05, **P < 0.01. BMI, Body Mass Index; TC, Total Cholesterol; TG, Triglycerides; LDL-C, Low-Density Lipoprotein Cholesterol; HDL-C, High-Density Lipoprotein Cholesterol; UA, Serum Uric Acid.

4 Discussion

This study explores the background of AH and its potential associations with metabolic-related diseases. AH is characterized by elevated blood uric acid levels without symptoms of conditions like gout. Despite a rising prevalence in the general population and its close links to health risks such as cardiovascular diseases, kidney stones, and metabolic syndrome, research on AH remains limited, particularly regarding its underlying pathophysiology and preventive strategies. This suggests that AH may serve as a precursor to more serious health issues, emphasizing the need for further investigation in this field.

This study investigates the observed association between changes in gut microbiota and AH. Various methods including clinical data collection, high-throughput sequencing, and microbiome data analysis were employed to analyze the gut microbiota characteristics of AH patients compared to healthy controls, and their relationship with clinical indicators. The results reveal significant differences in gut microbiota composition between AH patients and healthy individuals,

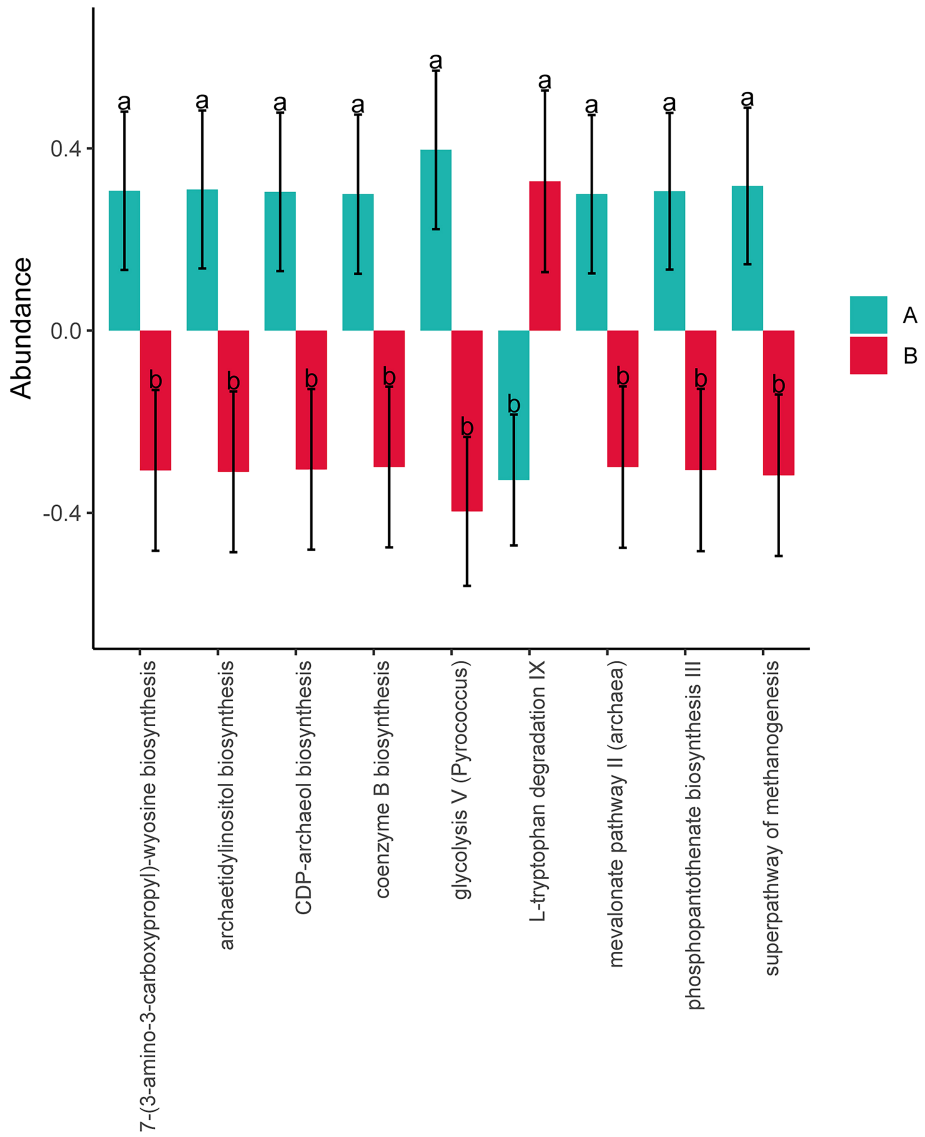

FIGURE 6
Significant differences in all METAcyc pathways identified through ANOVA and Duncan's test. The x-axis represents the names of pathways. Each pathway is color-coded to indicate a specific group. If two groups share the same letter above them, it signifies nonsignificant differences; otherwise, differences are considered significant.

suggesting new targets for future treatments. Through a thorough analysis of these findings, we aim to provide novel insights and evidence for the prevention and treatment of AH.

In this study, we revealed a potential association between AH and the gut microbiota by analyzing the characteristics of AH patients and their gut microbiomes. The results indicated significant variances between the AH group and the healthy control group in terms of body mass index (BMI) and metabolic indicators such as TG and TC. These variances suggest distinct metabolic features in AH patients compared to healthy individuals, providing foundational data for clinical screening and intervention strategies. Additionally, the prevalence of hypertension and fatty liver in the AH group was significantly higher than in the healthy group, further supporting a potential link between AH and metabolic syndrome (8).

In the analysis of microbiota data, this study observed a decrease in Alpha diversity in the AH group compared to the healthy group, indicating a reduction in overall richness and ecological diversity of the gut microbiota in the AH group. Beta diversity suggested differences in the composition of gut microbiota between the two groups. At the phylum level, a decrease in abundance of Acidobacteria and Verrucomicrobia was noted in the AH group. At the genus level, the relative abundance of Enhydrobacter, Dorea, Stenotrophomonas, Acinetobacter was higher, while Sphingobium, Candidatus_Koribacter, Anaerostipes, Oscillospira, Methanomethylovorans showed lower relative

abundance in the AH group. These microbial differences may be correlated with the pathogenesis of AH, providing clues for future research on the relationship between gut microbiota and AH. Previous studies have suggested that gut microbiota are associated with uric acid synthesis and excretion through metabolic pathways and immune responses (9).

Some studies suggest that Oscillospira is a genus associated with a healthy gut and has been predicted to be a potential producer of butyric acid (10). Anaerostipes strains are known to utilize inositol to generate propionic and acetic acids (11). SCFAs, particularly propionate and butyrate, have been reported to provide ATP to intestinal cells, potentially benefiting uric acid excretion (12). Our research also observed decreased abundance of Oscillospira and Anaerostipes in the AH group, indicating a possible association between AH and the reduction of these two genera.

Furthermore, the study revealed a positive correlation between serum uric acid levels in AH patients and specific gut microbiota such as Bordetella and Granulicatella, while showing a negative correlation with Oxalobacter and Methanomethylovorans ($P < 0.05$). These findings offer a novel perspective for biomarker research in AH, potentially aiding in early diagnosis and monitoring in clinical settings. Future research should explore the utility of microbiome analysis techniques for early diagnosis and investigate the prospects of these biomarkers in personalized medicine (13).

Finally, based on the PICRUSt2-predicted pathway abundances annotated by the METAcyc database, we observed significant differences in specific metabolic pathways, including downregulation of glycolysis V (Pyrococcus) and upregulation of L-tryptophan degradation IX in the AH group compared to the healthy group. However, as these functional predictions are derived from 16S rRNA gene sequences and not from metagenomic or metatranscriptomic data, they should be interpreted as in silico inferences with inherent limitations including dependence on reference genomes and lack of experimental validation.

Despite these predictive limitations, previous research has provided insights that may relate our findings to hyperuricemia pathogenesis. Potential inhibition of the glycolysis pathway could theoretically contribute to accumulation of metabolic intermediates such as 6-phospho-glucose and 3-phosphoglyceraldehyde, which can be diverted to produce 5-phosphoribose and subsequently ribose-5-phosphate. This could theoretically increased endogenous purine synthesis and elevated serum uric acid levels (14). It is noteworthy that the predicted glycolysis V pathway is specific to archaea (Pyrococcus), which implies a possible connection of archaeal metabolism in AH that warrants further investigation.

Regarding tryptophan metabolism, which encompasses the kynurenine, serotonin, and indole pathways, the production of bioactive compounds from tryptophan degradation can be associated with diverse physiological processes including inflammation, metabolism, and immune responses (15). Kynurenic acid, a major degradation product of L-tryptophan (16), was found elevated in AH rats, while indoxyl sulfate and tryptophan 2-C-glucoside were decreased, indicating alterations in tryptophan metabolism in AH (17). Although our predictive data suggest altered tryptophan degradation activity in the gut microbiome of AH patients, the nature of the relationship between microbial pathway activity and host metabolite levels requires experimental validation.

The limitations of this study primarily lie in sample size and experimental design. Although we compared high uric acid patients with a healthy control group, the relatively small sample size may impact the statistical significance and generalizability of the results. Furthermore, the observational design prevents causal inferences, and the lack of validation through wet lab experiments restricts the biological significance and clinical applicability of the findings. Additionally, important lifestyle factors including dietary patterns, fiber intake, physical activity, and probiotic use were not assessed in this study. These unmeasured confounders may influence both gut microbiota composition and uric acid levels, limiting the ability to isolate microbiome-specific effects. Moreover, the absence of long-term clinical follow-up data prevents the assessment of potential causality between microbiome changes and the progression of AH. These limitations suggest that future research should involve larger sample sizes, incorporate multiple experimental approaches, control for key lifestyle confounders, and include long-term follow-up to validate our findings and enhance their clinical relevance.

In conclusion, this study provides important foundational data for clinical management by analyzing the characteristics of patients with AH, differences in gut microbiota, and associated risk factors. Despite certain limitations, our findings suggest new research directions for early diagnosis and personalized treatment of AH. Future investigations into the relationship between microbiota and AH, combined with larger-scale clinical data, may contribute to the development of more effective prevention and treatment strategies.

Data availability statement

The datasets presented in this study can be found in online repositories.The data presented in this study are deposited in the NCBI Sequence Read Archive (SRA) repository https://www.ncbi.nlm.nih.gov/sra/, accession number PRJNA1336442.

Ethics statement

The studies involving humans were approved by Dongfang Hospital of Beijing University of Chinese Medicine. The studies were conducted in accordance with the local legislation and institutional requirements. The participants provided their written informed consent to participate in this study. Written informed consent was obtained from the individual(s) for the publication of any potentially identifiable images or data included in this article.

Author contributions

FC: Conceptualization, Investigation, Writing – original draft. WY: Formal analysis, Methodology, Writing – review & editing. MW: Investigation, Software, Writing – review & editing. AG: Data

curation, Writing – review & editing. TK: Data curation, Visualization, Writing – review & editing. XH: Resources, Supervision, Writing – review & editing.

Funding

The author(s) declare financial support was received for the research and/or publication of this article. This work was supported by the Key Specialty Project for the "12th Five-Year Plan" of the State Administration of Traditional Chinese Medicine (Preventive Healthcare Specialty) and the Scientific Research Project of Hebei Administration of Traditional Chinese Medicine (Grant No. B2026019).

Conflict of interest

The authors declare that the research was conducted in the absence of any commercial or financial relationships that could be construed as a potential conflict of interest.

Generative AI statement

The author(s) declare that no Generative AI was used in the creation of this manuscript.

Any alternative text (alt text) provided alongside figures in this article has been generated by Frontiers with the support of artificial intelligence and reasonable efforts have been made to ensure accuracy, including review by the authors wherever possible. If you identify any issues, please contact us.

Publisher's note

References

1. Zhu Y, Di S, Li Y, Liang W, Liu J, Nuermaimaiti R, et al. Integrative metabolomic and network pharmacological analysis reveals potential mechanisms of *Cardamine circaeoides* Hook.f. & Thomson in alleviating potassium oxonate-induced asymptomatic hyperuricemia in rats. *Front Pharmacol.* (2023) 14:1281411. doi: 10.3389/fphar.2023.1281411

2. Chen Y, Luo J, Ma XM, He X, Zhang W, Wu S, et al. Phosphorus modifies the association between body mass index and uric acid: Results from NHANES 2007-2018. *PLoS One*. (2024) 19:e0306383. doi: 10.1371/journal.pone.0306383

3. Guo Y, Wang S, Wu X, Zhao R, Chang S, Ma C, et al. Multi-omics reveals the role of arachidonic acid metabolism in the gut-follicle axis for the antral follicular development of holstein cows. *Int J Mol Sci*. (2024) 25:9521. doi: 10.3390/ijms25179521

4. Zhang X, Jiang J, Xin J, Sun N, Zhao Z, Gan B, et al. Preventive effect of *Lactobacillus johnsonii* YH1136 against uric acid accumulation and renal damages. *Front Microbiol*. (2024) 15:1364857. doi: 10.3389/fmicb.2024.1364857

5. Yin H, Liu N, Chen J. The role of the intestine in the development of hyperuricemia. *Front Immunol*. (2022) 13:845684. doi: 10.3389/fimmu.2022.845684

6. Wang Z, Li Y, Liao W, Huang J, Liu Y, Li Z, et al. Gut microbiota remodeling: A promising therapeutic strategy to confront hyperuricemia and gout. *Front Cell Infect Microbiol*. (2022) 12:935723. doi: 10.3389/fcimb.2022.935723

7. Yu Q, Sun Z, Wang Y, Du X, Huang J, Wang L. Hyperuricemia is accompanied by elevated peripheral CD4+ T cells. *Sci Rep*. (2023) 13:12537. doi: 10.1038/s41598-023-39775-2

8. Vafa L, Amini M, Kamran H, Aghakhani L, Hosseini SV, Mohammadi Z, et al. The impact of obesity surgery on serum uric acid in people with severe obesity: A retrospective study. *Clin Nutr Res*. (2023) 12:21–8. doi: 10.7762/cnr.2023.12.1.21

9. Ren L, Wang S, Liu S, Prasanthi HAC, Li Y, Cao J, et al. Postbiotic of *Pediococcus acidilactici* GQ01, a Novel Probiotic Strain Isolated from Natural Fermented Wolfberry, Attenuates Hyperuricaemia in Mice through Modulating Uric Acid Metabolism and Gut Microbiota. *Foods*. (2024) 13:923. doi: 10.3390/foods13060923

10. Gophna U, Konikoff T, Nielsen HB. Oscillospira and related bacteria - From metagenomic species to metabolic features. *Environ Microbiol*. 2017 Mar;19(3):835–841. doi: 10.1111/1462-2920.13658

11. Bui TPN, Mannerås-Holm L, Puschmann R, Wu H, Troise AD, Nijsse B, et al. Conversion of dietary inositol into propionate and acetate by commensal Anaerostipes associates with host health. *Nat Commun*. (2021) 12:4798. doi: 10.1038/s41467-021-25081-w

12. Wang K, Wu S, Li P, Xiao N, Wen J, Lin J, et al. Sacha inchi oil press-cake protein hydrolysates exhibit anti-hyperuricemic activity via attenuating renal damage and regulating gut microbiota. *Foods*. (2022) 11:2534. doi: 10.3390/foods11162534

13. Zhang Y, Chen Y, Chen X, Gao Y, Luo J, Lu S, et al. Unconjugated bilirubin promotes uric acid restoration by activating hepatic AMPK pathway. *Free Radic Biol Med*. (2024) 224:644–59. doi: 10.1016/j.freeradbiomed.2024.09.023

14. Bulbule S, Gottschalk CG, Drosen ME, Peterson D, Arnold LA, Roy A. Dysregulation of tetrahydrobiopterin metabolism in myalgic encephalomyelitis/chronic fatigue syndrome by pentose phosphate pathway. *J Cent Nerv Syst Dis*. (2024) 16:11795735241271675. doi: 10.1177/11795735241271675

15. Chen X, Xu D, Yu J, Song XJ, Li X, Cui YL. Tryptophan metabolism disorder-triggered diseases, mechanisms, and therapeutic strategies: A scientometric review. *Nutrients*. (2024) 16:3380. doi: 10.3390/nu16193380

16. Adeyemi OS, Obeme-Imom JI, Akpor BO, Rotimi D, Batiha GE, Owolabi A. Altered redox status, DNA damage and modulation of L-tryptophan metabolism contribute to antimicrobial action of curcumin. *Heliyon*. (2020) 6:e03495. doi: 10.1016/j.heliyon.2020.e03495

17. Zhang W, Cui Y, Zhang J. Multi metabolomics-based analysis of application of *Astragalus membranaceus* in the treatment of hyperuricemia. *Front Pharmacol*. (2022) 13:948939. doi: 10.3389/fphar.2022.948939

Frontiers in Endocrinology

Explores the endocrine system to find new therapies for key health issues

The second most-cited endocrinology and metabolism journal, which advances our understanding of the endocrine system. It uncovers new therapies for prevalent health issues such as obesity, diabetes, reproduction, and aging.

Discover the latest Research Topics

See more →

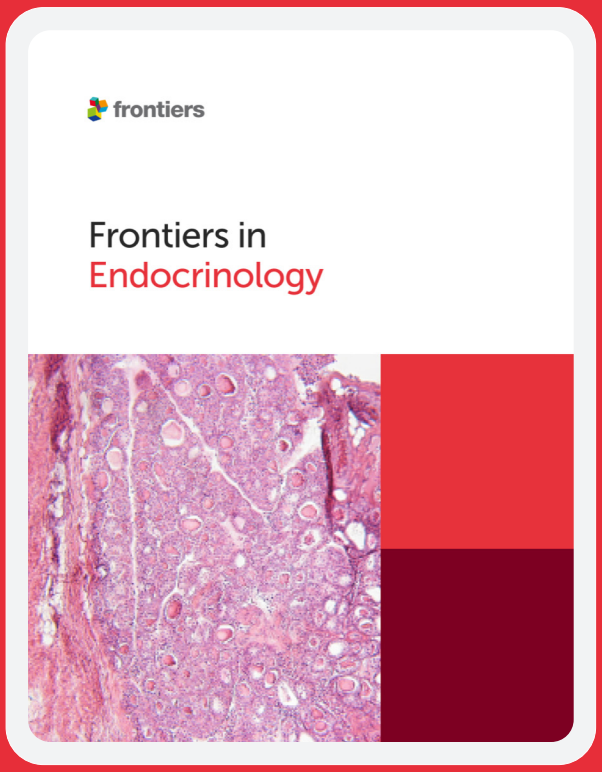

Frontiers

Avenue du Tribunal-Fédéral 34
1005 Lausanne, Switzerland
frontiersin.org

Contact us

+41 (0)21 510 17 00
frontiersin.org/about/contact